AD-A054 463 DOUGLAS AIRCRAFT CO LONG BEACH CALIF F/G 11/9
DAMPING, STATIC, DYNAMIC, AND IMPACT CHARACTERISTICS OF LAMINAT--ETC(U)
DEC 77 G F RHODES F33615-75-C-3105
UNCLASSIFIED MDC-J6944 AFFDL-TR-76-156 NL

1 OF 3
AD A054463

AFFDL-TR-76-156

DAMPING, STATIC, DYNAMIC, AND IMPACT CHARACTERISTICS OF LAMINATED BEAMS TYPICAL OF WINDSHIELD CONSTRUCTION

Douglas Aircraft Division
McDonnell Douglas Corporation
3855 Lakewood Boulevard
Long Beach, California 90846

DECEMBER 1977

TECHNICAL REPORT AFFDL-TR-76-156

Final Report for Period July 1975-November 1976

Approved for public release; distribution unlimited

AIR FORCE FLIGHT DYNAMICS LABORATORY
AIR FORCE WRIGHT AERONAUTICAL LABORATORIES
AIR FORCE SYSTEMS COMMAND
WRIGHT-PATTERSON AIR FORCE BASE, OHIO 45433

NOTICE

When Government drawings, specifications, or other data are used for any purpose other than in connection with a definitely related Government procurement operation, the United States Government thereby incurs no responsibility, nor any obligation whatsoever; and the fact that the Government may have formulated, furnished, or in any way supplied the said drawings, specifications, or other data, is not to be regarded by implication or otherwise as in any manner licensing the holder or any other person or corporation, or conveying any rights or permission to manufacture, use, or sell any patented invention that may in any way be related thereto.

This report has been reviewed by the Information Office (OI) and is releasable to the National Technical Information Service (NTIS). At NTIS, it will be available to the general public, including foreign nations.

This technical report has been reviewed and is approved for publication.

LT. LARRY G. MOOSMAN
Project Manager
Improved Windshield Protection ADPO
Vehicle Equipment Division

ROBERT E. WITTMAN
Program Manager
Improved Windshield Protection ADPO
Vehicle Equipment Division

FOR THE COMMANDER:

AMBROSE B. NUTT
Director
Vehicle Equipment Division

Copies of this report should not be returned unless return is required by security considerations, contractual obligations, or notice on a specific document.

AIR FORCE/56780/18 April 1978 — 150

UNCLASSIFIED

SECURITY CLASSIFICATION OF THIS PAGE (When Data Entered)

REPORT DOCUMENTATION PAGE	READ INSTRUCTIONS BEFORE COMPLETING FORM
1. REPORT NUMBER: AFFDL-TR-76-156	2. GOVT ACCESSION NO. / 3. RECIPIENT'S CATALOG NUMBER
4. TITLE (and Subtitle): DAMPING, STATIC, DYNAMIC, AND IMPACT CHARACTERISTICS OF LAMINATED BEAMS TYPICAL OF WINDSHIELD CONSTRUCTION.	5. TYPE OF REPORT & PERIOD COVERED: Final Report, Jul 75 - Nov 76
	6. PERFORMING ORG. REPORT NUMBER: MDC-J6944
7. AUTHOR(s): G. F. Rhodes	8. CONTRACT OR GRANT NUMBER(s): F33615-75-C-3105
9. PERFORMING ORGANIZATION NAME AND ADDRESS: Douglas Aircraft Company, McDonnell Douglas Corporation, Long Beach, California 90846	10. PROGRAM ELEMENT, PROJECT, TASK AREA & WORK UNIT NUMBERS: Project: 2202, Task: 02, Work Unit: 01
11. CONTROLLING OFFICE NAME AND ADDRESS: Air Force Flight Dynamics Laboratory (AFFDL/FEW), Air Force Systems Command (AFSC), Wright-Patterson Air Force Base, Ohio 45433	12. REPORT DATE: Dec 1977; 13. NUMBER OF PAGES: 284
14. MONITORING AGENCY NAME & ADDRESS (if different from Controlling Office)	15. SECURITY CLASS. (of this report): Unclassified; 15a. DECLASSIFICATION DOWNGRADING SCHEDULE

16. DISTRIBUTION STATEMENT (of this Report)

Approved for Public Release, Distribution Unlimited.

17. DISTRIBUTION STATEMENT (of the abstract entered in Block 20, if different from Report)

63211F

18. SUPPLEMENTARY NOTES

19. KEY WORDS (Continue on reverse side if necessary and identify by block number)

Beam Analysis	Damping Response	Laminates
Beam Testing	Empirical Analysis	Material Characteristics
Composites	Interlayer Material	Plastic Materials
Thermal Effects	Impact Test	Static Loading
Damping Characteristics		

20. ABSTRACT (Continue on reverse side if necessary and identify by block number)

This eight section report contains the test plans, test results and analyses for a series of monolithic and laminated transparent beams which represent aircraft windshield segments.

A method of imbedding strain gages, mounting strain gages, and the application of thermocouples is described.

DD FORM 1 JAN 73 1473 EDITION OF 1 NOV 65 IS OBSOLETE
S/N 0102-014-6601

SECURITY CLASSIFICATION OF THIS PAGE (When Data Entered)

116 400

19. KEY WORDS (continued)

Transparencies
Windshield Design

20. ABSTRACT (Continued)

The method of data collection was assessed for data reduction that could provide stress-strain relationships. These relationships were used for the determination of energy transfer, dynamic response, and displacements due to applied loads. Selected portions of the test data were correlated with data output in a math model representation of test specimens noted in Section IX of AFFDL-TR-77-1.

Eleven cantilevered damping specimens were tested at various levels in order to study the damping characteristics for each ply of the laminate utilizing strain recordings. The strain responses were checked for accuracy with respect to theoretical strains calculated as a function of the applied loads.

Four beam specimens were subjected to static and dynamic load tests under hot, cold or ambient temperatures with either fixed or simply supported end constraints. Three of these beams were also subjected to impact loads at room temperature. These tests were conducted in order to study the strain distribution characteristics between plies of each laminate. A correlation of a theoretical static analysis with data from one test condition was documented in technical report AFFDL-TR-76-114. These correlations were made on the basis of strains, loads, displacements and time.

FOREWORD

This report is one of a series of reports that describes work being performed by Douglas Aircraft Company, McDonnell Douglas Corporation, 3855 Lakewood Boulevard, Long Beach, California 90846, under the Windshield Technology Demonstrator Program. This work was sponsored by the U. S. Air Force Flight Dynamics Laboratory, Wright-Patterson Air Force Base, Ohio, under Contract F33615-75-C-3105, Project 2202/1926.

Mr. D. C. Chapin, Capt., USAF Ret., was the Air Force Project Manager during the conceptual phase of the work reported herein. Lieutenant L. G. Moosman (AFFDL/FEW) succeeded Mr. Chapin during the conduct of the program.

Mr. J. H. Lawrence, Jr., was Program Director for the Douglas Aircraft Company. Mr. G. F. Rhodes, Structural Engineering, was the responsible engineer and author of this report.

The principal investigators and contributing authors were:

P. H. Denke - Structures - Advanced Methods and Research
G. R. Eide - Structures - Advanced Methods and Research
D. A. Hunt - Structures - Advanced Methods and Research
L. R. Islander - Project Manager - Testing and Instrumentation
L. P. Koegeboehn - Environmental Engineering
J. H. Lawrence - Structures - Design
R. H. Magnusson - Structures - Stress

The authors wish to thank the many individuals in the commercial and military aircraft manufacturing industry, the glass and windshield manufacturers, and the commercial airlines for their excellent cooperation in sharing their experiences during the conduct of this work.

The authors are grateful to the Douglas secretaries for the layout and typing of the report in a timely manner.

This report was first submitted to the Air Force in November 1976 and the time period covered by this report was from July 1975 through November 1976.

CONTENTS

CONTENTS (Continued)

CONTENTS (Continued)

CONTENTS (Continued)

ILLUSTRATIONS

ILLUSTRATIONS (Continued)

ILLUSTRATIONS (Continued)

ILLUSTRATIONS (Continued)

ILLUSTRATIONS (Continued)

TABLES

TABLES (Continued)

LIST OF ABBREVIATIONS, ACRONYMS AND SYMBOLS*

A	Area
a	constant
AB	Aluminum Bushings
B	Beam width
b	Strip width of beam
C	Damping matrix
c	Distance from neutral axis to outer fiber
C_A	Damping matrix for air
c_A	An air damping constant
C_{A1}	Unit value of the air damping constant (c_A)
CASD	Computer Aided Structural Design
c_C	Critical damping coefficient
C_I	Damping matrix for interlayer
CIP	Cast In Place
c_V	Viscous damping factor
$\mathbb{\ell}$	Center Line
cps	Cycles per second
C_S	Damping matrix for structural plies
D	Dynamic
DR	Double Row of bolts
E	Modulus of elasticity
EI	Beam flexural rigidity
F_a	Allowable stress
FB	Fixed-base (cannot slide)
f	Stress
f_b	Bending stress
F_d	Damping force

*All subscripted symbols are not listed. Subscripts shown only for those symbols where clarity on the meaning is required.

f_d	Damped frequency
F_N	Normal force
f_n	Natural frequency
fps	Feet per second
f_s	Shear stress
f_t	Tensile stress
G	Shear Modulus
g	Gravity constant (386.1 inches per sec^2)
GF	Gage factor
H	Drop weight height
h	Damping to stiffness ratio
h_I	Interlayer material damping to stiffness ratio
h_S	Structural ply material damping to stiffness ratio
I	Moment of Inertia
K	Stiffness coefficient matrix
k	Stiffness coefficient
L	Beam length between supports
ℓ	L/6 (34-inch/6, Section V)
L'	Total beam length
LVDT	Linear Voltage Differential Transducer
M	Mass matrix
M	Bending moment
m	Mass
ms	Milli-seconds
N	Number of active legs in a bridge
n	Number of cycles
P	Load
p	First good rebound peak number, and subscript
PC	Polycarbonate
P/N	Part Number

Q	Fixity factor
q	Any peak number after the p-number at 1/2 cycles, and subscript
R	Reaction load
r	Constant
R_c	Calibration resistance
R_g	Strain gage resistance
RT	Room temperature
$\dot{\bar{R}}$	Strain Rate
S	Static
SB	Soft Elastic bushings
SG	Strain Gage
SR	Single Row of bolts
SS	Simple Supported edges
Sym	Symmetrical
T	Transformation matrix
T	*Temperature*
t	Time
t_i	Thickness (i = 1, 2, 3, . . .)
$t_{p,q}$	Time occurrance of the $p^{\underline{th}}$ or $q^{\underline{th}}$ peak amplitude
t*	Calculated time required for a 92% decay in amplitude
V	Shear load
v	Velocity
W	Weight for bullet-shaped drop weight
w	Uniform beam weight
W/S	Windshield
x	Horizontal distance from origin
y	Vertical variable dimension

Greek Symbols

β	Direction of applied load
γ	Damping Ratio
Δ	Column of matrix displacements
Δ_m	Column of matrix maximum displacements
δ	Deflection or displacement
δ_1	First rebound deflection
δ_L	Full-cycle logarithmic decrement
δ_{Lpq}	Half-cycle logarithmic decrement
δ_0	Initial end displacement of cantilevered beam
ε	Strain
ε_a	Allowable strain
θ	Slope of beam end
μ	Micro
ν	Poisson's Ratio
π	Constant (3.14159)
ρ	Density
Σ	Summation
ϕ	Phase angle
χ	Vibrating cantilevered beam tip displacement
X	Constant
ψ	Shear strain
ω_d	Damped frequency ($2 \pi f_d$)
ω_n	Natural frequency ($2 \pi f_n$)
Ω	Resistance

Superscripts

$\dot{}$	Velocity
$\ddot{}$	Acceleration
-	Transformed
T	Transposed matrix

Mathematical Symbols

$< >$	MacCauley's brackets used with step or ramp functions
$\propto$	Proportional to
e	Natural Logarithm base (2.71828 . . .)

SECTION I
INTRODUCTION

This report covers the test directions, instrumentation studies and development, results and analyses for laminated transparent beam specimens, representing aircraft windshield constructions, subjected to damping, static/dynamic, and impact tests. Strain gages and thermocouples, at specified locations, were bonded to the beam laminated structural plies to monitor the strains and temperatures through the beam sections. The beam specimens were tested at temperatures that were representative of a B-1 type aircraft windshield in a flight regime representative during a bird strike environment. It is believed that the tests conducted were unique and that comparable tests have not previously been accomplished.

Included in this report is a matrix analysis method for the determination of damping factors, and the correlation of beam strain response with theoretical analysis. Recommendations for further studies and testing are also contained within this report. Following are brief descriptions for Sections II through VIII.

Within Section II is a description of the test specimens, conditions, and objectives of the damping, static/dynamic, and impact tests. The damping tests provided the strain data for determining the damping characteristics of windshield materials. The static/dynamic beam tests provided data for determining the strain characteristics of beam laminates under various loads, with various edge restraints and under a variety of temperatures. The impact beam tests provided high-strain-rate data obtained by dropping a 60-pound weight from heights ranging from eleven to twenty feet. Also described, are the testing apparatus, the method used for loading and environmental temperature control, data acquisition means, and test procedures.

Test/analysis techniques to extract material damping factors from the strain response of vibrating cantilevered multi-layered laminated beams were developed to provide both structural ply and interlayer material stiffness/damping ratio values for various temperatures. The values were needed to permit realistic analytical calculations of structural responses from bird impacted laminated windshields. The instrumentation of the static/dynamic, and impact beams tests was unique in that strain gages were embedded in the laminated interlayer, and mounted directly on the structural ply surface. Each structural ply had its strain gages mounted back-to-back to allow for proper construction of the multi-strain diagrams within the structural plies.

Within Section III, a historical review of successful strain gage and thermocouple installations and procedures is presented. This section includes discussions of strain gages, surface preparation, strain-gage cements, system protection, and the best places for locating strain gages in laminates used for static/dynamic tests. This section also presents the general notes and related figures from Douglas detail drawings which are noted in Appendix A.

Sections IV, V, and VI present the test results and analysis for the damping, static/dynamic, and impact beam specimens, respectively.

Within Section IV, the actual dimensions for the damping beam specimens and test temperatures are provided. The development of the damping ratio equation and a sample calculation are also provided. The average damping ratios for the laminated beam are compared with temperature changes. The time-to-dampen data is also presented and compared.

Within Section V the static/dynamic beam specimens actual test temperatures are described. The practice of presenting "raw" strain test data in the form of strain diagrams is also described. By displaying the data in the form of strain diagrams, instead of stress diagrams,

logical strain distribution between structural plies can easily be assessed. Distorted diagrams that may evolve from stresses beyond the elastic limits does not affect the strain diagram as explained in Section V. The load versus strain curves for the test beams are investigated and also the effect of the edge restraints and temperature on strain distributions. The spring stiffness, damping characteristics, correlations between test strain data and simplified computer analyses, and an interlayer energy transfer analysis are also contained.

Within Section VI, the impact beam specimens strain distributions, strain rates, and beam failure modes are presented. Strain rates in the order of 10 inches per inch per second and strains above 30,000 μ in./in. were recorded.

Section VII provides a matrix analysis method for the determination of the laminated materials damping factors, and correlation of a damping beam and a static loaded beam strain responses with theoretical analyses. Close correlation between test and analysis was obtained. These correlations were made during the early development of the "Bird Impact Math Model" program, Reference 1. The math model is a computer program utilizing finite elements for calculating the transient dynamic responses of a windshield and its supporting structure to a bird impact. A complete description of the math model is given in Reference 1.

Conclusions and recommendations are provided in Section VIII for the three major types of testing. The objectives of these damping, static/dynamic, and impact beam test are reiterated.

The experience obtained during these tests provided Douglas with the instrumentation methods required to participate in a series of bird impact tests conducted at the USAF Arnold Engineering Development Center (AEDC).

SECTION II
TEST DIRECTION

The purpose of this section of the report is to present the test direction describing objectives, specimens, conditions, set-up, and procedure for a series of damping, static/dynamic and impact tests. The series of tests are illustrated in Figure 1.

TEST OBJECTIVES

The prime objectives of this series of tests were to determine beam damping characteristics, static/dynamic responses and impact responses for representative transparency laminated materials in the form of uniform straight beam sections.

In an endeavor to provide meaningful data each specimen was instrumented with strain gages, transducers or accelerometers, and, when required, thermocouples. The specimens were tested with various edge constraints under low, room and high temperature conditions.

Damping Beam Test Objective

The objective of this series of tests was to compile test data related to various transparency materials from which certain damping parameters were calculated.

The damping ratios were considered as basic material properties requirements for application to a bird impact math model (see Reference 1).

Static/Dynamic Beam Test Objective

The primary objective of this series of tests was to quantiatively evaluate the strain distribution due to load transfer between plies of various laminated transparency materials when subjected to varying load conditions, edge restraints and temperatures.

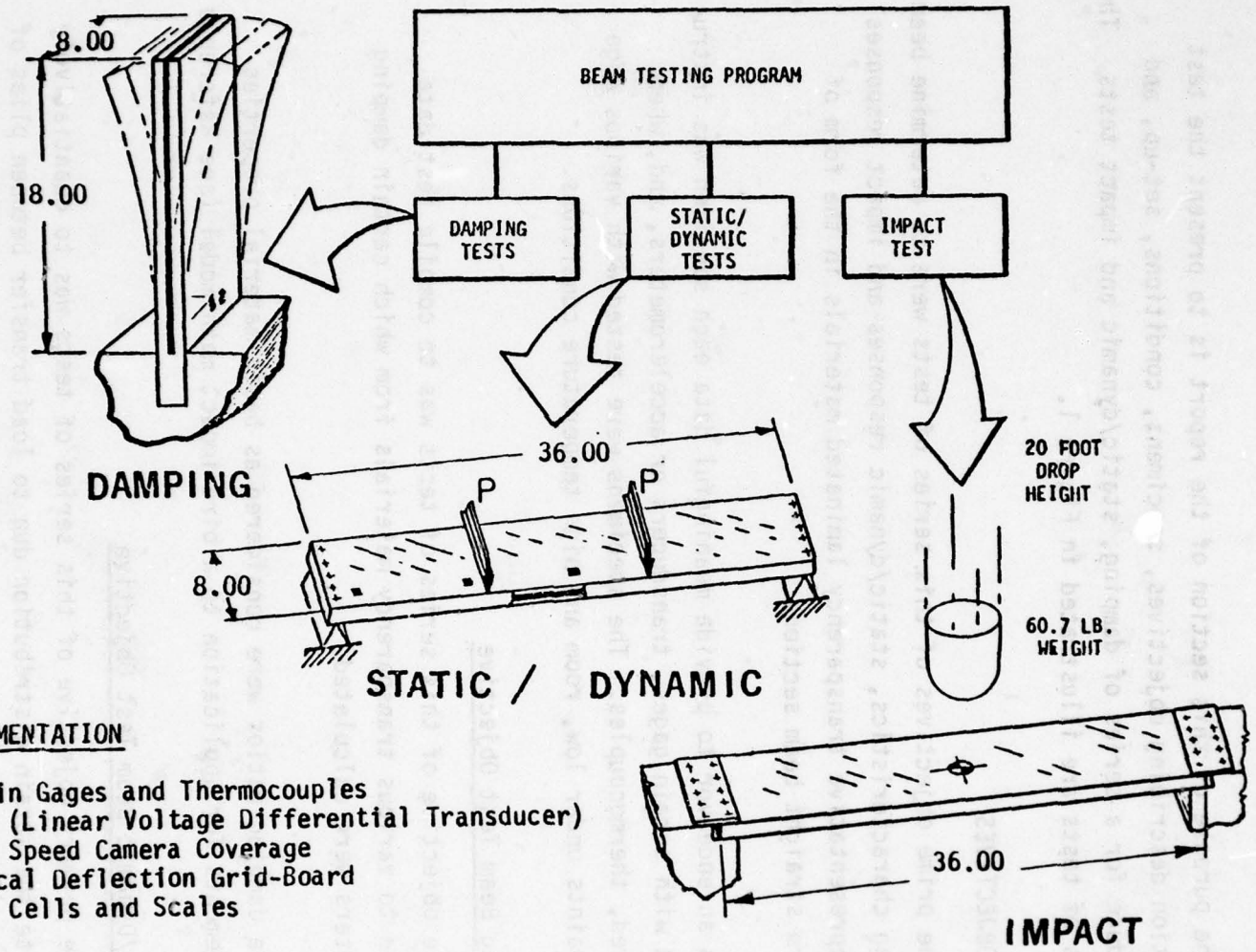

INSTRUMENTATION

- Strain Gages and Thermocouples
- LVDT (Linear Voltage Differential Transducer)
- High Speed Camera Coverage
- Optical Deflection Grid-Board
- Load Cells and Scales

Figure 1. Instrumented transparent beam testing.

Each surface of the laminate, internal and external, was instrumented with strain gages at three locations. The strains were measured and recorded. These strain responses were used for substantiating values predicted by mathematical analyses. Other parameters that were also recorded included the beam vibration frequencies, damping ratios and the effects of testing on the edge attachments.

The term "Static/Dynamic and Impact Beam" is used interchangeably with the term "36-inch beam" in this report.

Impact Beam Test Objectives

Selectively, some of the 36-inch laminated beams were subjected to impact testing to ascertain the strain rates of the materials under impact for subsequent comparisons to actual instrumented bird impact tests on canopies or windshields. The strain rates for bird impacted transparencies is believed to be in the range of 30 to 200 inch/inch/second. Equally important, was to determine the feasibility of compiling strain gage data during the fracture of each specimen.

This test data were made available for a math model application for data correlation; several math model applications are shown in Section VII.

TEST SPECIMEN DESCRIPTIONS

For this test program, there were eleven 20-inch length damping beam specimens and four 36-inch length beams used for the static/dynamic and impact tests.

Damping Beam Specimens

The damping beam specimens were eight inches wide by twenty inches long. In Figure 2, a typical damping beam is shown rigged in the test fixture.

The materials used in the construction of these damping beams are shown in Table 1.

Specimen Number 12 was a thin monolithic polycarbonate beam to compare with Specimens 7A and 7B which were thicker monolithic polycarbonate beams.

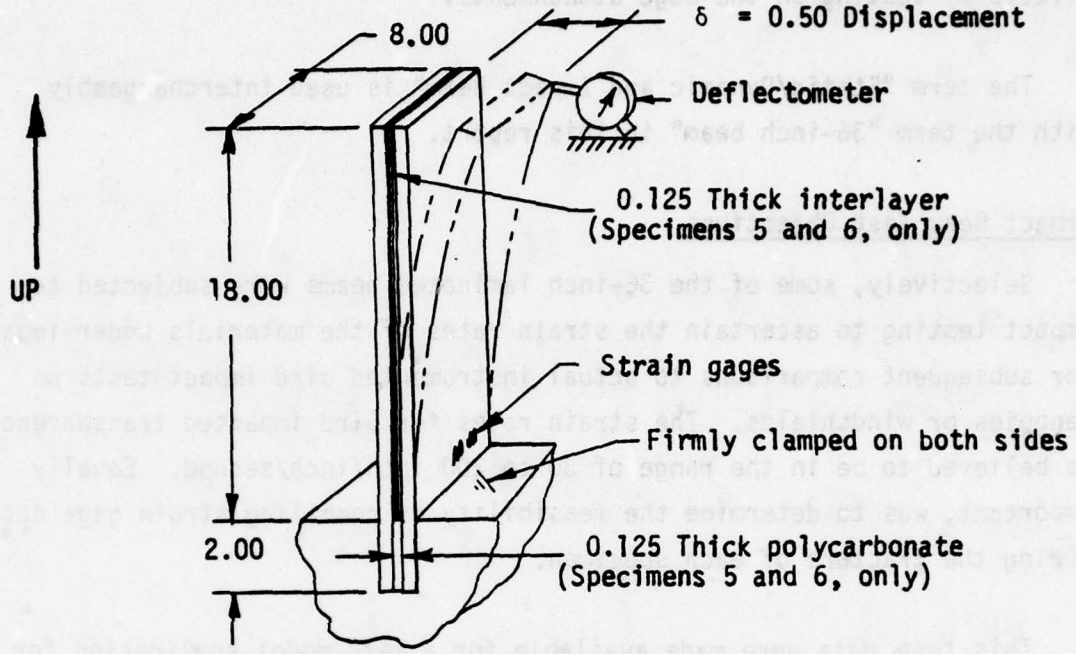

Figure 2. Typical damping beam test specimen set-up.

Static/Dynamic and Impact Beam Test Specimens

The 36-inch length beams were eight inches wide consisting of the laminated materials as noted in Table 2.

The lamination construction and the edge attachment design is illustrated in Figures 3 and 4.

TABLE 1. DAMPING BEAM SPECIMENS DESCRIPTION

SPECIMEN NO.	PLY THICKNESS (INCHES)	MONOLITHIC OR LAMINATE MATERIAL DESCRIPTION	NOTES	DRAWING NO. CONFIGURATION
5	0.250 0.125 0.250	Polycarbonate PPG 112 interlayer Polycarbonate	1 1	Z5942629 -1
6	0.250 0.125 0.250	Polycarbonate CIP Polycarbonate	1 2 1	Z5942629 -501
7A	0.625	Polycarbonate	1	Z5942629 -503(PPG)
7B	0.625	Polycarbonate	1	Z5942629 -503(Sierracin)
8	0.250	Aluminum	3	Z5942629 -505
9A 9B	0.625 0.625	Glass Glass	4	Z5942629 -507
9C	0.250	Glass	4	Z5942629 -509
10	0.625	Acrylic	5	Z5942629 -511
11	(Not Used)			
12	0.250	Polycarbonate	1	Z5942629 -513

Notes:
1. Polycarbonate per MIL-P-83310.
2. CIP= Sierracin S-100 Cast-in-place.
3. Aluminum alloy plate, 7075-T6, bare per QQ-A-250/12.
4. Fully tempered soda-lime glass per MIL-G-25667, Type I, Class A.
5. Stretched acrylic per MIL-P-25690.

TABLE 2. THIRTY-SIX INCH BEAM SPECIMENS DESCRIPTIONS

SPECIMEN NO.	LAMINATE THICKNESS (INCH) AND MATERIAL DESCRIPTION	NOTES	DRAWING CONFIGURATION
1	0.125 Glass 0.250 CIP 0.87 Polycarbonate	1 2 3	Z5942626-1
2	0.125 Glass 0.250 CIP 0.87 Polycarbonate 0.120 CIP 0.150 Polycarbonate	1 2 3 2 3	Z5942626-501
3	0.25 Acrylic 0.06 PPG 112 Interlayer 0.188 Polycarbonate	4 3	Z5942626-503
4	0.25 Acrylic 0.06 PPG 112 Interlayer 0.188 Polycarbonate 0.060 PPG 112 Interlayer 0.188 Polycarbonate 0.060 PPG 112 Interlayer 0.080 Acrylic	4 3 3 4	Z5942626-505

Notes:
1. Chemically strengthened glass per MIL-G-25667 Type V, Class A.
2. CIP = Sierracin S-100 Cast-in-place silicone interlayer.
3. Polycarbonate per MIL-P-83310, prior to fusion bonding.
4. Acrylic per MIL-P-8184.

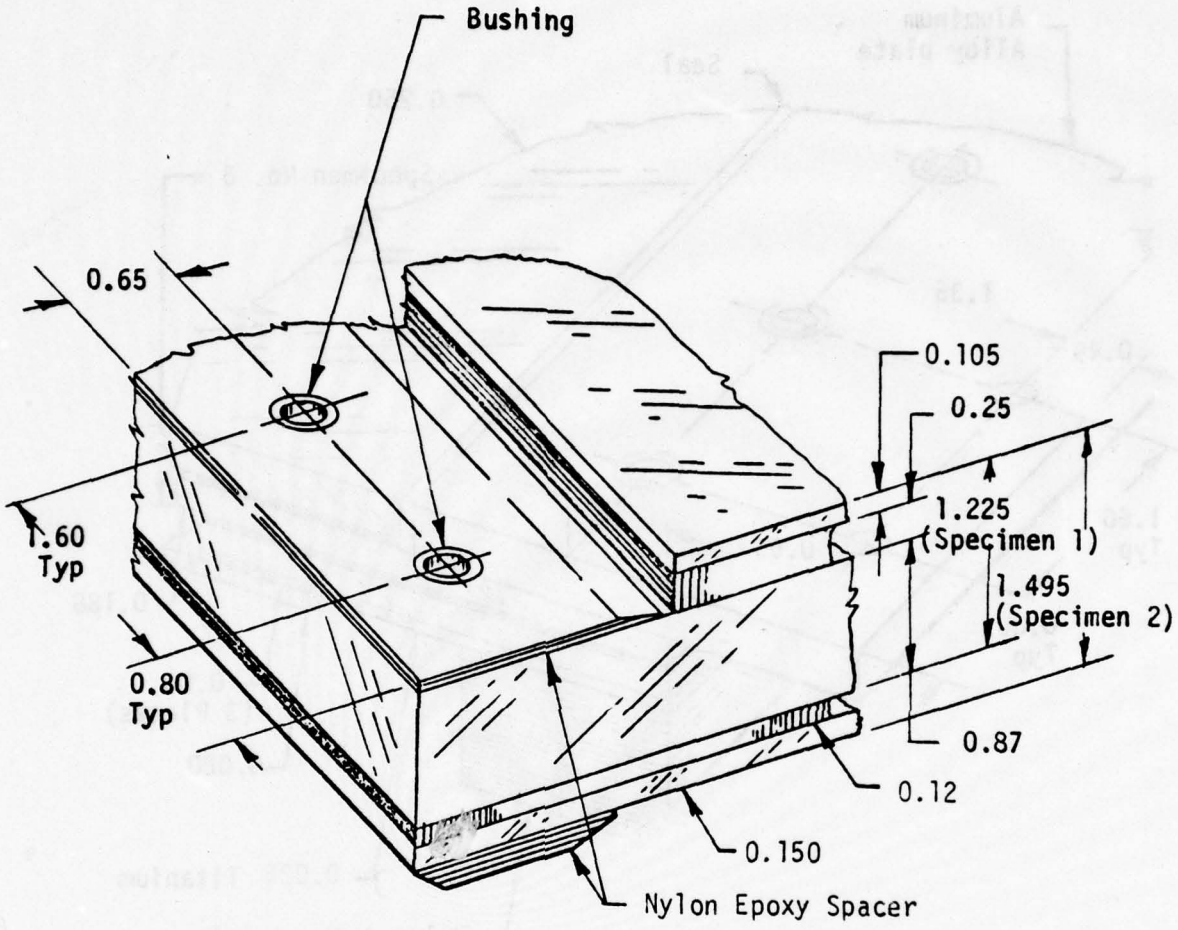

- o See Table 2 for material description.
- o Sierracin fabricated.
- o Specimen 2 shown.
- o Edge designs for specimen 1 and 2.
- o Specimen 1 has only three plies: 0.105" glass face ply, 0.25" silicone interlayer and 0.87 P.C. ply.

Figure 3. Glass-faced transparency laminate with thick polycarbonate (fusion bonded) core.

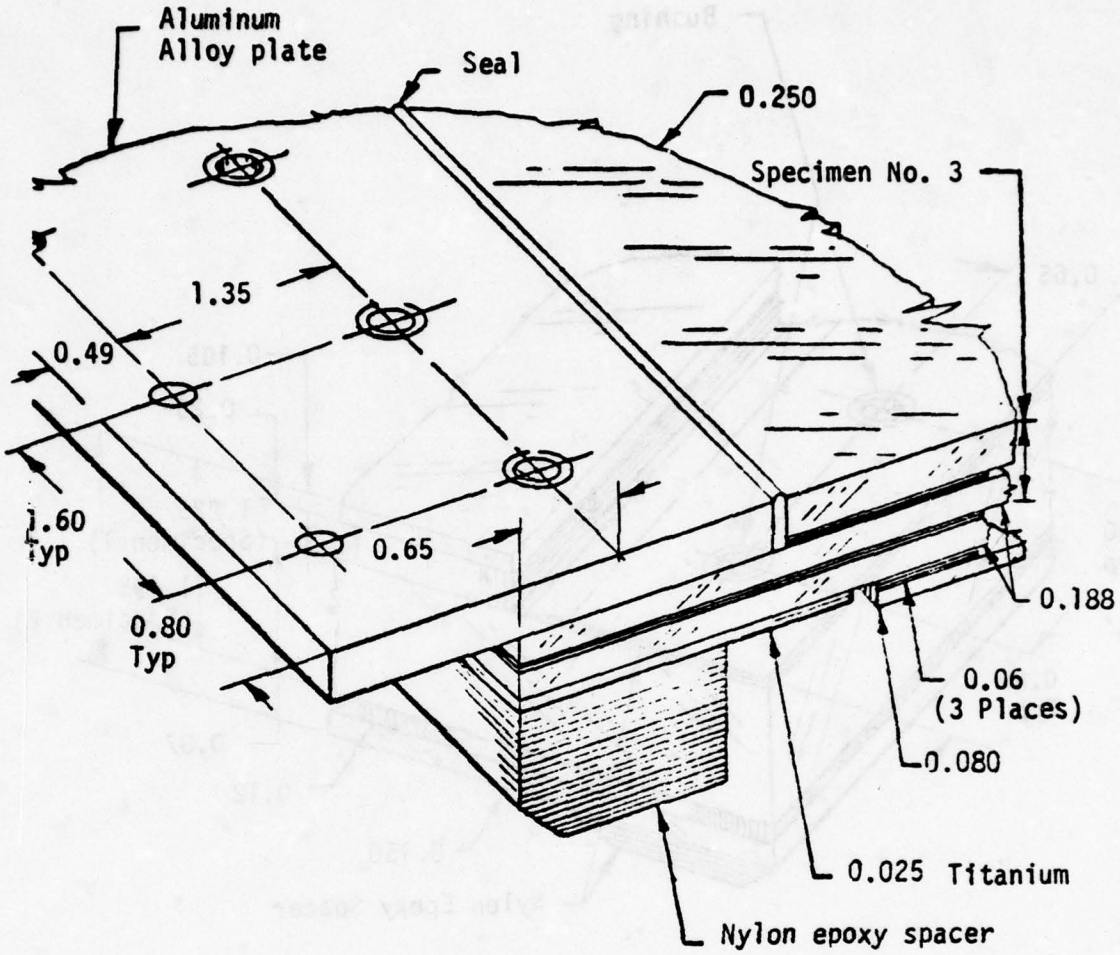

- o See Table 2 for material description
- o PPG Fabricated
- o Specimen 4 shown
- o Specimen 3 only has one upper 0.25 acrylic ply and one lower 0.188 polycarbonate ply with 0.06 PPG 112 interlayer

SPECIMENS 3 AND 4 END VIEW

Figure 4. Acrylic-faced transparency laminate with polycarbonate plies.

These four specimens were utilized in the static/dynamic tests and subsequently, three were used for impact tests.

TEST CONDITIONS

In general, each test specimen was subjected to different temperature conditions, edge restraint and modes of loading. Subsequent paragraphs describe the details for these test conditions.

It must be pointed out that during the testing program specimen shipments from various vendors were oftentimes delayed, and during the program additional testing was deemed necessary. Consequently, the sequence of test conditions was in order, but the grouping of specimens was not. For purposes of clarity, however, this report groups the types of specimens per type of test.

Damping Beam Test Conditions

In turn, each specimen base end was firmly clamped into the test fixture as shown in Figure 2. After the test specimen had stabilized at its test temperature, and with the environmental temperature control chamber removed, the cantilevered beam end was quickly displaced approximately one-half inch and released. The oscillating strain wave (near beam base) versus time was recorded on an oscillograph. Later, this data was analyzed to determine the beam's damping properties as described in detail in Section IV.

Table 3 depicts the test condition number and temperature requirements related to each specimen.

Temperature Conditions

Three temperature conditions were used for the damping beam tests. Each temperature condition had a tolerance of $\pm$ 10°F. The temperatures selected were low (-35°F), room temperature (75°F) and high (195°F).

TABLE 3. DAMPING BEAM TEST CONDITIONS

TEST CONDITION NO.	SPECIMEN NO.	DRAWING CONFIGURATION	TEMPERATURE GOALS (°F)
1 2 3	5	Z5942629-1	-35 RT 195
4 5 6	6	Z5942629-501	-35 RT 195
7a 8a 9a	7A	Z5942629-503 (PPG)	-35 RT 195
7b 8b 9b	7B	Z5942629-503 (Sierracin)	-35 RT 195
11a 11b	8	Z5942629-505	RT
89a.1 89a.2 89a.3 89a.4 89a.5 89a.6	9A	Z5942629-507	RT
89b.1 89b.2 89b.3	9B	Z5942629-507	RT
90 91 92	10	Z5942629-511	RT -35 200
97 101 103	12	Z5942629-513	RT -35 195
110	9C	Z5942629-509	RT

RT denotes room temperature.

Section IV of this report contains a further discussion of Environmental Temperature Conditions for the damping beams.

Load Conditions

A load was applied to the end of each damping beam specimen sufficient to cause a 1/2-inch displacement of the beam-end from its neutral position; then the load was released.

Static/Dynamic Beam Test Conditions

Each of the four 36-inch beams were subjected to a series of static and dynamic tests. The edge constraints were varied between one-row and a double-row of attachments utilizing simply supported conditions for comparison purposes. Each beam was loaded at two places and under each test condition the temperature was varied between -65°F and 272°F.

Table 4 lists the test condition number related to each specimen, temperatures, edge conditions, and allowable stress for any structural ply. Table 5 identifies the edge conditions and code identification noted in Table 4. These edge conditions are illustrated in Figure 5.

Temperature Conditions

Three temperature conditions were used for the 36-inch beam tests. Each temperature condition had a tolerance of $\pm$ 10°F. The temperatures selected were low (-65°F), room temperature (+75°F) and high temperature (272°F). For each case, the lower surface of each specimen was exposed to a 75°F environment. This temperature was measured six inches below each specimen. The static/dynamic specimen temperature profile requirements are described in Section V which includes a plot of the resulting test temperature gradient through the specimens.

The external temperatures noted in Table 4 refers to test chamber temperatures.

TABLE 4. STATIC/DYNAMIC BEAM TEST CONDITIONS

TEST COND. NO.	SPECIMEN NO.	DRAWING CONFIGURATION (See Table 1)	TEST CONDITION		
			CHAMBER TEMPERATURE (°F)	ALLOWABLE STRESS (psi)	EDGE CONDITION IDENTIFICATION (See Table 5)
13 14	2	Z5942626-501	-65	5200	SR/SS-PIV.
15 16			RT	4960	
17 18			272	3200	
19 20	2	Z5942626-501	-65	5200	SR/SB
21 22			RT	4960	
23 24			272	3200	
25 26	2	Z5942626-501	272	3200	DR/SB
27 28			RT	4960	
30 31			-65	5200	
29S 29D	2	Z5942626-501	RT	4960	DR/FB
32 33	4	Z5942626-505	-65	5200	SR/SS-PIV.
34 35			RT	4960	
36 37			200	3200	
38 39	4	Z5942626-505	-65	5200	SR/SB
40 41			RT	4960	
42 43			200	3200	
44 45	4	Z5942626-505	200	3200	DR/SB
46 47			RT	4960	
49 50			-65	5200	

NOTE: 1. The test data from Test Condition No. 15 was used to correlate theoretical dynamic analyses with test results.

2. The test data from Test Condition No. 27 was used to correlate theoretical static analyses with test results.

TABLE 4. (Continued)

TEST COND. NO.	SPECIMEN NO.	DRAWING CONFIGURATION (See Table 1)	TEST CONDITION		
			CHAMBER TEMPERATURE (°F)	ALLOWABLE STRESS (psi)	EDGE CONDITION IDENTIFICATION (See Table 5)
48S 49D	4	Z5942626-505	RT	3200	DR/FB
51 52	1	Z5942626-1	-65	5200	SR/SB
53 54			RT	4960	
55 56			272	3200	
57 58	1	Z5942626-1	272	3200	DR/FB
59 60			RT	4960	
61 62			-65	5200	
63 64	2	Z5942626-501	-65	5200	SR/FB-S
65 66			RT	4960	
67 68			272	3200	
69 70	3	Z5942626-503	-65	5200	SR/SB
71 72			RT	4960	
73 74			272	3200	
75 76	3	Z5942626-503	272	3200	DR/SB
77 78			RT	4960	
79 80			-65	5200	
81 82	4	Z5942626-505	-65	5200	SR/FB-S
83 84			RT	4960	
85 86			200	3200	
107A	2	Z5942626-501	RT	4960	/SS
107B	2	Z5942626-501	RT	4960	/SS-B

NOTE: 3. Static tests only were accomplished under Test Condition 107A and 107B.

TABLE 5. EDGE CONDITION - CODE IDENTIFICATION

CONDITION	CODE IDENTIFICATION
Double row attachments - both ends fixed - aluminum bushings-tight holes.	DR/FB
Double row attachments - one end fixed - one end attached to a sliding base - aluminum bushings - tight holes.	DR/SB
Single row attachments - both ends fixed - aluminum bushings-tight holes.	SR/FB
Single row attachments - both ends fixed - sealant - loose holes.	SR/FB-S
Single row attachments - one end fixed - one end attached to a sliding base - aluminum bushings - tight holes.	SR/SB
Single row attachments - both ends free to pivot - on simple supports - aluminum bushings - tight holes.	SR/SS-PIV
No attachments - simple supported - no bushings - open holes	/SS
No attachments - simply supported - aluminum bushings-open holes.	/SS-B

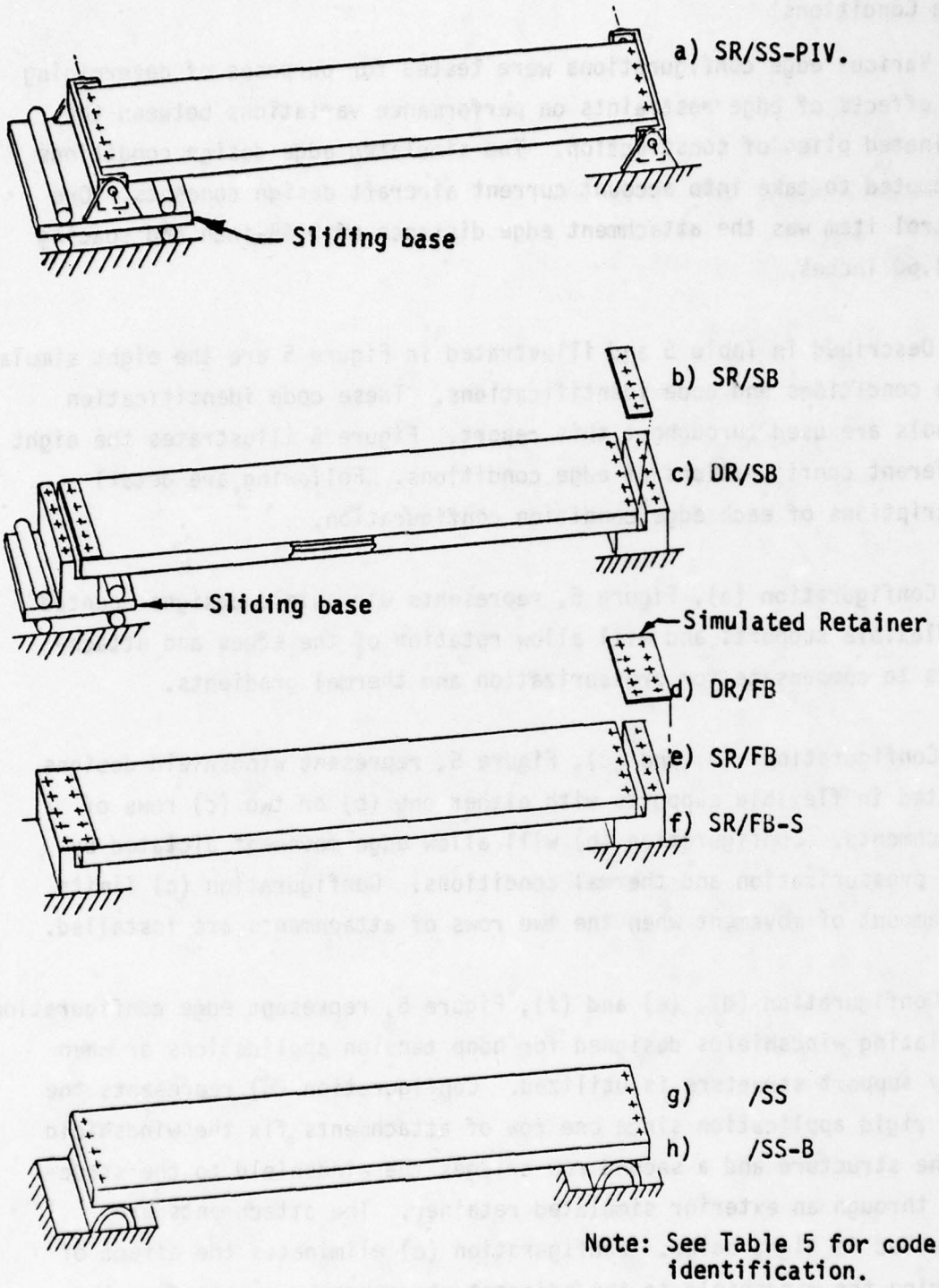

Figure 5. Static/Dynamic beam edge conditions.

Edge Conditions

Various edge configurations were tested for purposes of determining the effects of edge restraints on performance variations between the laminated plies of construction. The simulated edge design conditions attempted to take into account current aircraft design concepts. One control item was the attachment edge distance of 0.65-inch and spacing of 1.60 inches.

Described in Table 5 and illustrated in Figure 5 are the eight simulated edge conditions and code identifications. These code identification symbols are used throughout this report. Figure 5 illustrates the eight different configurations of edge conditions. Following are detail descriptions of each edge condition configuration.

Configuration (a), Figure 5, represents windshield designs mounted in flexible supports and will allow rotation of the edges and attachments to compensate for pressurization and thermal gradients.

Configurations (b) and (c), Figure 5, represent windshield designs mounted in flexible supports with either one (b) or two (c) rows of attachments. Configuration (b) will allow edge movement dictated by both pressurization and thermal conditions. Configuration (c) limits the amount of movement when the two rows of attachments are installed.

Configuration (d), (e) and (f), Figure 5, represent edge configurations simulating windshields designed for hoop tension applications or when heavy support structure is utilized. Configuration (d) represents the most rigid application since one row of attachments fix the windshield to the structure and a second row bridges the windshield to the structure through an exterior simulated retainer. The attachments are installed in tight holes. Configuration (e) eliminates the effect of bridging the windshield to the adjacent structure by eliminating the row of attachments common to the retainer and structure, but the row of attachments in the windshield are installed in tight holes. Configuration

(f) is identical to Configuration (e), except that one row of attachments are installed in loose holes and a rubber grommet is installed to represent a normal aircraft installation utilizing wet sealant to fill the voids between the attachments and metal bushings.

Configuration (g), Figure 5, edge condition test data was necessary for analyses in the determination of interlayer shear-load transfer capability. The bushings were removed to allow the laminate to act under load similar to a leaf-spring.

Configuration (h), Figure 5, is similar to Configuration (g), Figure 5, except bushings were installed in the holes in an effort to determine the amount of inner structural ply restraint obtainable, thus, minimizing the leaf-spring effect.

The application of the single attachment row concept allows potential bolt bending under pressurization, thermal and impact conditions. The double-row attachment concept provides double-shear conditions for the bolts.

Figure 6 illustrates the concept for both the tight and loose attachments with simulated sealant filling the voids between the bolt and bushing. The spacers noted in Figure 6, under the NAS 1304 bolt head, were interchanged with the simulated retainer shown in Figure 5.

Load Conditions

Static loads were applied to the 36-inch beams that caused the beams' center to displace a maximum of 3 inches or reach a limiting strain allowable, whichever came first. The polycarbonate structural ply strain gages, as developed and noted in Section III, were monitored to determine which strain gage presented the highest strain level. That particular gage was further monitored to make sure the maximum allowable strain was not exceeded. The maximum allowable strain ε_a, was approximated by the following equation:

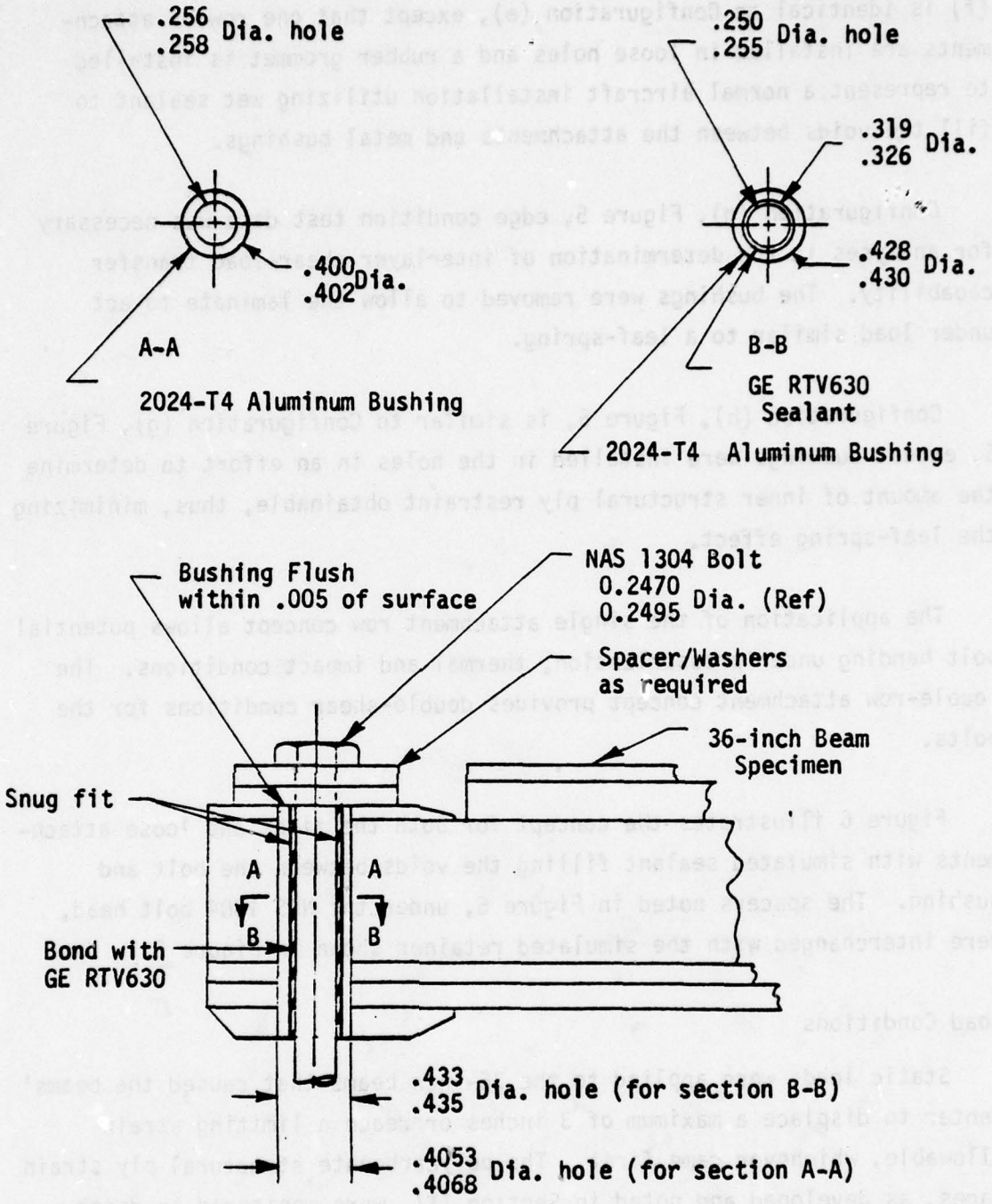

Figure 6. Edge attachment detail showing aluminum bushing and simulated sealant.

$$\varepsilon_a = \frac{F_a}{E} \qquad (1)$$

where

F_a = allowable stress as specified in Table 4.

E = 320,000 psi for polycarbonate material.
(Conservative for the 3 tested temperature ranges.)

Note that for clarity the more familiar allowable stress term was provided in Table 4 rather than the maximum allowable strain term.

The beams were statically loaded, as shown in Figure 7, to produce approximate beam center displacement levels of one-, two- and three-inches. After reaching the desired maximum center displacement, the beam was quickly released for the dynamic test. The oscillation curves of all strain gages versus time output was recorded. This data were made available for a math-model application for data correlation. Note that in Figure 7a, two ten-pound weights were secured to the beam specimen with tape. These weights served two purposes. First, the weights helped to properly distribute the loads across the beam width. Second, when the beam was released for the beam dynamic test, the weights tended to provide a constant bending moment section, although, the bending moment was further complicated by its uniform beam weight.

Impact Beam Test Conditions

Three of the 36-inch beams were utilized in the impact tests. These tests were performed at room temperature.

Listed in Table 6 are the test conditions, including the edge conditions and the height from which a 60.7 weight was dropped onto each specimen center.

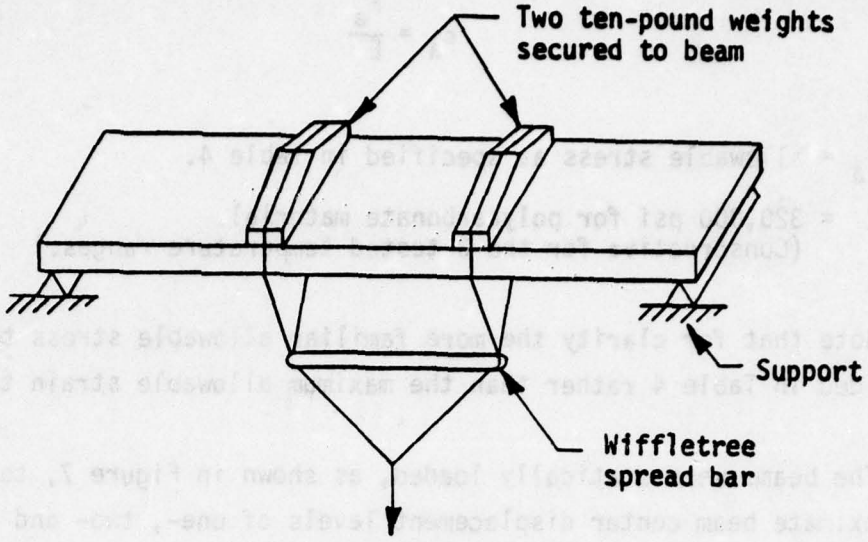

a) Beam specimen loading arrangement.

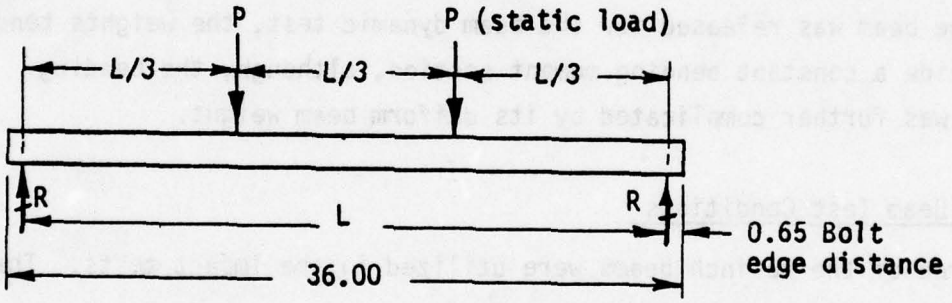

b) Beam loading diagram.

Figure 7. Static/Dynamic beam load definition.

Edge Conditions

As noted in Table 6 for Specimens Nos. 2 and 4, the edge conditions were those identified as Configuration (f) noted in Figure 5. This configuration utilizes one row of attachments installed in loose holes with simulated sealant that could represent the edge design for hoop tension applications.

TABLE 6. IMPACT BEAM TEST CONDITIONS

TEST CONDITION NO.	SPECIMEN NO.	DRAWING CONFIGURATION (see Table 1)	HEIGHT WEIGHT DROPPED (feet)	EDGE CONDITION IDENTIFICATION (see Table 5)
87	2	Z5942626-501	20	SR/FB-S
88	4	Z5942626-505	11	SR/FB-S
108	1	Z5942626-1	20	DR/SB

Specimen No. 1, as noted in Table 6, had edge conditions identified as Configuration (c) in Figure 5. This configuration utilizes two rows of attachments installed in tight holes that could represent the edge design of a windshield when mounted in flexible structure.

Load Conditions

For the three beams selected, a series of impact tests were established that would impose sufficient forces to fail each specimen.

Rather than design a special fixture, a bullet shaped 60.7-pound weight was found that could be utilized as a drop weight. Because of the difficulty in determining the impact load required to fail a laminated specimen comprised of various combinations of materials, an approximate height, H, was determined for a monolithic beam specimen.

To determine the approximate minimum drop height for material failure the following method of analysis, noted in Reference 2, Page 474, was used:

$$f_t = \sqrt{\frac{6WHEc^2}{LI}} \quad . \tag{2}$$

Rearranging eq. (2) to determine H, gives

$$H = \frac{f_t^2 \, LI}{6WEc^2} \quad . \tag{3}$$

The dynamic deflection of the beam (δ_D), is

$$\delta_D = \sqrt{2H\delta} \quad ; \tag{4}$$

from standard static deflection (δ) equations:

$$\delta \text{ (Simple support)} = \frac{WL^3}{48EI} \quad , \text{ and} \tag{5}$$

$$\delta \text{ (Fixed ends)} = \frac{WL^3}{192EI} \quad . \tag{6}$$

where

W = Bullet wt [lb.]

H = Drop height [in.]

E = Modulus of elasticity [PSI]

c = Outer fiber distance to [in.] neutral axis (Beam)

L = Beam length [in.]

I = Beam moment of inertia [in.^{4}]

f_t = Tensile stress [PSI]

B = Beam width [in.)

The rationale for using static equations for a dynamic condition follows from assuming that the total work done by a falling object is determined by total transformance of kinetic energy of the equivalent impact spring. By dividing the falling object weight by the spring constant, the equivalent static deflection term is introduced into the final equations.

Then, utilizing Section 4 for Condition No. 88, the following analysis was performed (assuming: $I = 2c^3B/3$), where

$W = 60.7$ lb.

$c = 0.443$ in.

$I = 0.464$ in.

$B = 8.00$ in.

$E = 320{,}000$ psi

$L = 36$ in.

$f_t = 9300$ psi

and utilizing the above equations:

$H = 63$ in. (from eq. 3)

$\delta = 7.11$ in. (simple supported) (from eq. 5)

$\delta = 3.55$ in. (fixed ends) (from eq. 6)

To ensure that Specimen 4 would fracture under the impact load, this calculated drop weight height was more than doubled. The test height selected was 11 feet. For the heavier specimens, 1 and 2, 20 feet was arbitrarily selected.

TEST SETUP

One test fixture, constructed from standard "erector set" beams, turnbuckles, tension rods, and pull-off fittings, was to be used for all tests. The setup for static, dynamic and drop tests is shown in Figure 8, and the damping test setup is shown in Figure 9.

Loading Methods

The damping test specimen loads are applied as shown in Figure 9. The specimen was installed between rigid supports bolted to the test fixture. The lateral applied load (P) deflected the specimen a given distance at which time the loading bracket was released, and the oscillation-damping characteristic was recorded.

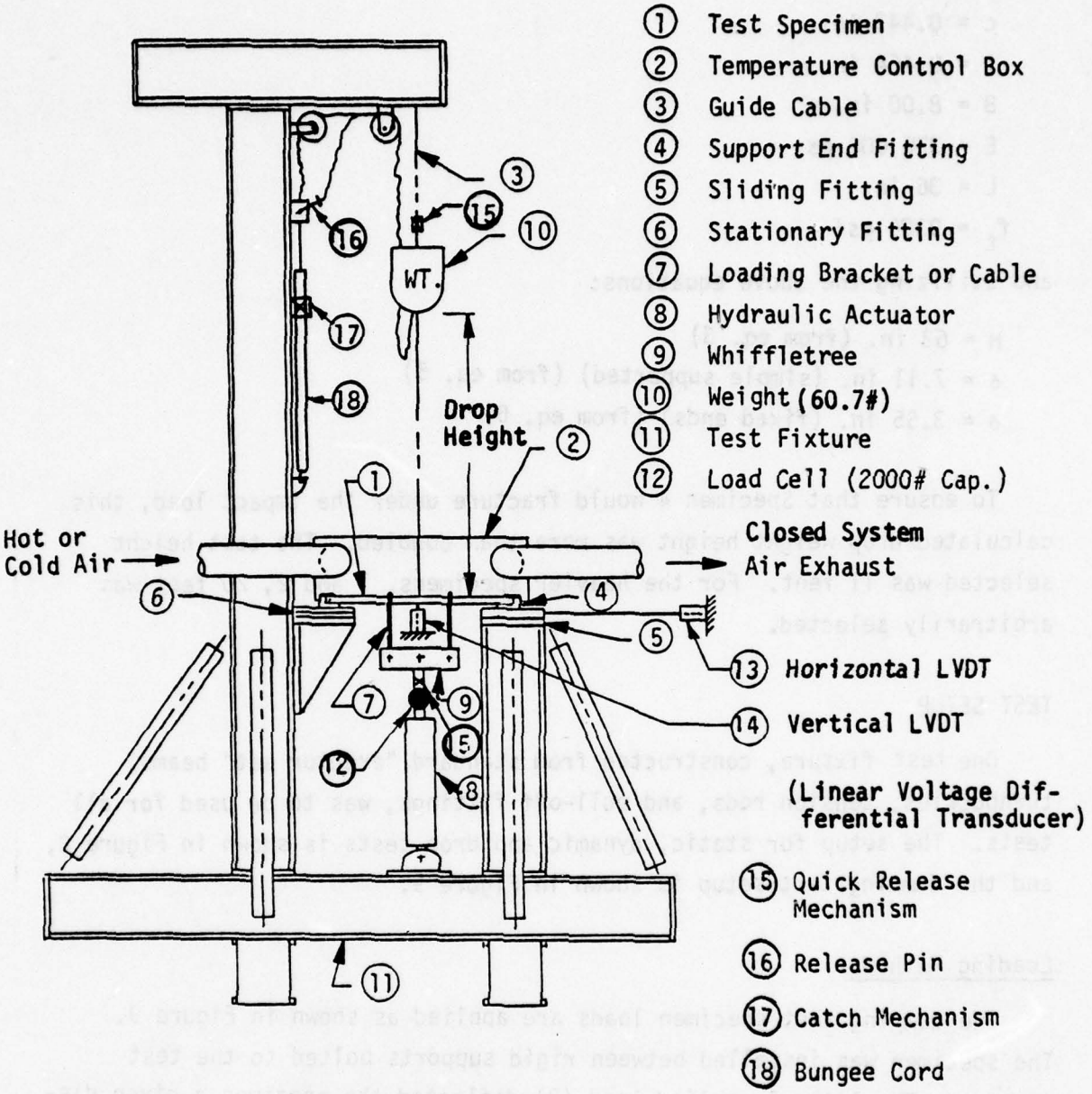

Figure 8. Test set-up.

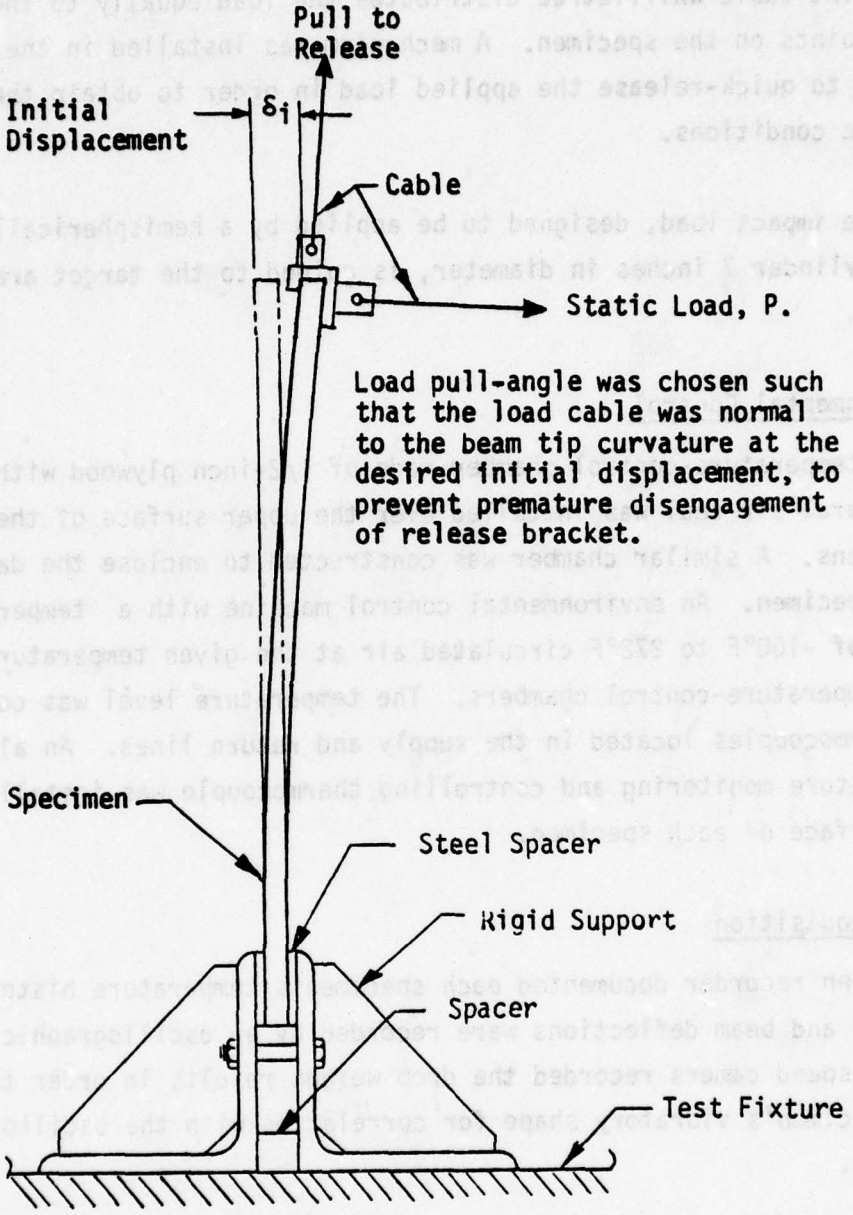

Note: Temperature control box was omitted in this view for clarity.

Figure 9 . Test setup for specimen damping.

The dynamic and static loads are applied by a hydraulic actuator mounted directly under the 36-inch beam specimen at mid-span. A two-point cable whiffletree distributes the load equally to the two load points on the specimen. A mechanism was installed in the loading system to quick-release the applied load in order to obtain the required dynamic conditions.

The impact load, designed to be applied by a hemispherically ended lead cylinder 7 inches in diameter, is guided to the target area by cables.

Environmental Control

A temperature-control chamber made of 1/2-inch plywood with a peripheral air seal was installed over the upper surface of the 36-inch specimens. A similar chamber was constructed to enclose the damping test specimen. An environmental control machine with a temperature range of -100°F to 272°F circulated air at the given temperature through the temperature-control chambers. The temperature level was controlled by thermocouples located in the supply and return lines. An alternate temperature monitoring and controlling thermocouple was installed on the surface of each specimen.

Data Acquisition

A pen recorder documented each specimen's temperature history. Loads, strains and beam deflections were recorded by an oscillographic recorder. A high-speed camera recorded the drop weight results in order to define the specimen's vibratory shape for correlation with the oscillograph records.

A test data sheet for each test condition is shown in Appendix B.

TEST PROCEDURES

The test procedure for each type of test is described in the following paragraphs.

Damping Test Procedure

The damping tests were permitted to be the first tests since these test specimens were available. The specimens were set up as shown in Figure 9. The procedural steps used were:

1. Verify specimen number, temperature, deflection, or load condition to be included in each specific test.
2. Notify the Instrumentation Group of test start time; start recorders.
3. Attach deflectometer extension cable to top end of specimen (typical).
4. Install environmental control chamber over specimen (if required).
5. Turn on hot or cold air machine and bring specimen to steady-state temperature gradient; hold this temperature for 6 minutes.
6. Remove environmental control chamber and shut off machine.
7. Position quick-release bracket to top edge of specimen (see Figure 9).
8. Check out the specimen instrumentation for proper operation and calibration-step at test temperature.
9. Apply load to deflect beam free end 1/2-inch from its relaxed (stress-free) position.
10. Record the load required.
11. Detach deflectometer extension cable at top end of specimen; note any change in load.
12. Increase strain chart recorder speed for free-vibrating beam test (approximately 16 inches per second chart speed).
13. Quickly release beam end.
14. Check recording for accuracy.

15. Examine specimen and instrumentation for damage.

16. Change over for next condition.

Note: Steps 6 through 13 took approximately 30 seconds.

Static/Dynamic Beam Test Procedure

Instrumented beams, Specimens 1 through 4, were set up in accordance with conditions listed in Table 4 and loads applied as described in the test load requirements. The static load, P, was applied in increments until the maximum stress, as specified in Table 4, was attained.

The specimen instrumentation was checked for proper operation and calibration at test temperature. Steady-state temperature was achieved before the test proceeded and precautions taken to limit the load time during the high-temperature test.

After reaching the maximum desired static load, the load quick-release mechanism was activated. This procedure provided the dynamic response data.

1. Verify specimen number, temperature, deflection, or load condition and end condition to be included in each specific test.
2. Notify the Instrumentation Group of test start time and turn on recorder.
3. Install environmental control chamber over specimen (if required).
4. Turn on hot or cold air machine and bring specimen to steady-state temperature gradient, hold this temperature for 6 minutes.
5. Preload hydraulic actuator to 50 pounds.
6. Shut off temperature control machine.
7. Remove environmental control chamber.
8. Calibrate each strain gage channel; observe and check recorded calibration steps.

9. Pump actuator to obtain desired load or deflection.
10. Obtain approval from engineering for all recordings.
11. Increase strain chart recorder speed for dynamic test (approximately 16 inches per second chart speed).
12. Actuate quick release mechanism.
13. Check recording for accuracy.
14. Examine specimen and instrumentation for damage.
15. Change over for next condition.

Note: Steps 7 through 12 took approximately 20 seconds

Impact Test Procedures

After completion of the static/dynamic beam tests, Specimens 1, 2 and 4 were set up for the drop test at room temperature. Figure 8 shows the test setup. The hydraulic actuator (8), whiffletree (9), cable (7), and hood (2) were removed for the impact tests (numbers in parentheses refer to parts shown in Figure 8). The following procedural steps were then applied:

1. Verify specimen number and edge condition.
2. Preload bungee cord and install release pin; check for proper arming of the drop weight catch mechanism.
3. Check the center alignment and conformation of the drop weight guide cables.
4. Raise the 60.7-pound drop weight to the designated height above the specimen upper surface.
5. Start recorders and check out each strain gage calibration stop.
6. Increase chart recorder speed to approximately 20 inches per second and actuate high-speed camera (for Specimen 2 only) and quick release drop weight mechanism.

7. Check chart recording of strain versus time for accuracy.

8. Change over for next condition.

SECTION III
TEST INSTRUMENTATION STUDIES AND DEVELOPMENT

A purpose for this series of tests was to develop instrumentation techniques for measuring the strains and damping characteristics of monolithic and laminated transparency materials under applied loads.

This section describes the rationale for the instrumentation selected, the development necessary to attach strain gages and thermocouples to transparency materials, the analysis to define strain gage optimum locations, and the equipment required for data documentation.

INSTRUMENTATION SELECTION

This series of tests utilized strain gages and thermocouples attached to various transparent materials. These materials included glass, acrylic, and polycarbonate.

Instruments considered to be standard are:

- o Linear Variable Differential Transformer (LVDT)
- o Deflectometers
- o Load Indicator Cells
- o Load Indicator Spring Scale
- o Recording Equipment.

Selection of Strain Gages

The selection of strain gages for application to the various beams in this series of tests had to be directed toward future applications to full size windshield systems that might be subjected to high strain response under the impact of four-pound birds at velocities up to 950 feet per second.

Additional constraints on the selection of the strain sensor systems were:

- o Gage and installation had to be of low mass
- o Gage had to be reasonably temperature compensated
- o System had to be capable of withstanding shock environment.

A set of general requirements was then established as follows:

1. Materials used in contact with transparencies must be compatible. Solvents, cements, gages, wiring, or sealants can not affect the transparency material mechanical or optical properties.

2. Transparent materials used must have high elongation properties; therefore, the bonded sensors, strain gages, thermocouples, and cements must also have elongation capabilities.

3. Sensor assemblies embedded in laminated transparencies must be a design that will not produce significant occlusions in the laminate; creating neither debonding between the sensor and transparency, nor stress risers or delaminations that would affect the structural integrity of the laminate.

4. Shock due to impact must not create failures (sensor debonding or lead wire detachment) in the sensor systems.

5. Sensor materials must be capable of withstanding temperatures in the range of -65°F to 272°F.

6. Strain sensor output signals must be recorded in millivolts versus time. It was estimated that time in milliseconds should be used for the beam test specimens, but microsecond measurements might be required for bird impact tests.

Strain gages and thermocouples are manufactured in many different shapes and with the direction of the lead wire terminating at different angles with respect to the gage axis. Therefore, for this series of tests conventional gages and thermocouples were chosen for exterior applications where lead wire direction was not important. The selection for embedded strain gages had to be made so that the gage lead wires would be of minimum length in the laminate.

External Surface Mounted Strain Gages

The "post yield" strain gages for mounting on the external surfaces were Micro-Measurements (M-M) Part Number EP-08-125AV-120 Option B-64. These gages were required for strains predicated for the beam static and impact tests. The M-M Part Number EA-13-125BZ-350 Option W strain gages used for the damping beams were conveniently available, and were used because high strain rates were not expected on these parts during testing.

The Option B-64 strain gage has a ribbon tab approximately four inches long; thus, precluding the possibility of damaging either the transparency material or the actual gage due to soldering of the leads. Although there were some objections to this long ribbon tab design concept, namely geometry and mismatch of temperature compensation, it was decided to use these strain gages since time constraints and cost factor for new gage development were not acceptable. The long flat copper coated ribbon tabs of approximately 4 inches in length allowed close proximity of the gage package to the specimen surface and the wire attachment mass to be located away from the strain measuring points.

After installation, the EP-08-125AV-120 Option B-64 strain gages were calibrated by checking the data output from the gage, using a 6250 ohm calibration resistance and utilizing the following equation (noted in Reference 3):

$$\varepsilon_{CAL_{SB}} = \frac{R_G}{(GF)\ (N)\ (R_C + R_G)} \qquad (7)$$

where:

R_G = Strain gage resistance, 120 ohms

R_C = Calibration resistance, 6,250 ohms

GF = Gage factor, 2.08

N = Number of active legs, 1

$\varepsilon_{CAL_{SB}}$ = Strain calibration for the static beam, μ in./in.

hence,

$$\varepsilon_{CAL_{SB}} = 9{,}057\ \mu \text{ in./in.}$$

After installation, the M-M Part Number EA13-125BZ-350 Option W strain gages were calibrated. Four active strain gages were wired into a full-bridge bending installation, so that all strain gages indicated the accumulated strain. This strain signal was then divided by four to provide an average strain gage output. The gages were calibrated by checking the data output from the gages using 50,000 ohm calibration resistance and the following equation.

$$\varepsilon_{CAL_{SB}} = \frac{R_G}{(GF)\ (N)\ (R_C + R_G)}\ , \qquad (8)$$

where:

R_G = Strain gage resistance, 350 ohms

R_C = Calibration resistance, 50,000 ohms

GF = Gage factor, 2.12

N = Number of active legs in the bridge, 4

$\varepsilon_{CAL_{DB}}$ = Strain calibration for damping beam, μ in./in.

hence,

$$\varepsilon_{CAL_{DB}} = 820\ \mu \text{ in./in.}$$

Embedded Strain Gages

The strain gages selected for embedding within laminated transparency specimens were M-M Part Number EP-08-S1128-120 Option 78. The Option 78 strain gages are identical to the Option B-64 strain gages, except the axes were turned 90 degrees to each other relative to the lead wires contained in the ribbon tab.

These strain gages had to be bonded to the monolithic plies of the laminate prior to lamination. Since plastic components of transparencies are not cut to final size until final lamination, problems occurred for the vendors. The vendors trimmed the specimens to within 1/4-inch of the ribbon tabs and then had to trim the plies by hand. Frequently, the vendors, because of the thin ribbon tabs, accidently cut the tabs off. When this occurred, they had to dig out some of the interlayer and solder wires to the ribbon tabs. During the methodology development at the various vendors, it was determined that strain gages could be embedded in the laminate for flat or slightly curved parts. For parts that were compound contoured or formed to a sharp radius, it was felt that strain gage wiring would have to accommodate large amounts of stretching to be operative, thus the wiring method used for the specimens during forming would leave the gages inoperative.

The Option 78 strain gages were calibrated in the identical manner noted for the Option B-64 strain gages.

Selection of Thermocouples

For this series of tests, both foil type and crimped wire type of thermocouples were used. The external mounted foil type thermocouple shock resistant requirement predicated the same method of attachment as that used for the external strain gage. These gages, Part Number 20114-L10, Type T, manufactured by RdF Corporation, 23 Elm Avenue, Hudson, New Hampshire, 03051 were installed by Douglas. The selected internal temperature sensors were Douglas fabricated thermocouples made from copper-constantan wire whose thermal sensor junction was

twisted and crimped in accordance with the Instrument Society of America (ISA) standards. These "wire made" thermocouples were used due to the lower cost factor. The vendors, PPG and Sierracin, embedded these interlaminate temperature sensors in contact with the structural ply surfaces by holding the sensors with the PPG-112 interlayer sheet material and by pre-bonding the sensor to the structural ply with Sierracin S-100 silicone material, respectively.

Standard Instrumentation Components

The selection and development of strain gages and thermocouples as an important part of this test program justified the foregoing presentation in this report. The standard laboratory instrumentation requirements and application techniques will not be presented in detail in this report; although, a brief description with schematics of peripheral equipment is presented. Some items of instrumentation have been identified as described in the Test Setup descriptions noted in Section II.

STRAIN GAGE AND THERMOCOUPLE ATTACHMENT DEVELOPMENT

Currently, polycarbonate has the greatest potential for meeting the requirements imposed by high energy transfer occurring during bird strikes; however, the mechanical properties of the materials are easily and quickly degraded by contact with many common chemicals.

The presentations that follow detail the materials investigation and development for bonding the strain gages and thermocouples to polycarbonate materials and the techniques evolved to prevent the lead wires from tearing the gages loose under high impact load.

Strain Gage and Thermocouple Bonding

A library survey was made of the airframe industry, the Air Force, technical socieites, and vendors in an endeavor to find a suitable method of bonding the strain gages to the polycarbonate. The method selected

had to have inherent features that would not cause polycarbonate degradation, would retain the gages and thermocouples, and would not impair the elongation and yield capabilities of the gages or the surface preparation bonding and sealing materials.

Surface Preparation

Grit-blast and chemical etching methods were not allowed since both methods would affect the material properties of the plastic substrates. Only Freon cleaning and light sanding were found to be acceptable. A 400 grit silicone carbide paper rather than coarser grits was used, as the polycarbonate tends to "gum" when extensively abraded. Chemical surface conditioners were not allowed. Distilled water was used to purge the polycarbonate surfaces of particle and chemical residue. All surface preparation was accomplished in the cleanest environment practical.

Selection of Bonding Material

Adhesive used in bonding strain gages to polycarbonate material were thoroughly investigaged and evaluated from various standpoints. The cured adhesive system had to have sufficient elongation capability to withstand the high deflection during bird impact test; to be capable of withstanding extreme temperatures and thermal shock conditions; to be compatible with polycarbonate material.

The curing and handling characteristics of the adhesive system were evaluated for ease of application with respect to time and temperature required for curing.

To determine the stress craze effects of various adhesives, a series of tests were performed, in accordance with MIL-P-83310, to the following:

1. A series of 1" x 7" x 0.250-inch craze test specimens were machined from fusion bonded polycarbonate made from polycarbonate sheets per MIL-P-83310.

2. The specimens were annealed and conditioned for two (2) hours at 120°C (248°F) in a circulating air oven and followed by 48 hours at standard testing conditions.

3. The craze test specimens were placed in a cantilever beam fixture as shown in Figure 1 of MIL-P-83310, and the load necessary to produce a minimum outer fiber stress of 2000 psi was applied. After a ten (10) minute load period, the test material was applied to the specimen over the fulcrum and allowed to remain in contact for 30 minutes. At the conclusion of the test period the specimen was removed and the fluid wiped off. The polycarbonate specimen was then visually examined for crazing.

The materials tested and the test results are shown in Table 7. The materials were then tested by cementing strain gages to polycarbonate specimens. The results of this series of tests are shown in Table 8. The elongation, temperature range, and minimum curing requirements were obtained from vendor supplied data. The other data was from informal tests conducted at Douglas.

The two materials determined to be acceptable for strain gage and thermocouple attachment were M-Bond AE-15 and M-Bond GA-2. Both are two-component, room temperature adhesives.

Selection of Sealant Materials

In addition to determining a material for bonding strain gages to the transparent materials, it was also determined that the loose wires must be attached to the specimens for routing and to meet shock resistant characteristics. For this application, commercially available sealants were evaluated.

RTV 118 silicone sealant was tested, as noted in Table 7, and found to be an acceptable material. Further, conversations with three transparency manufacturers revealed that RTV 630 silicone sealant was also compatible with polycarbonate.

Silastic S-140 silicone sealant was found to be an acceptable material for adhering the strain gage and lead wires to glass and metal parts; however, S-140 sealant has acetic acid as a component which may or may not be compatible with polycarbonate or acrylic materials.

TABLE 7. STRESS CRAZE EFFECTS OF VARIOUS BONDING MATERIALS ON POLYCARBONATE

BONDING MATERIALS OR SOLVENTS	OUTER FIBER STRESS LEVEL (PSI)	CRAZE EFFECTS
Isopropyl Alcohol	3750	Incipient Crazing
M-Bond 43B Adhesive	3500	Severe Crazing - 5 Minutes
M-Bond 600 Adhesive	3500	Severe Crazing - 5 Minutes
M-Bond 610 Adhesive	3500	Severe Crazing
M-Bond 200 Adhesive	3500	Extreme Craze
M-Bond 200 Catalyst	3500	Instant Craze on Contact
M-Bond GA-2 Catalyzed	3000	No Craze
RTV 118 Silicone	3750	No Craze
M-Bond AD-15 (Epoxy + Hardener)	3750	Severe Crazing
M-Bond AE-15 (Epoxy + Hardener)	2500	No Craze
Hardener 15	3750	Instant Craze
Epoxy + Hardener	3750*	No Craze

*Applied after 18 hours

TABLE 8. STRAIN GAGE BONDING CEMENTS TESTED

	CEMENT IDENTIFICATION					
	M-Bond 200 (E-910)	M-Bond 600	M-Bond 610	M-Bond AE15	M-Bond GA-2	M-Bond GA-60
Elongation*	Fresh 15% embrittles with time	3% H.T. 3% R.T. 1% L.T.	3% H.T. 3% R.T. 1% L.T.	10-15% R.T. 3% R.T.	2% R.T.	
Temp, Range °F (Long term)*	±30° to 150°F	-450° to 500°F	-450° 500°F	-450° 200°F	-320° to 200°F	-100° to 500°F
Minimum Curing Requirement*	None	175°F 4 hours	210°F 4 hours	150°F w hrs. 125°F 6 hrs.	150°F 1 hr. R.T. 6 hrs.	250°F 6 hours
Shock Resistant	Poor	Good	Good	Good	N/A	N/A
Compatibility with P/C No Load Loaded	Good Poor	Good Poor	Good Poor	Good Fair	Good N/A	Good N/A
Base of Application	Excellent (Except for precise positioning)	Fair	Fair	Fair	Fair	Poor

*Data Supplied by Vendors.

N/A = Not Available

M-Bond cements are commercially available strain gage cement from Micro-Measurements, Inc.

H.T. = High Temperatures

R.T. = Room Temperatures

L.T. = Low Temperatures

All three sealants are room temperature curing and can be applied in accordance with the labels on the material.

Primers were not used prior to the application of sealants because the sealants adhered adequately to the polycarbonate and acrylic.

Lead Wire Shock Resistance Development

The prime requisite of the instrumentation for this series of tests, and any high impact tests, is to demonstrate strain gage and thermocouple retention when the mounting surface is subjected to large deflections and high level impact load.

During an impact, if the lead wires are not secured to the specimen, the mass of the wires, solder joint, and ribbon tab could pull the strain gages loose. It is not as important that the thermocouples remain secure at impact, because the temperature at the instant of impact would have been recorded. It is important that the strain gages remain secure and are readable during this critical event.

It was determined that for static loading and minor impact forces an acceptable installation could be accomplished by installing a block of styrofoam below the ribbon tab and encapsulating it with sealant, as shown in Figure 10.

Under high impact forces, the added mass of the sealant causes the block to "jump" about four inches. This action hyper-extends the ribbon tab, thus, causing gage failure.

To eliminate the hyper-extension of the ribbon tab a free space loop of approximately one inch was made and the solder joint juncture was mounted on a pad of sealant. This method generally worked for most high impact conditions. Refer to Figure 11 for the installation.

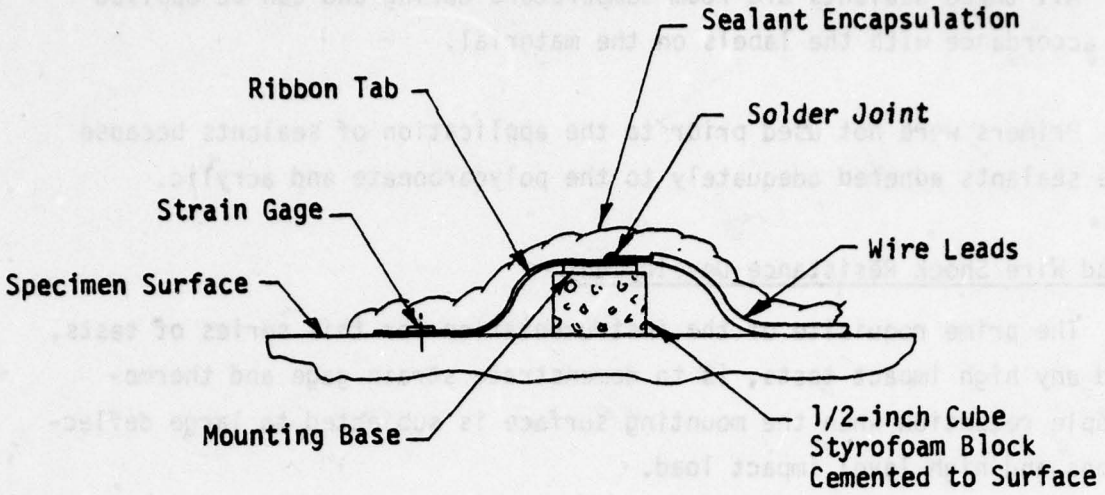

Figure 10. Styrofoam block shock absorber.

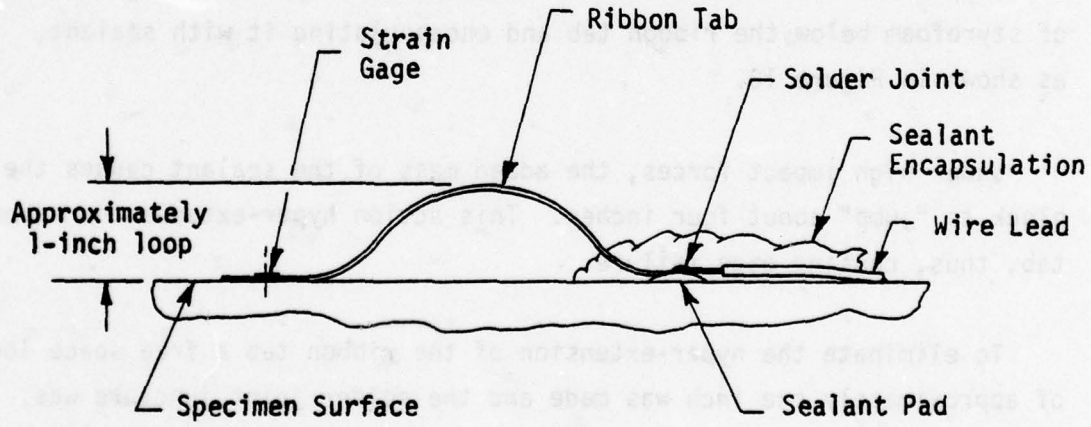

Figure 11. High impact shock resistant gage installation.

STRAIN GAGE AND THERMOCOUPLE INSTALLATION PROCEDURES

At the conclusion of this investigative effort, a series of requirements and installation procedures were developed. Applicable procedures were then included on the specimen drawings, in test plans, and in procurement specifications.

The following subsections utilized these developed procedures.

Damping Beam Instrumentation Installation Procedures

Requirements and procedures for installation of strain gages were developed for application to the damping beam specimens. The procedure was applicable to both acrylic and polycarbonate specimens. The procedure was also applied to the glass specimens except standard glass cleaning procedures were utilized.

The instrumentation installation procedures for external bonding of strain gages to the damping beams are as follows:

1. Solder No. 28 AWG., Teflon Insulated, 6 feet long, lead wires to EA-13-125BZ-340, Option W (or equivalent) strain gage ribbon tabs with M-M 361A-20R (or equivalent); CAUTION: Solder prior to cementing gage to specimen.

2. Position strain gage ribbon tabs to allow a one-inch loop, and at solder joint juncture provide a base of sealant. Encapsulate junction with sealant and attach leads to specimen with sealant.

3. Strain gages are to be bonded to the specimen surfaces using M-M M Bond GA-2 adhesive system per M-M Instruction Bulletin B-137-2 with the following exceptions:

   Par III Step 1 - CAUTION: Do not use Chlorothene Nu.

Step 2 - Use 400 grit silicone carbide paper in place of 270 or 320. CAUTION: Do not use conditioner.

Par IV Cure one hour at 200°F to insure bond.

Par V No protective coating required.

4. Sealant to be RTV 118 (or equivalent).

5. Use isopropyl alcohol to clean polycarbonate.

6. Use naptha to clean acrylic followed by cleaning with a detergent soap and water.

7. Clean glass with a detergent soap and water.

8. Bridge - full bridge to measure bending strains.

9. Strain gages will be acceptable when:
   - Electrical continuity is maintained.
   - Grid to specimen resistance is 10 megohms or greater.
   - Strain gage resistance is approximately 120 ohms plus or minus 2 ohms.

A typical strain gage installation to a damping beam specimen is shown in Figure 12.

Beam Embedded Instrumentation Installation Procedures

Procedures for installation of strain gages and thermocouples were developed for the respective vendors to laminate strain gages and thermocouples internal to the 36-inch beam specimens and are as follows:

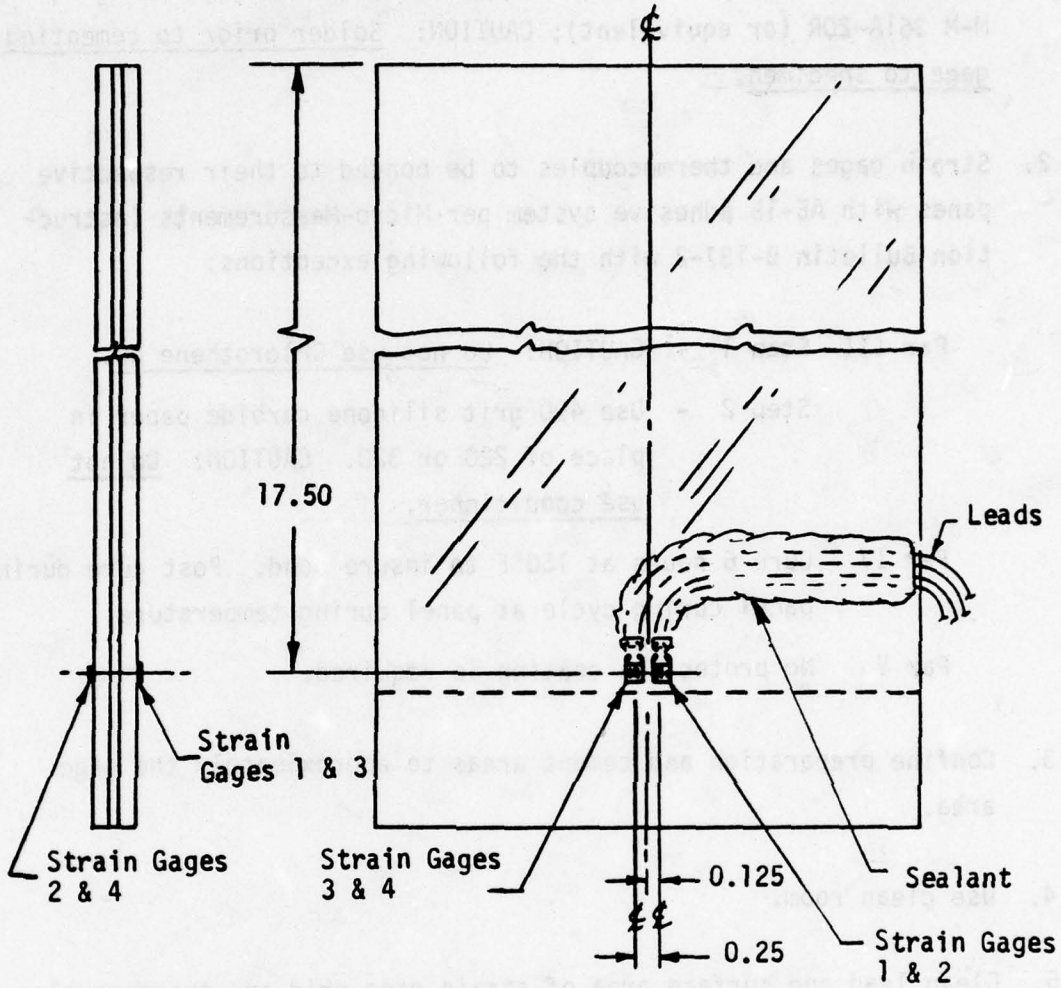

Figure 12. Typical damping beam strain gage instrumentation detail.

1. Solder No. 28 AWG., Teflon insulated, 6 feet long, lead wires to EP-08-S1128-120 Option 78 (or equivalent) strain gage using M-M 361A-20R (or equivalent); CAUTION: Solder prior to cementing gage to specimen.

2. Strain gages and thermocouples to be bonded to their respective panes with AE-15 adhesive system per Micro-Measurements Instruction Bulletin B-137-2 with the following exceptions:

   Par III Step 1 - CAUTION: Do not use Chlorothene Nu.

   Step 2 - Use 400 grit silicone carbide paper in place of 220 or 320. CAUTION: Do not use conditioner.

   Par IV Cure 6 hours at 150°F to insure bond. Post cure during panel curing cycle at panel curing temperature.

   Par V No protective coating is required.

3. Confine preparation and cement areas to approximately the gage area.

4. Use clean room.

5. Clean lead and surface area of strain gage grid and thermocouples just before laminating process to avoid surface contaminants affecting both leads, grid and laminate materials.

6. All gas bubbles must be carefully pressed out of cement-gage assembly during cementing process. Higher clamping pressure during curing than recommended by Micro-Measurements may be required. CAUTION: Take care not to damage gage.

7. Strain gages will be acceptable when:

   - Electrical continuity is maintained.
   - Grid to specimen resistance is 10 megohms or greater.

- Strain gage resistance is approximately 120 ohms plus or minus 2 ohms.

- Visual inspection of beam assembly indicates strain gages are completely bonded to specimen surface indicated on the respective drawing.

8. Internal copper-constantan thermocouples will be acceptable when:

   - Continuity is maintained.
   - Thermocouple is bonded directly to surface indicated on the respective drawing.

9. The vendor must provide adequate means of protecting the instrument leads from damage during handling.

10. When CIP interlayers are used, the thermocouple must be bonded to the structural ply.

Externally Mounted Instrumentation Installation Procedures

Procedures for installation of external strain gages and thermocouples on the 36-inch beam specimens are as follows:

1. Solder No. 28 AWG., Teflon insulated, 6 feet long lead wires to EA-13-125BZ-350 Option W (or equivalent) strain gage using M-M 361A-20R (or equivalent); CAUTION: Solder prior to cementing gage to specimen.

2. Strain gages and thermocouples to be bonded to their respective specimen surfaces with AE-15 adhesive system per Micro-Measurements Instruction Bulletin B-137-2 with the following exceptions:

Par III Step 1 - Do not use Chlorothene Nu.

Step 2 - Use 400 grit silicone carbide paper in place of 220 or 320. CAUTION: Do not use conditioner.

Par IV Cure one hour at 200°F to insure bond.

Par V No protective coating required.

3. Confine preparation and cement areas to approximately the gage area.

4. Use clean room procedures in handling and installing the strain gages.

5. Clean lead wires and surface area of strain gage grid and thermocouples just before bonding to specimen to avoid surface contaminants affecting both grids, leads and specimen surface.

6. All gas bubbles must be carefully pressed out of cement-gage assembly during bonding process. Higher clamping pressure during curing than recommended by M-M may be required. CAUTION: Take care not to damage gage.

7. Use isopropyl alcohol to clean polycarbonate.

8. Use naptha to clean acrylic followed by cleaning with a detergent soap and water.

9. Clean glass with a detergent soap and water.

10. Clean strain gages, thermocouples, and lead wires, if required, in accordance with normal laboratory procedures.

11. Bend exposed ribbon tabs from embedded strain gages and bond to specimen edge with RTV 118 (or equivalent), as shown in Figure 13.

12. For static or low impact specimens, a 1/2-inch cube of styrofoam may be placed under the ribbon tabs and bonded to the specimen with RTV 118 (or equivalent) sealant. Pot around gages and block with RTV 118 sealant.

13. For high impact specimens, a loop of approximately one inch must be accomplished. Bond and pot ribbon tab in area of solder joint terminals to specimen with RTV 118 (or equivalent) sealant.

14. Strain gages will be acceptable when:

    - Electrical continuity is maintained.
    - Grid to specimen resistance is 10 megohms or greater.
    - Strain gage resistance is approximately 120 ohms plus or minus 2 ohms.
    - Visual inspection of beam assembly indicates strain gages are completely bonded to specimen surfaces indicated on the respective drawing.

15. Copper-constantan thermocouples will be acceptable when:

    - Continuity is maintained.
    - Thermocouple is directly in contact with surface indicated on the respective drawing.

16. Extreme care must be taken to protect instrumentation from damage during handling.

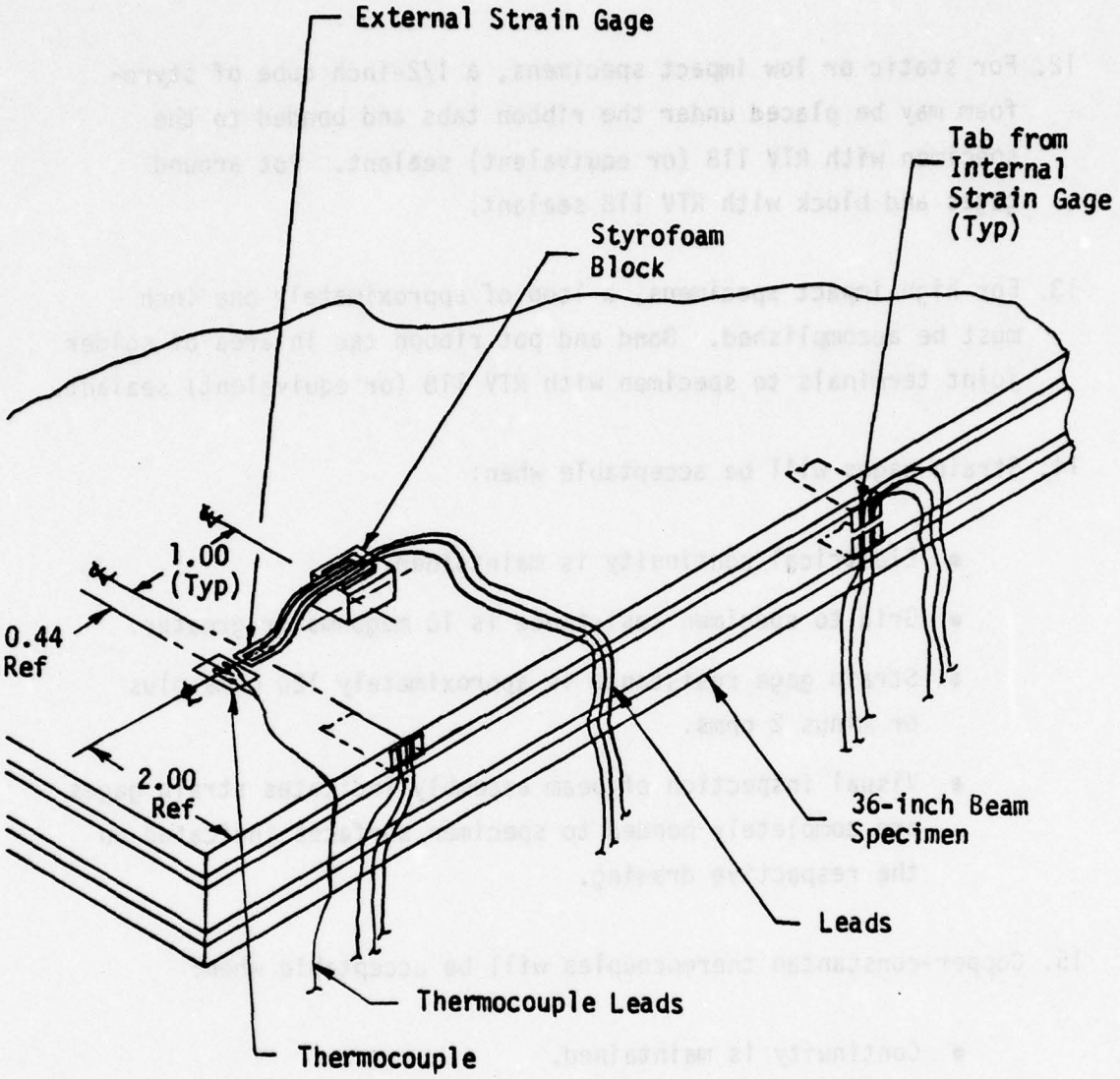

Figure 13. Typical 36-inch beam instrumentation details.

Typical strain gage and thermocouple installations to 36-inch beams are shown in Figure 13.

OPTIMIZED STRAIN GAGE LOCATION SELECTION

Subsequent to the strain gage selections and installation developments, a series of studies were undertaken to establish the optimum locations for strain gages for the damping and 36-inch beams.

Damping Beam

Four active strain gages were wired into a full-bridge bending installation where two strain gages were installed on each side of each damping beam to provide a balanced electrical output. As shown in Figure 12, the strain gages were located as close as practicable to the base of each specimen where maximum strains would occur and the center of each specimen to minimize the edge effects on the strain gage readings.

Thirty-Six-Inch Bending Beams

In an endeavor to select optimum locations for strain gage installations for the 36-inch beams, shear, bending moment, and deflection analyses theories were utilized.

The bending beam test conditions varied from simply supported ends to totally fixed ends. The two theoretical extreme conditions are illustrated in Figure 14.

Even though the various beam end conditions noted in Table 5 indicate a vast difference, it is doubtful that actual conditions would totally match either theoretical extreme, but in most cases would be somewhere in between.

The conventional deflection and moment equations that apply to these diagrams, from Reference 2, Pages 193 and 254, are presented in the following discussion.

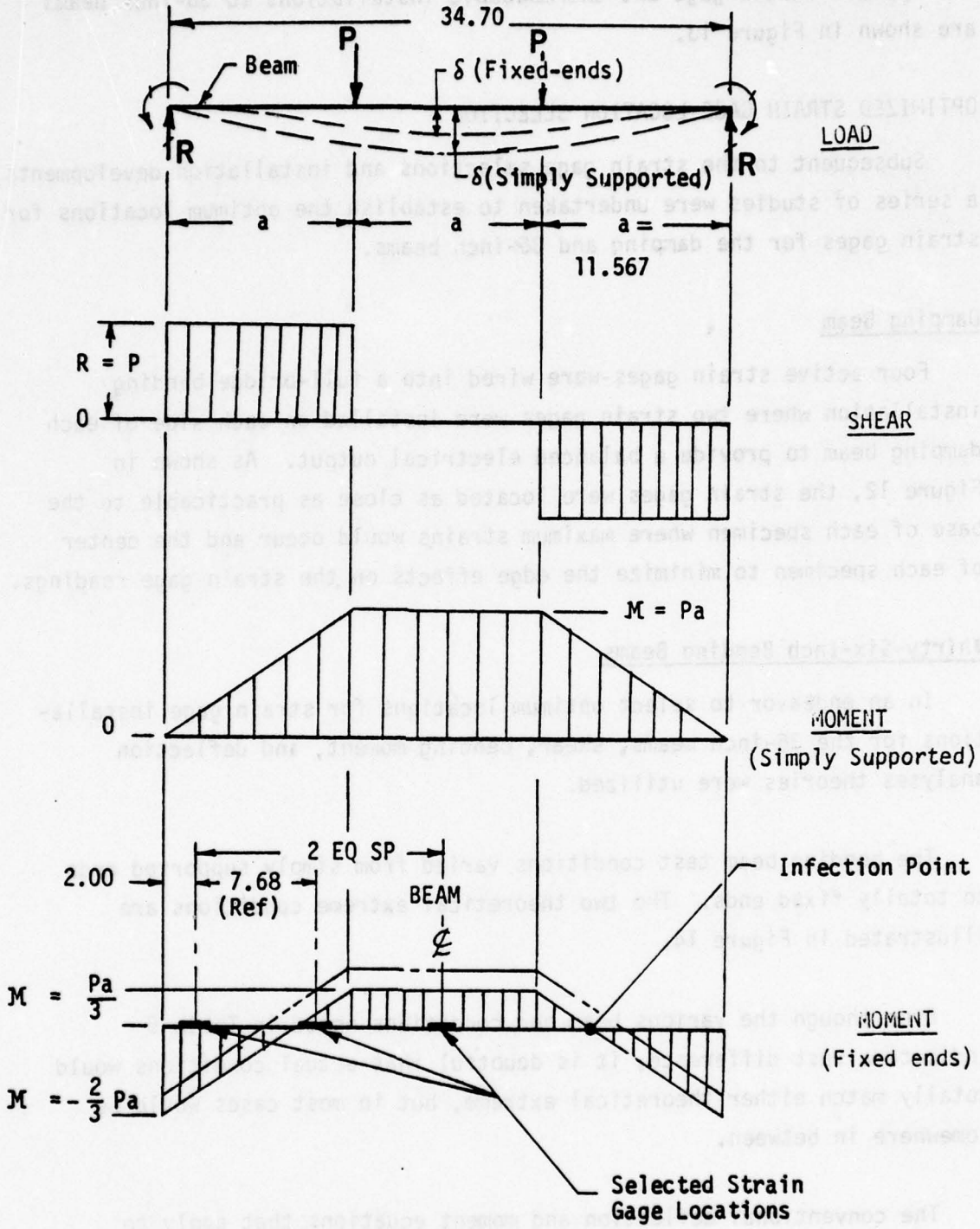

Figure 14. Strain gage optimum location definition, 36-inch beam specimens.

1. For simply supported beams:

   a. The maximum beam center deflection is:

$$\delta = \frac{23Pa^3}{24EI} \quad . \tag{9}$$

   b. The maximum bending moment occurs in the constant bending moment section between the two load points. This bending moment is:

$$M_{max} = Pa \quad . \tag{10}$$

   c. The bending moments at the beam ends are zero for simply supported beams.

2. For fixed-end beams:

   a. The maximum beam center deflection is:

$$\delta = \frac{5Pa^3}{24EI} \quad . \tag{11}$$

   b. The maximum negative bending moment occurs at the beam fixed ends and is:

$$M = -\frac{2}{3} Pa \quad . \tag{12}$$

   c. The maximum positive bending moment occurs between the two load points and is:

$$M = \frac{Pa}{3} \quad , \tag{13}$$

where:

P = Load (pounds)

a = 1/3-beam segment lengths (in.)

E = Modulus of elasticity (psi)

I = Moment of inertia ($in.^4$)

δ = Beam center maximum displacement (in.)

M = Bending moment (in.-lb.)

Since the loaded beam strains are assumed to be proportional to its bending moments, strain diagrams can be constructed that are proportional to the conventional simply supported or fixed-end beam moment diagrams. Therefore, the moment diagrams shown are representative of the relative strain magnitudes. By observation and an overlay comparison of these diagrams, the optimum locations for placing a minimum number of strain gages along the beam length can be determined. The gages should be placed away from the predicted zero strain reading areas; such as, the beam ends for the simply supported beam and the inflection point for the fixed-end beam.

The strain gage optimum locations selected are shown in Figure 15 for both external and internal surfaces. Figures 16 and 17 indicate the locations for the strain gages and thermocouples within multilayered specimens.

INSTRUMENTATION DOCUMENTATION

The damping and 36-inch beams strain, temperature, load, and deflection sensors with their associated recording equipment are described in the following subsections.

Damping Beam

The damping beams were instrumented with four active strain gages (Micro-Measurement Part Number EA-13-125BZ-350, Option W) that were wired into a full-bridge bending installation, so that all strain gages indicated the accumulated strain. This signal was then divided by four to provide the average strain output. Refer to Figure 12 for the strain gage locations. A schematic diagram of the full-bridge bending measure-

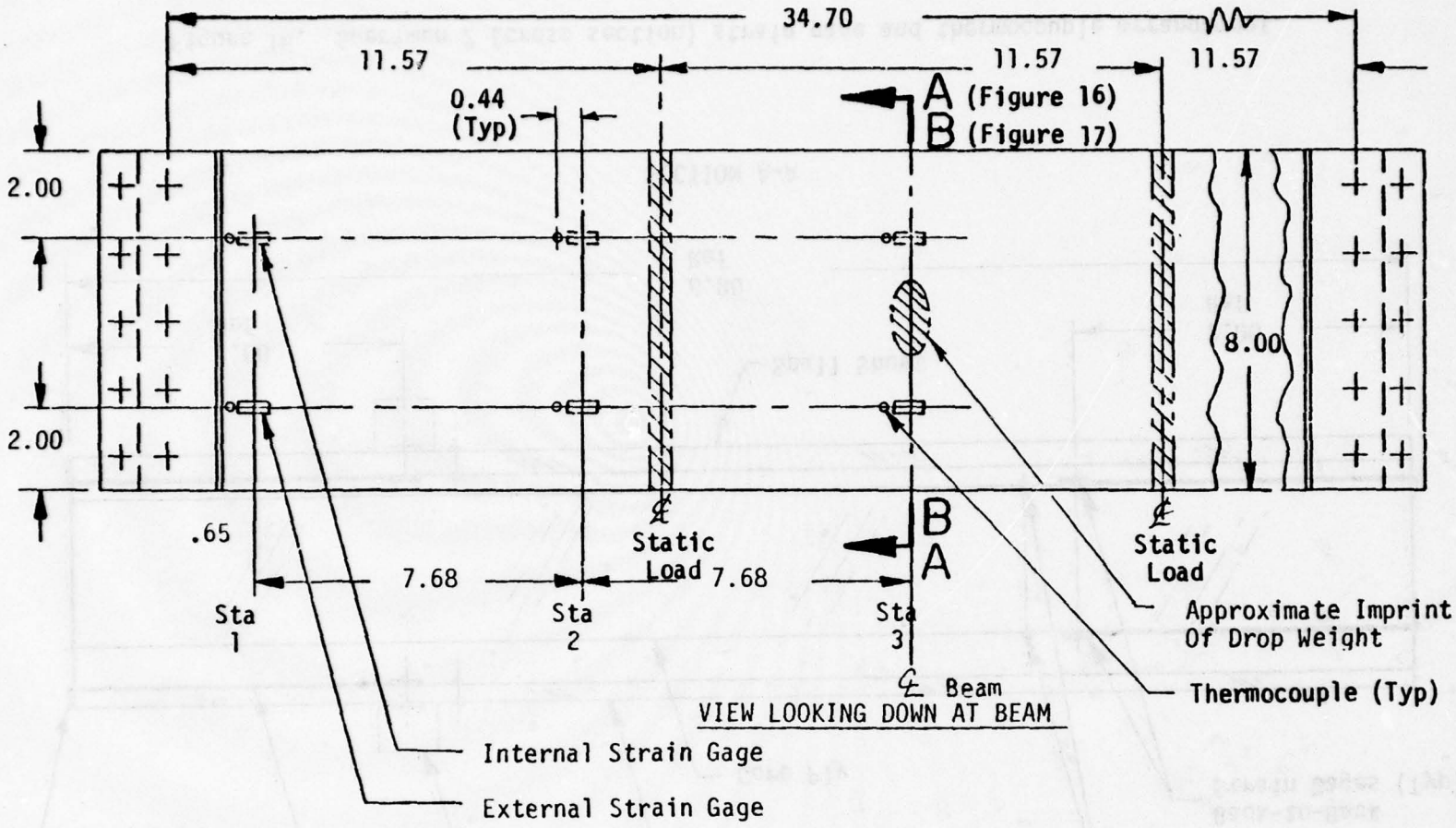

Figure 15. Strain gage and thermocouple arrangement, 36-inch beam specimens.

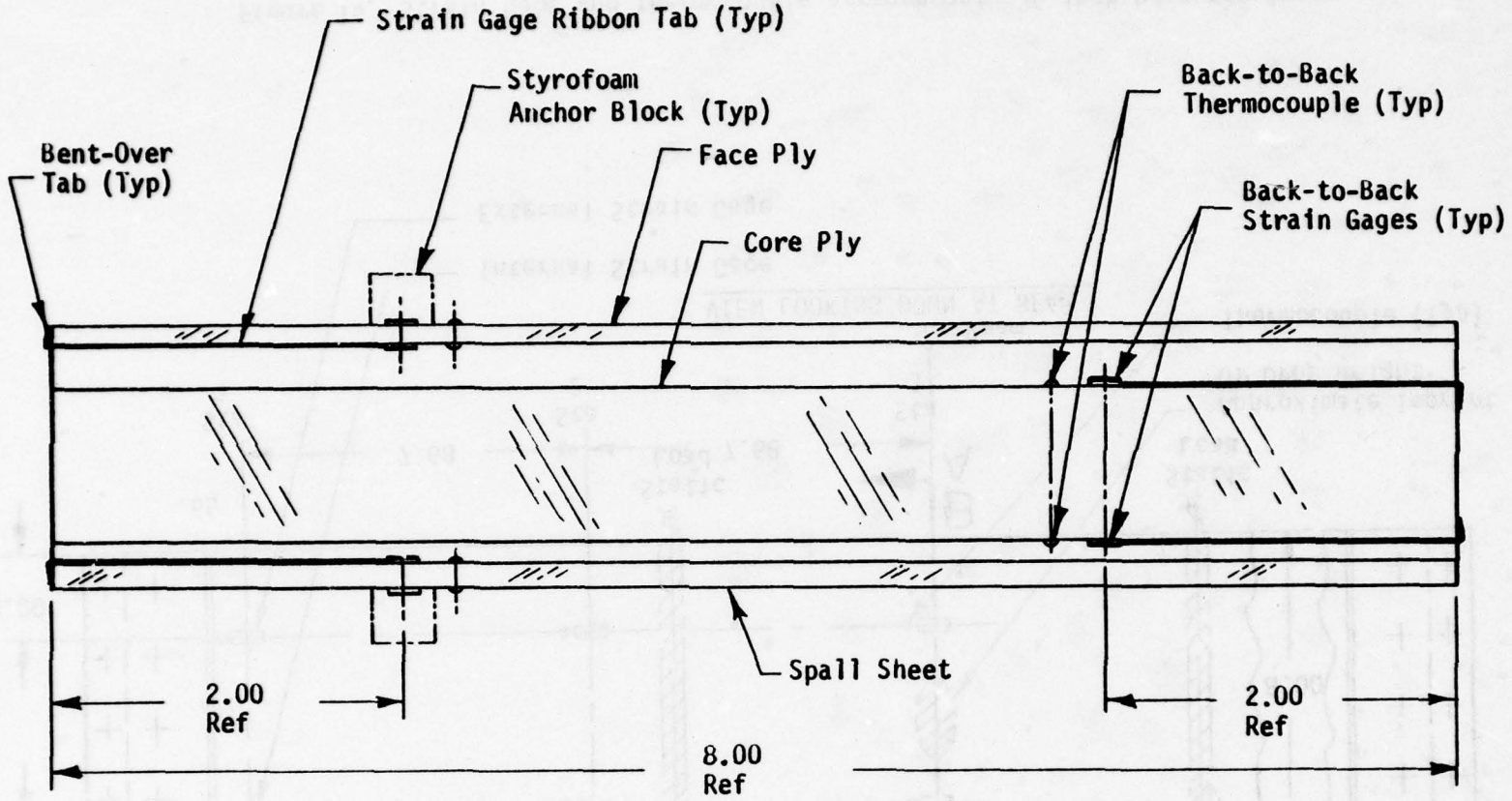

SECTION A-A

Figure 16. Specimen 2 (cross section) strain gage and thermocouple arrangement.

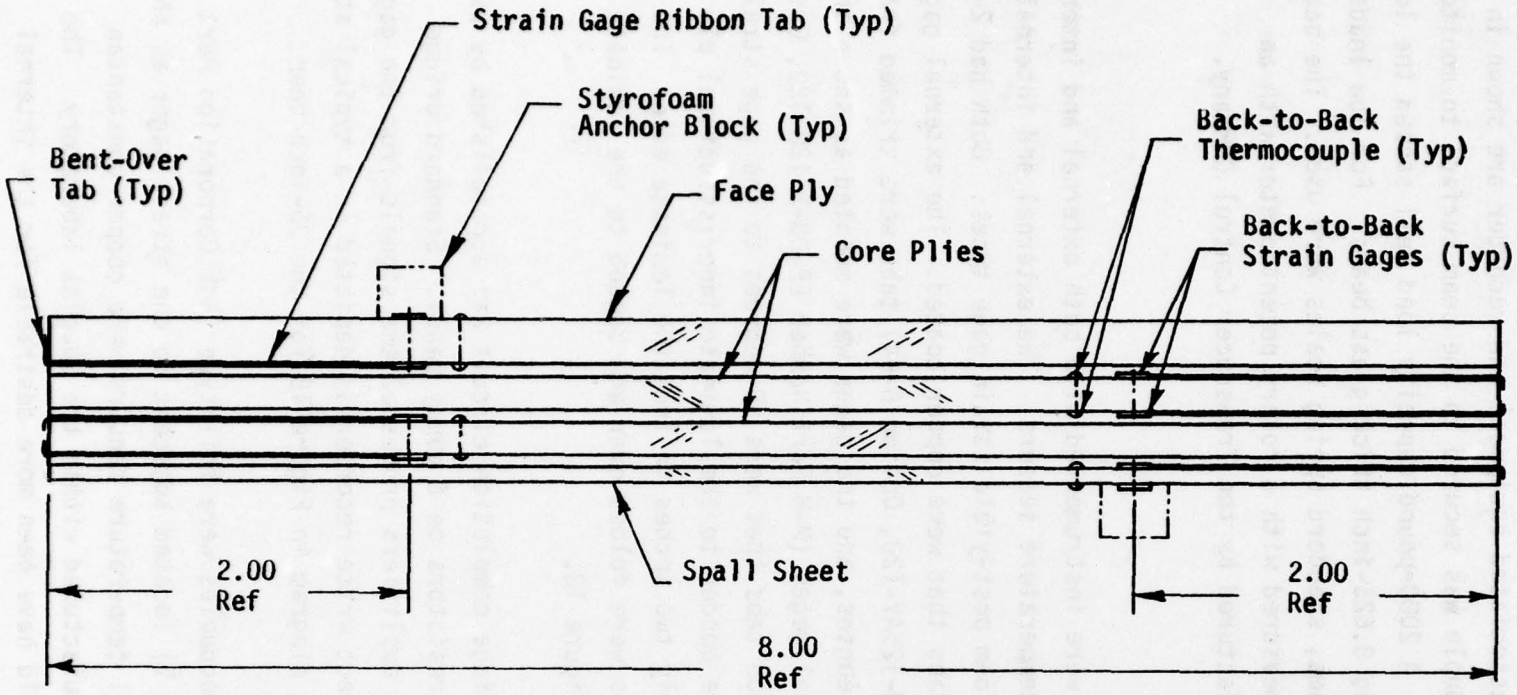

SECTION B-B

Figure 17. Specimen 4 (cross section) strain gage and thermocouple arrangement.

ment circuit and its associated equipment and recorder are shown in Figure 18. A thermocouple was secured to the beam surface to monitor its test temperature. A 2000-pound capacity load cell sensed the load required to deflect the 0.625-inch thick glass beams. For low loads applied to damping beams, standard spring scales were used. The beam tip displacement was measured with a rotary potentiometer with an extension cable, manufactured by the Transducer Control Company.

Thirty-Six-Inch Beam

The 36-inch beams were instrumented with both external and internal laminated strain and temperature sensors. The external and internal strain gages were 120 ohm post-yield strain gage types. Both had 2-inch long integral ribbon tabs that were copper coated. The external gage (m-M Part Number EP-08-125AV-120, Option B-64) tabs were trimmed from four-inch ribbon tab lengths, and the gages were mounted as shown in Figure 13. The internal gages (M-M Part Number EP-08-S1128-120, Option 78) had four-inch ribbon tabs that were 90 degrees to the gage strain axis. These gages were bonded to the laminate inner structural ply surface at approximately two inches in from the laminate edge. The ends of the ribbon tabs were folded over and bonded to the laminate edge as indicated in Figure 13.

The strain gage bridge completion circuit was accomplished by use of 3/4 bridge completion resistors on a dummy panel. Standard bridge balancing controls and amplifiers processed the signals from the gages to an oscillograph direct write recorder as depicted in a typical strain gage channel schematic diagram in Figure 19 for the 36-inch beam.

The external thermocouples were foil type (RdF Corporation Part Number 20114-L10, Type T) located adjacent to the strain gages as shown in Figure 13. Internal temperature sensors were copper-constantan wire thermocouples manufactured within the Douglas laboratory. The foil type thermocouples would have been more desirable for the internal

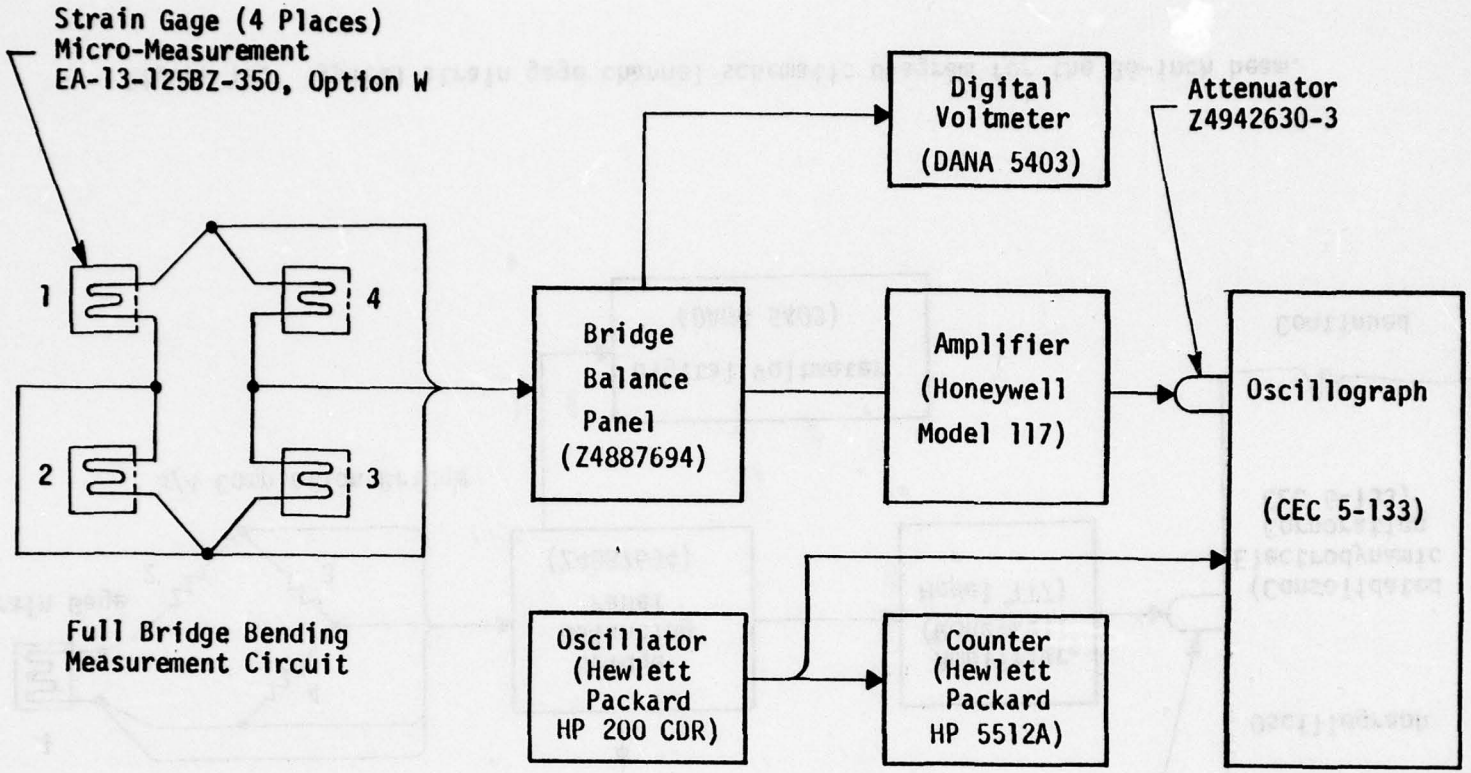

Figure 18. Schematic diagram of damping beam strain gage instrumentation.

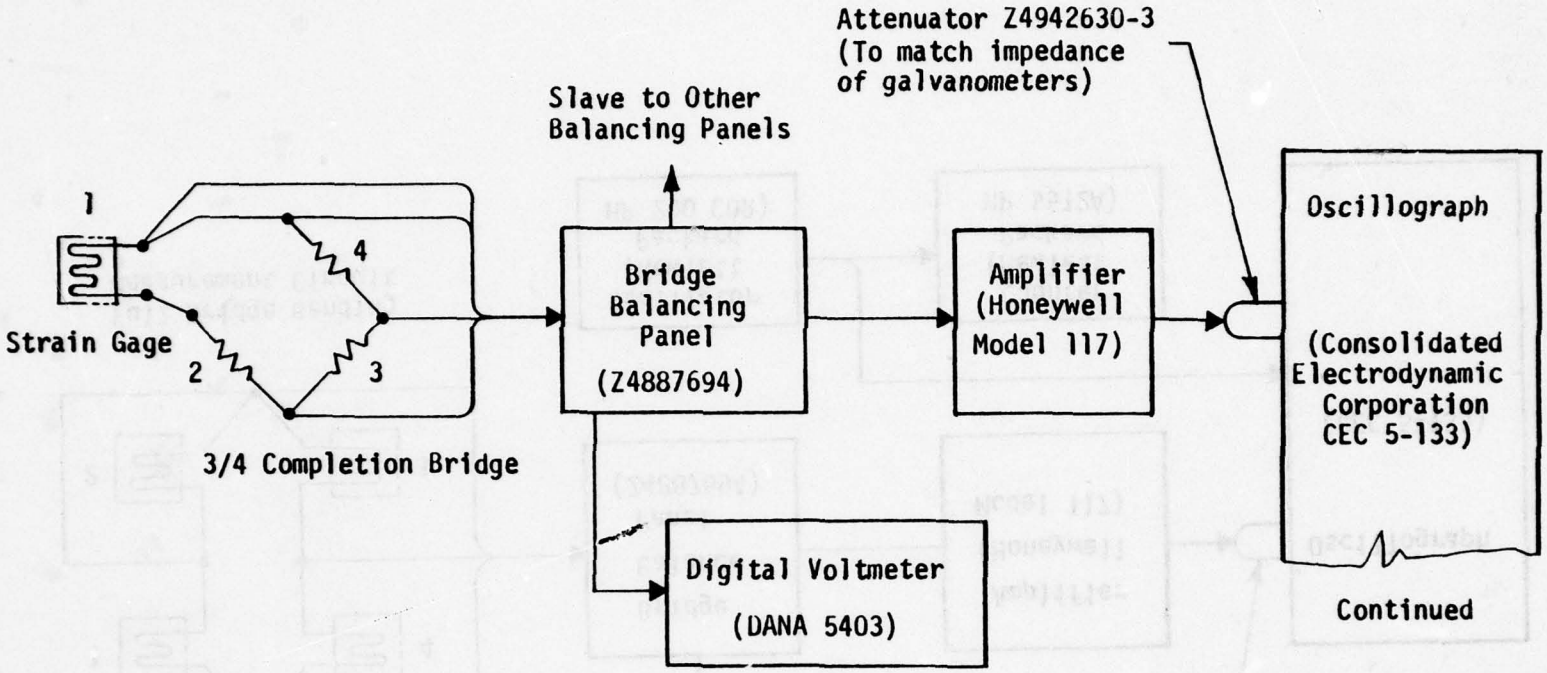

Figure 19. Typical strain gage channel schematic diagram for the 36-inch beam.

temperature sensors, but the additional cost was the deciding factor. The temperature sensor signals were processed through a "Leed and Northrup" temperature strip chart recorder.

The load sensor was a bonded resistance strain gaged load ring (2000 pound load capacity), manufactured by Douglas. Figure 20 shows a schematic diagram of the load cell channel to the recorders. The beam vertical and horizontal deflection sensors were Linear Variable Differential Transformers (LVDT). The schematic diagram for the vertical and horizontal sensor channels is shown in Figure 21. In addition to the oscillograph strip chart recordings of the beam strains, load, horizontal and vertical displacement, a sinusodial timing wave of approximately 20 Hertz was recorded. Figure 22 depicts a schematic diagram of this timing reference channel.

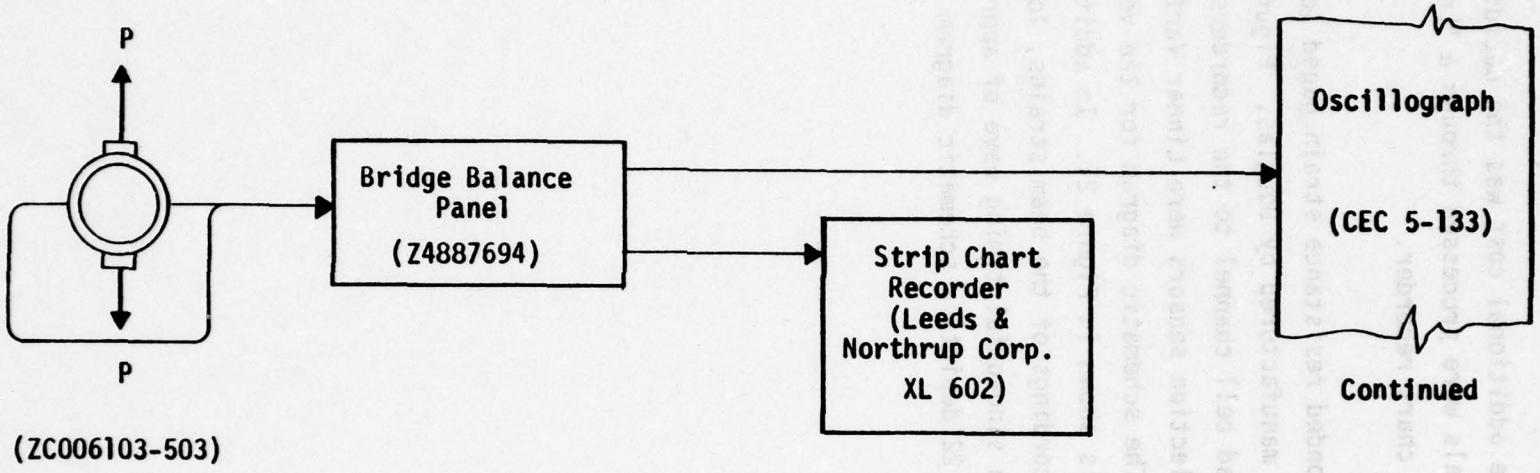

Figure 20. Load cell channel schematic diagram for 36-inch beam.

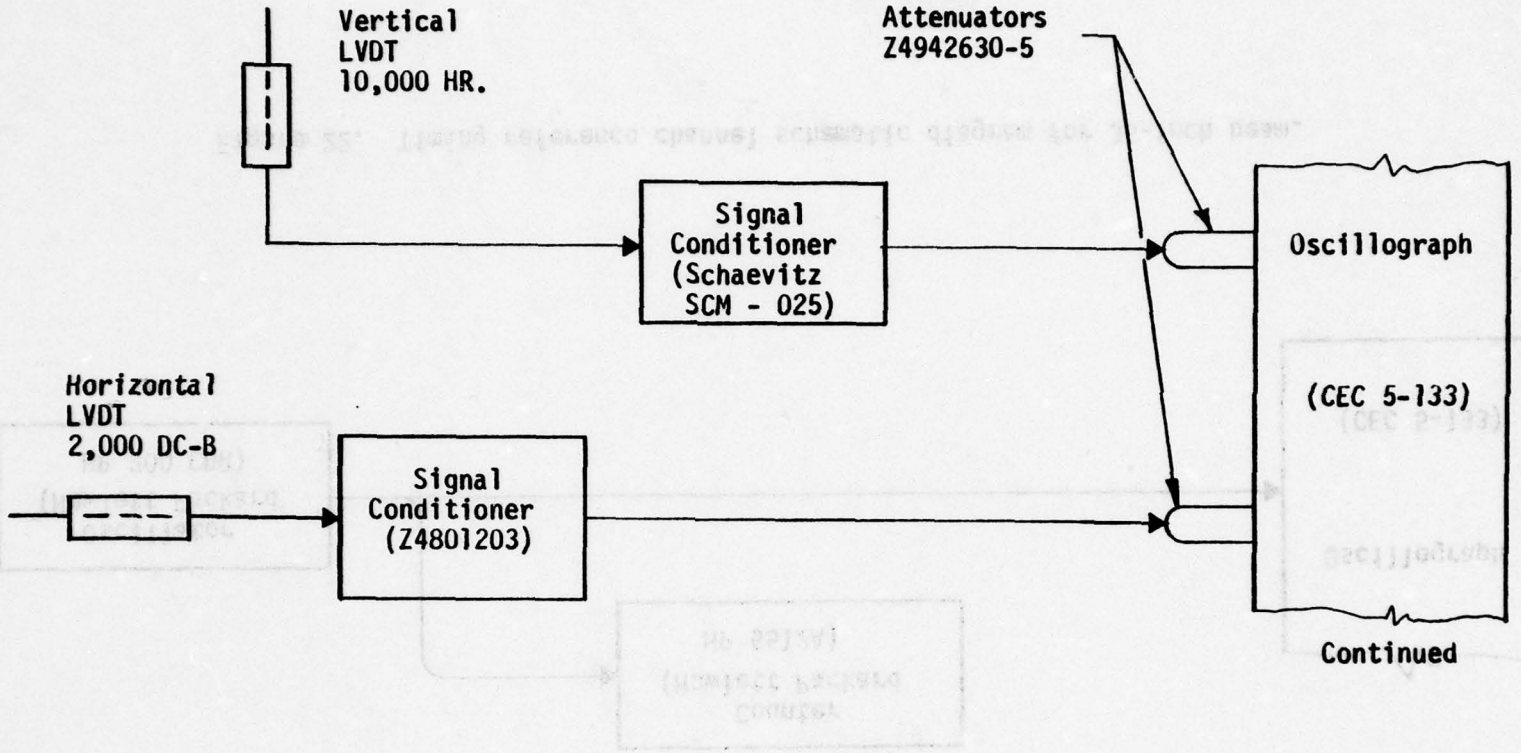

Figure 21. Linear Variable Differential Transformers (LVDT) channel schematic diagram for 36-inch beam.

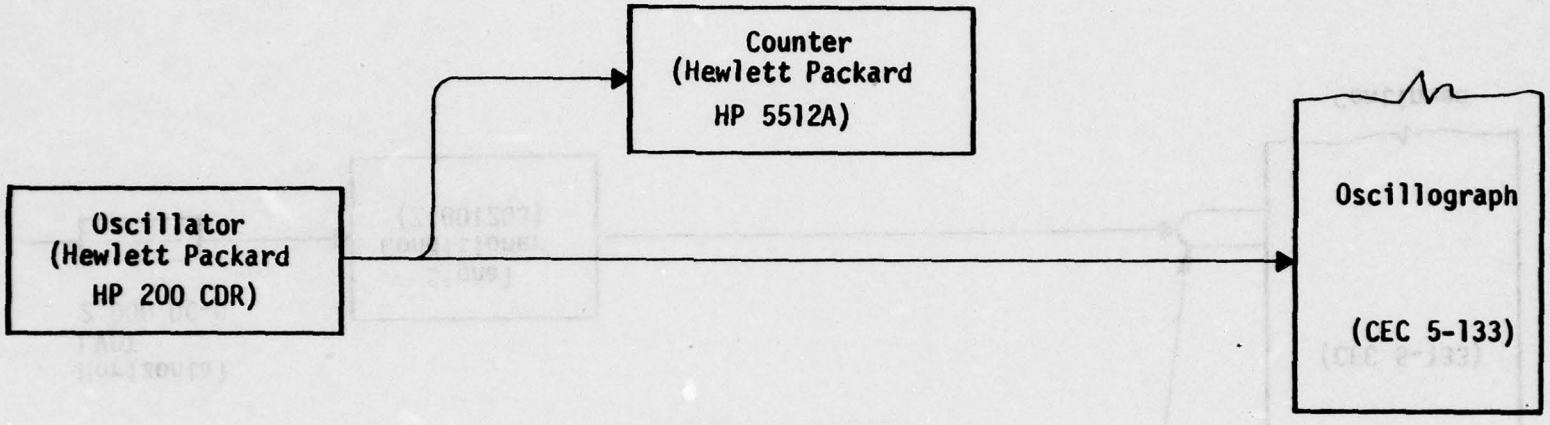

Figure 22. Timing reference channel schematic diagram for 36-inch beam.

SECTION IV

TESTS RESULTS AND ANALYTICAL DEVELOPMENT FOR DAMPING BEAM SPECIMENS

Within Section II a complete presentation was made regarding the Test Direction pertaining to this entire series of specimen tests. Included were the test specimen descriptions, test conditions, test set-up, and test procedures for the damping beam specimens.

The rationale and final development for the selection of strain gages and thermocouples, as well as the method of documentation for this series of specimen tests was described in Section III.

The purpose of the damping beam test series was to obtain test data for various windshield materials, such that certain damping properties could be ascertained. Within this section the damping beam test results and analyses are covered.

SPECIMEN DEFINITION AND TEST TEMPERATURES

Even though engineering drawings and test plans clearly delineate requirements for vendors to manufacture parts, test engineers to perform testing, and specifically defined test data to be compiled, variations always occur. Subsequent paragraphs will define these variations.

Specimen Definition

As noted previously in Table 1, the engineering drawing requirements were established for each damping specimen, and Figure 12, Section III, illustrates the planned locations of the strain gages.

The actual as-manufactured dimensions are tabulated in Table 9 for each damping specimen.

Test Temperatures

The damping beam specimens were to be tested at the individual

TABLE 9. DAMPING BEAM SPECIMEN DIMENSIONS

SPECIMEN NO.	DRAWING NO. CONFIGURATION	L_1* (in.)	L* (in.)	B* (in.)	THICKNESS* (in.)	VENDOR
5	Z5942629-1	17.15	18.03	8.00	t_1 = .250 t_2 = .121 t_3 = .254 t_4 = .625	PPG
6	Z5942629-501	17.15	17.97	8.03	t_1 = .246 t_2 = .120 t_3 = .248 t_4 = .614	SK
7A	Z5942629-503A	17.15	18.03	8.03	0.621	PPG
7B	Z5942629-503B	17.15	18.03	8.00	0.636	SK
8	Z5942629-505	17.00	18.06	8.00	0.250	DAC
9A	Z5942629-507	16.57	18.00	8.00	0.638	PPG
9B	Z5942629-507	17.20	18.06	8.00	0.639	PPG
9C	Z5942629-509	---	18.00	8.00	0.250	PPG
10	Z5942629-511	17.00	18.09	8.06	0.679	DAC
11	(N O T U S E D)					
12	Z5942629-513	17.00	18.00	8.00	0.250	DAC

NOTES:

Refer to Table 2 for material description.

PPG - PPG Industries

SK - Sierracin Corp., Inc.

DAC - Douglas Aircraft Co.

*Refer to Figure 23 for dimension locations.

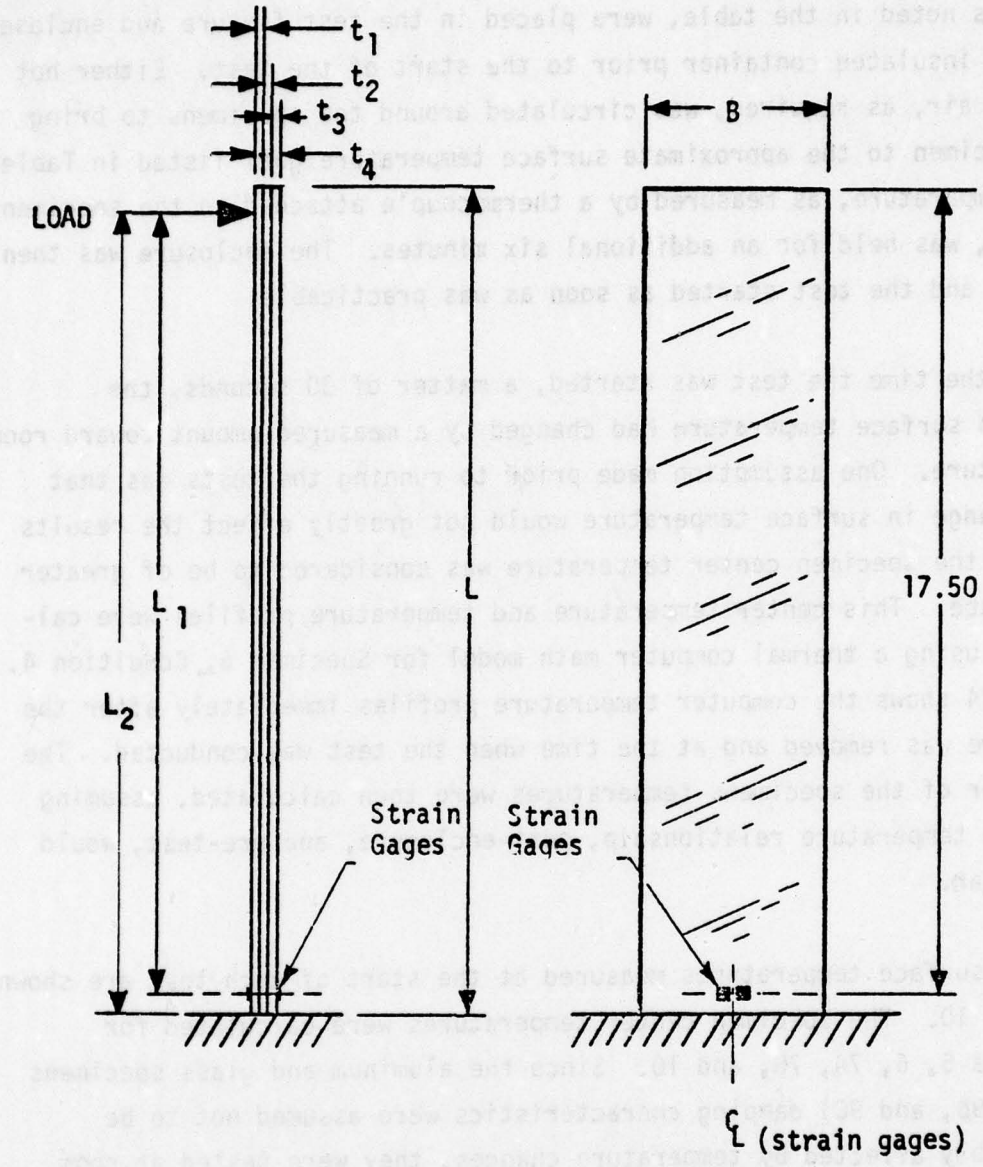

Figure 23. Damping beam dimensional measurement locations.

temperature goals noted in Table 3, Section II. Those specimens, 5, 6, 7A, 7B, 10 and 12, that were to be tested at three different temperature goals as noted in the table, were placed in the test fixture and enclosed with an insulated container prior to the start of the test. Either hot or cold air, as required, was circulated around the specimens to bring the specimen to the approximate surface temperature goal listed in Table 10. This temperature, as measured by a thermocouple attached to the specimen surface, was held for an additional six minutes. The enclosure was then removed and the test started as soon as was practicable.

By the time the test was started, a matter of 30 seconds, the specimen surface temperature had changed by a measured amount toward room temperature. One assumption made prior to running the tests was that this change in surface temperature would not greatly effect the results because the specimen center temperature was considered to be of greater importance. This center temperature and temperature profiles were calculated using a thermal computer math model for Specimen 6, Condition 4. Figure 24 shows the computer temperature profiles immediately after the enclosure was removed and at the time when the test was conducted. The remainder of the specimens temperatures were then calculated, assuming that the temperature relationship, post-enclosure, and pre-test, would be similar.

The surface temperatures measured at the start of each test are shown in Table 10. The specimen center temperatures were calculated for Specimens 5, 6, 7A, 7B, and 10. Since the aluminum and glass specimens (8, 9A, 9B, and 9C) damping characteristics were assumed not to be appreciably affected by temperature changes, they were tested at room temperature only.

DATA DOCUMENTATION AND ASSESSMENT

During each damping beam test, data were compiled and assessments made regarding the accuracy of the test equipment, recording apparatus and problems associated with the test program.

TABLE 10. TEMPERATURE GRADIENT FOR DAMPING BEAMS

TEST CONDITION NUMBER *	SPECIMEN NUMBER	SPECIMEN TEMPERATURE GOAL (°F)	SPECIMEN SURFACE TEMP (°F) (MEASURED)	CENTER OF SPECIMEN - TEMP (°F) (CALCULATED)
1	5	- 35	- 10	- 32
2		75	65	65
3		195	127	180
4	6	- 35	- 10	- 30
5		75	76	76
6		195	162	187
7a	7A	- 35	- 20	- 33
8a		75	75	75
9a		195	171	190
7b	7B	- 35	- 21	- 34
8b		75	66	66
9b		195	172	190
11a	8	75	75	75
11b		75	75	75
89a.3	9A	75	75	75
89a.6		75	75	75
89b.1	9B	75	78	78
89b.2		75	78	78
89b.3		75	75	75
90	10	75	75	75
91		- 35	- 16	- 30
92		200	176	197
97	12	75	75	---
101		- 35	- 30	---
103		195	135	---
110	9C	75	75	---

*See Table 3, Section II.

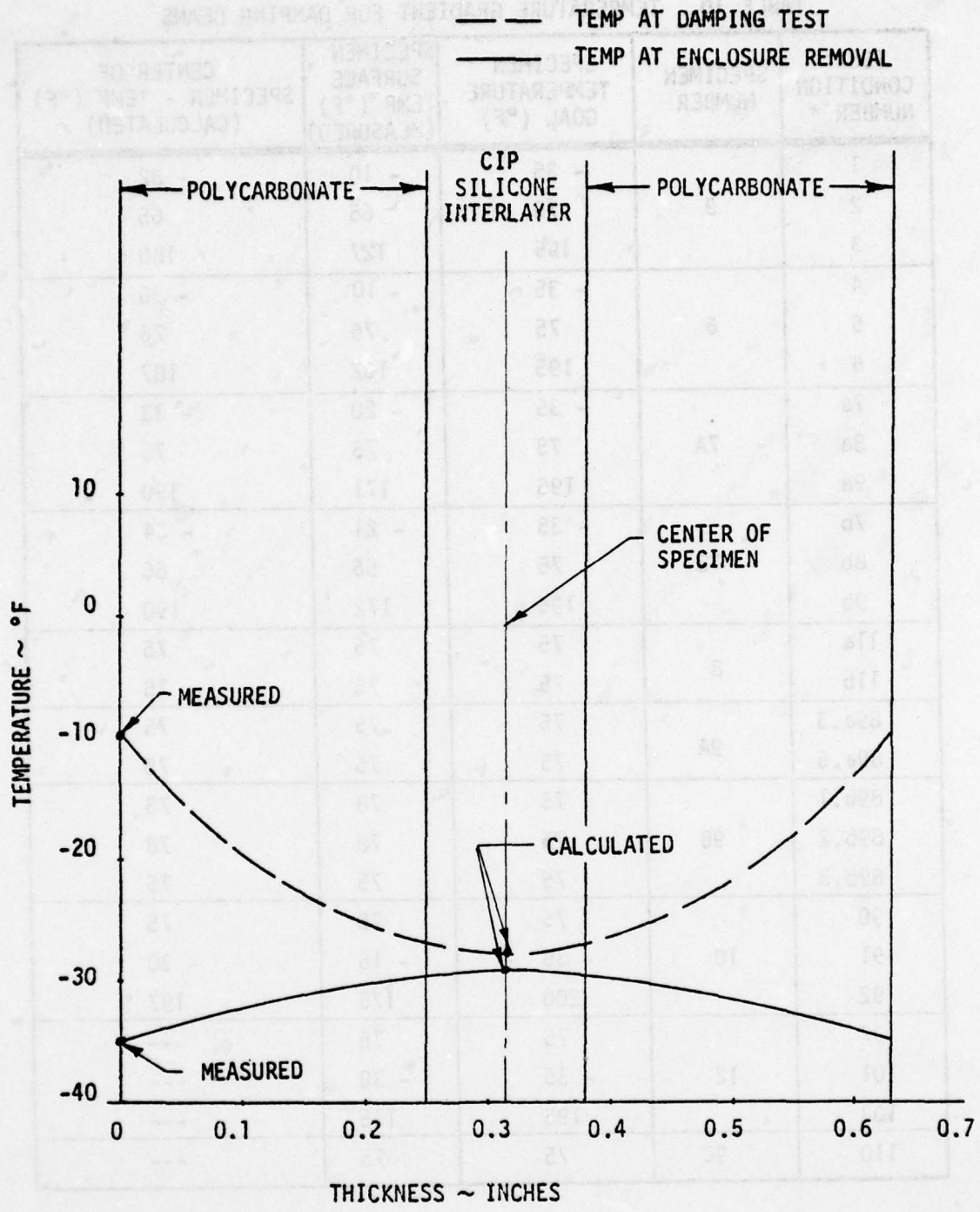

Figure 24. Calculated temperature profile for Specimen 6, Condition 4, damping beam test.

The damping beam test variables are graphically illustrated in Figure 25 and are tabulated in Table 11.

Test Results

Tables 11A, B, and C present the test results for each identified damping beam specimen including specimen number, specimen type (whether the beam is of laminate or monolithic construction), and test condition number. Also provided are reference values for the structural plies, Poisson's Ratio (ν) and modulus of elasticity (E). Overall values for the laminates were not required within this report. Also ν and E values for the interlayer materials were not required.

This table provides information for the following:

- The measured surface temperatures (T) at the instant the damping tests started (see Table 10 for the calculated temperature at center).

- The load (P) required to deflect the end of each specimen some displacement (δ_o) as depicted in Figure 25.

- The first rebound deflection (δ_1), was obtained by factoring method, derived by comparing the initial beam displacement amplitude to its corresponding strain.

- The measured damped frequency (f_d) was determined (from the vibratory strain versus time recording) by counting the number of full cycles within a selected time span, and dividing this event by the time increment.

- The measured strain (ε_o) is that recorded static strain, near the beam base support, just prior to beam release. These data were used as a countercheck for comparison with that obtained through beam theory analysis for the monolithic beams.

AD-A054 463 DOUGLAS AIRCRAFT CO LONG BEACH CALIF F/G 11/9
DAMPING, STATIC, DYNAMIC, AND IMPACT CHARACTERISTICS OF LAMINAT--ETC(U)
DEC 77 G F RHODES F33615-75-C-3105
UNCLASSIFIED MDC-J6944 AFFDL-TR-76-156 NL

2 OF 3
AD
A054463

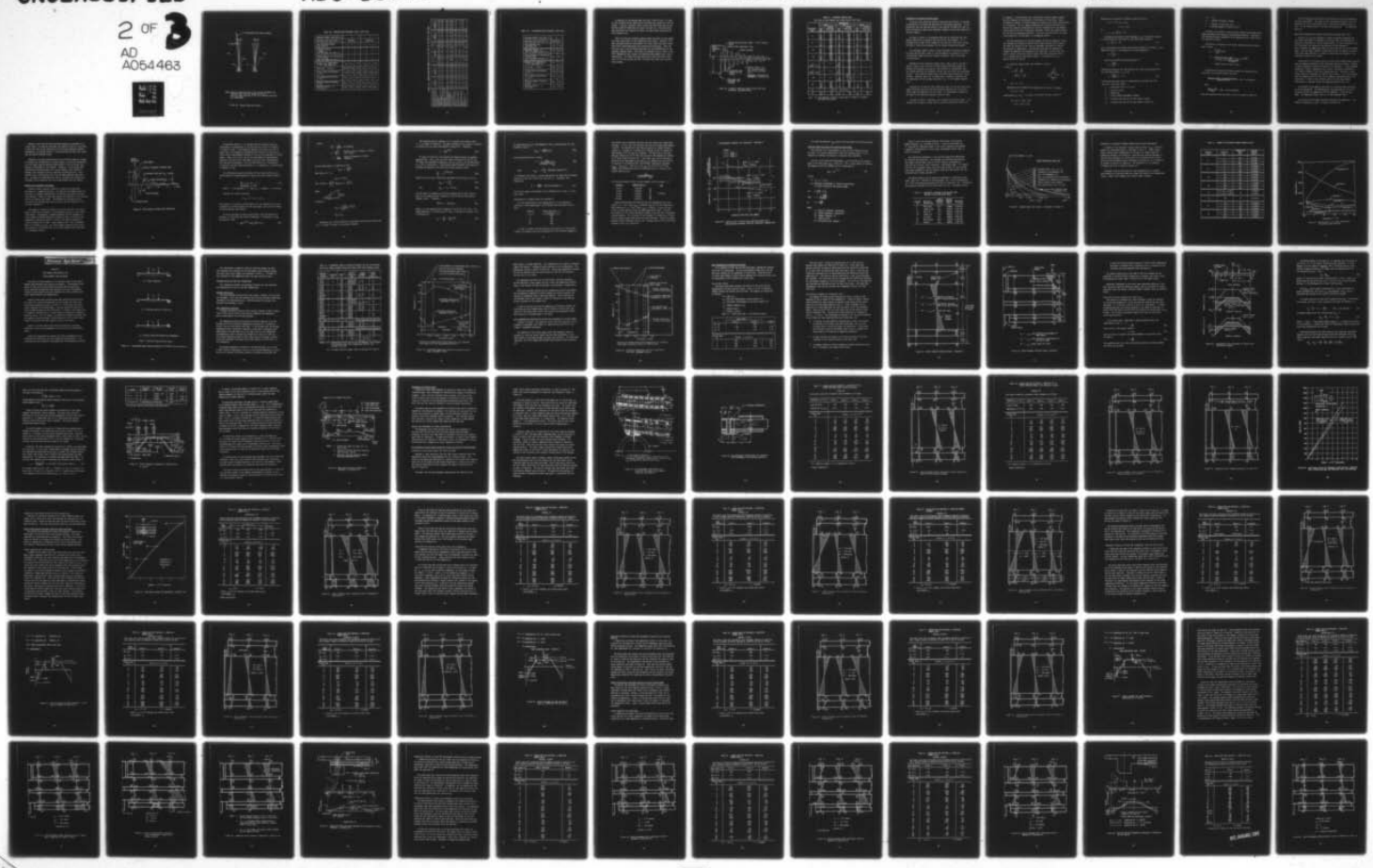

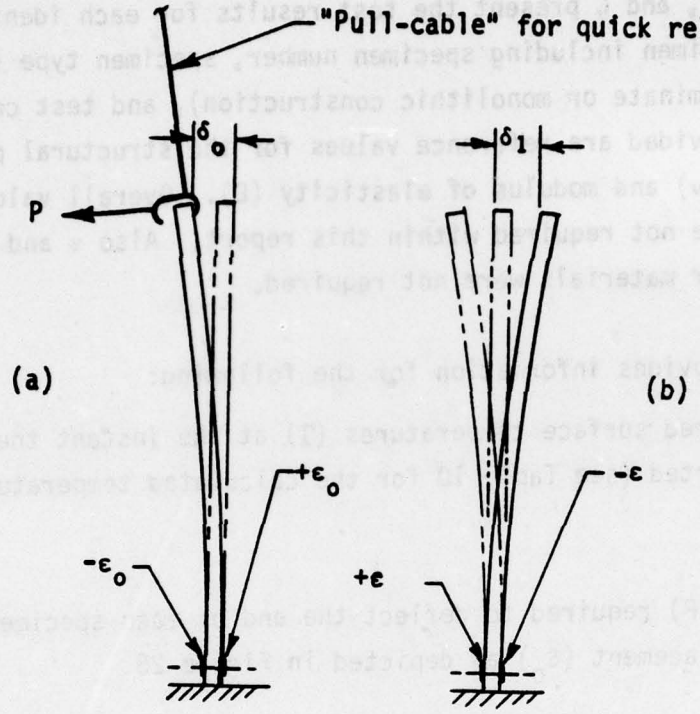

NOTE: View (a) shows the beam in its initial deflected (δ_o) position, just prior to release of load P.
View (b) shows the beam in its first rebound deflected (δ_1) mode-shape.

Figure 25. Damping beam test method.

TABLE 11A. DAMPING BEAM SPECIMENS 5 AND 6 TEST DATA.

Specimen Number (see Table 1)	5			6		
Specimen Type (see Table 1)	Laminate			Laminate		
Test Condition Number (See Table 3)	1	2	3	4	5	6
Poisson's Ratio, ν (Ratio) (Ref MIL-HDBK-17A, Part II)	-	-	-	-	-	-
Tension Modulus of Elasticity, E ($\times 10^{-5}$ psi) (Ref. MIL-HDBK-17A, Part II)	-	-	-	-	-	-
Surface Test Temperature, T (°F), (see Table 10)	-10	65	127	-13	76	162
Test Load, P (Lbs.)	19.51	17.93	11.17	8.6	6.7	6.7
Initial Beam Displacement, δ_0 (in.)	0.510	0.510	0.515	0.495	0.505	0.560
First Rebound Deflection, δ_1 (in.)	0.33	0.53	0.51	0.59	0.54	0.45
Measured Damped Frequency, f_d (H_z)	18.2	17.0	15.0	13.9	12.6	12.2
Measured Strain, ε_0 (μ in./in.)	1720	1607	1451	1138	1130	1284

TABLE 11B. DAMPING BEAM SPECIMENS 7A, 7B, 9A, 9B, 9C, 10, AND 12 TEST DATA

Specimen Number (see Table 1)	7A			7B			9A		9B			9C	10			12		
Specimen Type (see Table 1)	Monolithic			Monolithic			Monolithic						Monolithic			Monolithic		
Test Condition No. (see Table 3)	7a	8a	9a	7b	8b	9b	89a.3	89a.6	89b.1	89b.2	89b.3	110	90	91	92	101	97	103
Poisson's Ratio, ν (Ref. MIL-HDBK-17A, Part II)	0.38	0.38	0.38	0.38	0.38	0.38	0.22	0.22	0.22	0.22	0.22	0.22	0.35	0.35	0.35	0.38	0.38	0.38
Tension Modulus of Elasticity, E ($\times 10^{-5}$ psi) (Ref. MIL-HDBK-17A, Part II)	3.66	3.41	3.25	3.66	3.41	3.25	10	10	10	10	10	10	4.0	8.0	1.8	3.66	3.41	3.25
Surface Test Temperature, T (°F) (see Table 10)	-20	75	171	-21	66	172	75	75	78	78	75	75	75	-16	176	-30	75	135
Test Load, P (LB)	19.5	16.38	13.13	21.47	18.67	15.36	477	903	200	302	828	–	25.8	45.8	11.1	2.12	1.75	1.50
Initial Beam Displacement, δ_0 (in.)	0.591	0.576	0.579	0.485	0.521	0.485	0.470	–	0.493	0.611	1.70	0.50	0.507	0.406	0.305	1.0	1.0	1.0
First Rebound Deflection, δ_1 (in.)	0.66	0.65	0.54	0.63	0.47	0.52	0.43	–	0.22	0.25	–	0.11	0.31	0.25	0.21	–	–	–
Measured Damped Frequency, f_d (H_z)	18.3	17.4	16.4	19.3	18.2	17.4	56	–	42.2	38.1	–	23.8	25.0	28.6	19.4	6.98	7.22	6.62
Measured Strain, ε_0 (μ in./in.)	1608	1429	1407	1525	1515	1365	861	2827	563	849	2432	–	1047	1470	1470	845		

TABLE 11C. AIR DAMPING BEAM SPECIMEN 8 TEST DATA.

Specimen Number (see Table 1)	8	
Specimen Type (see Table 1)	Monolithic	
Test Condition No. (see Table 3)	11a	11b
Poisson's Ratio, ν (Ref. MIL-HDBK-17A,Part II)	0.33	0.33
Tension Modulus of Elasticity E ($x10^{-5}$ psi) (Ref. MIL-HDBK-17A,Part II)	104	104
Surface Test Temperature, T (°F) (see Table 10)	75	75
Test Load, P (lbs.)	24.8	60.6
Initial Beam Displacement, δ_0 (in.)	0.494	0.998
First Rebound Deflection, δ_1 (in.)	0.63	1.09
Measured Damped Frequency, f_d (H_z)	23.1	23.2
Measured Strain, ε_0 (μ in./in.)	516	1047

In addition to the damping beam test data listed in Table 11, data for the vibratory strain amplitude of selected peak numbers are also required. A typical vibratory strain versus time data recording and the various points of definition are shown in Figure 26. The half-cycled peak amplitudes are numbered as shown, with peak number one being the first rebound point.

Table 12 lists the vibratory damping beams test data of peak numbers and strain amplitudes for the temperature goals noted. Generally (for data averaging accuracy requirements) four peak points and their associated strain double amplitudes were measured and tabulated. These raw data are used in the following subsection for the determination of the specimens damping ratios. Note that for Specimen 5 and 6, shown in the 195°F temperature data column, the beginning peak numbers were 4 and 6, respectively. For these two cases the earlier peak point strain data were not utilized because the data indicated that there were secondary waves present.

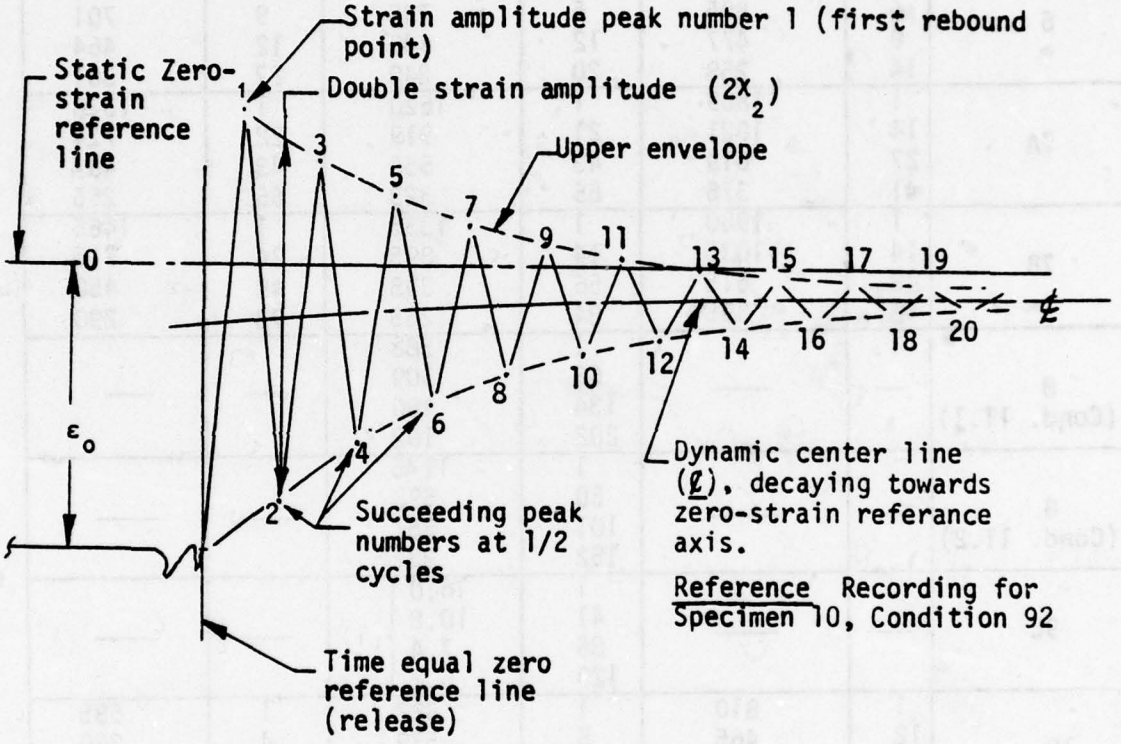

Figure 26. A typical vibratory strain versus time data recording and definitions.

TABLE 12. VIBRATORY DAMPING BEAM

TEST DATA OF PEAK NUMBERS AND STRAIN DOUBLE AMPLITUDES

SPECIMEN NO.	TEMPERATURE					
	-35°F		RT		195°F	
	PEAK NO.	STRAIN AMPLITUDE μ in./in.	PEAK NO.	STRAIN AMPLITUDE μ in./in.	PEAK NO.	STRAIN AMPLITUDE μ in./in.
5	1	1125	1	1700	4	1459
	15	643	12	1049	14	989
	30	370	26	579	30	531
	45	225	39	338	47	289
6	1	1357	1	1210	6	1042
	4	895	6	735	9	701
	9	477	12	440	12	464
	14	258	20	240	27	301
7A	1	1809	1	1620	1	1326
	14	1021	21	919	22	724
	27	619	43	555	43	434
	41	376	65	323	66	265
7B	1	1980	1	1335	1	1465
	14	1035	14	895	24	715
	28	615	56	395	48	450
	42	395	84	265	72	290
8 (Cond. 11.1)	—	——	1	588	—	—
			66	309		
			134	180		
			202	102		
8 (Cond. 11.2)	—	——	1	1145	—	—
			50	598		
			101	351		
			152	232		
9C	—	——	1	16.0 (1)	—	—
			41	10.8		
			86	7.4		
			129	5.2		
10	1	810	1	882	1	585
	12	465	5	539	4	360
	23	280	9	333	8	190
	36	160	14	181	12	105
11	(N O T U S E D)					
12	1	119	1	124	1	100
	45	26	51	49	29	42

NOTE: (1) Accelerometer readings of amplitude in number of recorded divisions (no scale).

Assessment of Testing and Data Output

Since each test condition could be monitored very closely it provided an opportunity to observe the operation of the testing apparatus. It was determined that the specimen having a high modulus of elasticity such as glass, aluminum, or very thick laminates, tended to force some rotation of the base support.

As noted in Table 11, on occasion there was an indication that the rebound deflection was greater than the initial displacement. It is believed that at the initial release of the load (P), there was a slight increase in load which accounted for the larger rebound displacement.

Two specimens noted in Table 11 were laminated of dissimilar materials for which the Poisson's ratio (ν) and the modulus of elasticity (E) had insignificant usage within this report; therefore, these values were not determined.

Specimen 9A, test condition numbers 89a.1, 89a.2, 89a.4, and 89a.5, noted in Table 3, were run but the strain gage recordings showed the presence of secondary wave motion, that resulted in unacceptable data. The clamped base was re-tightened, and the test was re-run for acceptable results. Test condition numbers 89a.3 and 89a.6 were successfully accomplished. Condition 89a.6 was a rupture test; therefore, readings were not obtainable for the rebound deflection (δ_1), or the damped frequency (f_d).

Specimen 9C utilized for Test Condition Number 110 did not have strain gages installed since the time and available resources did not justify strain gage instrumentation of this beam. An accelerometer attached to the beam tip provided the necessary vibratory data.

As noted in Table 1, Specimen 8 was a monolithic aluminum plate. This specimen was included in these tests to provide information relative to

air damping. Aluminum beams have insignificant internal damping characteristics because of the material's high modulus of elasticity. Hence, the apparent damping in aluminum beams was assumed to be totally attributable to air damping. This air damping component was required specifically so that the air damping characteristics could be screened out of the damping values obtained for the transparency specimens, leaving the damping values for the basic transparency materials. This was true particularly for monolithic materials, as described in a subsequent section.

With the undertaking of any test program, errors are expected. Since this program was designed to obtain strain gage readings during loading and after the release of the load, an assessment was made to determine the accuracy of these tests. Calculations were made for comparative purposes to determine the accuracy of the test data. In this case, the beam is totally within the elastic range, hence the calculated strain ε_c, is proportional to the applied load, P. An expression for ε_c may be derived as follows:

In a biaxial stress field, with stresses f_1 and f_2:

f_1 and f_2,

$$\varepsilon_1 = \frac{f_1}{E} - \nu\frac{f_2}{E}$$

$$= \frac{1}{E}[f_1 - \nu f_2]$$

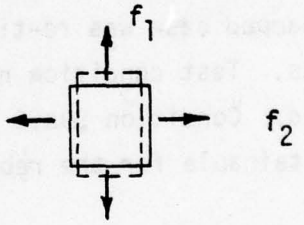

or,

$$E\varepsilon_1 = f_1 - \nu f_2 .$$

Rearranging this equation, the expression for stress f_1 becomes

$$f_1 = E\varepsilon_1 + \nu f_2 .$$

Substituting $f_2 = E\varepsilon_2 + \nu f_1$, which is similarly derived, results in

$$f_1 = E\varepsilon_1 + \nu\,(E\varepsilon_2 + \nu f_1)$$

$$= E\varepsilon_1 + \nu E\varepsilon_2 + \nu^2 f_1 .$$

Rearranging this equation to separate stress and strain:

$$f_1 (1 - \nu^2) = E\varepsilon_1 + \nu E\varepsilon_2$$

$$= E (\varepsilon_1 + \nu\varepsilon_2)$$

or,

$$\varepsilon_1 + \nu\varepsilon_2 = \frac{f_1}{E} (1 - \nu^2)$$

Considering the lateral strain component, $\nu\varepsilon_2$, as negligible results in an expression for the strain in the longitudinal direction

$$\varepsilon_1 = \frac{f_1}{E} (1 - \nu^2) . \qquad (14)$$

Now, in any beam of unit-width cross-section properties of height, t_1, and moment-of-inertia I, and subjected to a bending moment, M:

$$f_1 = \frac{M t_1}{2I} .$$

Referring to definitions below results in

$$f_1 = \frac{PL_1 t_1}{2I} . \qquad (15)$$

Substituting Equation (15) into Equation (14) gives the expression for the calculated strain, $\varepsilon_1 = \varepsilon_c$ as:

$$\varepsilon_c = \frac{PL_1 t_1}{2EI} (1 - \nu^2) \qquad (16)$$

which establishes that strain is proportional to the beam load (for monolithic beams only) where:

ε_c = calculated strain (μ in./in.)

ν = Poisson's ratio

P = loads (lb)

δ_o = initial beam displacement (inches)

L_1 = distance from load (P) to strain gages (inches)

L_2 = distance from load (P) to beam support (inches) ref.

M = PL_1

t_1 = specimen thickness (inches)

E = modulus of elasticity (psi)

I = specimen moment of inertia ($in.^4$).

Initially, this series of tests was also aimed at evaluating strain gage performance when mounted on polycarbonate materials. Specimen 7A was selected to make a comparison of the measured strain values versus the theoretical values.

Substituting in Equation 16 the actual required data from Tables 9 and 11 gives:

$$\varepsilon_c = \frac{PL_1\, t_1}{2\, EI}(1-\nu^2)$$

$$\varepsilon_c = \frac{16.08 \times 17.15 \times 0.621}{2 \times 3.41 \times 10^5 \times \frac{8.03 \times 0.621^3}{12}}(1-0.38^2)$$

$$= .001341 \text{ in/in or } 1341\ \mu \text{ in/in.}$$

To determine the percent difference between the measured versus calculated, the following formula was used:

$$\frac{\text{Measured Strain - Calculated Strain}}{\text{Measured Strain}} \times 100 = \%\ \text{Difference}$$

Then:

$$\frac{1429 - 1341}{1429} \times 100 = 6.16\%\ \text{Difference}$$

Where the measured strain was 1429 μ in./in. as noted in Table IIB.

The 6.16 percentage difference was considered to be within reasonable accuracy requirements. The cause of this percentage difference could be attributed to either experimental error, theoretical equation error, or both. It was assumed that all the data collected had a similar degree of accuracy.

ANALYTICAL DEVELOPMENT OF DAMPING RATIOS AND AMPLITUDE DECAY TIME

Analysis of a typical laminated aircraft windshield, employing the Bird Impact Math Model of Reference 1, requires that the windshield or canopy be represented by a finite element model, in which structural plies and interlayers are separately represented by finite elements. Mass, stiffness and damping matrices are calculated for the finite element model. The math model computer program then solves an equation of motion, based upon these matrices, as a means of predicting the response of the windshield system to bird impact.

Calculations of the damping matrix for the finite element model requires that the damping properties of the interlayer material be known. Damping in most structures, including windshields, is nonlinear. In the laminated windshield, however, damping has only a small influence on response to bird impact, because of the short loading duration. Therefore, linear viscous damping is assumed, to simplify the analysis. It is also assumed that the damping matrix for any finite element, representing part of an interlayer, is equal to the stiffness matrix for the same element multiplied by a constant called the damping/stiffness ratio, h_I.

The purpose of the damping beam tests is to provide data from which h_I can be determined. The determination is accomplished by first calculating the ratio of damping to critical damping, γ, from the test data. The damping/stiffness ratio h_I is then computed from γ.

This section of the report explains the method of computing γ. The method of computing h_I from γ is given in Section VII.

Because of the fact that the interlayer damping was assumed to be linear, when it is actually nonlinear, the measured value of γ was found to vary with time as the vibration of the test beam gradually decayed. Consequently, an average value of γ was established for each test, based upon the actual measured values.

Although a real beam theoretically has an infinite number of degrees of freedom, and consequently an infinite number of modes and frequencies, only the lowest mode was excited significantly in any particular test, because of the method of tip release. Therefore, it was assumed that the cantilevered beam behaves as a viscous damped, single degree of freedom, free vibration system in deriving the damping ratio. Which implies, and is confirmed by test, that the beam specimens obey Hooks Law. The beam tip displacement can then be assumed to be directly proportional to the reading of the strain gage located near the support.

Damping Ratio Equation Development

Figure 27 shows a typical history of a beam strain amplitude. The motion is a damped oscillation. The positive and negative peaks of the waves are numbered consecutively as indicated, beginning with the first rebound. These half wave peak numbers are important in the development of an accurate math model. For determining the damping ratio, a time span was selected away from any noise, one end labeled "p" and the other labeled "q".

The method of releasing the beam tip was such that only the lowest mode of vibration was present in the subsequent motions, to any significant degree. Consequently, standard equations for the response of a single degree of freedom mechanical system can serve as the basis for computing an effective value of γ, which is the ratio of damping to critical damping for the beam. Note, however, that γ for a laminated beam is an effective value. The actual damping constant of the interlayer material is obtained from γ by a finite element method described in a subsequent section.

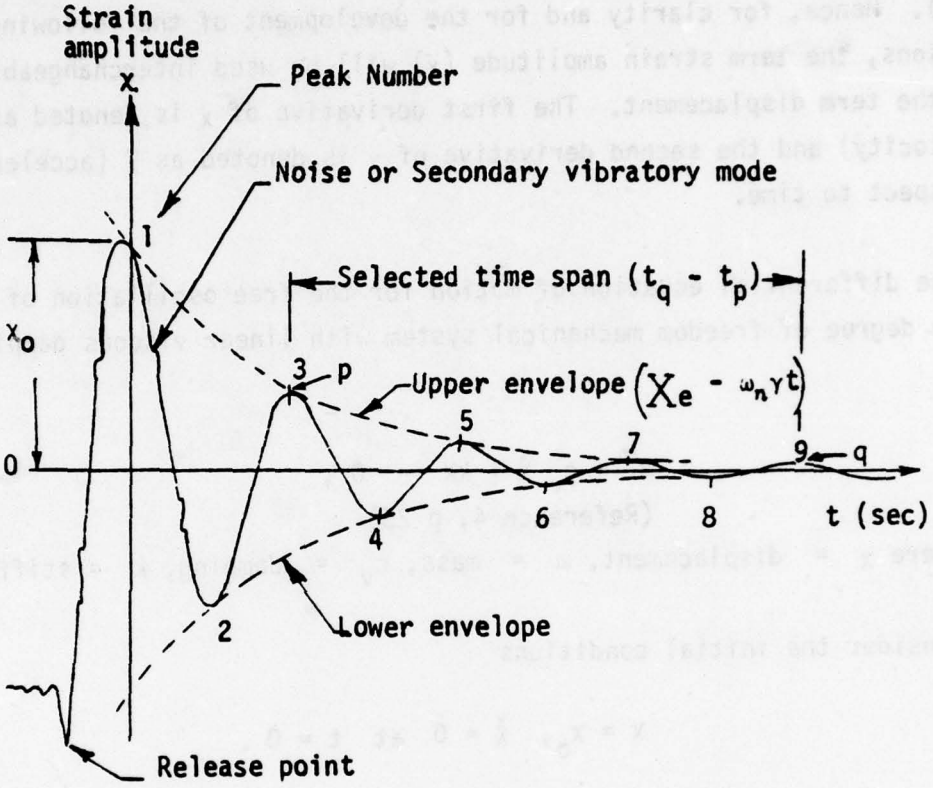

Figure 27. Time history of beam strain amplitude

As mentioned earlier, it is assumed that the vibratory beam tip displacement is proportional to the beam strain, next to its support, in respect to time. This assumption appears to be valid, as will be shown later, when comparing the damping ratio results for Specimen 12 (which had an accelerometer attached to its tip) with Specimen 7B (strain gaged). Hence, for clarity and for the development of the following equations, the term strain amplitude (χ) will be used interchangeably with the term displacement. The first derivative of χ is denoted as $\dot{\chi}$ (velocity) and the second derivative of χ is denoted as $\ddot{\chi}$ (acceleration) in respect to time.

The differential equation of motion for the free oscillation of a single degree of freedom mechanical system with linear viscous damping is

$$m\ddot{X} + c_v \dot{X} + kX = 0 , \qquad (17)$$

(Reference 4, p 25)

where χ = displacement, m = mass, c_v = damping, k = stiffness.

Consider the initial conditions

$$X = X_o, \quad \dot{X} = 0 \quad \text{at} \quad t = 0 .$$

Then Equation 17 provides a satisfactory basis for determining the ratio of damping to critical damping for the test beams, since only the lowest vibration mode was significant.

It can be verified, by direct substitution, that the solution of Equation 17, satisfying the initial conditions, is (Reference 4, Page 26, Equation 1-44)

$$\chi = Xe^{-\omega_n \gamma t} \sin(\omega_n \sqrt{1-\gamma^2}\, t - \phi) , \qquad (18)$$

where

$$X = \frac{-x_0}{\sqrt{1-\gamma^2}} \quad \text{(a constant)}$$

$$\omega_n = \sqrt{\frac{k}{m}} \quad \text{(natural angular frequency, radians/unit time),}$$

$$\gamma = \frac{c_v}{2\sqrt{km}} \quad \text{(ratio of damping to critical damping),}$$

and the phase angle ϕ is defined so that

$$\tan \phi = \frac{\sqrt{1-\gamma^2}}{-\gamma} .$$

Note that, at $t = 0$,

$$x_{t=0} = -X \sin \phi .$$

But, if $\tan \phi = \frac{\sqrt{1-\gamma^2}}{-\gamma}$, then $\sin \phi = \sqrt{1-\gamma^2}$,

where,

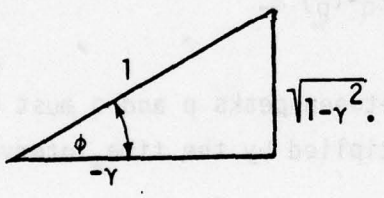

Therefore,

$$x_{t=0} = -\left(\frac{-x_o}{\sqrt{1-\gamma^2}}\right)\sqrt{1-\gamma^2},$$

or

$$x_{t=0} = x_0 .$$

Therefore, the initial condition is satisfied, and the strain amplitude at $t = 0$ shown in Figure 27 is correctly labeled.

The response given by Equation 18 is a decaying oscillation, when $\gamma < 1$, as shown in Figure 27. The upper envelope of this motion is obtained by letting the sine term from Equation 18 equal one. Therefore,

$$x = Xe^{-\omega_n \gamma t} \quad . \tag{19}$$

As shown in Figure 27, the positive and negative peaks are numbered consecutively. Let t_p and t_q be the time of occurrence of the p^{th} and q^{th} peaks (not necessarily adjacent), and let x_p and x_q be the amplitudes at t_p and t_q respectively. Substituting these variables into Equation 19 provides two equations, and division of these equations gives

$$\frac{x_p}{x_q} = e^{\omega_n \gamma (t_q - t_p)} \quad . \tag{20}$$

Define the "half cycle" logarithmic decrement for the peaks p and q as

$$\delta_{Lpq} = \ln \frac{x_p}{x_q} \quad , \tag{21}$$

then

$$\delta_{Lpq} = \omega_n \gamma (t_q - t_p) \quad . \tag{22}$$

Now the number of complete oscillations between peaks p and q must be equal to the damped natural frequency multiplied by the time interval between p and q. Therefore,

$$\frac{1}{2}(q-p) = f_d (t_q - t_p) \quad , \tag{23}$$

where f_d is the damped natural frequency in cycles per unit time. This damped frequency, in radians per unit time, is defined by (Equation 1-42 of Reference 4):

$$f_d = \frac{\omega_d}{2\pi} = \frac{\omega_n}{2\pi} \sqrt{1-\gamma^2} \tag{24}$$

By substituting $(t_q - t_p)$ from Equation 23 and f_d from Equation 24, into Equation 22 gives

$$\delta_{Lpq} = \frac{\pi\gamma}{\sqrt{1-\gamma^2}}(q-p) \quad . \tag{25}$$

Solving Equation 25 for γ results

$$\gamma = \frac{\delta_{Lpq}}{\sqrt{\pi^2(q-p)^2 + \delta^2_{Lpq}}} \tag{26}$$

where $\delta_{Lpq} = \ln \frac{x_p}{x_q}$ (reference Equation 21)

In literature, the symbol δ_L usually designates the logarithmic decrement occurring in one full cycle, i.e., for q-p = 2. Therefore, from Equation 25

$$\delta_L = \frac{2\pi\gamma}{\sqrt{1-\gamma^2}} \quad \text{(See also Appendix C)} \tag{27}$$

This result agrees with Equation 3.24 of Reference [5], where γ is less than 0.0001.

Determination of Damping Ratio for Specimen 6

For the determination of the damping ratio (γ) for Specimen 6, Condition 5 (room temperature), the following test data from Table 12 apply

PEAK NO.	STRAIN AMPLITUDE (x) μ IN./IN.
1	1210
6	735
12	440
20	240

In order to present accurate damping ratio values to 5 significant figures, the damping ratio was calculated for five different segments of

oscillation over a selected time span, and then these five values were averaged. In this case, the selected time span was between peak numbers 1 and 20. The damping ratio was then calculated for segment Numbers 1 through 6, 1 through 12, 1 through 20, 6 through 20 and 12 through 20, approximately 1/3, 2/3 and full segments. The beginning of each segment was labeled as the p^{th} peak and the end of the segment was labeled as q^{th} peak (refer to Figure 27). From these data, the corresponding relative strain amplitude x_p at p and x_q at q segment ends were applied to Equation 21 to determine the "half-cycled" logarithmic decrement ($\delta_{Lpq} = \ln[x_p/x_q]$). Then this value δ_{Lpq} and the p^{th} and q^{th} peak numbers were substituted into the final Equation 26 to determine that segment damping ratio

$$\gamma = \frac{\delta_{Lpq}}{\sqrt{\pi^2(q-p)^2 + \delta_{Lpq}^2}}$$

The resulting damping ratios for each segment and the average γ is:

SEGMENT	DAMPING RATIO (Y)	γ_{AVG}
1⟶6	0.031720	
1⟶12	0.029260	
1⟶20	0.027092	0.027524
6⟶20	0.025439	
12⟶20	0.024110	

Similar calculations were made for tne low temperature test (condition 4, T = -35°, where γ_{AVG} = 0.040953) and for the high temperature test (Condition 6, t = 195°, where γ_{AVG} = 0.018947). Figure 28 shows a plot of these damping ratios for each temperature level. The plot for Condition 5 also shows horizontal segment lines with their corresponding peak numbers. The mid-point of each segment is plotted and a faired line is drawn through these points for each condition. Since this method produces smooth continuous curves, the γ average value of five significant figures is felt to be justified.

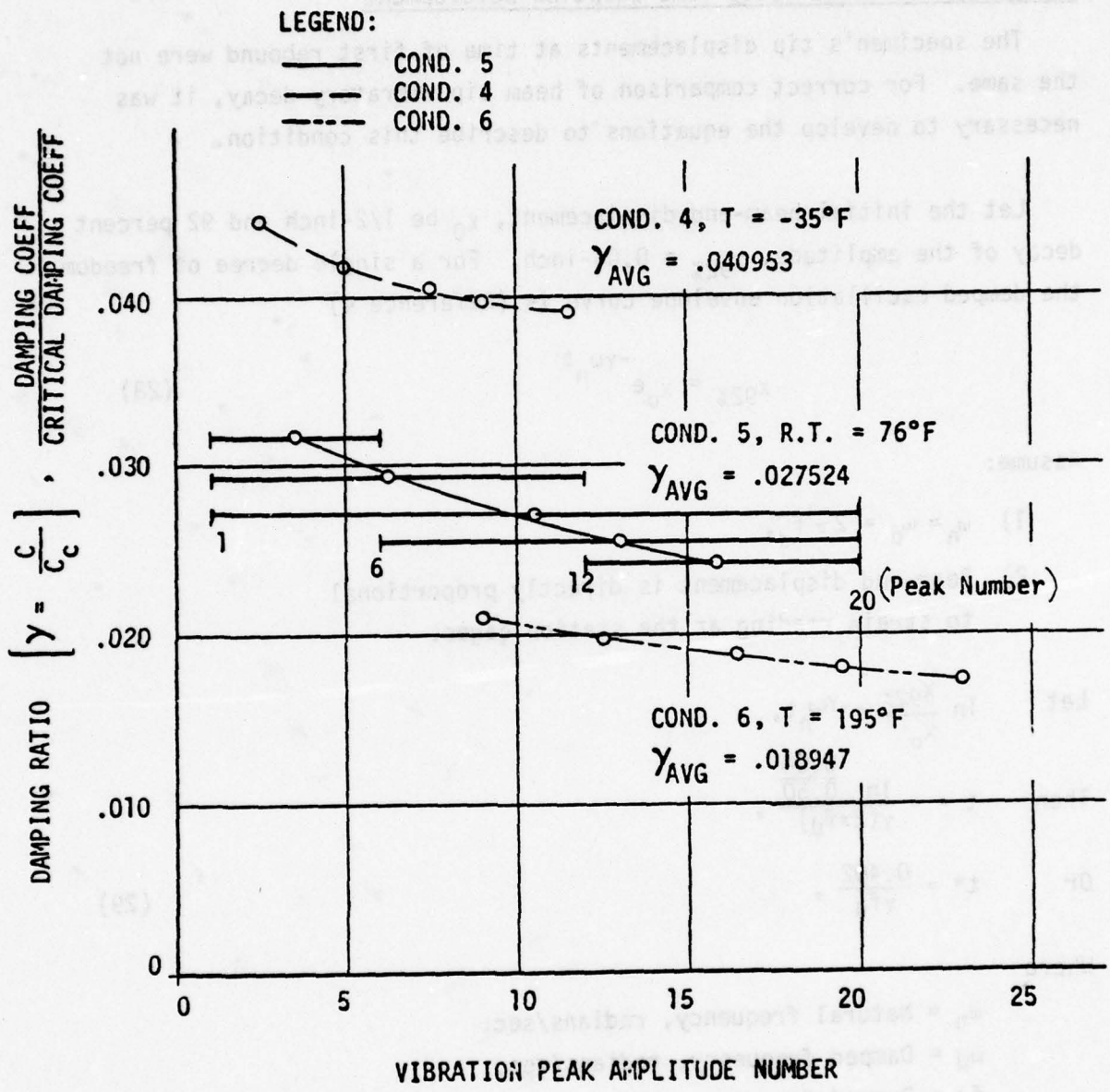

Figure 28. Damping ratio γ versus peak amplitude number for a polycarbonate laminate, with CIP interlayer, damping test.

The remaining specimen γ_{AVG} values were calculated by the same approach.

Vibratory Amplitude Decay Time Equation Development

The specimen's tip displacements at time of first rebound were not the same. For correct comparison of beam tip vibratory decay, it was necessary to develop the equations to describe this condition.

Let the initial beam-end displacement, x_0 be 1/2-inch and 92 percent decay of the amplitude, $x_{92\%}$ = 0.04-inch. For a single degree of freedom, the damped oscillation envelope curve is (Reference 4)

$$x_{92\%} = x_0 e^{-\gamma\omega_n t} \tag{28}$$

Assume:

1) $\omega_n \approx \omega_d = 2\pi f_d$,
2) Beam-end displacement is directly proportional to strain reading at the station gages.

Let $\ln \frac{x_{92\%}}{x_0} = -\gamma\omega_n t$,

Then $t = -\frac{\ln \frac{0.04}{0.50}}{\gamma(2\pi f_d)}$,

Or $t^* = \frac{0.402}{\gamma f_d}$, (29)

Where

ω_n = Natural frequency, radians/sec.
ω_d = Damped frequency, radians/sec.
f_d = Damped frequency, Hz
γ = Damping ratio
t^* = Calculated time, seconds.

Table 13 lists the specimen material description, the observed damped frequency, f_d, the damping ratio, γ, and the calculated time, t*, required for 92-percent decay of the initial beam-end displacement. A graphical representation of this data, displacement versus time, is shown in Figure 29.

The interesting phenomenon is the relative decay-time experienced by different beam materials. As expected, the aluminum beam required the longest time to decay from an initial beam-end displacement of 0.50-inch to 0.04-inch, which represents a 92-percent decay. The longest time for this 92-percent decay point was 5.883 seconds for the aluminum plate beam, Specimen 8; and the shortest time was 0.394 seconds for the stretched acrylic beam, Specimen 10.

The second longest time to decay and subsequent, in decreasing time order, were (7B) - Sierracin's Polycarbonate; (7A) - PPG's Polycarbonate; (5) - PPG's Polycarbonate Laminate with PPG-112 Interlayer; (6) - Sierracin's Polycarbonate Laminate with CIP Interlayer; and (10) - Stretched Acrylic.

TABLE 13. SPECIMENS 5 THROUGH 10 CALCULATED TIME FOR 92% INITIAL AMPLITUDE DECAY

SPECIMEN NO.	BEAM MAT'L DESCRIPTION	DAMPED FREQUENCY, f_d [HZ]	AVERAGE DAMPING RATIO	CALCULATED t* [SEC]
5	PPG'S LAM.	17.0	.013558	1.744 SEC
6	SIERR'S LAM.	15.0	.027524	0.974 SEC
7A	PPG'S PC	17.4	.008120	2.845 SEC
7B	SIERR'S PC	18.2	.006672	3.311 SEC
8	AL PLATE	23.1	.002958	5.883 SEC
9C	PPG'S GLASS	23.8	.003128	5.400 SEC
10	ACRYLIC	25.2	.038857	0.394 SEC

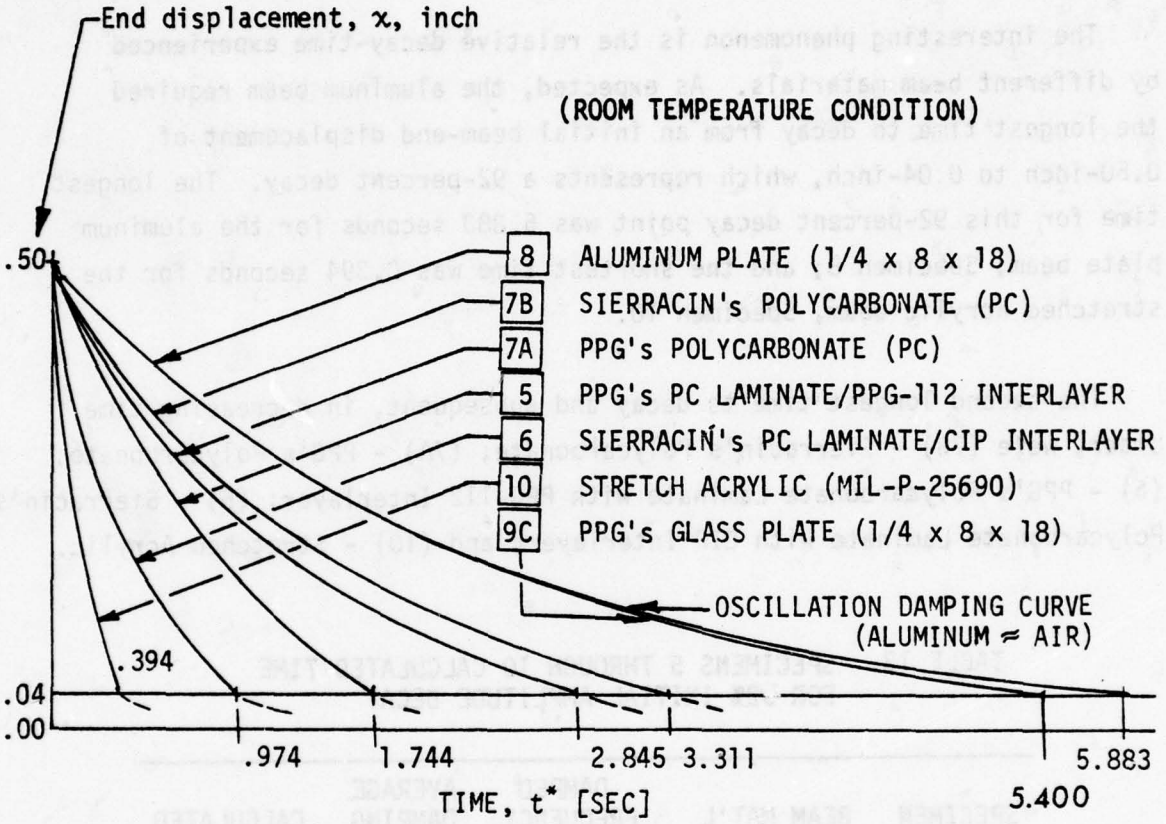

Figure 29. Damping beam test results. Specimens 5 through 10.

COMPARISON OF SPECIMENS' AVERAGE DAMPING RATIO VERSUS TEMPERATURE

A summary of the specimens' average damping ratios (γ_{avg}), condition numbers and temperature goals is provided in Table 14. These average damping ratios versus temperature are plotted on a common graph for comparison purposes, see Figure 30. Note that the aluminum specimen, 8, and the glass specimen, 9C, cruves show very low damping ratio values; these low valued damping ratios indicated, are mainly due to air damping, as assumed in Section VII analysis. The conversion of γ to damping/stiffness ratio (h) is shown in Section VII.

Specimens 8 and 9C were tested at room temperature only, because their modulus of elasticity does not change significantly with temperature change. Hence, their damping ratio should remain constant.

TABLE 14. SUMMARY OF SPECIMENS' AVERAGE DAMPING RATIOS

Specimen No.	Condition No.	Temperature Goal (°F)	Average Damping Ratio
5	1	-35	0.01165
	2	RT	0.01356
	3	195	0.01190
6	4	-35	0.040953
	5	RT	0.027524
	6	195	0.018947
7A	7a	-35	0.012542
	8a	RT	0.008120
	9a	195	0.007921
7B	7b	-35	0.012639
	8b	RT	0.006672
	9b	195	0.007399
8	11.1 (δ_0 = 0.63")	RT	0.002801
	11.2 (δ_0 = 1.09")		0.003376
9C	110	RT	0.002738
10	90	RT	0.038857
	91	-35	0.014805
	92	200	0.049654
12	97	RT	0.005884
	101	-35	0.011063
	103	195	0.009707

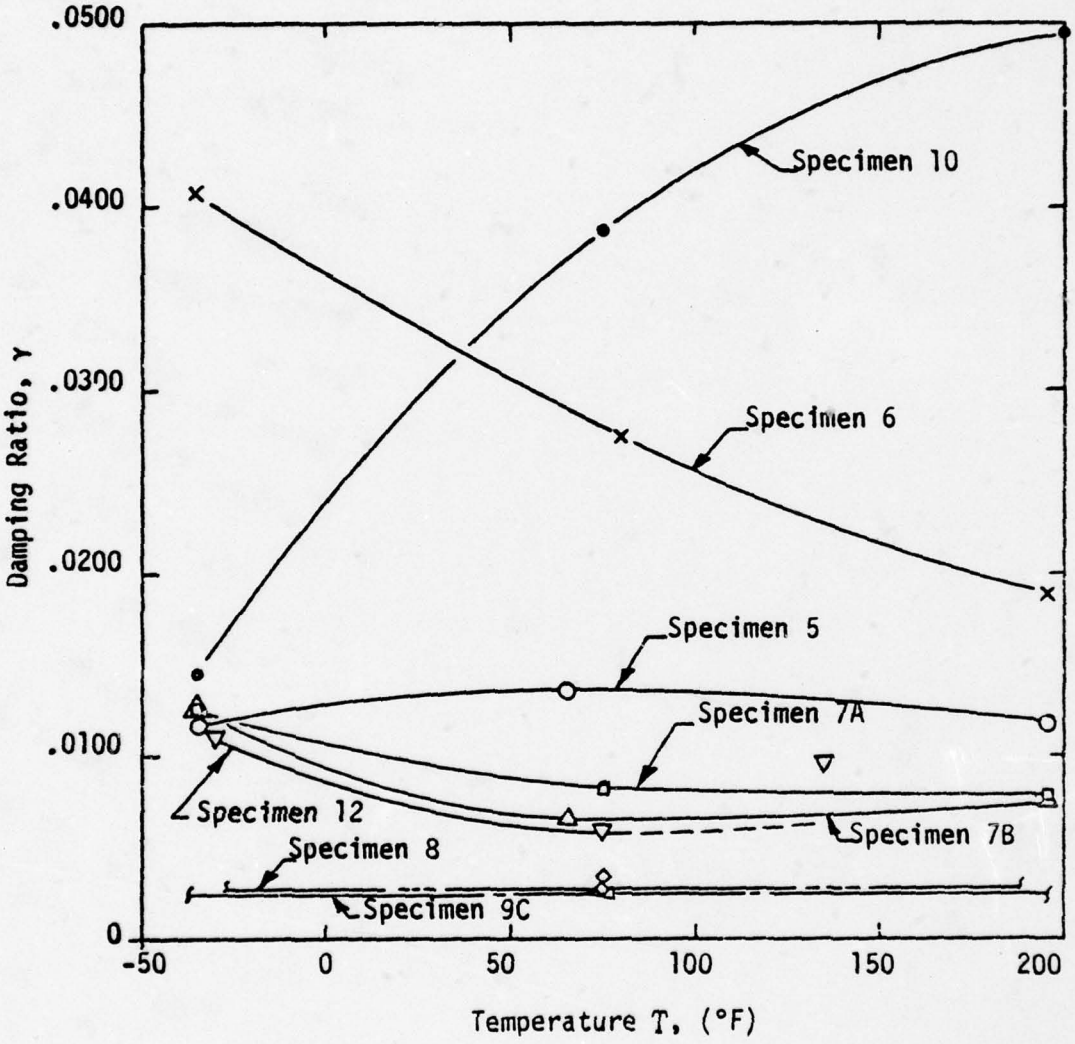

Figure 30. Damping Ratio (γ) versus temperature for damping beam specimens.

SECTION V

TEST RESULTS AND ANALYSIS FOR STATIC/DYNAMIC BEAM SPECIMENS

The series of tests covered in this section relate to the static/dynamic beam specimens test results and analysis. The purpose of this series of tests was to quantitatively evaluate the stress/strains within laminated transparency beam specimens that were instrumented internally and externally, and were subjected to various loading conditions, edge restraints and temperatures.

Figure 5 shows eight different beam edge restraint configurations. For simplicity, these configurations can be grouped into three basic beam loading diagrams as shown in Figure 31. These beams are either simply supported or fixed-end beams. The main purpose of testing the simply supported beams was for calibration. In theory, these beams have no tangential restraint; but, in real aircraft windshields, tangential loads may exist. For this reason, the beams were tested with either both end supports locked to prevent sliding inwards or with one end support locked in place and the other support free to slide inward.

Section II of this report described the objectives, specimens, conditions, set-ups, and procedures for this series of static/dynamic tests.

Section III described the rational and final development for the selection and installation of strain gages and thermocouples. Also described were the supporting instrumentation and documentation systems.

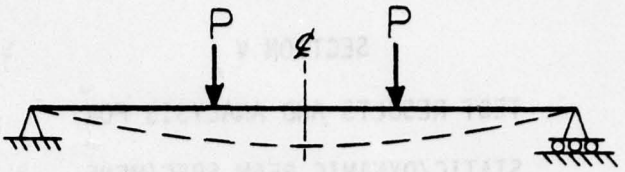

a) Simply Supported

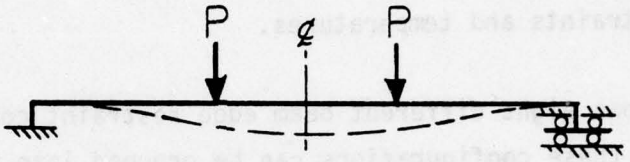

b) Fixed-end beam with single row

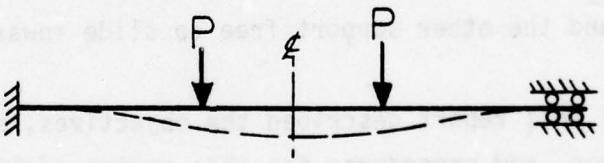

c) Fixed-end beam with double-row attachments

(Note: Fixed base condition not shown)

Figure 31. Instrumented beam loading diagrams for different edge restraints.

For convenience, a numerical index of condition numbers for each test specimen with reference to the forthcoming strain diagram figures and strain data table numbers are presented in Table 15. Included for each specimen are the temperature goals and edge restraint codes.

SPECIMEN DEFINITION AND TEST TEMPERATURES

This subsection presents the specimens selected for data reduction and presentation as well as the test temperatures.

Specimen Definition

Four beam specimen configurations were tested. However, the test data for Specimens 1 and 3 were not reduced since the data provided insufficient information for complete analysis. Sufficient data for analyses were obtained from Specimens 2 and 4.

Test Temperature Selection

A Douglas windshield transient heat transfer computer program, identified as E1GG, was utilized to analytically determine the temperature profile requirements for each beam specimen.

The temperature profiles selected for Sierracin Specimen 2 are the maximum and minimum windshield temperatures expected for a supersonic aircraft during flight below 8,000 feet. It was assumed that the maximum temperature occurs following a supersonic cruise and a subsequent high-speed descent to 8,000 feet; this is at Mach 0.85 in a hot atmosphere. The temperature profile through the windshield is shown in Figure 32. The minimum temperature shown in this figure occurs following a subsonic cruise and subsequent high-speed (Mach 0.85) descent to 8,000 feet in a cold atmosphere.

The maximum temperature selected for the PPG Specimen 4 was limited to 200°F external temperature, as this is the maximum temperature at which acrylic will maintain sufficient rigidity to prevent the specimen from

TABLE 15. A NUMERICAL INDEX OF CONDITION NUMBERS FOR THE 36-INCH BEAM TESTS WITH STRAIN DIAGRAM FIGURE AND STRAIN DATA TABLE NUMBERS LISTED.

COND NO. STATIC/ DYNAMIC	SPECIMEN NO.	TEMP(1) °F	EDGE(2) RESTRAINT CODE	STRAIN DIAGRAM FIG. NO.	STRAIN DATA TABLE NO.
13/14	2	-65	SR/SS-PIV	-	-
15/16		RT	SR/SS-PIV	37, 46	19
17/18		272	SR/SS-PIV	-	-
19/20	2	-65	SR/SB	55, 57	26
21/22		RT	SR/SB	37, 47, 57	20
23/24		272	SR/SB	56, 57	27
25/26	2	272	DR/SB	-	-
27/28		RT	DR/SB	37, 48	21
29S/29D		RT	DR/FB	49, 51	22
30/31		-65	DR/SB	-	-
32/33	4	-65	SR/SS-PIV	-	-
34/35		RT	SR/SS-PIV	45, 58, 59,	28
36/37		200	SR/SS-PIV	60, 61 -	-
38/39	4	-65	SR/SB	62, 65	29
40/41		RT	SR/SB	63, 65	30
42/43		200	SR/SB	64, 65	31
44/45	4	200	DR/SB	-	-
46/47		RT	DR/SB	-	35
48S/48D		RT	DR/FB	-	36
49/50		-65	DR/SB	-	-
51 62	1			Data Reduction not Required	
63/64	2	-65	SR/FB-S	52, 54	24
65/66		RT	SR/FB-S	50, 51, 54	23
67/68		272	SR/FB-S	53, 54	25
69 86	3			Data Reduction not Required	
81/82	4	-65	SR/FB-S	66	32
83/84		RT	SR/FB-S	67	33
85/86		200	SR/FB-S	68	34
107 A	2	RT	/SS	38, 41, 43,	17
107 B		RT	/SS-B	44 - 38, 42, 43, 44	18

NOTES: (1) Temperatures shown are for the environmental test chamber. For specimen actual test temperature profile, see Figures 32 and 33.

(2) For edge restraint codes, refer to Section III, Table 5.

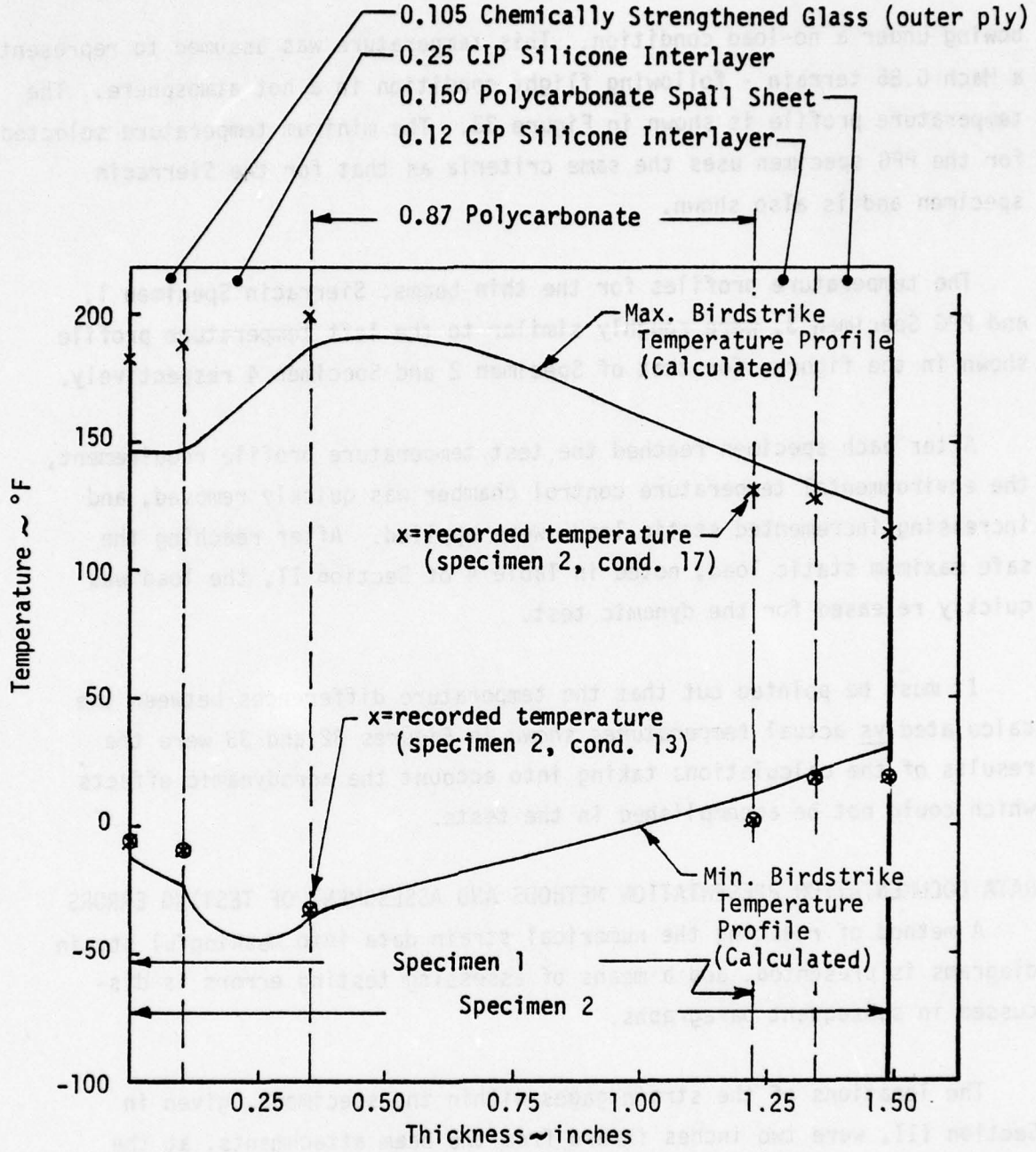

Maximum and minimum bending beam temperature for laminated thick beam, with 0.87 polycarbonate core-ply.

Figure 32. Windshield temperature profile as applied to test beam, specimens 1 and 2.

bowing under a no-load condition. This temperature was assumed to represent a Mach 0.85 terrain - following flight condition in a hot atmosphere. The temperature profile is shown in Figure 33. The minimum temperature selected for the PPG specimen uses the same criteria as that for the Sierracin specimen and is also shown.

The temperature profiles for the thin beams, Sierracin Specimen 1, and PPG Specimen 3, were roughly similar to the left temperature profile shown in the figures for that of Specimen 2 and Specimen 4 respectively.

After each specimen reached the test temperature profile requirement, the environmental temperature control chamber was quickly removed, and increasing incremented static loads were applied. After reaching the safe maximum static load, noted in Table 4 of Section II, the load was quickly released for the dynamic test.

It must be pointed out that the temperature differences between the calculated vs actual temperatures shown in Figures 32 and 33 were the results of the calculations taking into account the aerodynamic effects which could not be accomplished in the tests.

DATA DOCUMENTATION PRESENTATION METHODS AND ASSESSMENT OF TESTING ERRORS

A method of reducing the numerical strain data into meaningful strain diagrams is presented, and a means of assessing testing errors is discussed in subsequent paragraphs.

The locations of the strain gages within the specimens, given in Section III, were two inches inward from the beam attachments, at the beam midpoint, and midway between the above two locations. At these three locations, the strain gages were mounted back-to-back on each structural ply.

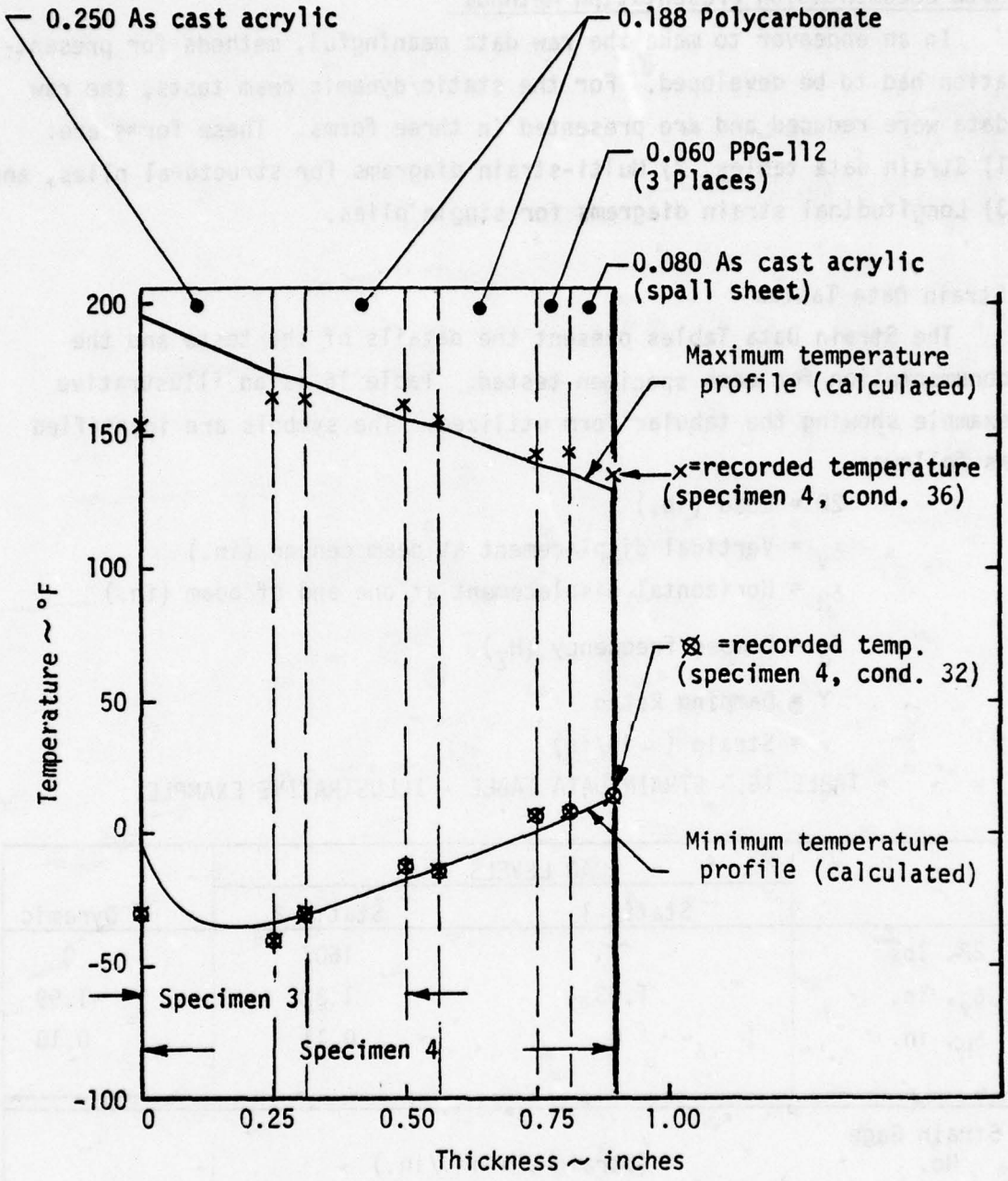

Maximum and minimum bending beam temperature for laminated thick beam, with multi-layers of 0.188 PC-plies.

Figure 33. Windshield temperature profile as applied to test beam, specimens 3 and 4.

Data Documentation Presentation Methods

In an endeavor to make the raw data meaningful, methods for presentation had to be developed. For the static/dynamic beam tests, the raw data were reduced and are presented in three forms. These forms are: 1) Strain data tables, 2) Multi-strain diagrams for structural plies, and 3) Longitudinal strain diagrams for single plies.

Strain Data Tables

The Strain Data Tables present the details of the tests and the documentation for each specimen tested. Table 16 is an illustrative example showing the tabular form utilized. The symbols are identified as follows:

$2P$ = Load (lb.)

δ_v = Vertical displacement at beam center (in.)

δ_H = Horizontal displacement at one end of beam (in.)

f_d = Damped frequency (H_Z)

γ = Damping Ratio

ε = Strain (μ in/in)

TABLE 16. STRAIN DATA TABLE - ILLUSTRATIVE EXAMPLE.

	LOAD LEVELS		
	Static 1	Static 2	Dynamic
2P, lbs	~	1607	0
δ_v, in.	1.03	1.82	-1.99
δ_H, in.	0	0.11	0.10
Strain Gage No.	(Strain μ in./in.)		
1	354	354	-552
2	-402	-673	403
3	-667	-1972	953

With each table is shown the documentation for a load that was applied (two places) and identified in sum as 2P. These loads were applied initially to reach an approximate one-inch deflection identified as δ_N; held until the deflection stabilized under Static 1; then the two loads were increased until an approximate two-inch deflection stabilized under Static 2. The loads 2P and the deflections δ_V and δ_H were measured and recorded. The loads were quickly released and the deflections measured for the dynamic response at the first rebound. The strains of the materials were measured and recorded on tape for each strain gage. The tapes were subsequently read and the readings were documented as shown, for each load level.

Multi-Strain Diagrams For Structural Plies

The formats for these strain diagrams are shown in Figure 34 (for Specimen 2) and in Figure 35 (for Specimen 4). Figure 34 shows a typical strain diagram for gages located on opposite sides (back-to-back strain gage set) at strain gage numbers 14 and 17. Strain diagrams will be shown for all strain gage sets for each structural ply of the laminated beams. Positive strain will be to the right side of the vertical (zero strain) reference line. The positive strain magnitude is indicated as xxxx (ϵ, μ in./in.). The advantages of showing all of the strain diagrams in one figure for each beam condition and related data, are:

- To provide a scaled graphical representation, drawn with respect to specimen ply thickness and strain magnitude, that would be of great value in assisting checks for continuity. These graphs also provide a check on the strain sense; that is, whether the strain data are of positive or negative orientation.

- To show visually the effects of a failed structural ply on the remainder of the structural plies, when under load.

- To compare slopes of strain diagrams on several structural plies; this is allowed by the common scale factor.

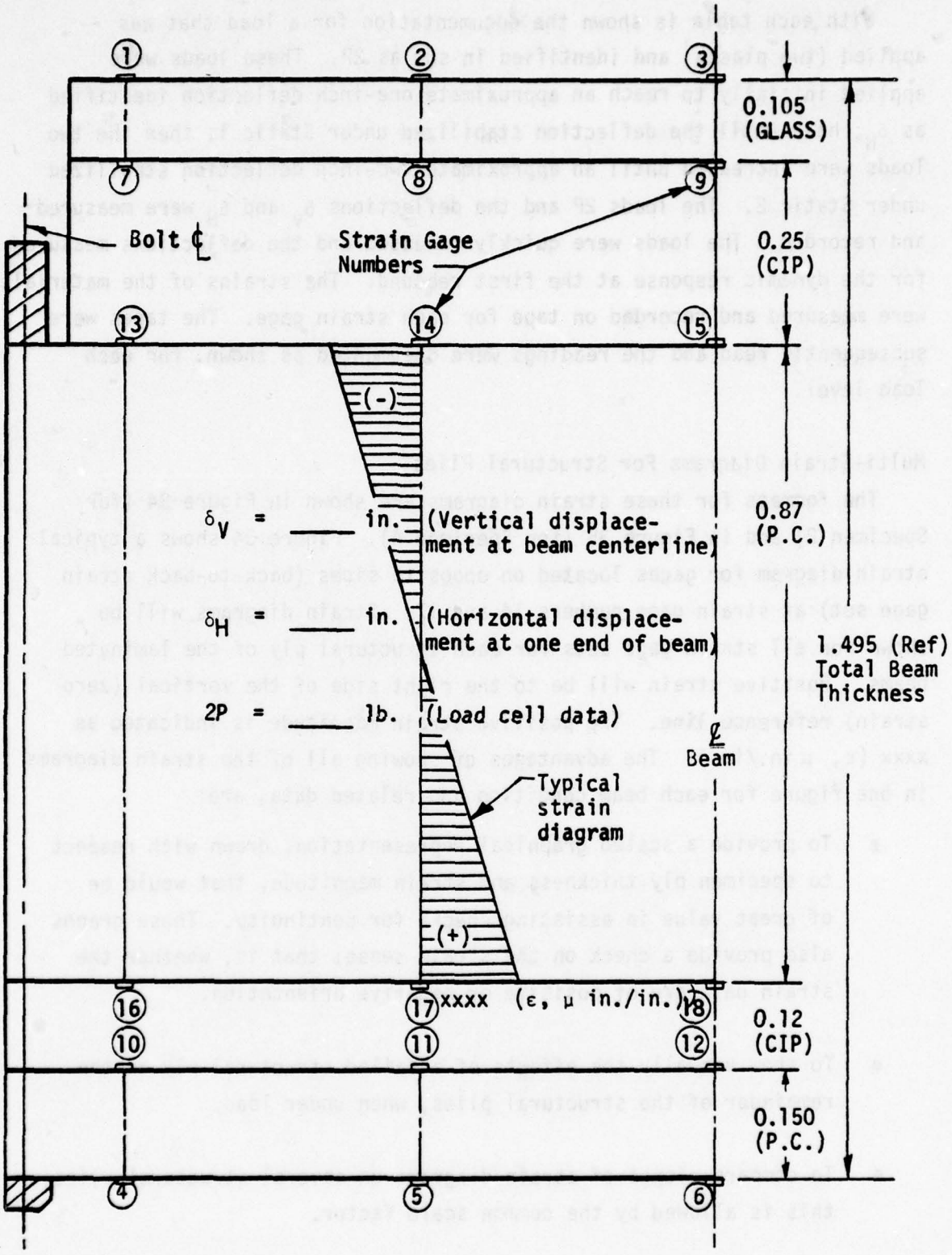

Figure 34. Strain diagram labeling format - Specimen 2.

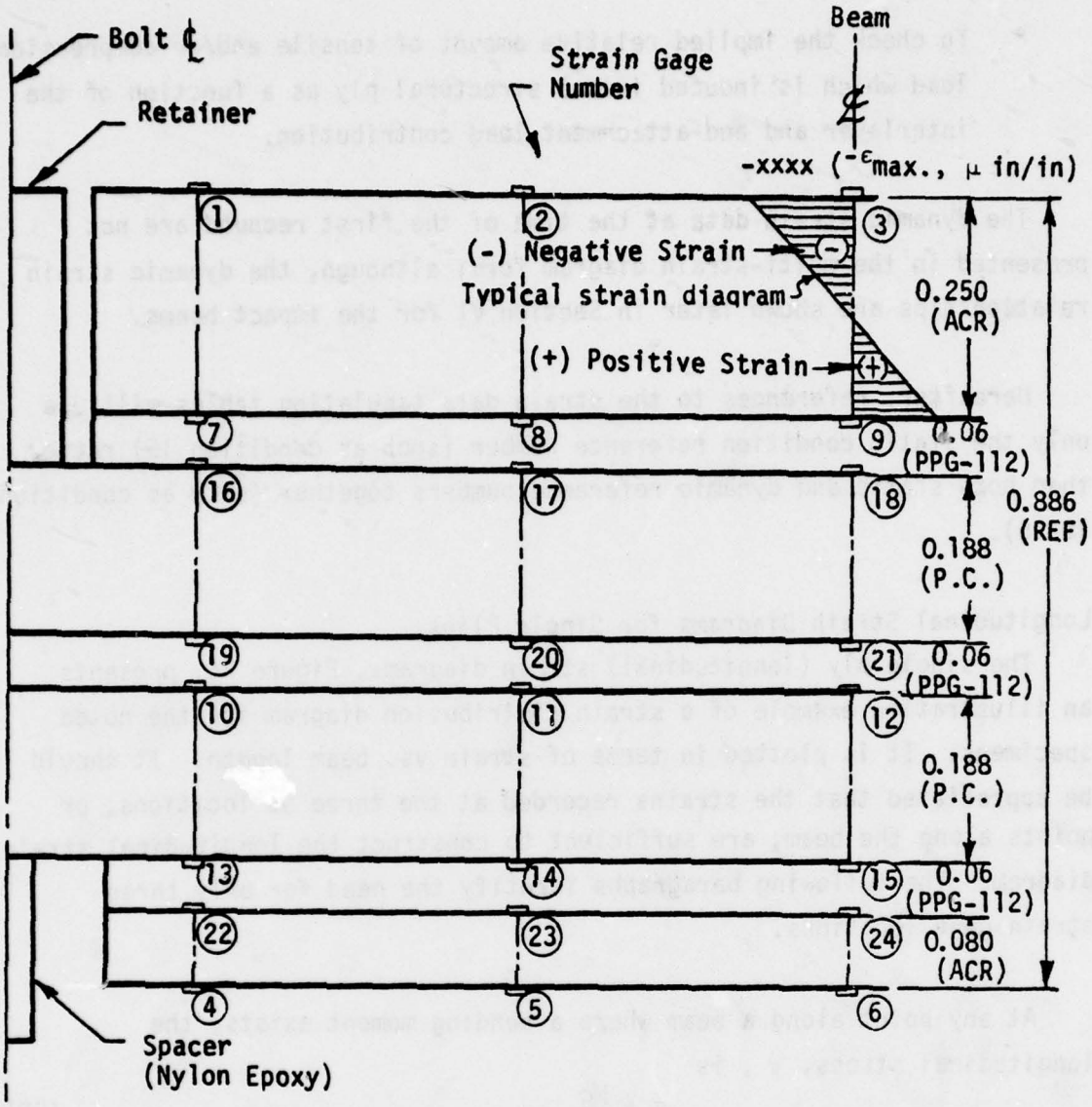

δ_V = _____ inch (Vertical displacement at beam center)

δ_H = _____ inch (Horizontal displacement at one end of beam)

2P = _____ pound (Load cell data)

Figure 35. Strain diagram labeling format, Specimen 4.

- To check the implied relative amount of tensile and/or compression load which is induced into a structural ply as a function of the interlayer and end-attachment load contribution.

The dynamic strain data at the time of the first rebound are not presented in the multi-strain diagram form; although, the dynamic strain relationships are shown later in Section VI for the impact beams.

Hereafter, references to the strain data tabulation tables will use only the static condition reference number (such as condition 15) rather than both static and dynamic reference numbers together (such as condition 15/16).

Longitudinal Strain Diagrams for Single Plies

The single ply (longitudinal) strain diagrams, Figure 36, presents an illustrative example of a strain distribution diagram for the noted specimens. It is plotted in terms of strain vs. beam length. It should be appreciated that the strains recorded at the three SG locations, or points along the beam, are sufficient to construct the longitudinal strain diagram. The following paragraphs identify the need for only three strain gage locations.

At any point along a beam where a bending moment exists, the longitudinal stress, σ , is

$$\sigma = \frac{Mc}{I} . \tag{30}$$

Since strain in the elastic range is

$$\sigma = \varepsilon E, \tag{31}$$

then the strain in terms of the bending moment at any section along the beam is

$$\varepsilon = \frac{Mc}{EI} . \tag{32}$$

This equation shows the linear relationship between the bending moment and strain at any point.

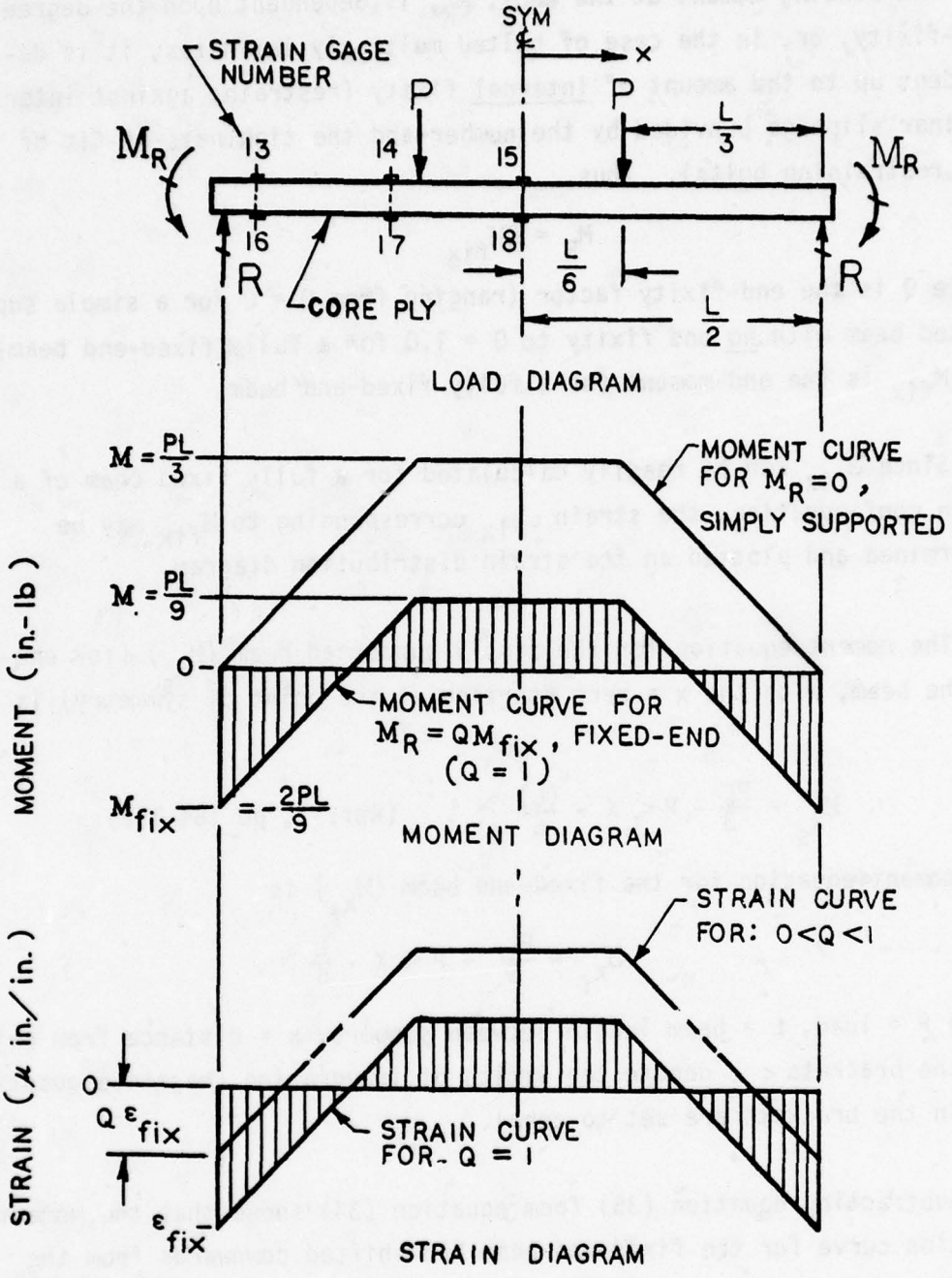

Figure 36. Longitudinal strain diagrams for single plies - illustrative example.

The bending moment at the ends, M_R, is dependent upon the degree of end-fixity, or, in the case of bolted multi-ply laminates, it is dependent up to the amount of internal fixity (restraint against inter-laminar slippage provided by the number and the tightness-of-fit of the restraining bolts). Thus,

$$M_R = QM_{fix} \tag{33}$$

where Q is the end-fixity factor (ranging from Q = 0 for a simple supported beam with no end fixity to Q = 1.0 for a fully fixed-end beam), and M_{fix} is the end-moment for a fully fixed-end beam.

Since M_{fix} can be readily calculated for a fully fixed beam of a given configuration, the strain ε_{fix} corresponding to M_{fix} may be determined and plotted on the strain distribution diagram.

The moment equation for the simply supported beam (M_{x_s}) (for one-half of the beam, with the x = zero starting at the point of symmetry) is

$$M_{x_s} = \frac{PL}{3} - P\left\langle X - \frac{(L)}{6}\right\rangle . \quad \text{(Ref. 1, pp 184-192)} \tag{34}$$

The moment equation for the fixed-end beam (M_{x_f}) is

$$M_{x_f} = \frac{PL}{9} - P\left\langle X - \frac{L}{6}\right\rangle , \tag{35}$$

where P = load, L = beam length between suppors, x = distance from origin, and the brackets $\langle\ \rangle$ denote the limits of integration (negative quantities within the brackets are set to zero).

Subtracting equation (35) from equation (34) shows that the moment equation curve for the fixed-end beam had shifted downwards from the simply supported beam moment equation curve by a constant value of $\frac{2PL}{9}$. That is

$$(M_{x_s} - M_{x_f}) = \left(\frac{PL}{3} - \frac{PL}{9}\right) = \frac{2PL}{9}, \text{ or } \frac{2}{3}\left(\frac{PL}{3}\right).$$

Hence, for the fixed-end beam, the maximum negative bending moments at the ends of the beam are

$$\frac{2}{3}\left(\frac{PL}{3}\right), \text{ where } x = L/2.$$

The maximum positive bending moment (between load points in the constant bending moment area) is

$$\frac{PL}{9} \text{ or } 1/3\left(\frac{PL}{3}\right).$$

Figure 37 shows the typical method of presentation for the superimposed "longitudinal" strain diagrams. The strain data shown for Conditions 21 and 27 have been ratioed (adjusted) to the 2P base load of Condition 15. A common base load for all three conditions provide relative strains that can be easily compared. The strain diagram construction method follows.

The strain diagram for Condition 15 (SR/SS-PIV) was constructed by drawing a horizontal line through the strain point of 8705 μ in./in. at Station 3. A straight line was passed through three points: the zero-strain point at the origin (attachment area), strain point of 1700 μ in./in. (Station 1), and strain point of 7701 μ in./in. (Station 2). These two straight lines were then faired as shown in the figure.

Similarly, the strain diagram for Condition 21 (SR/SB), was constructed from test data. In this case, through means of geometry and calculations, the intercept was determined by passing a straight line through Station 1 and 2 strain data points, with a vertical line drawn through the beam attach point. For Condition 27 (DR/SB), the same method was used. The straight line equation used to determine the intercept strain values is

$$\varepsilon_o = -\left(\frac{\varepsilon_2 - \varepsilon_1}{3.84}\right) + \varepsilon_1 . \text{(Straight line equation theory.)} \qquad (36)$$

For example (Condition 21), let ε_1 = -5008μin./in. and ε_2 = 4701μin./in. (data shown in Figure 37 at Stations 1 and 2). Substituting these values in the equation gives the intercept value ε_o of 7536 μ in./in.

Legend	Condition Number	Edge Cond. Code	2P Load (lb)	Strain Factor
○- - - - - -○	15	SR/SS - PIV	1365*	1
△—— - ——△	21	SR/SB	1607	0.85
□—— - ——□	27	DR/SB	2009	0.68
———	Theoretically fixed-ends		1365*	1

*The 2P base load was 1365 pounds from Condition 15

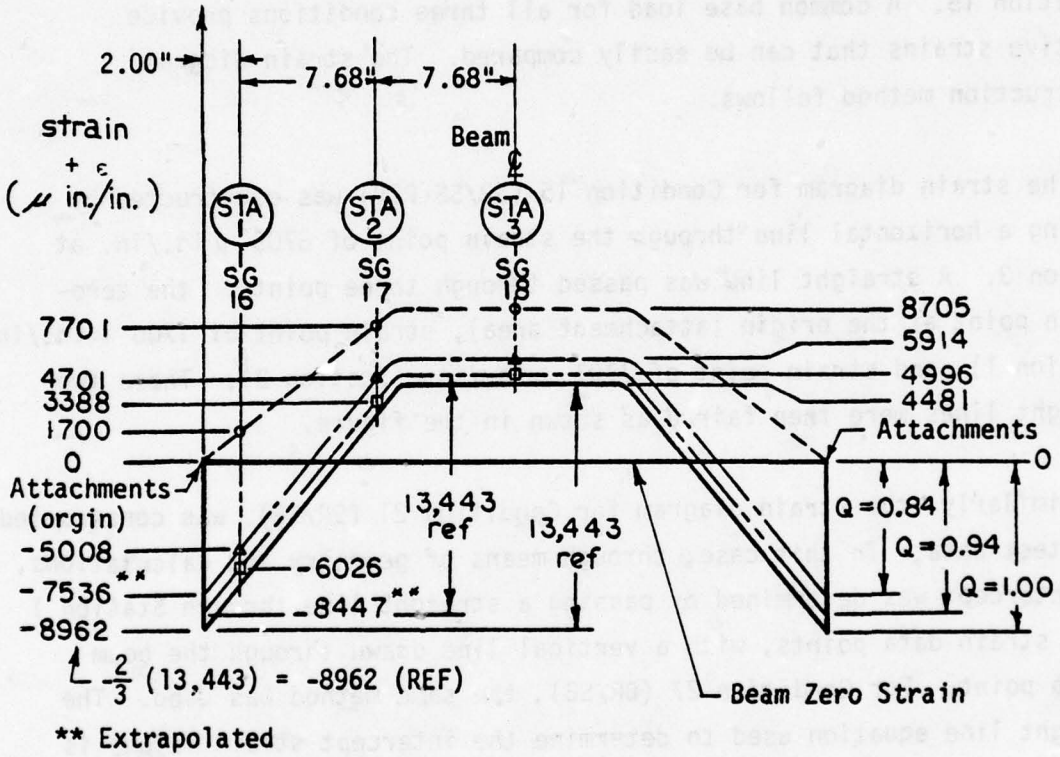

Figure 37. Strain diagrams for Specimen 2; Conditions 15, 21, and 27.

In theory, the maximum moment (or strain) for a simply supported beam is equal to the sum of absolute values of the maximum positive and negative moments (or strains) of a fixed-end beam, under the same symmetrically loaded condition.

As previously mentioned, the beam strain is directly proportional to its bending moment along the beam length (ϵ_ℓ : M_ℓ). For a theoretically fixed-end beam, based on this relationship and taking 1/3 and 2/3 of the sum of the absolute values of the strain test data for Condition 27 (4996 + 8447, μ in./in.), resulted in a maximum negative theoretical strain value of -8962 μ in./in. and a maximum positive theoretical strain value of 4481 μ in./in., as shown in Figure 37. It should be noted that the test data strain curve for the simply supported beam is not exactly parallel to that of the fixed-end beam. This is probably because the beam equivalent stiffness value (EI) is greater for the simply supported beam, since the edge attachment bolts lock the plies together preventing the structural ply slippage.

The end-fixity factor (Q) corresponding to these specimens are: Q = 0 assumed for simply supported beam Condition 15; Q = 0.84 for fixed-end beam with single row of attachments Condition 21; and Q = 0.94 for fixed-end beam with double row of attachments Condition 27. The fixity factors of 0.84 and 0.94 were obtained by ratioing their extrapolated strain (at the attach point) to that of the theoretical beam with 100 percent fixed-ends.

To recapitulate, for the selected beam specimens, the strain data were tabulated. From this, multi-layered strain diagrams were constructed, and then several selected conditions of single ply (longitudinal) strain diagrams were superimposed for comparison and evaluation purposes.

The lower surface of the main core ply for beam Specimen 2, Figure 38, and the lower surface of the lowest polycarbonate structural ply for Specimen 4 (reference Figure 61), were selected for displaying the single ply (longitudinal) strains.

Details are in Figures 39 and 40.

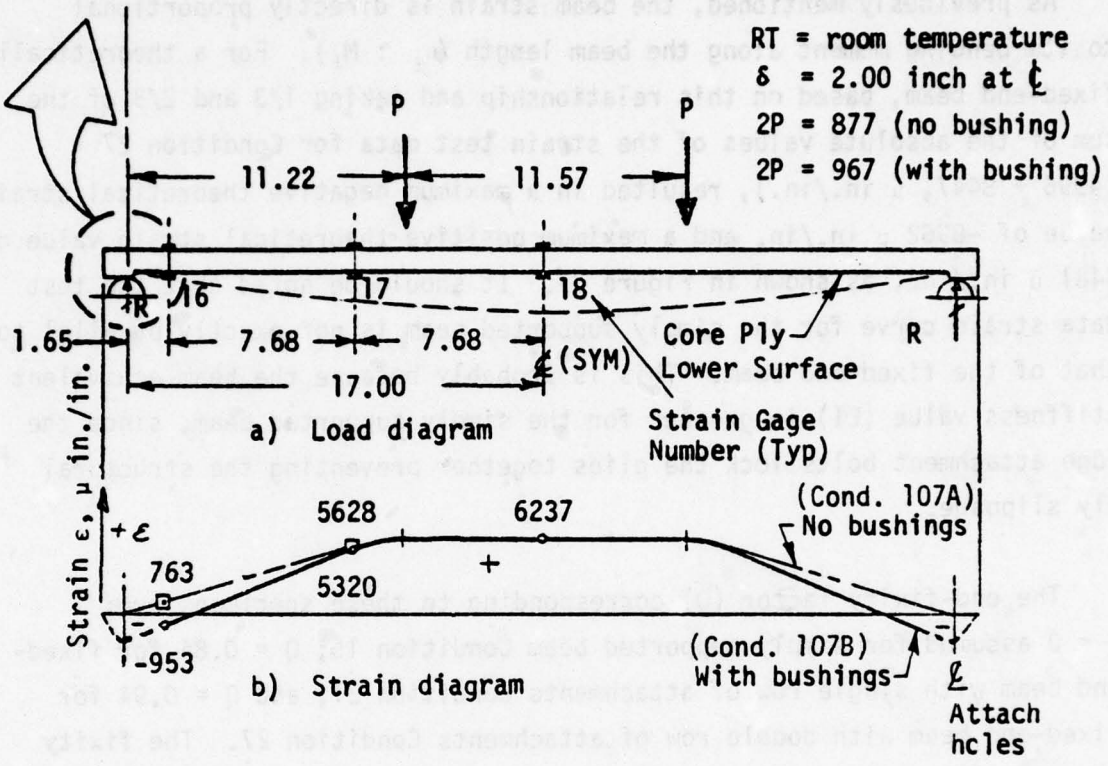

NOTES:
1. Strains are shown for gages 16, 17, and 18 only.
2. Condition 107B has bushings installed with no bolts (/SS-B).
3. Condition 107A has bushings removed from end-attachment bolts.

Figure 38. Beam load and strain diagram for Specimen 2, Condition 107.

Assessment of Testing Errors

Conventional beam theory methods for monolithic beams do not apply to laminated beams; thus, assessment of testing errors becomes an engineering judgment. Within the multi-layered strain diagrams, the slope of the strain diagrams could have been compared to theoretical strain diagram slopes as a function of the bending beam instantaneous bend radii. However, this was not practical because of time and expense constraints.

The method used for the assessment of testing errors was by inspection, comparison, and engineering judgment. The diagrams were evaluated for continuity and direction of slopes where, for any particular section, the slopes of the strain diagrams should be parallel. This has been analytically verified in Section VII, where a direct comparison is made between the results of a finite element math model and the test data.

RESULTS AND ASSESSMENT OF STRAIN DISTRIBUTION

The paragraphs that follow present the results and assessment of the test data for the thick core and multi-layered beam specimens. Hereafter, the thick core beam refers to Specimen 2 and the multi-layered beam refers to Specimen 4. A comparative analysis is made of each separate configuration for linearity of load versus strain, an assessment of strain distribution and a comparison of their respective stiffness.

The Linearity of Load Versus Strain for Thick Core and Multi-Layered Beams

Linearity of Load Versus Strain for Thick Core Beam

Specimen 2, test conditions 107A and 107B (simply supported under room temperature conditions) were selected for this linearity study. The center of the beams were deflected to a maximum of two inches with resulting loads (2P) of 877 pounds and 967 pounds respectively. Based on this data, the load and longitudinal strain diagrams for these two conditions are shown in Figure 38.

The detail for the end attachment configuration for Condition 107A

(under load) showing interlayer deformation is shown in Figure 39. The detail for the end attachment for condition 107B unloaded is shown in Figure 40.

The strain shown in Figure 38 are from gages 16, 17, and 18 only, as tabulated in Tables 17 and 18. Note that the strain curve for conditions 107A appears to be zero near the attachment hole area. The strain curve for condition 107B appears to have an inter-laminate fixity effect near the beam ends. Table 17 is a tabulation of the strain data for Specimen 2, condition 107A, a simply supported beam with bolts and bushings removed. Four static load (2P) levels were tested causing 0.50, 1.00, 1.50, and 2-inch beam center deflections (δ), respectively. The negative strain numbers (-) are compression strains. The strain data for the 2-inch deflection are plotted in a multi-layered strain diagram shown in Figure 41.

Similarly, Table 18 is a tabulation of the strain data for Specimen 2, Condition 107B, the same simply supported beam, but with bushings in place (no bolts) that lock the structural plies together to prevent slippage. Figure 42 shows its multi-layered strain diagrams. The following, Figure 43, shows a composite strain diagram of conditions 107A and 107B. Note that the two strain diagram line types are approximately parallel. The small arrows indicate that higher tensile and compression loads (in the form of strain magnitudes) are caused by the locking of the structural plies together through means of the bushings.

The strain output gage 18 (bottom, center strain gage mounted on the main polycarbonate core ply) was selected for the load versus strain linearity check for the thick core beam. The 2P load versus strain for the four static load levels for both conditions 107A and 107B were plotted as shown in Figure 44. The results indicate that both beams had linear relationships between load and strain. The beam with the bushings in place provided an apparently stiffer beam which is consistent with the foregoing.

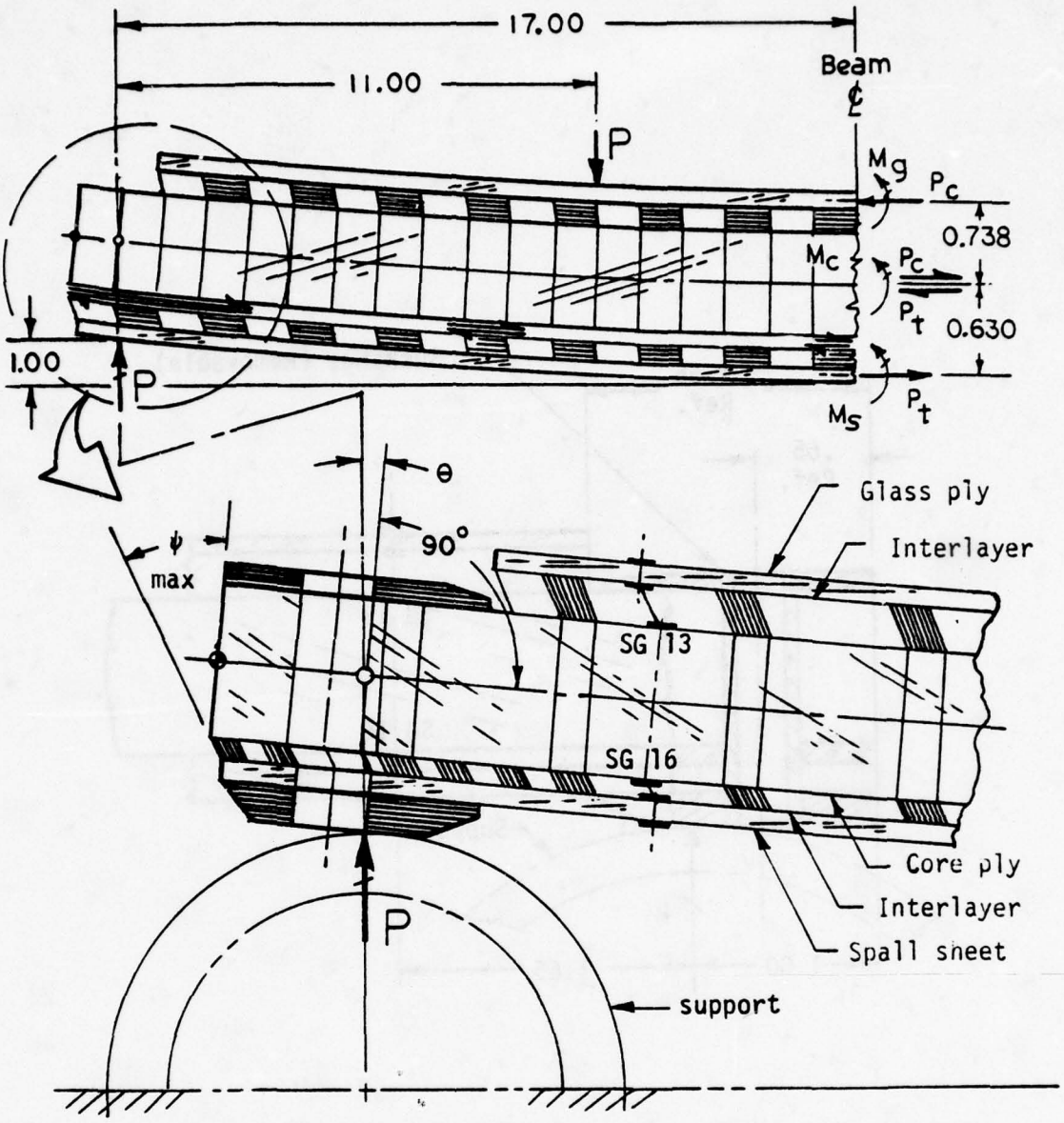

Notes: 1. θ is the slope of beam end.
2. ψ is the varying angular shear strain for the CIP interlayer, decreasing (approximately) linearly from ψ_{max} at beam end to zero at beam center.

Figure 39. End attachment configuration for Condition 107A under load, showing interlayer deformation.

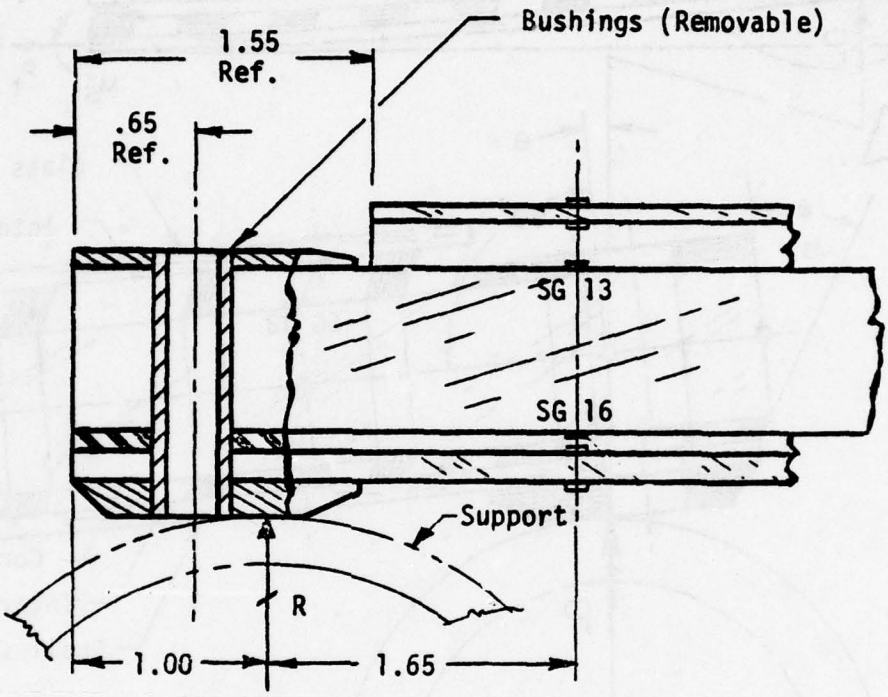

Figure 40. End-attachment configuration for Condition 107B (unloaded), with bushings installed.

TABLE 17. STRAIN DATA FOR SPECIMEN 2, CONDITION 107 A, SIMPLY-SUPPORTED BEAM, WITHOUT BUSHINGS

(/SS), RT

Four static runs with increasing load increments as follows:

Condition ⟶	Static 1	Static 2	Static 3	Static 4
Load 2P (lbs)	229	439	638	877
Deflection δ (in.)	0.50	1.00	1.50	2.00
Strain Gage No.	Strain ε (μ in./in.)(1)			
1	91	91	319	546
2	-183	-320	-457	-778
3	-183	-457	-595	-823
4	253	557	860	1164
5	1089	2079	3019	4058
6	1253	2409	3585	4866
7*	—	—	—	—
8	47	142	237	474
9	147	343	490	539
10	253	506	658	911
11	503	961	1418	1875
12	616	1233	1849	2608
13*	—	—	—	—
14	-1126	-2581	-3754	-5303
15	-1370	-3004	-4418	-6097
16	238	281	572	763
17	1495	2858	4177	5628
18	1623	3204	4614	6237

(1) Negative numbers (-) are compression strains.

*Gages Inoperative.

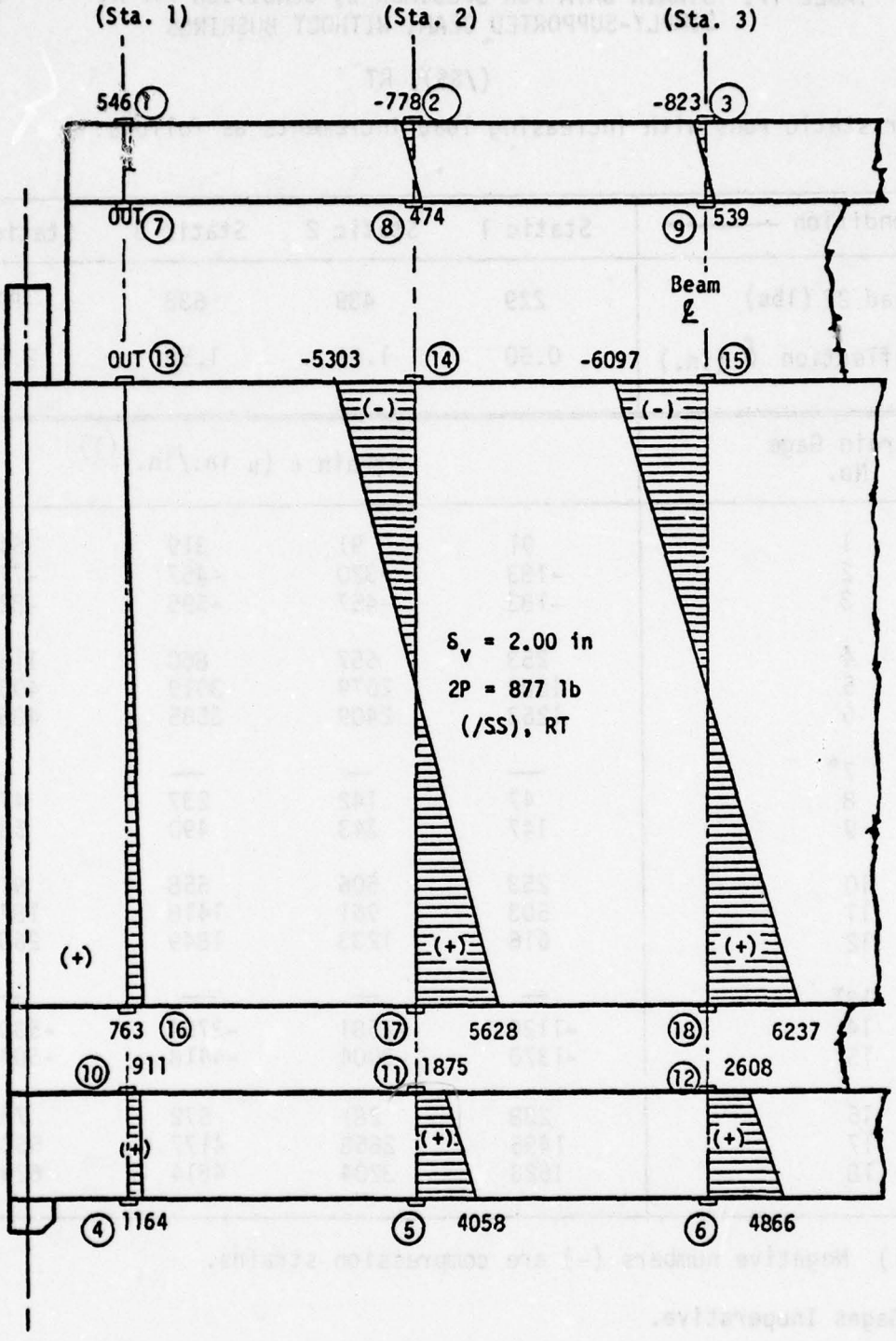

Figure 41. Strain diagrams within structural plies of Specimen 2, Condition 107A without bushings.

TABLE 18. STRAIN DATA FOR SPECIMEN 2, CONDITION 107 B, SIMPLY-SUPPORTED BEAM, WITH BUSHINGS IN PLACE

(/SS-B), RT

Four static runs with increasing load increments as follows:

Condition ⟶	Static 1	Static 2	Static 3	Static 4
Load 2P (lbs)	202	469	678	967
Deflection δ (in.)	0.50	1.00	1.50	2.00
Strain Gage No.	Strain ε (μ in./in.)(1)			
1	0	-91	-137	-137
2	-137	-229	-457	-778
3	-229	-457	-640	-915
4	658	1417	2226	3188
5	841	2128	3860	5939
6	1445	2891	4384	7082
7*	Out	Out	Out	Out
8	0	142	285	285
9	196	343	392	539
10	658	1316	2176	3086
11	778	1510	2333	3385
12	806	1706	2608	3746
13*	Out	Out	Out	Out
14	-1408	-2722	-4036	-5631
15	-1590	-3225	-4683	-6627
16	-95	-381	-667	-953
17	1407	2682	3737	5320
18	1581	2991	4400	6237

(1) Negative numbers (-) are compression strains.

*Gages Inoperative.

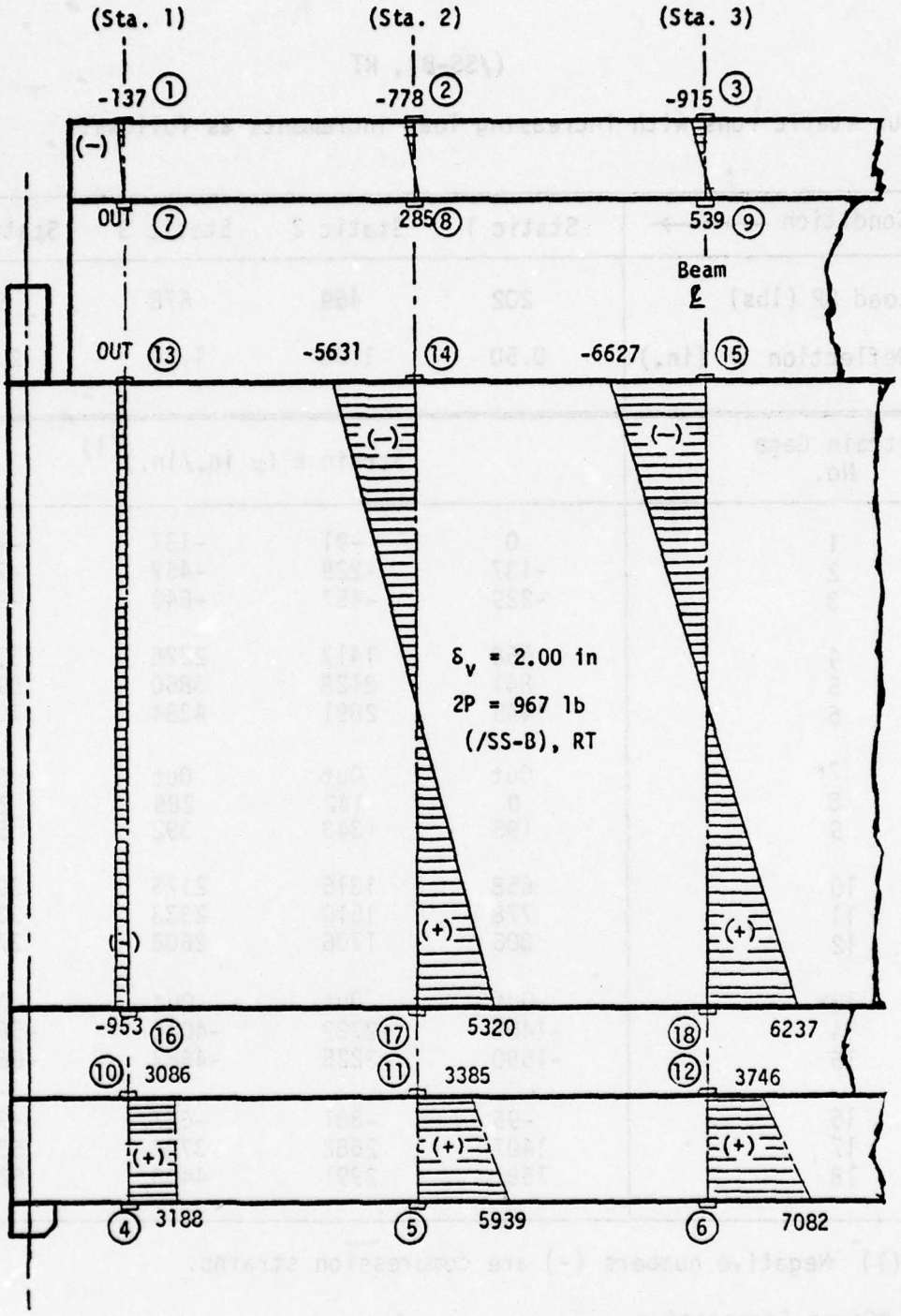

Figure 42. Strain diagrams within structural plies of Specimen 2, Condition 107B, with bushings.

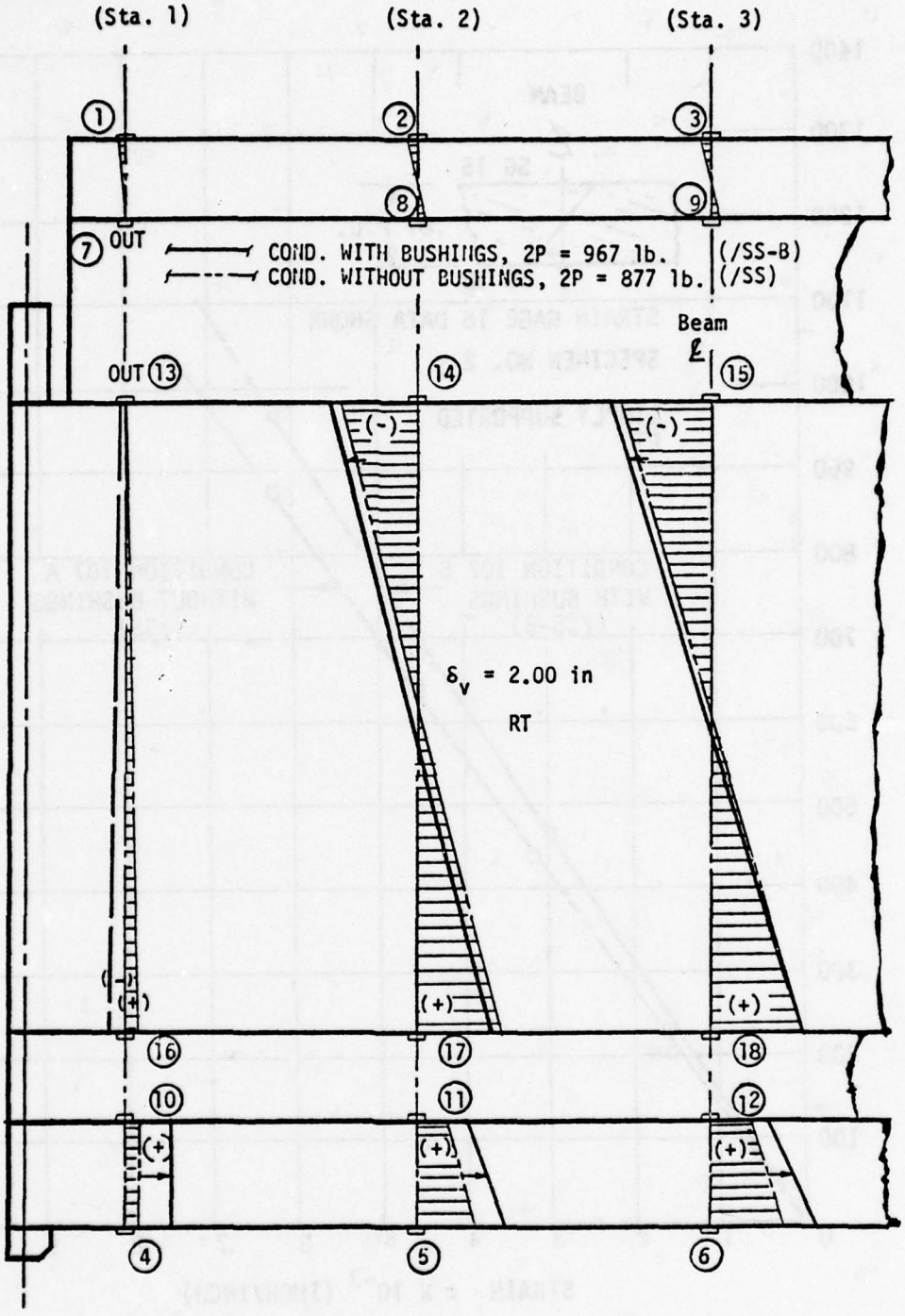

Figure 43. Composite strain diagram Conditions 107A and 107B.

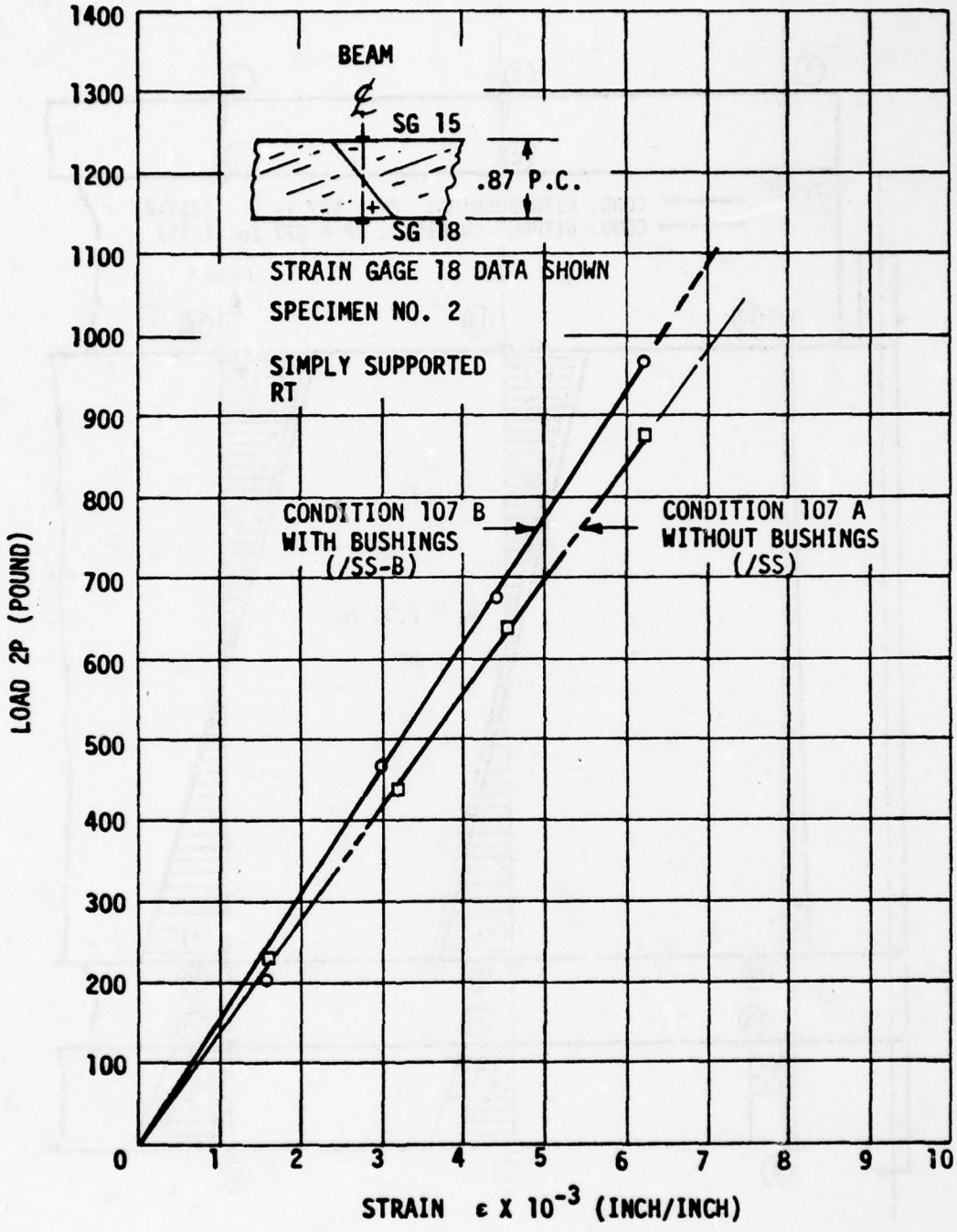

Figure 44. Load versus strain for Specimen 2, main core ply, Condition 107A, without bushings, and Condition 107B, with bushings.

Linearity of Load Versus Strain for Multi-Layered Beam

Specimen 4, calibration condition 34 (a simply supported beam, pin-ended, with a single row of bolts and bushings) was selected for this linearity study. Figure 45 shows the curve for the 2P load versus strain data for gage 15. The curve displays non-linearity, but good continuity.

Strain Distribution From Edge Effects on Thick Core Beam

The results and assessment of strain distribution, caused by the edge effect, for the thick core beam specimen follows. The simply supported and fixed-end beams are compared. (The single row attached beam with sealant are compared with double row attached beam.) The effect of temperature is presented for the single row attached beams with sealant (loose holes) and with tight fitting aluminum bushings.

Simply Supported and Fixed-End Beams

A comparison was made of the strain distribution for the thick core beam, simply supported (condition 15), fixed-end with single row of attachments (condition 21), and fixed-end with double row of attachments (Condition 27). These tests were run at room temperature, and the beam had one support free-to-slide and the other support was locked in place. The strain data test results and strain diagrams within the structural plies for condition 15 are shown in Table 19 and Figure 46. In the figure, the slope of the strain diagrams at Station 2 and 3 appear to be parallel, indicating a common beam bending radius; at Station 1, the slopes are negligible, indicating zero radius (station definition was provided in Figure 15 of Section III). Note that the strain diagrams show the main core ply positive and negative strain magnitudes as approximately equal; whereas the strain diagrams for the lower spall sheet have translated to the right, indicating an induced tension strain component. If this laminated beam was totally monolithic, then the strain diagram slope would be continuous from the beam's upper to lower surfaces. The relative position of the slopes, suggest the lack of shear-load transfer between structural plies, caused by the characteristic of soft silicone interlayers.

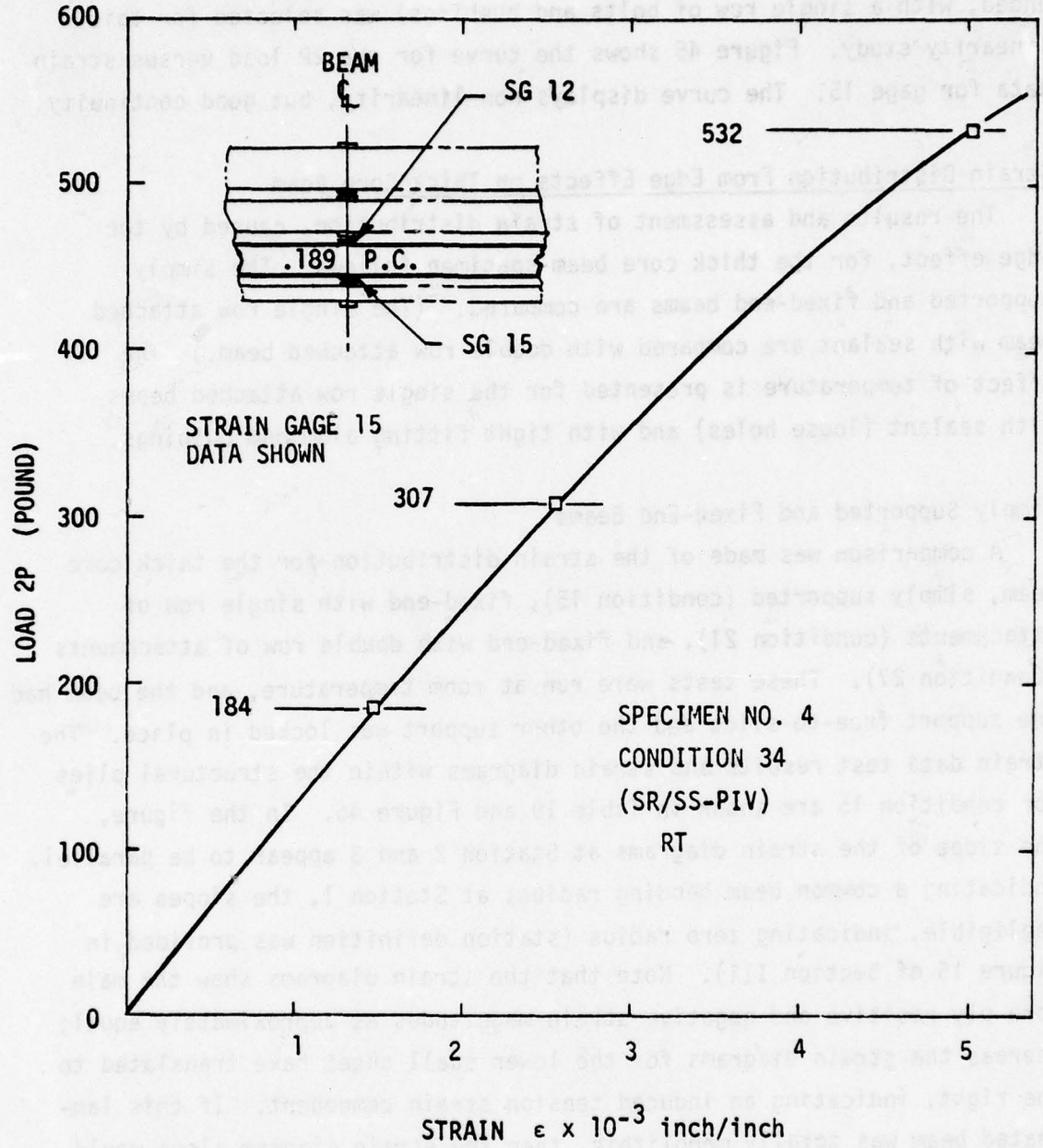

Figure 45. Load versus strain for Specimen 4, Condition 34.

TABLE 19. STRAIN DATA FOR SPECIMEN 2, CONDITION NUMBER 15/16.

(SR/SS-PIV), RT

Three static runs with increasing load increments denoted as Condition 15 and a dynamic condition denoted as Condition 16 are as follows:

Load levels →	STATIC 1	STATIC 2	STATIC 3	Dynamic*
2P (lbs)	476	992	1365	0
δ_V (in.)	0.98	1.96	2.75	-2.35
δ_H (in.)	0.52	1.42	2.25	**
Strain Gage No.	**Strain ε, (μin./in.)**			
1**	—	—	—	—
2	-414	-932	-1190	906
3	-481	-1094	-1400	1203
4	1769	3496	4971	-4213
5	3033	5898	8257	-6869
6	3297	6551	9233	-7694
7**	—	—	—	—
8	260	520	693	- 672
9	340	693	910	- 823
10	656	3500	4813	-7482
11	1867	3828	5182	-4272
12	2184	4187	5871	-4915
13	0	221	353	**
14	-2339	-5953	-8717	8674
15	-4386	-7311	-9829	8326
16	510	1276	1700	- 850
17	1800	5688	7701	-5907
18	3078	6155	8705	-7035

f_d = 12 Hz $\qquad\qquad$ γ = 0.0407

*Strain ε_d at first rebound, and related beam center displacement δ_V.

**Gage Inoperative.

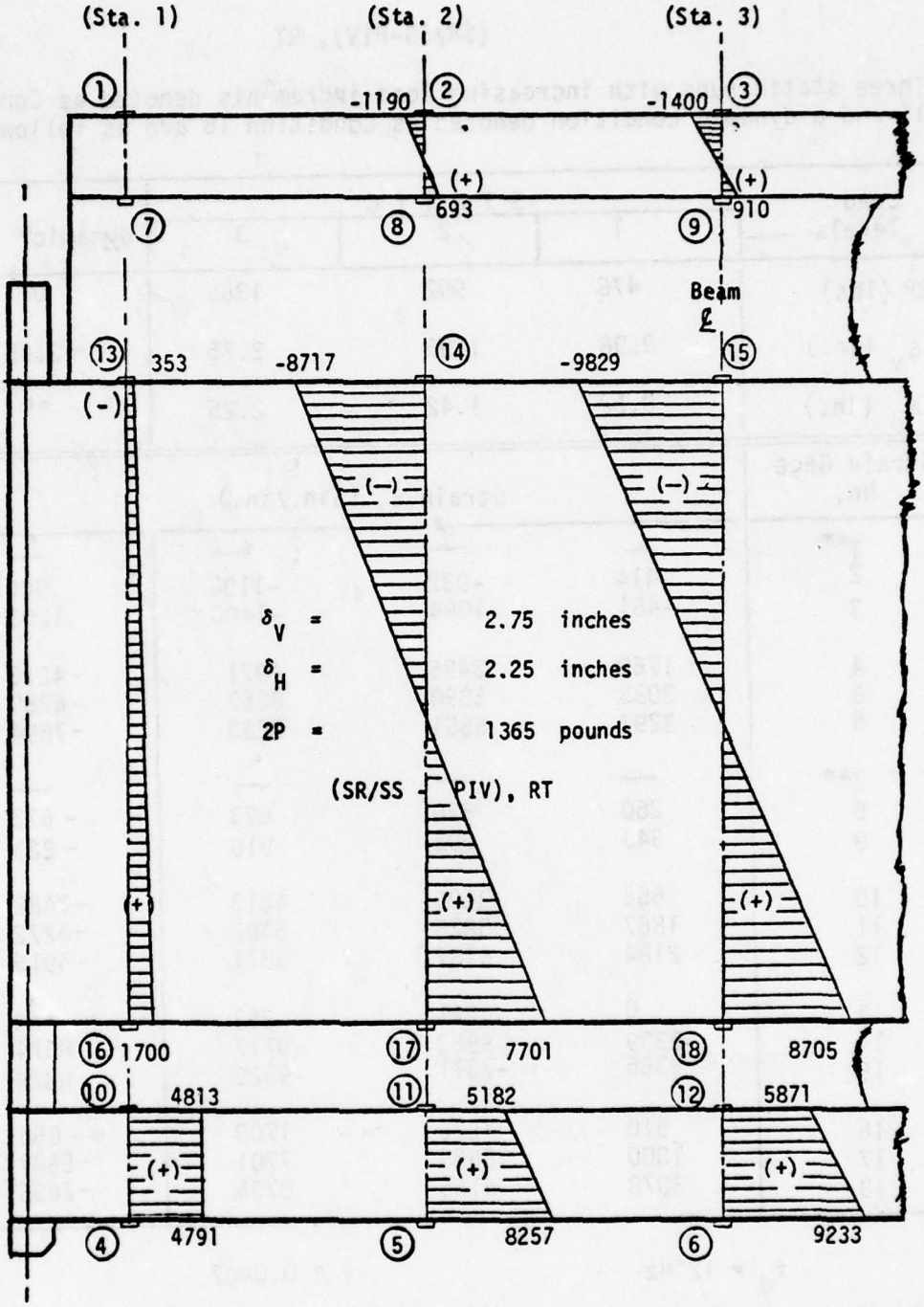

Figure 46. Strain diagrams within structural plies of Specimen 2, Condition 15.

Table 20 and Figure 47 show the strain data results and strain diagrams within the structural plies for condition 21 (single row of attachments). As expected for a fixed-end beam, shown in the figure, the slope of the strain diagrams at Station 1 reversed, providing tensile strain at the upper surface and compression strain at the lower surface of the structural plies.

Table 21 and Figure 48 show the strain data results and strain diagrams within the structural plies for condition 27 (double row of attachments). As expected, greater strain magnitudes occurred at Station 1, with respect to condition 21. This was probably caused by the higher applied load (2009 pounds versus 1607 pounds) and the greater edge restraint of Condition 27.

Single Row with Sealant Versus Double Row Tight Attachments

A comparison was made of the strain distribution for the thick core beams with the single row of attachments, whose loose holes were filled with sealant, and with the double row of attachments, provided with tight fitting aluminum bushings. *These conditions* had both supports locked in place and were run at room temperature.

The strain data test results and strain diagram within the structural plies for condition 29S are shown in Table 22 and Figure 49. In Figure 49, ε_C, ε_T, and ε_M strain reference components for the shaded diagrams are shown in μin./in., where ε_C is the compression component, ε_T is the tensile component, and ε_M is the (plus and minus) bending strain component. These components are shown for reference purpose only and were determined by assuming a neutral bending axis located at the centerline of the structural ply. A vertical line was constructed through the strain diagram intercept with the centerline forming the shaded diagrams. The compression and tensile strain components are caused by the interlayer shear load (energy) transfer from one structural ply to another and/or inter-ply reaction loads induced from tne edge attachments.

TABLE 20. STRAIN DATA FOR SPECIMEN 2, CONDITION NUMBER 21/22.

(SR/SB), RT

Two static runs with increasing load increments denoted as Condition 21 and a dynamic condition denoted as Condition 22 are as follows:

Load levels →	Static 1	Static 2	Dynamic*
2P (lbs)	~	1607	0
δ_v (in.)	1.03	1.82	-1.99
δ_H (in.)	0	0.11	0.10
Strain Gage No.	Strain ε, (μ in./in.)		
1	354	354	-552
2	-402	-673	403
3	-667	-1972	953
4	-1275	-1539	1825
5	2454	4060	-1874
6	2808	4891	-4030
7	0	0	0
8	350	438	-394
9	496	676	-721
10	2094	2958	-1638
11	980	1867	-1214
12	1333	2345	-2161
13	4010	6227	-5708
14	-3261	-5298	2649
15	-4290	-7150	6483
16	-3821	-5896	5189
17	3293	5535	-3591
18	4142	6963	-6144

f_d = 17.6 Hz γ = 0.053103

* Strain ε_d at first rebound, and related beam center displacement δ_v.

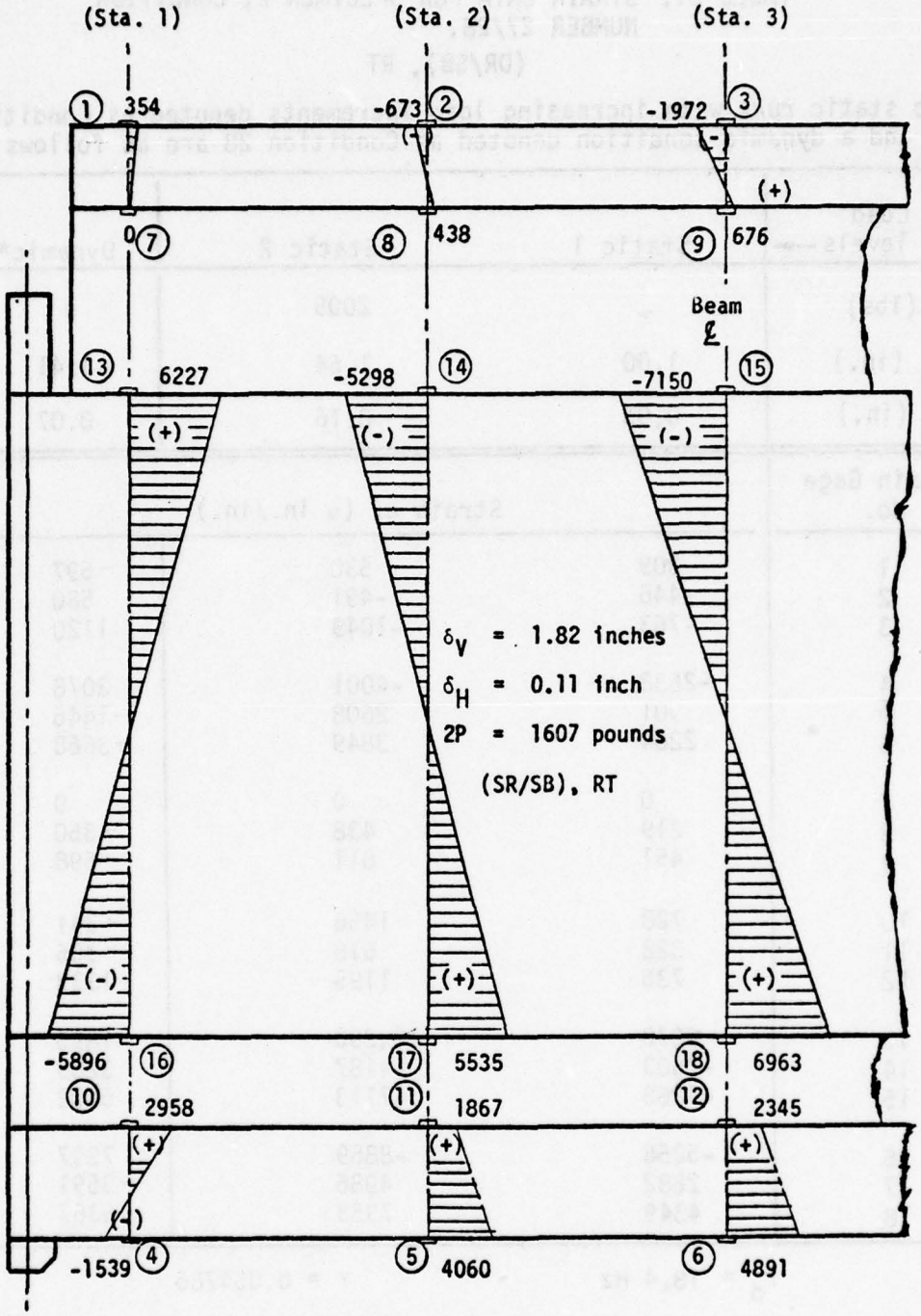

Figure 47. Strain diagrams within structural plies of Specimen 2, Condition 21.

TABLE 21. STRAIN DATA FOR SPECIMEN 2, CONDITION NUMBER 27/28.

(DR/SB), RT

Two static runs with increasing load increments denoted as Condition 27 and a dynamic condition denoted as Condition 28 are as follows:

Load levels →	Static 1	Static 2	Dynamic*
2P (lbs)	~	2009	0
δ_v (in.)	1.00	1.64	-1.41
δ_H (in.)	0.03	0.16	0.07
Strain Gage No.	**Strain ε, (μ in./in.)**		
1	309	530	-597
2	-446	-491	580
3	-763	-1049	1120
4	-2638	-4001	3078
5	901	2608	-1446
6	2264	3849	-3668
7	0	0	0
8	219	438	-350
9	451	811	-698
10	728	1456	-341
11	328	516	-305
12	736	1195	-1333
13	6070	10,290	-7895
14	-2503	-4187	3209
15	-4268	-7113	6402
16	-5256	-8869	7297
17	2882	4986	-3591
18	4349	7353	-6367

f_d = 18.4 Hz γ = 0.054786

* Strain ε_d at first rebound, and related beam center displacement δ_v.

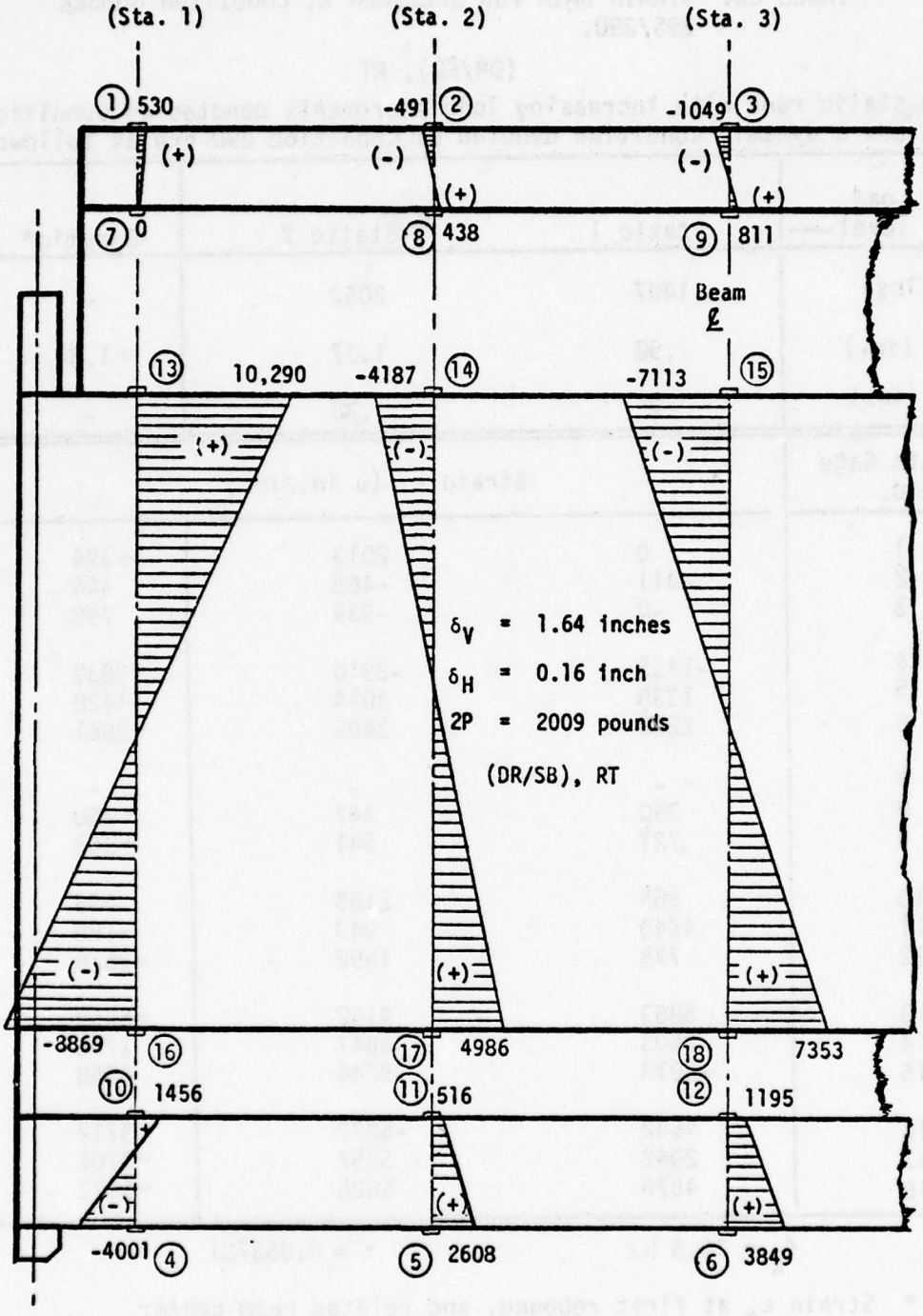

Figure 48. Strain diagram within structural plies of Specimen 2, Condition 27.

TABLE 22. STRAIN DATA FOR SPECIMEN 2, CONDITION NUMBER 29S/29D.

(DR/FB), RT

Two static runs with increasing load increments denoted as Condition 29S and a dynamic condition denoted as Condition 29D are as follows:

Load level →	Static 1	Static 2	Dynamic*
2P (lbs)	1407	2052	-
δ_v (in.)	.98	1.37	-1.32
δ_H (in.)	0	.38	-
Strain Gage No.	**Strain ε, (μ in./in.)**		
1	0	2013	-394
2	-311	-488	444
3	-0	-939	798
4	-1455	-2910	2839
5	1338	3034	-1428
6	2298	3695	-2861
7	-	-	-
8	390	347	-260
9	721	541	-563
10	865	2185	455
11	4245	943	-189
12	778	1692	-2516
13	5863	9152	-6459
14	-2503	-3641	2776
15	-8913	-5244	4958
16	4642	-6872	5712
17	2942	5057	-3701
18	4576	6626	-5172

f_d = 19.5 Hz γ = 0.053781

* Strain ε_d at first rebound, and related beam center displacement δ_v.

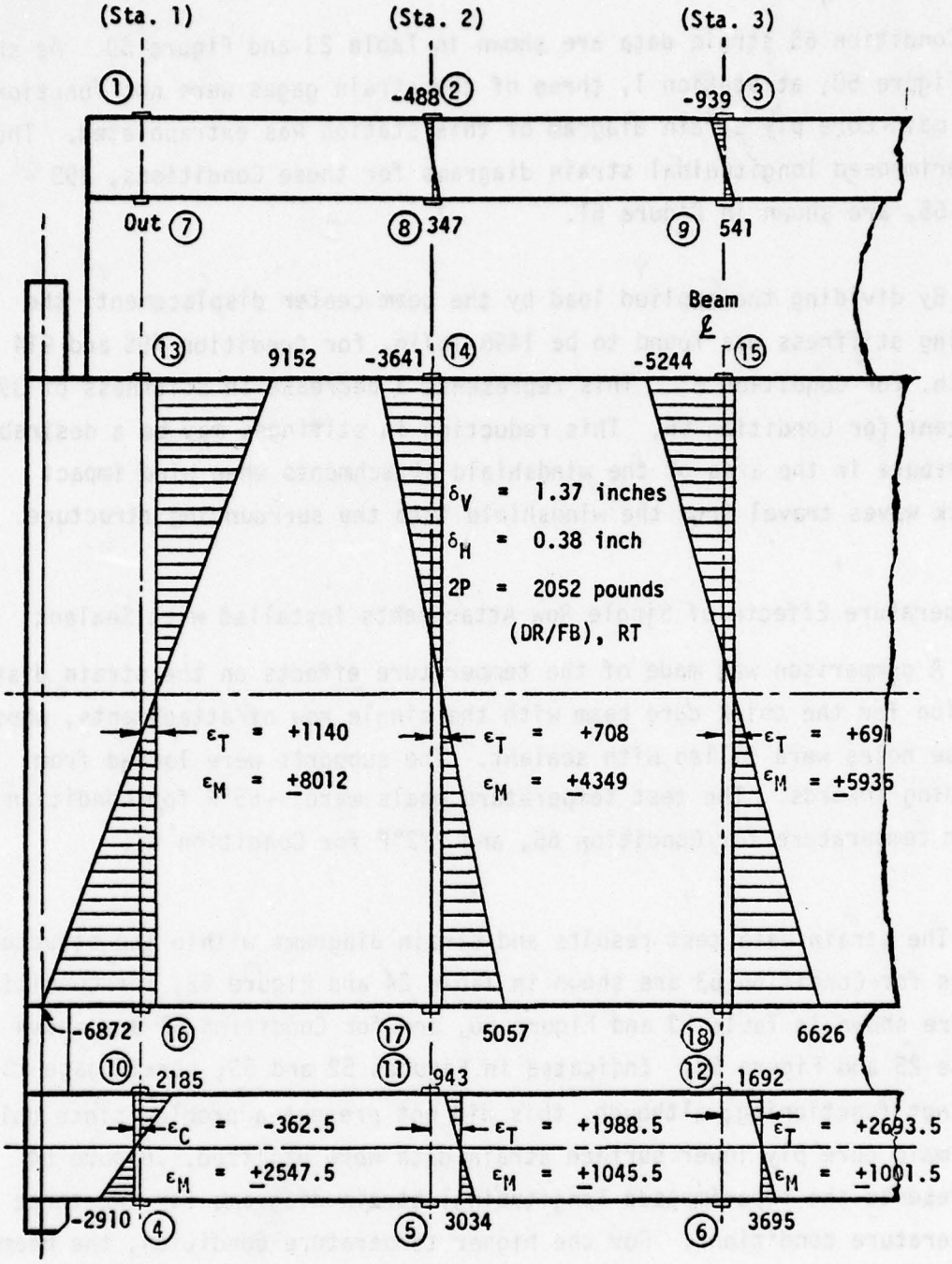

Figure 49. Strain diagrams within structural plies of Specimen 2, Condition 29S.

Condition 65 strain data are shown in Table 23 and Figure 50. As shown in Figure 50, at Station 1, three of the strain gages were not functioning. The main core ply strain diagram of this station was extrapolated. The superimposed longitudinal strain diagrams for these Conditions, 29S and 65, are shown in Figure 51.

By dividing the applied load by the beam center displacement, the spring stiffness was found to be 1498 lb/in. for Condition 29S and 914 lb/in. for Condition 65. This represents a decrease in stiffness of 39 percent for Condition 65. This reduction in stiffness may be a desirable attribute in the area of the windshield attachments when bird impact shock waves travel from the windshield into the surrounding structure.

Temperature Effects of Single Row Attachments Installed with Sealant

A comparison was made of the temperature effects on the strain distribution for the thick core beam with the single row of attachments, whose loose holes were filled with sealant. The supports were locked from sliding inwards. The test temperature goals were: -65°F for Condition 63, room temperature for Condition 65, and 272°F for Condition 67.

The strain data test results and strain diagrams within the structural plies for Condition 63 are shown in Table 24 and Figure 52, for Condition 65 are shown in Table 23 and Figure 50, and for Condition 67 are shown in Table 25 and Figure 53. Indicated in Figures 52 and 53, strain gage 13 was not functioning; although, this did not present a problem since only the main core ply lower surface strain data were utilized. Figure 54 represents the superimposed longitudinal strain diagrams for the three temperature conditions. For the higher temperature condition, the beam stiffness has been reduced by 18 percent with respect to the room temperature condition. The majority of this beam stiffness reduction may be attributed to the softening of the sealant; although, a post inspection of the sealant showed no apparent permanent set.

TABLE 23. STRAIN DATA FOR SPECIMEN 2, CONDITION NUMBER 65/66.

(SR/FB-S), RT

Two static runs with increasing load increments denoted as Condition 65 and a dynamic condition denoted as Condition 66 are as follows:

Load level →	Static 1	Static 2	Dynamic*
2P (lbs)	864	1646	~
δ_v (in.)	1.01	1.80	-1.38
δ_H (in.)	(Fixed Base)	(Fixed Base)	0.05
Strain Gage No.	**Strain ε, (μ in./in.)**		
1	142	142	-190
2	-392	-784	566
3	-543	-1177	860
4			
5	2588	4744	-2674
6	2948	5255	-3631
7	0	0	0
8	1356	317	-294
9	438	656	-481
10	1538	3119	-1239
11	1022	2415	-1393
12	1126	3019	-1919
13	0	0	0
14	-3276	-3420	4288
15	-2800	-6126	2647
16	-4385	-6483	5291
17	3464	6038	-3415
18	4191	6696	-4914

f_d = 5.97 Hz γ = 0.051791

* Strain ε_d at first rebound, and related beam center displacement δ_v.

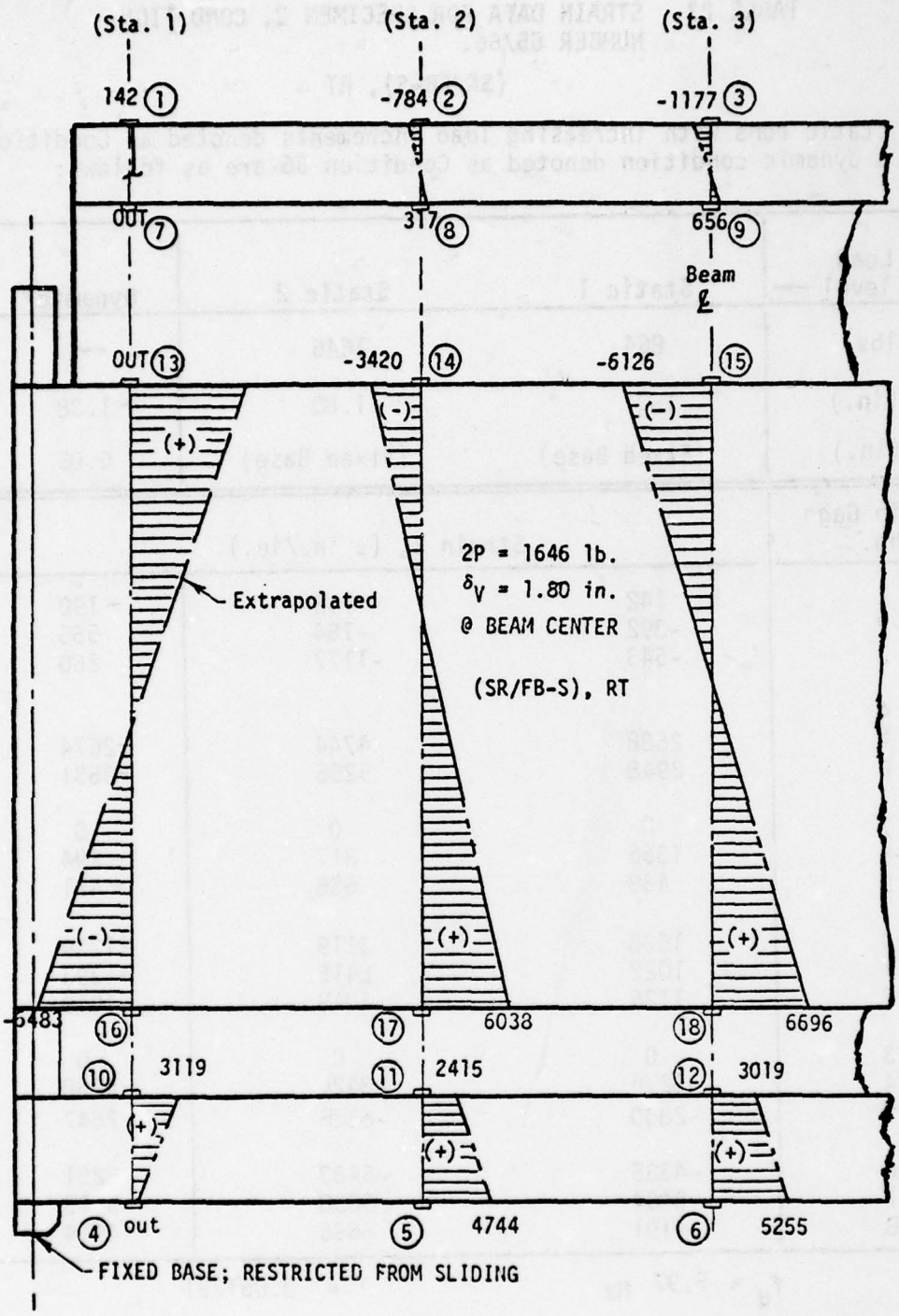

Figure 50. Strain diagrams within structural plies of Specimen 2, Condition 65.

o——o Condition 65 (SR/FB-S), RT.

△- - -△ Condition 29S (DR/FB), RT.

*2P = 2052 lb/condition 29S as base load.

** Extrapolated

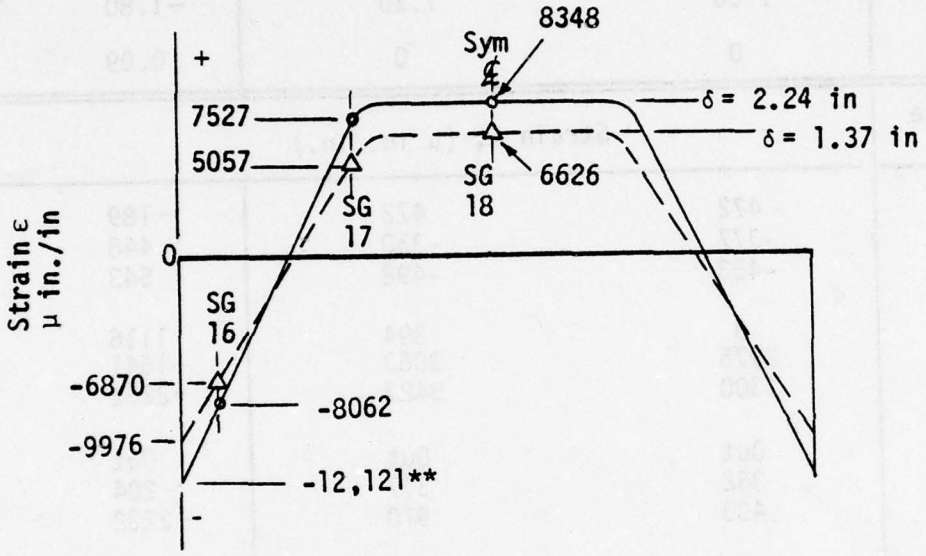

Figure 51. Strain Diagrams for Beam Specimen 2 - thick core ply Condition 29S and 65.

TABLE 24. STRAIN DATA FOR SPECIMEN 2, CONDITION NUMBER 63/64.

(SR/FB-S) T=-65°F

Two static runs with increasing load increments denoted as Condition 63 and a dynamic condition denoted as Condition 64 are as follows:

Load level →	Static 1	Static 2	Dynamic*
2P (lbs)	1153	1235	0
δ_V (in.)	1.00	1.20	-1.80
δ_H (in.)	0	0	0.09
Strain Gage No.	Strain ε, (μ in./in.)		
1	472	472	-189
2	-377	-330	448
3	-453	-498	543
4	0	394	1116
5	2975	3063	-1641
6	1300	3423	-2232
7	Out	Out	Out
8	362	317	-204
9	433	910	-2232
10	1356	1881	0
11	1254	1440	-604
12	1526	1832	-1272
13	Out	Out	Out
14	-3272	-4125	332
15	-2613	-2749	2298
16	-3642	-4332	3126
17	3442	4030	-2491
18	4020	4529	-3119

f_d = 7.41 Hz γ = 0.067730

* Strain ε_d at first rebound, and related beam center displacement δ_V.

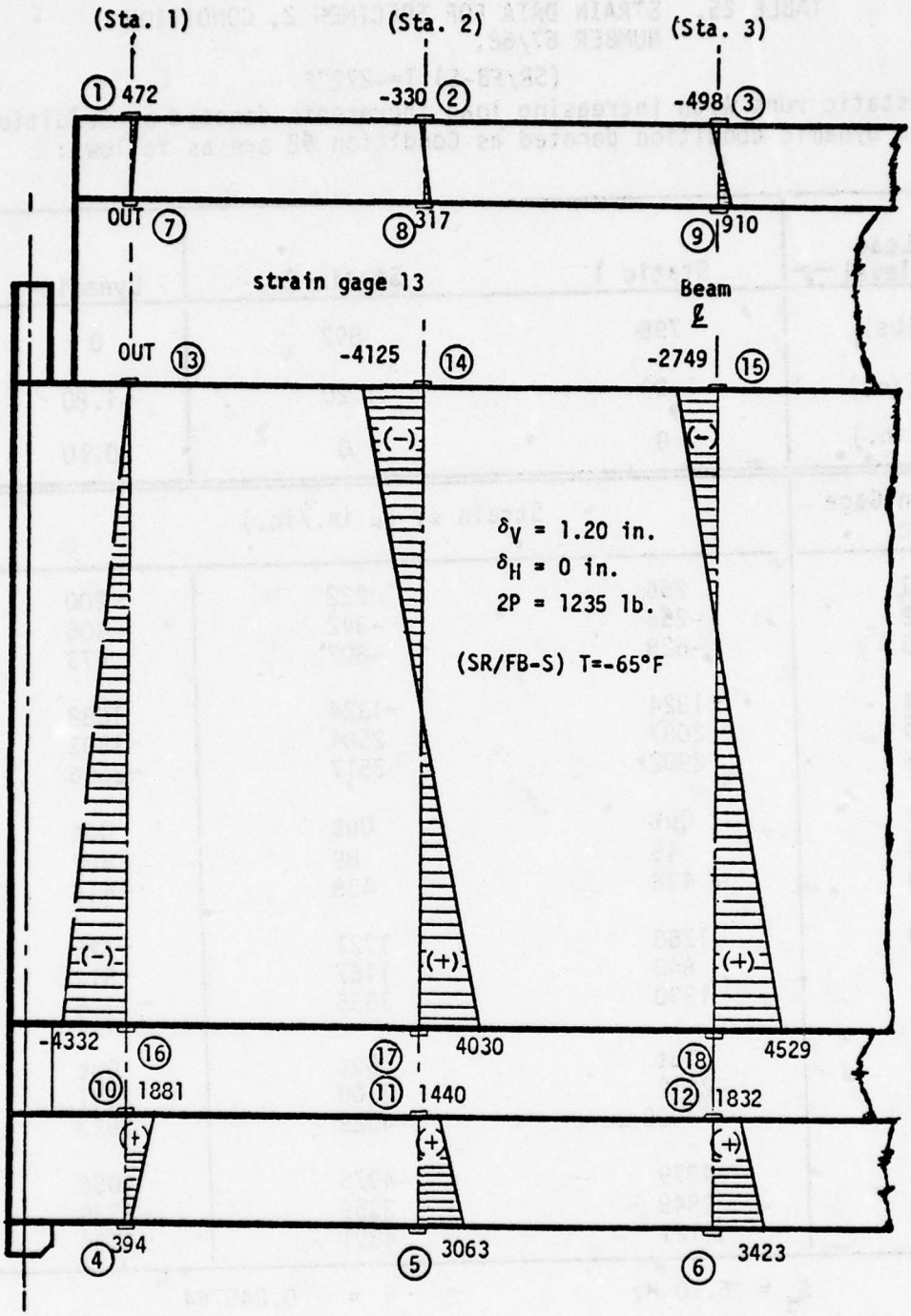

Figure 52. Strain diagrams within structural plies of Specimen 2, Condition 63.

TABLE 25. STRAIN DATA FOR SPECIMEN 2, CONDITION NUMBER 67/68.

(SR/FB-S) T=-272°F

Two static runs with increasing load increments denoted as Condition 67 and a dynamic condition denoted as Condition 68 are as follows:

Load level →	Static 1	Static 2	Dynamic*
2P (lbs)	798	897	0
δ_v (in.)	1.00	1.20	-1.80
δ_H (in.)	0	0	0.10
Strain Gage No.	**Strain ε, (μ in./in.)**		
1	266	222	-200
2	-256	-342	406
3	-628	-807	673
4	-1324	-1324	1688
5	2087	2504	-1503
6	2902	3517	-2506
7	Out	Out	Out
8	45	89	-402
9	438	438	-416
10	1268	1721	-725
11	840	1167	-514
12	1330	1535	-1126
13	Out	Out	Out
14	-2712	-3100	2591
15	-4030	-4529	3623
16	-4379	-4976	4056
17	2849	3359	-2339
18	4121	4891	-3736

f_d = 6.70 Hz γ = 0.045764

* Strain ε_d at first rebound, and related beam center displacement δ_v.

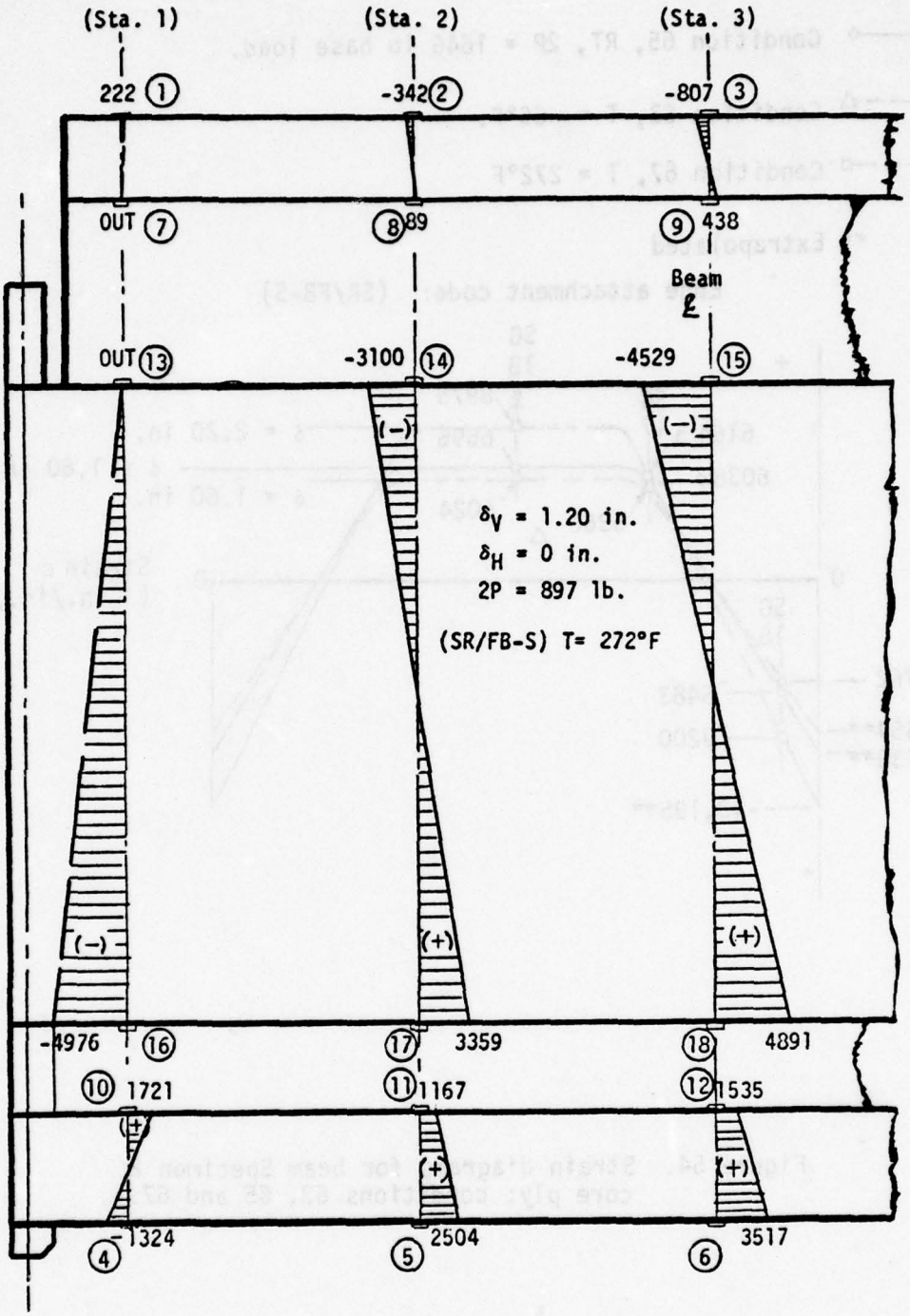

Figure 53. Strain diagrams within structural plies of Specimen 2, Condition 67.

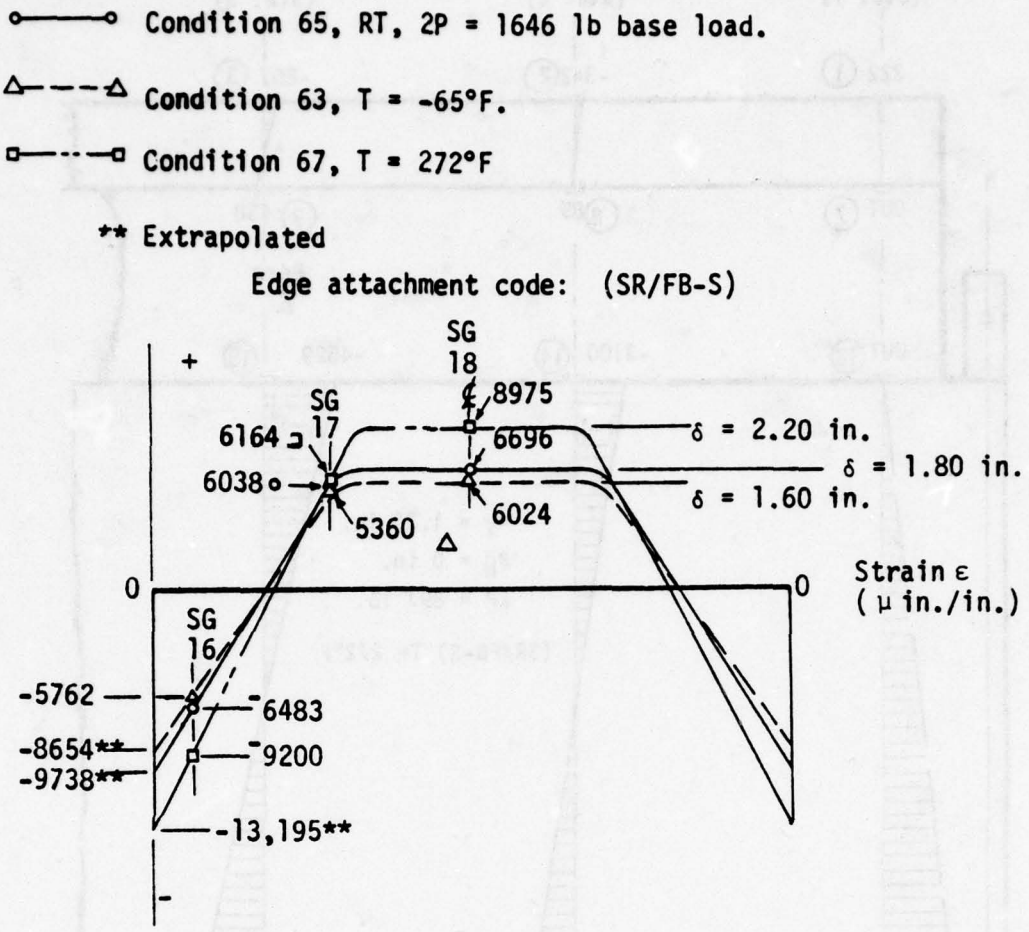

Figure 54. Strain diagrams for beam Specimen 2 core ply; conditions 63, 65 and 67.

Temperature Effects on Single Row Attachments Installed with Aluminum Bushings

A comparison was made of the temperature effects on the strain distribution for the beam with a single row of attachments and using tight fitting aluminum bushings. The temperature goals were -65°F for Condition 19, room temperature for Condition 21, and 272°F for Condition 23.

The strain data test results and strain diagrams within the structural plies for Condition 19 are shown in Table 26 and Figure 55, for Condition 21, shown in Table 20 and Figure 47, and for Condition 23, shown in Table 27 and Figure 56. The superimposed longitudinal strain diagrams for these conditions are shown in Figure 57. Note that the strain diagram curves appear to coincide for the room temperature Condition 21 and the low temperature (-65°F), Condition 19. Most likely, any major difference between the strain values at the attachment area was caused by the higher temperature (Condition 23) weakening the beam's polycarbonate structural plies.

Strain Distribution From Edge Effects On A Multi-Layered Beam

The results and assessment of strain distribution caused by the edge effect for the multi-layered specimen follow. First, a simply supported pin-ended beam with single row of attachments and aluminum bushings is evaluated. Second, a fixed-end beam with single row of attachments and tight fitting aluminum bushings is evaluated for the effects of temperature. Third, a fixed-end beam consisting of single row of attachments with loose holes filled with sealant is evaluated for temperature effect. Lastly, miscellaneous strain data tables are presented.

Simply Supported Pin-Ended Beam

A comparison was made of the strain distribution for two static load levels applied to a simply supported, pin-ended, multi-layered beam (Condition 34 at room temperature, a calibration test). The strain data

TABLE 26. STRAIN DATA FOR SPECIMEN 2, CONDITION NUMBER 19/20.

(SR/SB), T=-65°F

Two static runs with increasing load increments denoted as Condition 19 and a dynamic Condition denoted as condition 20 are as follows:

Load level →	Static 1	Static 2	Dynamic*
2P (lbs)	1003	1806	~
δ_v (in.)	1.02	2.04	-1.53
δ_H (in.)	~	~	~
Strain Gage No.	**Strain ε,(μ in./in.)**		
1	Out	Out	Out
2	-530	-707	574
3	-516	-939	939
4	-656	-1094	1422
5	2320	4640	-2498
6	2958	5644	-4233
7	Out	Out	Out
8	261	523	-305
9	404	897	-605
10	2083	3306	-1381
11	1027	2054	-1167
12	1502	2731	-2162
13	3641	6443	-5252
14	-3154	-6083	3695
15	-4198	-8161	6038
16	-3754	-6570	5265
17	3261	6023	-3781
18	4055	7976	-5858

f_d = 17.5 Hz γ = 0.066057

* Strain ε_d at first rebound, and related beam center displacement δ_v.

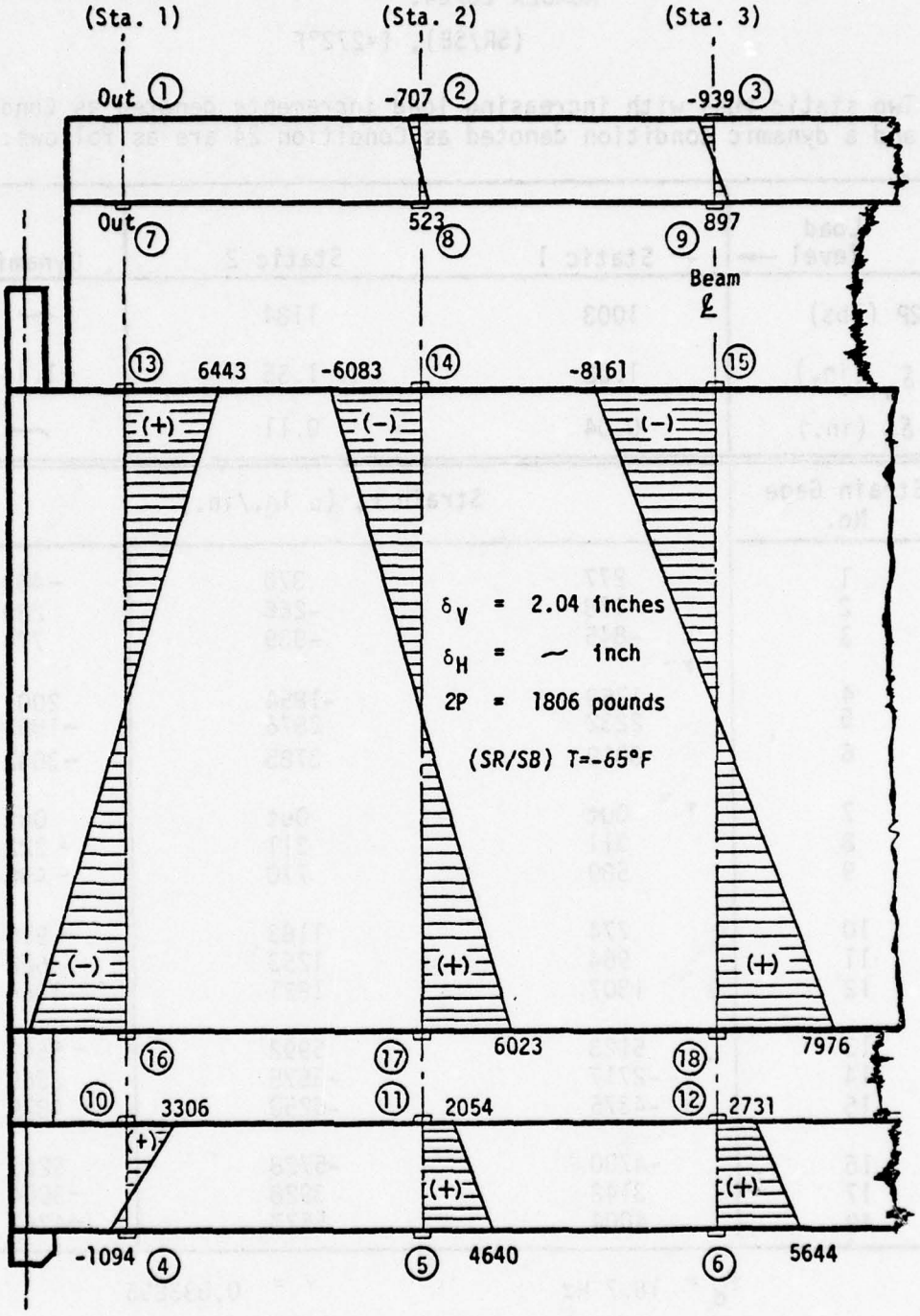

Figure 55. Strain diagrams within structural plies of Specimen 2, Condition 19.

TABLE 27. STRAIN DATA FOR SPECIMEN 2, CONDITION NUMBER 23/24.

(SR/SB), T=272°F

Two static runs with increasing load increments denoted as Condition 23 and a dynamic condition denoted as Condition 24 are as follows:

Load level →	Static 1	Static 2	Dynamic*
2P (lbs)	1003	1184	~
δ_v (in.)	1.02	1.35	-1.14
δ_H (in.)	0.04	0.11	~
Strain Gage No.	**Strain ε, (μ in./in.)**		
1	277	370	-462
2	-178	-266	289
3	-845	-939	774
4	-1769	-1854	2001
5	2232	2876	-1803
6	3019	3785	-3042
7	Out	Out	Out
8	311	311	- 222
9	589	770	- 498
10	774	1183	- 910
11	964	1253	- 626
12	1307	1821	-1354
13	5123	5992	-5649
14	-2717	-3575	2669
15	-4375	-5250	4879
16	-4700	-5728	5263
17	3142	3928	-3004
18	4004	5577	-4767

f_d = 18.7 Hz γ = 0.033855

* Strain ε_d at first rebound, and related beam center displacement δ_v.

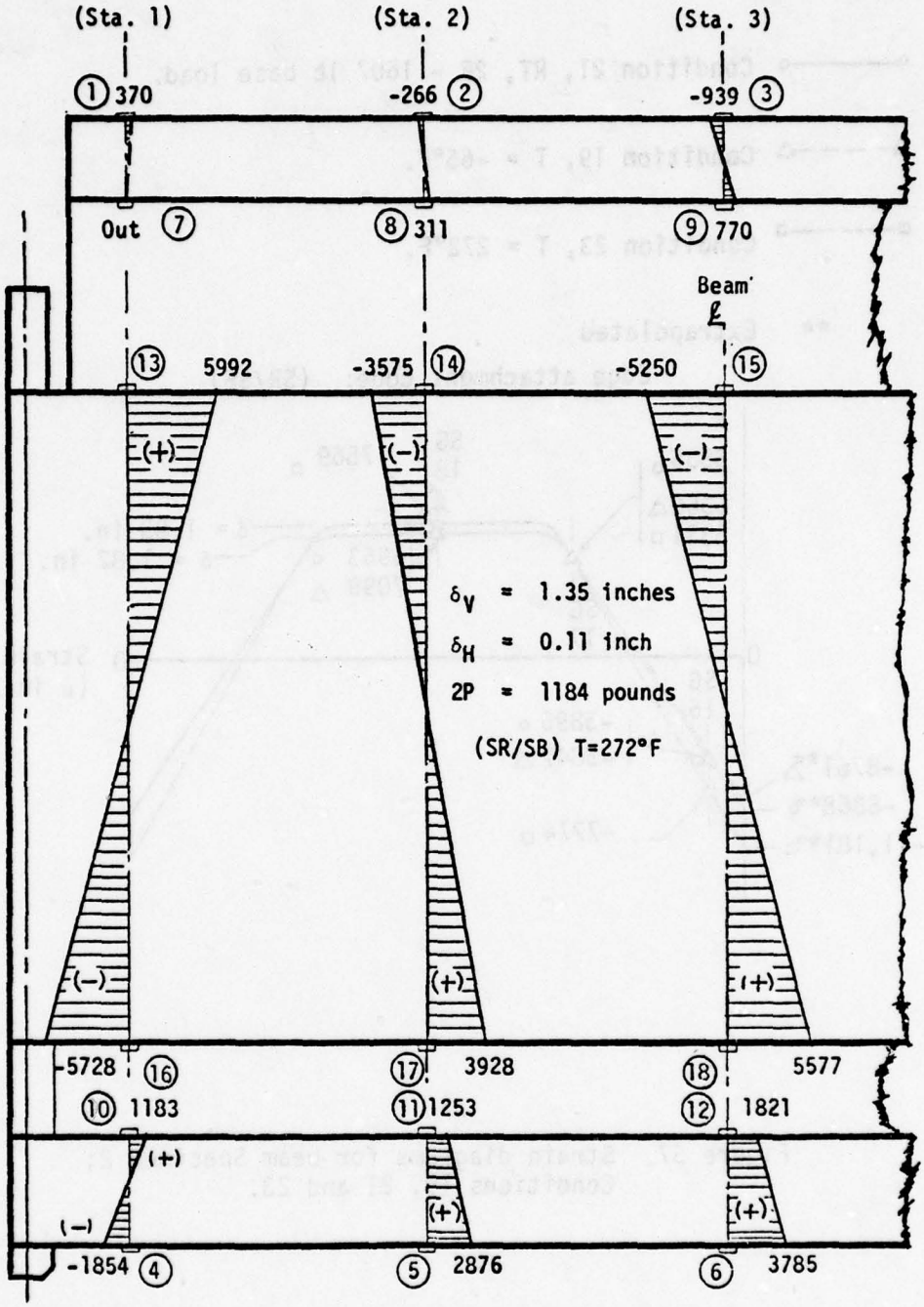

Figure 56. Strain diagrams within structural plies of Specimen 2, Condition 23.

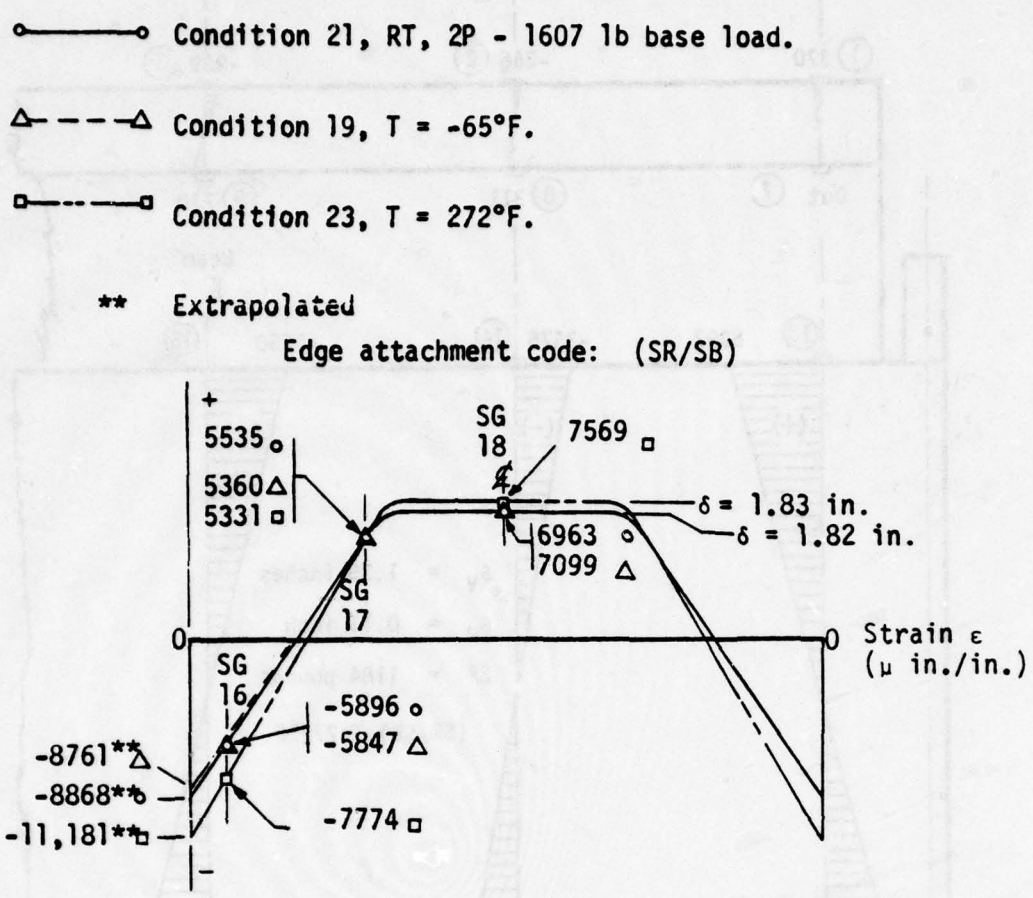

Figure 57. Strain diagrams for beam Specimen 2; Conditions 19, 21 and 23.

test results are shown in Table 28. Strain diagrams within the structural plies are shown in Figures 58, 59 and 60. Figure 58 strain data are for the Static 2 load level where 2P = 532 pounds, causing a 2.07-inch beam center deflection. Figure 59 strain data are for the Static 3 load level where 2P = 818 pounds, causing the lower spall sheet to accidently crack at a beam center deflection of approximately 3.10 inches. Strain distribution in the lower spall sheet was caused by a crack in the spall sheet that went unnoticed for several weeks before being discovered during the refurbishing of the edge attachments. During this two-week period, twenty test conditions for Specimen 4 were ran before the cracked spall sheet was discovered. Since the math could be easily revised to simulate the cracked spall sheet condition and due to the high cost of replacing this specimen and the time constraint, it was decided to run the remaining six conditions "as is". Figure 60 is a composite of these strain diagrams for static load levels 2 and 3. It must be noted that at Station 2 the sloped diagrams are almost in line through all plies. This indicates that this laminate, with PPG112 interlayers, acts almost like a monolithic beam. At Station 3, for Static 3 load level, the strain diagram indicates a lag of shear load transfer at the upper ply, possibly caused by interlayer delamination.

Figure 61 shows the longitudinal strain diagrams for the bottom surface of the lowest polycarbonate structural ply depicting the strain diagrams for Static 2 and 3 load levels. The solid line strain diagram is for the Static 2 load level where 2P = 532 pounds at a beam center deflection of 2.07 inches. The phantom line strain diagram is for the Static 3 load level where 2P = 818 pounds at a beam center deflection of 3.10 inches. The constant bending strain diagram section shape was changed to the approximate shape shown at the time when the spall sheet cracked. The maximum recorded strain was 13, 137 μ in./in. at strain Gage 15. The maximum extrapolated strain in the spall sheet would be approximately 17,000 μ in./in. For reference purposes, the bending modulus of strain for rupture of this spall sheet should be approximately 31,000 μ in./in. The beam's large deflection allowed the beam ends to bottom out on the support fixtures causing an end-fixity condition. This is represented by the negative strain (-4000 μ in./in.) as shown.

TABLE 28. STRAIN DATA FOR SPECIMEN 4, CONDITION NUMBER 34/35.
(SR/SS-PIV), RT

Three static runs with increasing load increments denoted as Condition 34 and a dynamic condition denoted as Condition 35 are as follows:

Load level→	Static 1	Static 2	Static 3	Dynamic
2P (lbs)	307	532	818	~
δ_V (in.)	1.03	2.07	3.10	-1.92
δ_H (in.)	0	0.11	0.57	0.18
Strain Gage No.	Strain ε, (μ in./in.)			
1	-1169	-1315	-974	1290
2	-1969	-4769	-6301	3981
3	-3363	-5829	-11433	6726
4	508	601	970	-693
5	4069	5688	7876	-3391
6	2756	6563	1663	-3063
7	Out	Out	Out	Out
8	-934	-1634	-2101	1401
9	-1254	-2415	-1254	999
10	453	453	1041	-498
11	953	1647	2167	-1387
12	1144	1464	5947	-2470
13	1344	1493	1991	-1319
14	2330	4221	5276	-3166
15	2541	5037	13170	-7648
16	-460	-919	-690	690
17	-332	-948	-1328	830
18	-1053	-1053	-2843	1448
19	0	226	453	-204
20	755	1271	1907	-1076
21	915	1327	5260	-3065
22	277	462	647	-416
23	2962	4722	6524	-4056
24	3302	6068	446	~

f_d = 10 Hz $\quad\quad$ γ = 0.072503

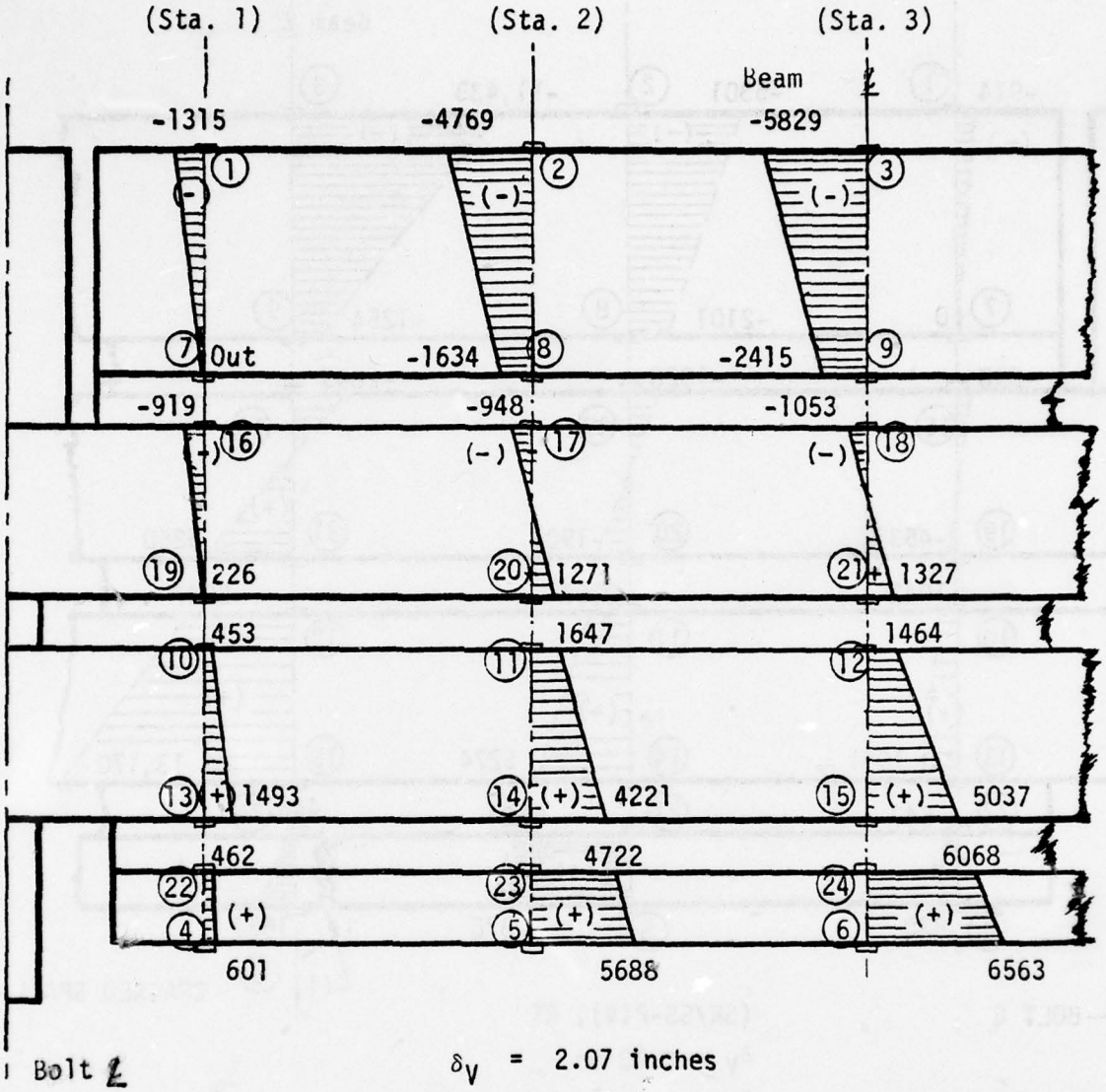

Figure 58. Strain diagrams within structural plies of Specimen 4, Condition 34 (Static 2 data).

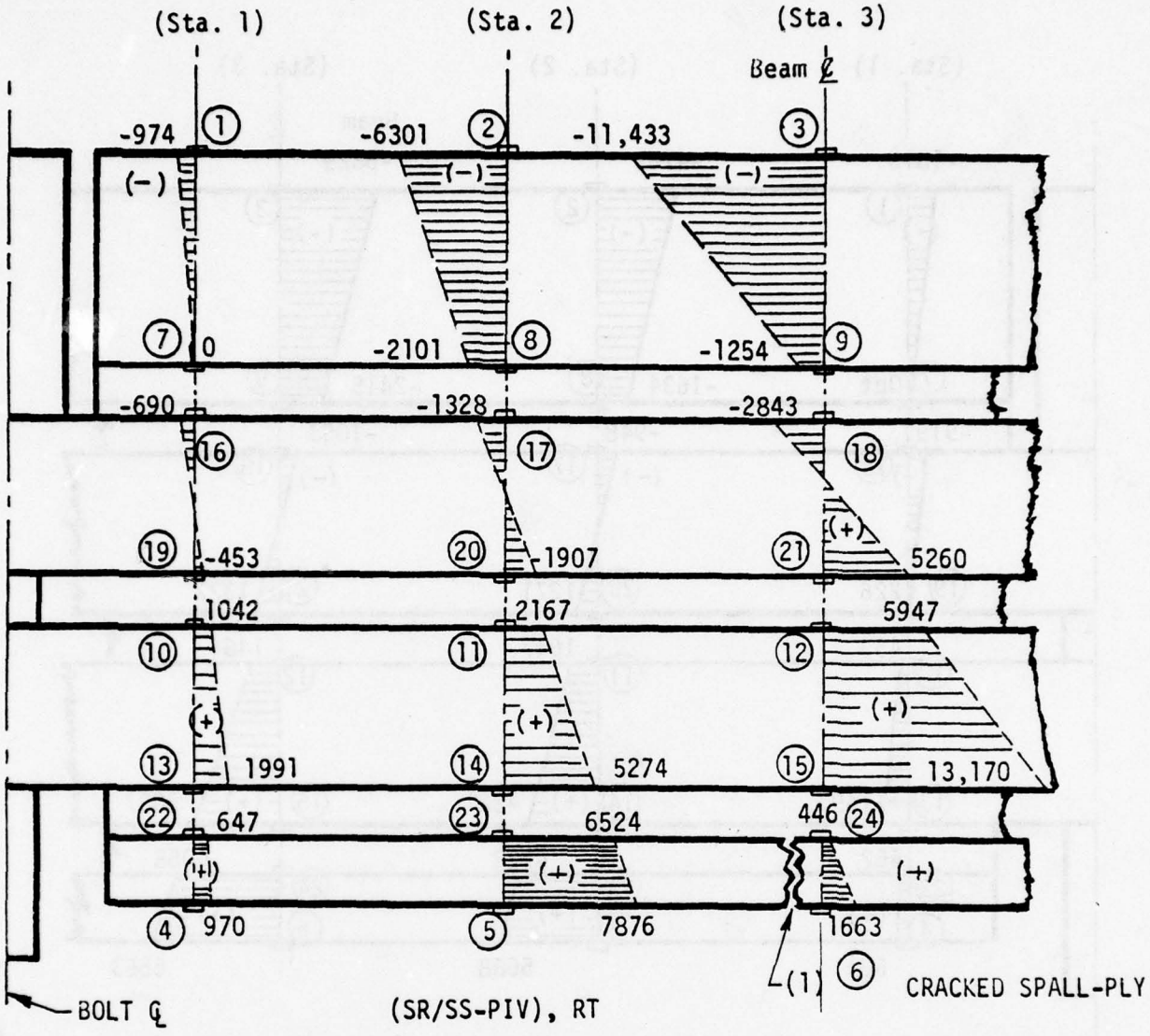

Figure 59. Strain diagrams within structural plies of Specimen 4, Condition 34 (Static 3 data).

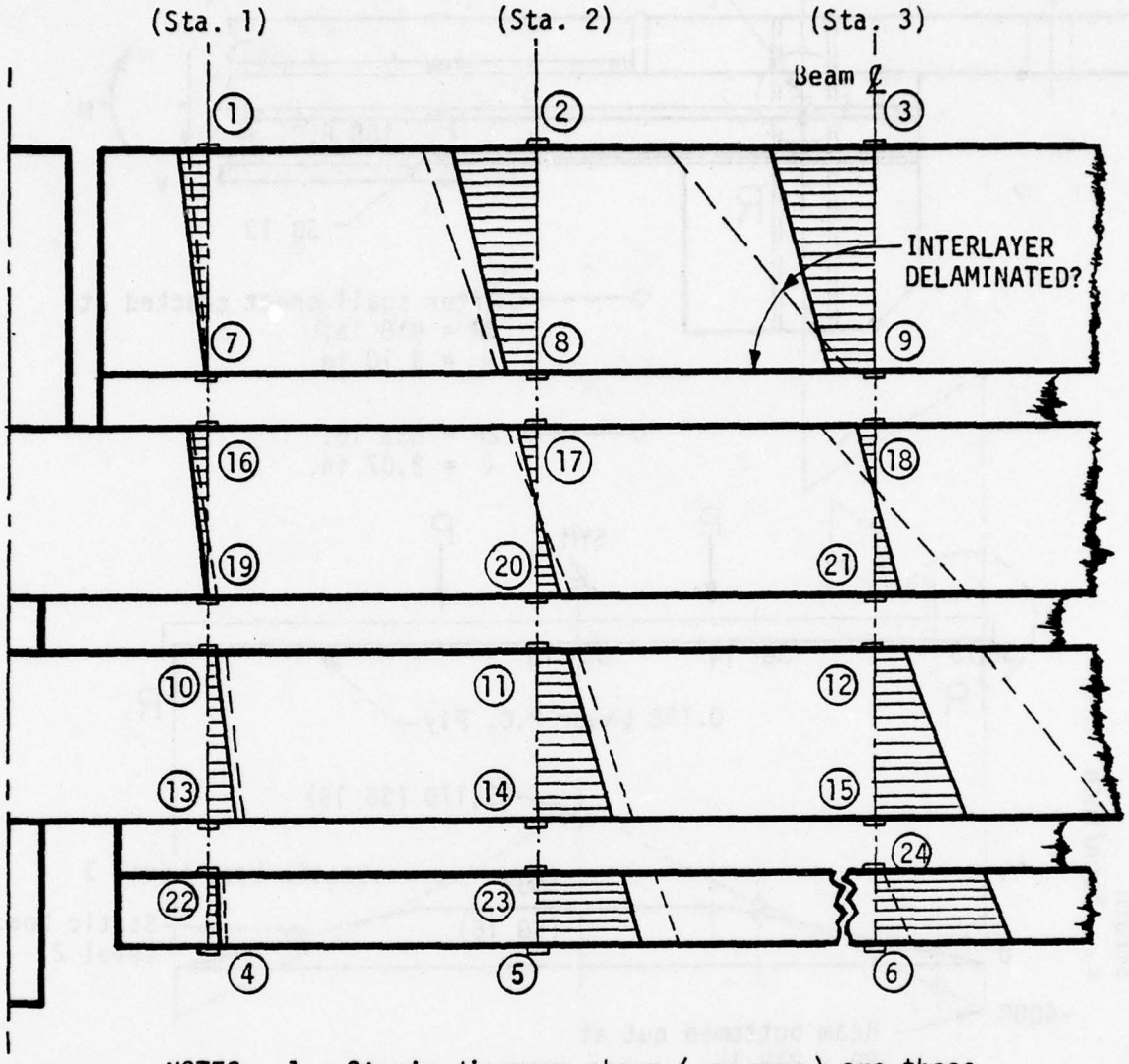

NOTES:
1. Strain diagrams shown (———) are those for the middle readings, static 2 load level.
2. (— — — —) denotes strain diagrams due to load redistribution when lower ply cracked, static 3 load level.
3. At δ = 3.10 inches, the ends of beam bottomed-out on support fixture.

Figure 60. Composite strain diagram of Specimen 4, Condition 34.

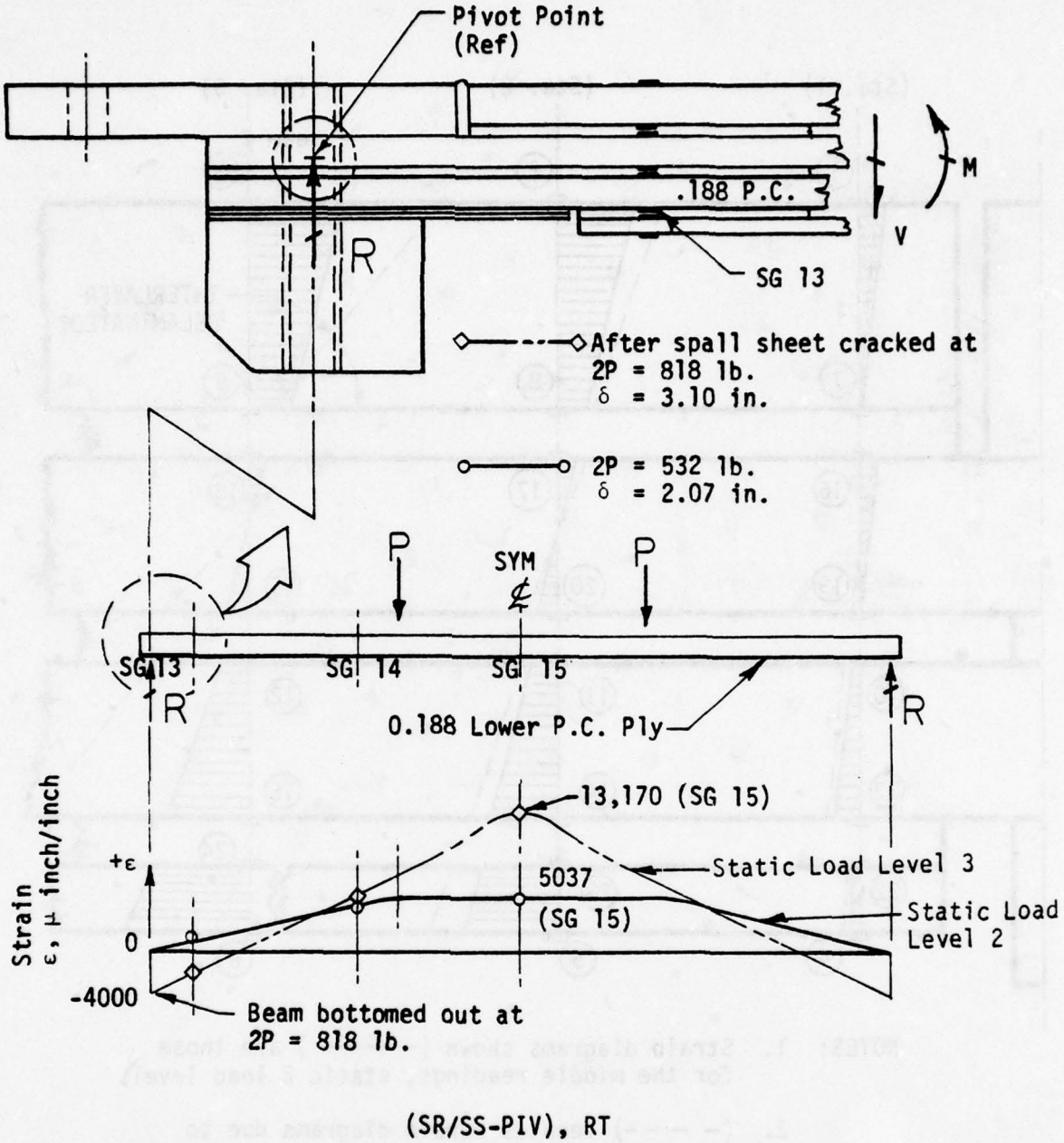

(SR/SS-PIV), RT

Figure 61. Single ply load and strain diagram for calibration of beam, Specimen 4, Condition 34.

Temperature Effects on Single Row Attachments Installed With Aluminum Bushings

A comparison was made of the low, room, and high temperature effects on the strain distribution for a multi-layered beam with a single row of attachments installed in tight fitting aluminum bushings. The temperature goals were -65°F for Condition 38, room temperature for Condition 40, and 200°F for Condition 42.

The strain data test results and strain diagrams within the structural plies for Condition 38 are shown in Table 29 and Figure 62, for Condition 40, shown in Table 30 and Figure 63, and for Condition 42, shown in Table 31 and Figure 64. The superimposed longitudinal strain diagrams for these conditions are shown in Figure 65. As expected, the low temperature test Condition 38, indicated a stiffer beam than the room temperature test; and the high temperature test, Condition 42, indicated a more flexible beam than the room temperature test Condition 40.

Temperature Effects on Single Row Attachments Installed with Sealant

The beam Specimen 4 was tested to determine the temperature effect on the strain distribution for the multi-layered beam with a single row of attachments and loose attachment holes filled with sealant. The temperatue goals were -65°F for Condition 81, room temperature for Condition 83, and 200°F for Condition 85. The strain data test results and strain diagrams within the structural plies for Condition 81 are shown in Table 32 and Figure 66, for Condition 83, shown in Table 33 and Figure 67, and for Condition 85, shown in Table 34 and Figure 68. Since the spall sheet was cracked, only the strain data tables and figures for depicting the strain diagrams within the structural plies are provided.

It should be recalled that in the beam specimens with single row attachments and sealant filled holes, the support bases are always locked from sliding. At no time during this program were tests conducted on beam specimens with single row attachments, tight fitting bushings and support bases locked from sliding. Therefore, a comparison between beam

TABLE 29. STRAIN DATA FOR SPECIMEN 4, CONDITION NUMBER 38/39, (SR/SB), T=-65°F

Static runs with increasing load increments denoted as Condition 38 and a dynamic condition denoted as Condition 39 are as follows:

Load level→	Static (Maximum)	Dynamic
2P (lbs)	762	0
δ_V (in.)	1.12	-.85
δ_H (in.)	0	0
Strain Gage No.	Strain ε, (μ in./in.)	
1	1573	~
2	-2200	1811
3	-4860	3512
4	-1144	1006
5	3369	-2560
6	1794	~
7	132	-352
8	-836	627
9	-819	728
10	-1524	829
11	1121	-819
12	3504	2526
13	-2415	1258
14	2550	-1803
15	6587	-4620
16	549	-114
17	-429	358
18	-576	288
19	-226	498
20	878	-658
21	2896	-1977
22	-878	809
23	2890	-2070
24	446	~

f_d = 16.75 H_z $\quad\quad$ γ = 0.060577

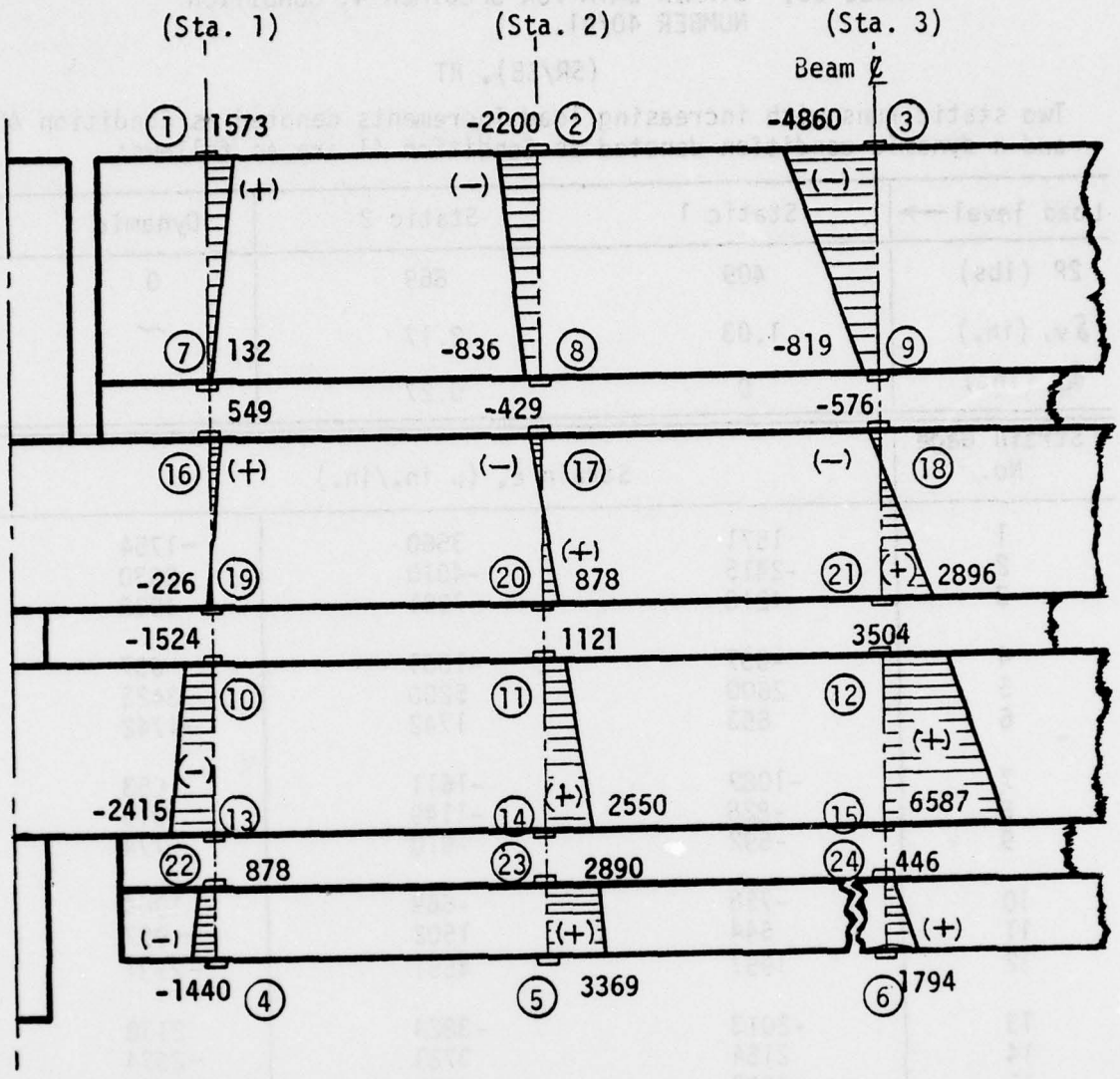

δ_V = 1.12 inches

δ_H = 0 inch

2P = 762 pounds

(SR/SB), T=-65°F

Figure 62. Strain diagrams within structural plies of Specimen 4, Condition 38.

TABLE 30. STRAIN DATA FOR SPECIMEN 4, CONDITION NUMBER 40/41.

(SR/SB), RT

Two static runs with increasing load increments denoted as Condition 40 and a dynamic condition denoted as Condition 41 are as follows:

Load level →	Static 1	Static 2	Dynamic
2P (lbs)	409	869	0
δ_V, (in.)	1.03	2.17	~
δ_H (in.)	0	0.27	~
Strain Gage No.	Strain ε, (μ in./in.)		
1	1571	3560	-1754
2	-2415	-4010	2630
3	-4218	-7991	4928
4	-637	-1001	637
5	2600	5200	-3423
6	653	1742	-1742
7	-1089	-1611	653
8	-828	-1149	919
9	-592	-910	774
10	-758	-669	1004
11	644	1502	-987
12	1957	4551	-2731
13	-2013	-3824	2138
14	2154	3781	-2374
15	4689	9011	-5747
16	1793	3908	-1586
17	-667	-763	596
18	-1059	-1907	1086
19	181	634	-453
20	561	1363	-1603
21	1821	3828	-2311
22	0	418	0
23	2154	4397	-2270
24	0	628	-1278

$f_d = 13.6\ H_z$ $\quad\quad$ $\gamma = 0.066847$

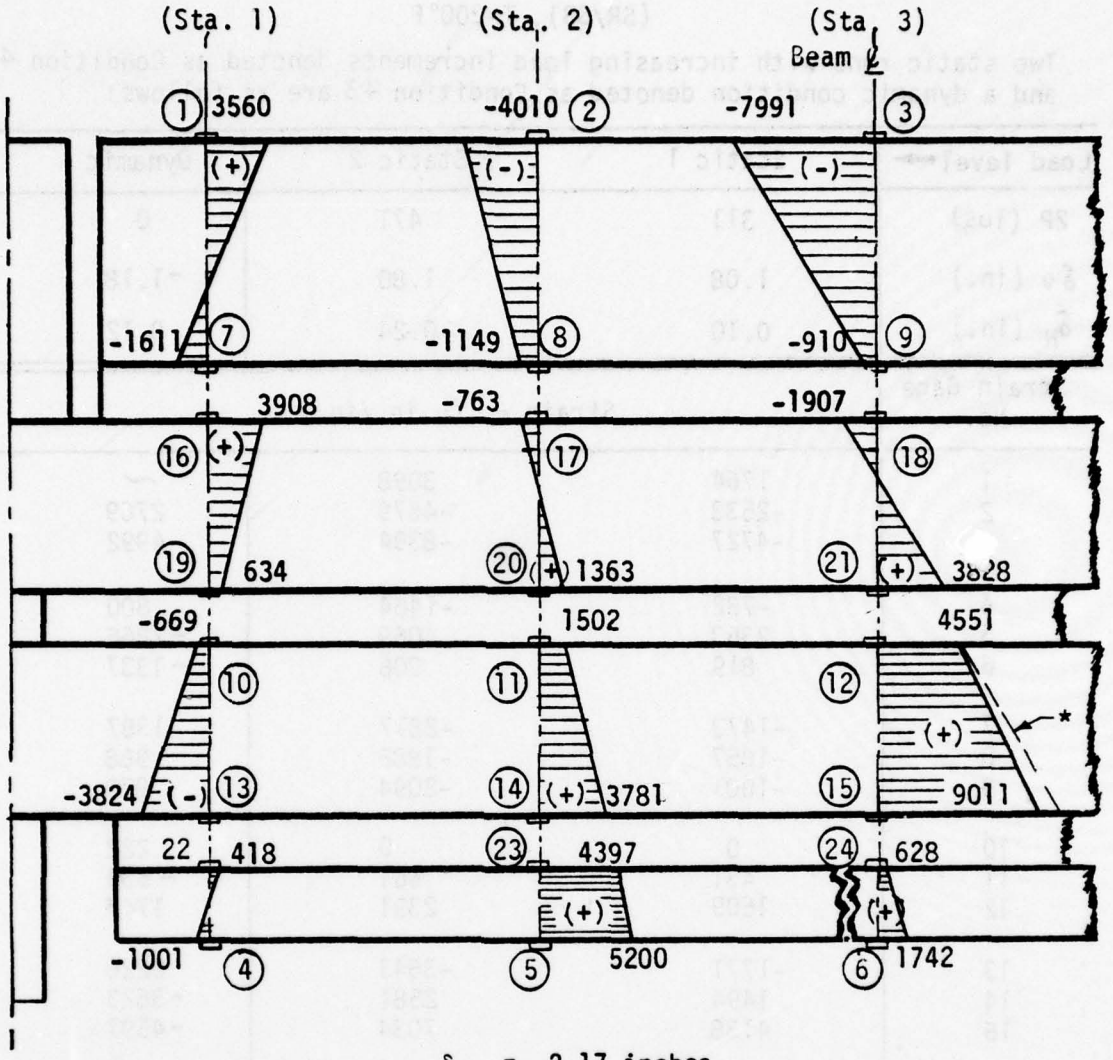

δ_V = 2.17 inches

δ_H = 0.27 inch

2P = 869 pounds

(SR/SB), RT

* Extrapolated

Figure 63. Strain diagrams within structural plies of Specimen 4, Condition 40

TABLE 31. STRAIN DATA FOR SPECIMEN 4, CONDITION NUMBER 42/43.

(SR/SB), T=200°F

Two static runs with increasing load increments denoted as Condition 42 and a dynamic condition denoted as Condition 43 are as follows:

Load level→	Static 1	Static 2	Dynamic
2P (lbs)	311	471	0
δ_V (in.)	1.08	1.80	-1.18
δ_H (in.)	0.10	0.24	0.12
Strain Gage No.	Strain ε, (μ in./in.)		
1	1764	3098	~
2	-2533	-4679	2769
3	-4727	-8394	4992
4	-732	-1464	800
5	2363	4069	-2866
6	819	906	-1337
7	-1473	-2817	1387
8	-1057	-1885	988
9	-1001	-2094	979
10	0	0	222
11	431	561	-539
12	1609	2391	1747
13	-1771	-3643	2226
14	1494	2581	-3623
15	4138	7034	-4597
16	Out	Out	Out
17	-664	-1280	854
18	-1474	-2633	1501
19	0	0	~
20	477	636	-516
21	1533	2276	-1626
22	231	185	-185
23	1829	3048	-2221
24	0	0	~

f_d = 11.25 H γ = 0.054825

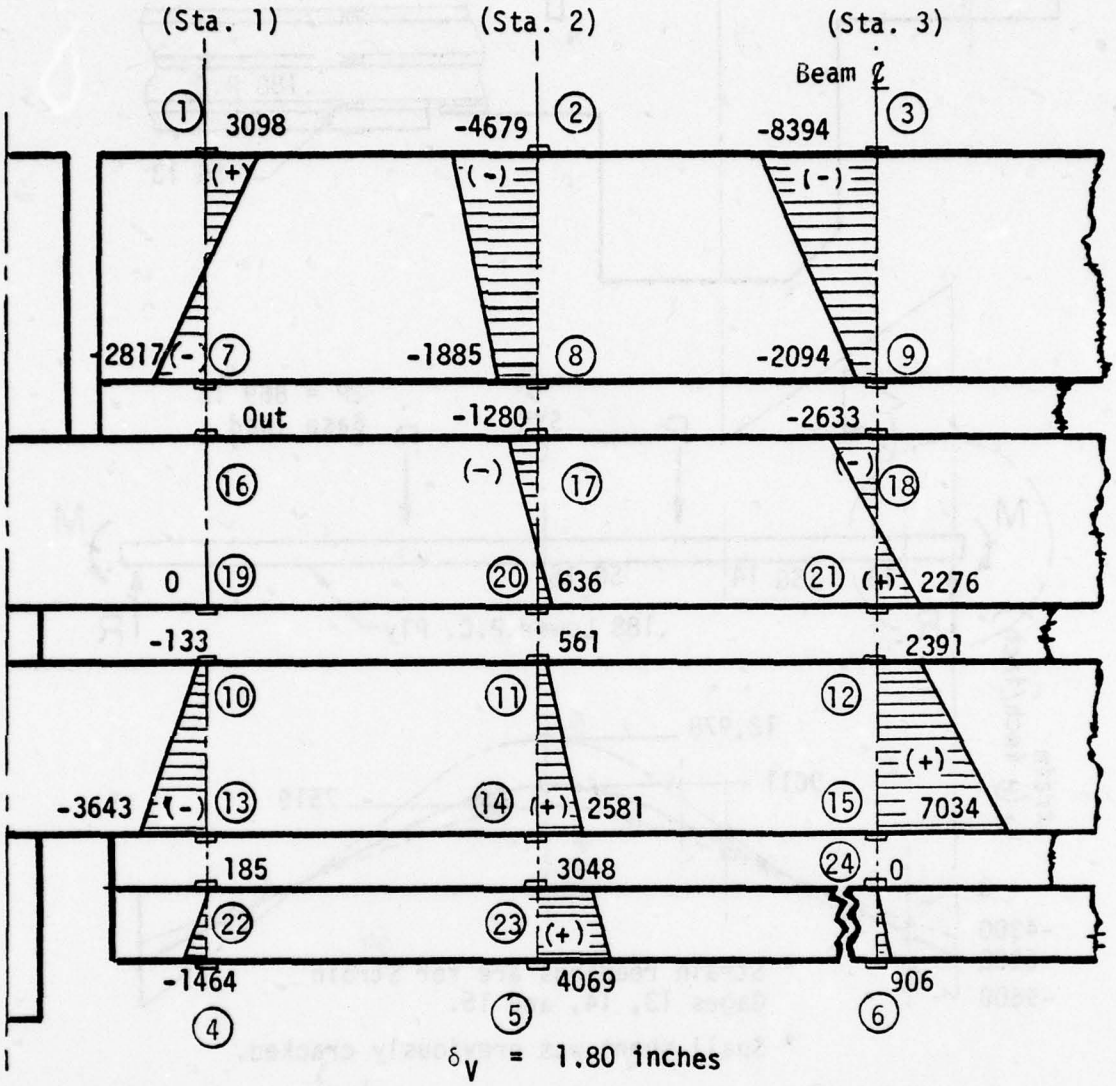

δ_V = 1.80 inches

δ_H = .24 inch

2P = 471 pounds

(SR/SB), T=200°F

Figure 64. Strain diagrams within structural plies of Specimen 4, Condition 42.

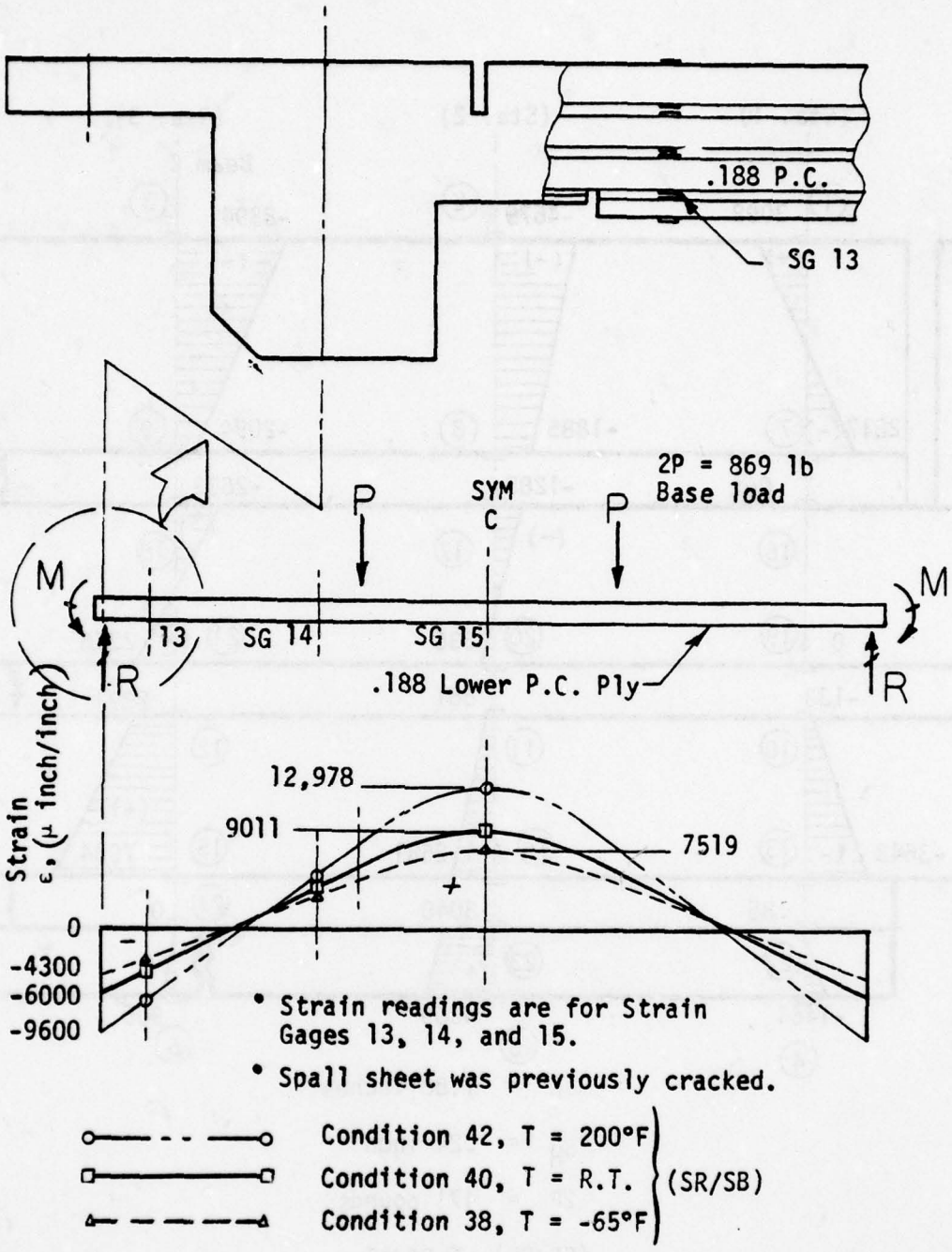

Figure 65. Load and strain diagrams for Specimen 4, Conditions 38, 40, and 42.

TABLE 32. STRAIN DATA FOR SPECIMEN 4, CONDITION 81/82

(SR/FB-S), T=-65°F

One static runs with increasing load increments denoted as Condition 81 and a dynamic condition denoted as Condition 81 are as follows:

Load level	Static 1	Dynamic*
2P (lbs)	821	-----
δ_{V}, (in.)	0.90	-1.4
δ_{H}, (in.)	0	-----
Strain Gage No.	Strain ε, (μ in./in.)	
1	572	-572
2	-2353	1598
3	-2758	2850
4	-444	533
5	3063	-2198
6	533	-599
7	519	-236
8	-422	563
9	-230	621
10	-831	788
11	1281	-755
12	2381	-3822
13	-1081	1036
14	2252	-1462
15	5183	-2054
16 (OUT)	-----	-----
17	0	-294
18 (OUT)	-----	0
19	644	0
20	1085	-590
21	2355	-1608
22	-219	394
23	2536	-1857
24 (OUT)	-----	-----

f_d = 19.3 H_z Y= 0.047426

* Strain (ε_d)@ first rebound, and related beam center displacement δ_v.

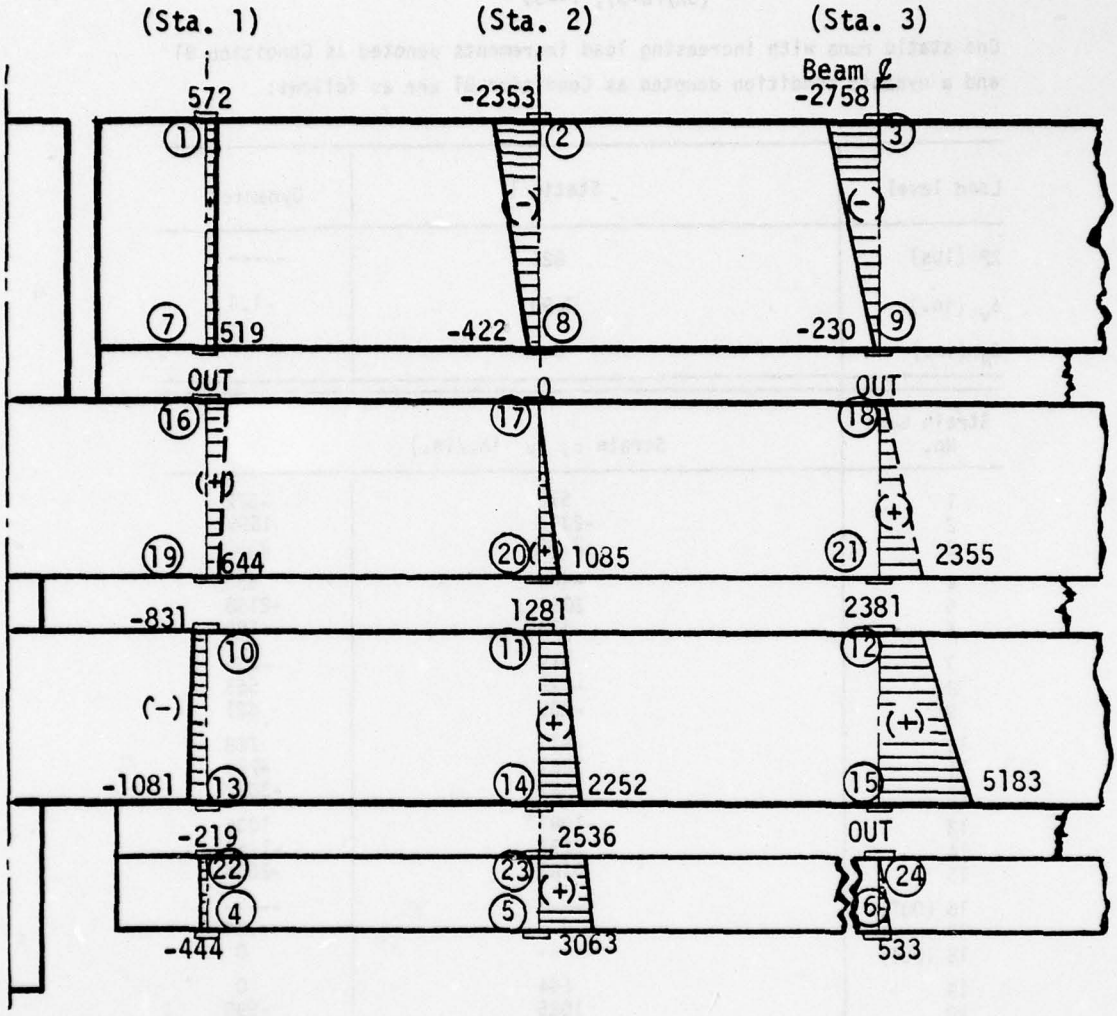

(SR/FB-S), T=-65°F

δ_V = 0.90 inches

δ_H = 0

2P = 21 pounds

----- denotes extrapolted

Figure 66. Strain diagrams within structural plies of Specimen 4, cond. 81

AD-A054 463 DOUGLAS AIRCRAFT CO LONG BEACH CALIF F/G 11/9
DAMPING, STATIC, DYNAMIC, AND IMPACT CHARACTERISTICS OF LAMINAT--ETC(U)
DEC 77 G F RHODES F33615-75-C-3105

UNCLASSIFIED MDC-J6944 AFFDL-TR-76-156 NL

3 OF 3
AD
A054463

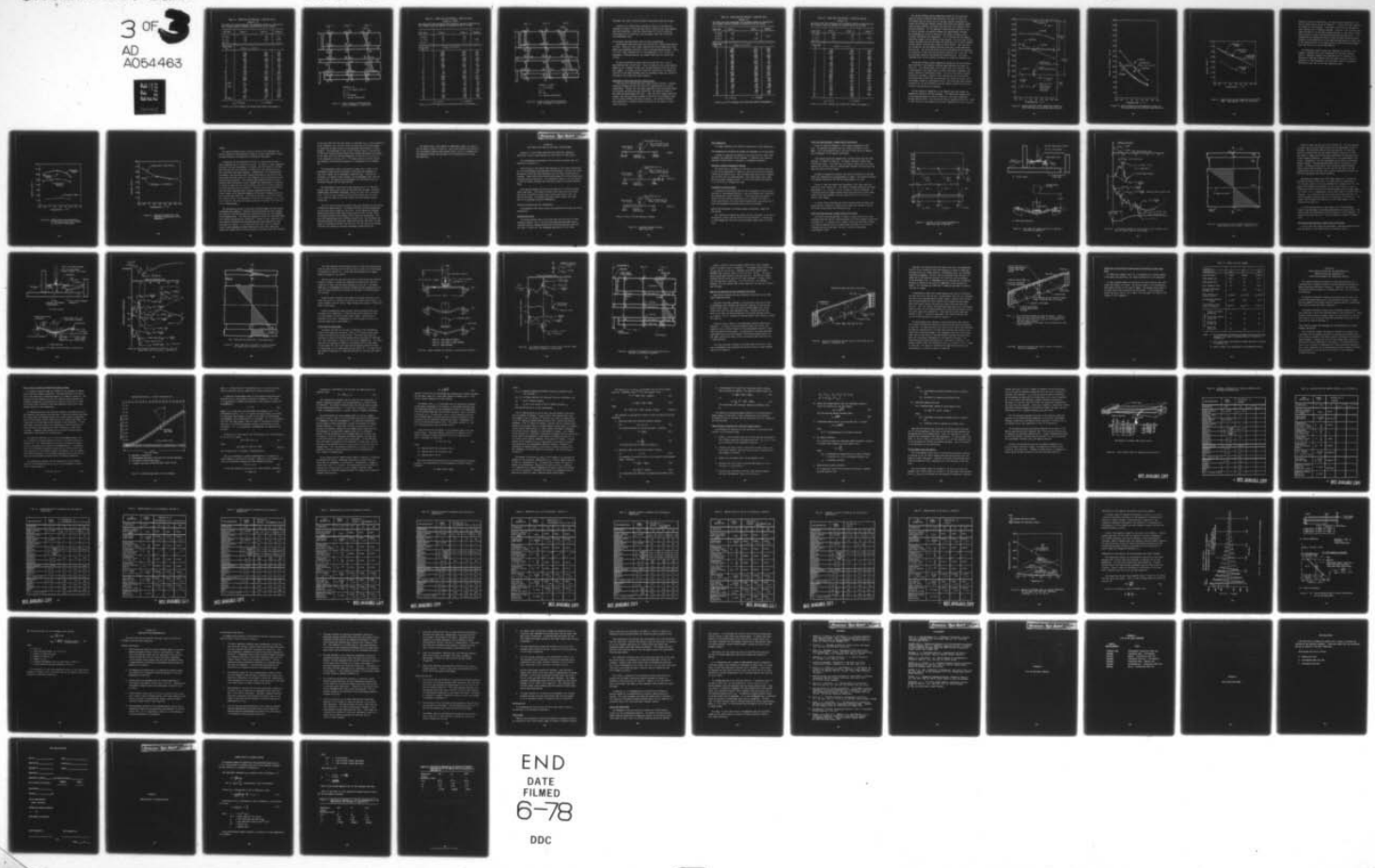

END
DATE
FILMED
6-78
DDC

TABLE 33. STRAIN DATA FOR SPECIMEN 4, CONDITION 83/84.

(SR/FB-S), RT

Two static runs with increasing load increments denoted as Condition 83 and a dynamic condition denoted as Condition 84 are as follows:

Load level	Static 1	Static 2	Dynamic*
2P (lbs)	494	798	-----
δ_V (in.)	1.02	1.35	-0.96
δ_H (in.)	0	0	-----
Strain Gage No.	**Strain ε (μ in./in.)**		
1	1150	1677	-1006
2	-1988	-2342	1966
3	-3816	-4781	3816
4	-577	622	-533
5	2638	3913	-2682
6	525	700	-503
7	-739	693	-531
8	-457	549	-663
9	-362	-317	566
10	-260	217	-780
11	878	1432	-901
12	2159	3191	2229
13	-1352	-1262	1622
14	1859	2669	-1811
15	4607	6282	4502
16 (OUT)	-----	-----	-----
17	-457	-229	412
18 (OUT)	-----	-----	-----
19	736	1241	-713
20	751	1267	-774
21	2094	2230	-2185
22	0	704	-1894
23	2231	3257	-2253
24 (OUT)	-----	-----	-----

$f_d = 14.35\ H_Z$ $\quad\quad$ $\gamma = 0.051091$

* Strain ε_d at first rebound, and related beam center displacement δ_V.

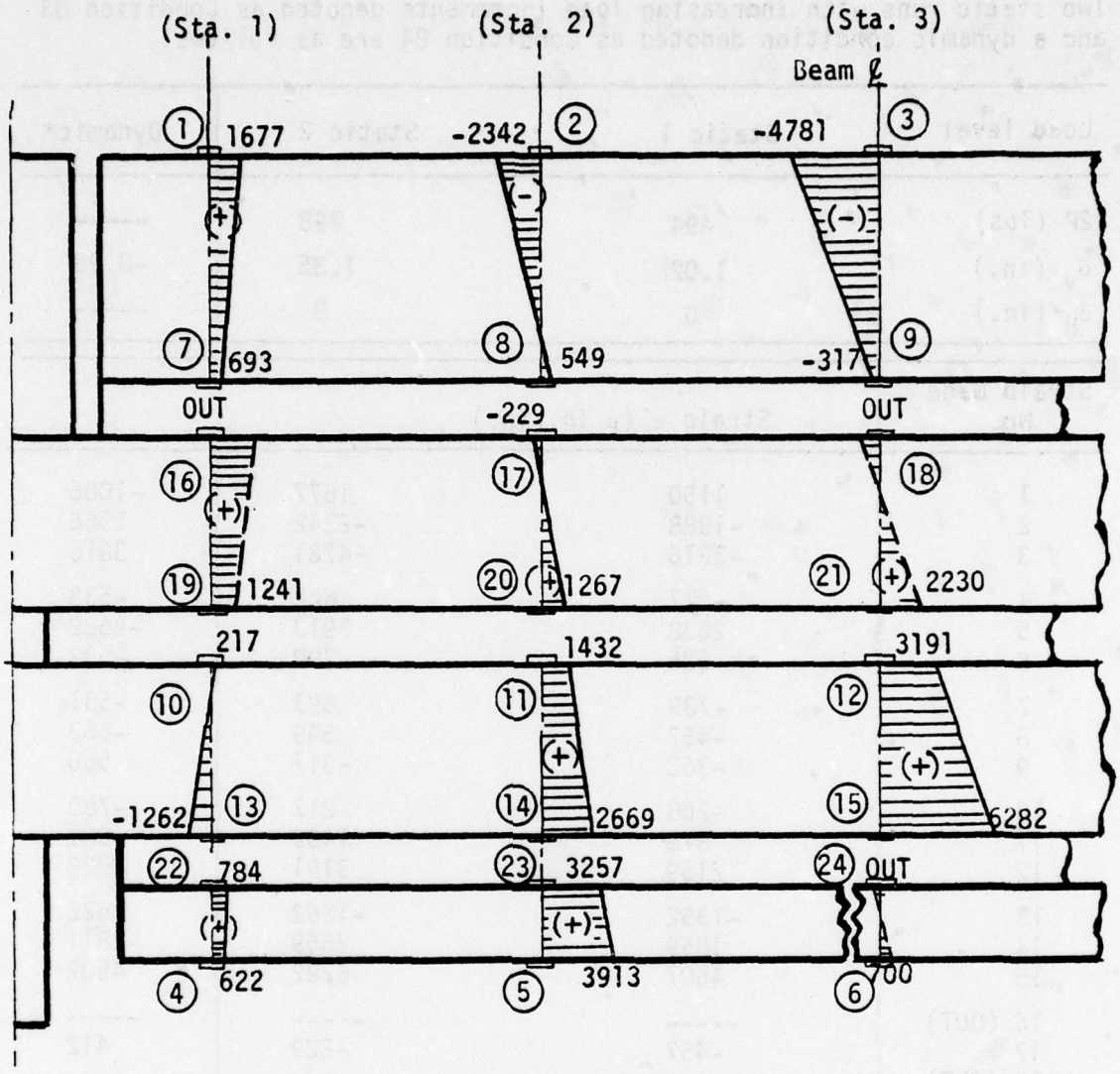

(SR/FB-S), RT

δ_V = 1.35 inches (static 2)

δ_H = 0

2P = 798 pounds

---- denotes extrapolated

Figure 67. Strain diagrams within structural plies of Specimen 4, Condition 83.

TABLE 34. STRAIN DATA FOR SPECIMEN 4, CONDITION 85/86.

(SR/FB-S), T=200°F

Two static runs with increasing load increments denoted as Condition 85 and a dynamic condition denoted as Condition 86 are as follows:

Load level	Static 1	Static 2	Dynamic*
2P (lbs)	191	602	
δ_v (in.)	.98	1.70	-1.08
δ_H (in.)	0	0	0
Strain Gage No.	**Strain ε (μ in./in.)**		
1	-1294	-2109	1869
2	-2545	-4011	1763
3	-4870	-6827	4005
4	-747	-879	769
5	2200	4658	-2560
6	OUT	OUT	OUT
7	-1659	-2197	1211
8	-888	-1066	644
9	-747	-1011	769
10	0	513	-449
11	418	1254	-743
12	276	3035	-1657
13	-1838	-2018	2287
14	1542	3276	-1710
15	1587	7179	-4335
16	OUT	OUT	OUT
17	1092	-592	592
18	OUT	OUT	OUT
19	457	1555	-274
20	511	1347	-650
21	1524	2780	-1569
22	0	388	-151
23	1963	3302	-1829
24	OUT	OUT	OUT

f_d = 9.8 H_Z γ = 0.045597

* Strain ε_d at first rebound, and related beam center displacement δ_v.

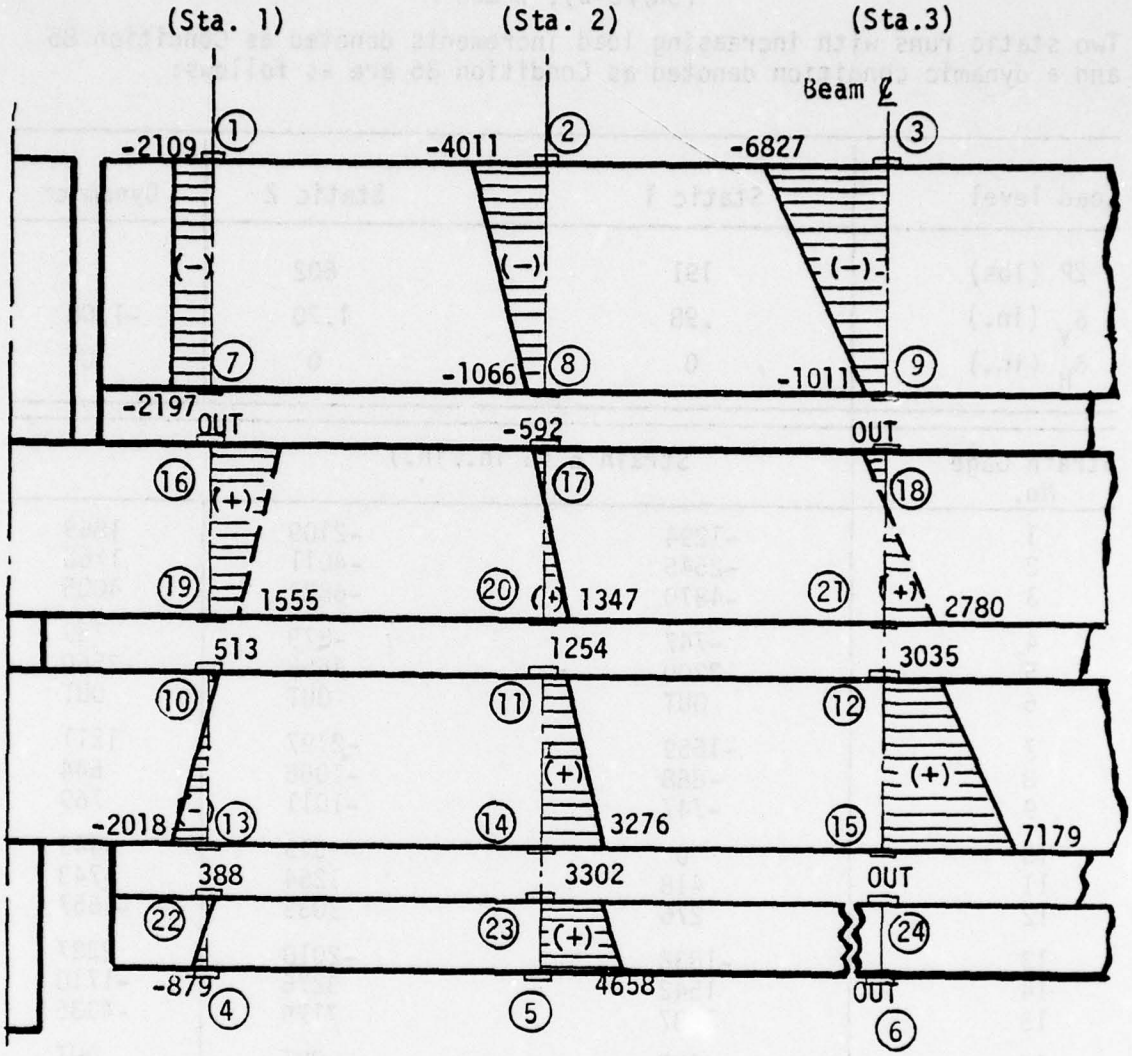

Figure 68. Strain diagrams within structural plies of Specimen 4, Condition 85.

specimens with tight fitting and loose fitting holes could not be made.

Figures 66, 67 and 68 strain diagrams at Station 2 show that the diagrams are almost in line and have similar slopes for all three temperature test conditions. Note that strain gages 16, 18 and 24 were not functioning for all conditions, and that gage 6 "went out" during the high temperature test.

Miscellaneous Tabulated Strain Data for Multi-Layered Beam

Miscellaneous tabulated strain data for the multi-layered beam specimen 4 follow. Table 35 is for a beam, condition 46 at room temperature, with double row attachments installed in tight fitting aluminum bushings. Table 36 is for a beam, Condition 48S at room temperature, with a double row attachments, aluminum bushings, and support bases that are locked from sliding.

The spring constant for beam Condition 46 was 391 lb/in. and for beam Condition 48S, of 680 lb/in. Thus, the beam with the locked supports appears to be 74 percent stiffer than the beam condition with one sliding base support. In actual aircraft windshield installation, the tangential restraint at the edge attachment would be somewhere between the restraints provided by the sliding and locked supports.

Comparison of Thick Core and Multi-Layered Beams

Since the multi-layered beam spall sheet had been cracked, a complete comparison between the thick core and multi-layered beams could not be accomplished. However, for the simply supported single row attached beams with pivoting end configurations (SR/SS-PIV), the spring stiffness of each beam was approximately 500 lb/in. After the multi-layered beam spall cracked, the spring stiffness changed to 264 lb/in; the percentage reduction of spring stiffness was about 47 percent. The spring stiffnesses were determined by dividing the applied load 2P by the amount the beam center displaced.

TABLE 35. STRAIN DATA FOR SPECIMEN 4, CONDITION 46/47 (DR/SB), RT

Two static runs with increasing load increments denoted as Condition 46 and a dynamic condition denoted as Condition 47 are as follows:

Load level	Static 1	Static 2	Dynamic*
2P (lbs)	406	782	
δ_v (in.)	1	2	-1.18
δ_H (in.)	0.17	0.26	
Strain Gage No.	**Strain ε (μ in./in.)**		
1	1438	3115	-1342
2	-2264	-4137	2721
3	-4283	-8120	5019
4	-739	-1294	693
5	2651	5081	-3424
6	569	2188	-875
7	-884	-1811	751
8	-828	-1379	919
9	-595	-1052	800
10	-669	-892	1026
11	474	1294	-1014
12	1951	3809	-1626
13	-2137	-4223	2442
14	1998	3463	-2331
15	4713	9288	-5776
16	2023	4460	-2552
17	-620	-453	596
18	-1225	-2025	1145
19	181	362	-249
20	479	1197	-798
21	1997	3762	-2346
22	0	280	0
23	2121	4241	-2805
24	0	0	-1121

f_d = 13.6 H_Z γ = 0.069769

* Strain ε_d at first rebound, and related beam center displacement δ_v.

TABLE 36. STRAIN DATA FOR SPECIMEN 4, CONDITION 48S/48D. (DR/FB), RT

Two static runs with increasing load increments denoted as Condition 48S and a dynamic condition denoted as Condition 48D are as follows:

Load level	Static 1	Static 2	Dynamic*
2P (lbs)	620	803	0
δ_v (in.)	1.00	1.18	-0.66
δ_H (in.)	0	0	0
Strain Gage No.	Strain ε (μ in./in.)		
1	1390	1581	-934
2	-1742	-2134	1633
3	-3391	-4149	3034
4	416	462	-347
5	3048	3534	-2496
6	700	963	-350
7	-530	-751	398
8	-368	-414	505
9	-183	-229	823
10	134	982	-402
11	1078	1294	-1294
12	2322	2787	-1486
13	-1069	-1221	1170
14	2264	2575	-1776
15	4852	5730	-4020
16	2437	2988	-1954
17	0	0	0
18	-533	-533	613
19	1132	1359	-679
20	997	1197	-738
21	2276	2601	-1742
22	233	280	0
23	2518	3093	-4020
24	0	224	

$f_d = 14.2\ H_Z$ $\gamma = 0.061075$

* Strain ε_d at first rebound, and related beam center displacement δ_v.

The spring stiffness versus temperature change for the thick core beam with several different edge restraints are shown in Figure 69. The plotted data and curves are for the edge restraint conditions of: Single row/sliding base (SR/SB), double row/sliding base (DR/SB), double row/fixed base (DR/FB), and single row/fixed base, with sealant filled bushings (SR/FB-S). For the specimen 2 edge restraint conditions, 19, 21 and 23, (SR/SB), the spring stiffness was approximately constant. For Conditions 63, 65 and 67 (SR/FB-S), the spring stiffness varied linearly, decreasing with temperature. This indicated that the change was mainly caused by the softening of the sealant. As can be seen in the figure, the beams with the end restraint conditions, 25, 27 and 30 (DR/SB), and 29S (DR/FB), provided much higher spring stiffness. Only one point was plotted for the 29S (DR/FB) condition since only a room temperature test was run. The spring stiffness curve for the DR/SB would be expected to be parallel to the cruve for the SR/SB condition; but it was not. This may have been caused by instrumentation recording error. The simply supported beams relative spring stiffnesses are shown for reference only.

The spring stiffness versus temperature change for the multi-layered beam (Specimen 4) with several different edge restraints are shown in Figure 70. This laminate beam (acrylic face plies, two structural plies of polycarbonate, and three layers of PPG112 interlayers) appeared to be greatly affected by temperature change. The curves for SR/SB and DR/SB practically coincided. Actually, the Conditions 44, 46 and 49 (DR/SB) should have been stiffer than the Conditions 38, 40 and 42 (SR/SB); this was probably caused by load reading errors. The fixed base edge restraint Conditions 81, 83 and 85 (SR/FB-S) and 48S (DR/FB), showed higher spring stiffness characteristics as expected.

The last method of comparison is the damping ratio with respect to temperature change for the two specimens. The abbreviated damping ratio by the alternate method as shown in Appendix C, was used to determine average damping ratios. The results are shown in graphical form only. Figure 71 shows the curves for damping ratio versus temperature for thick core ply

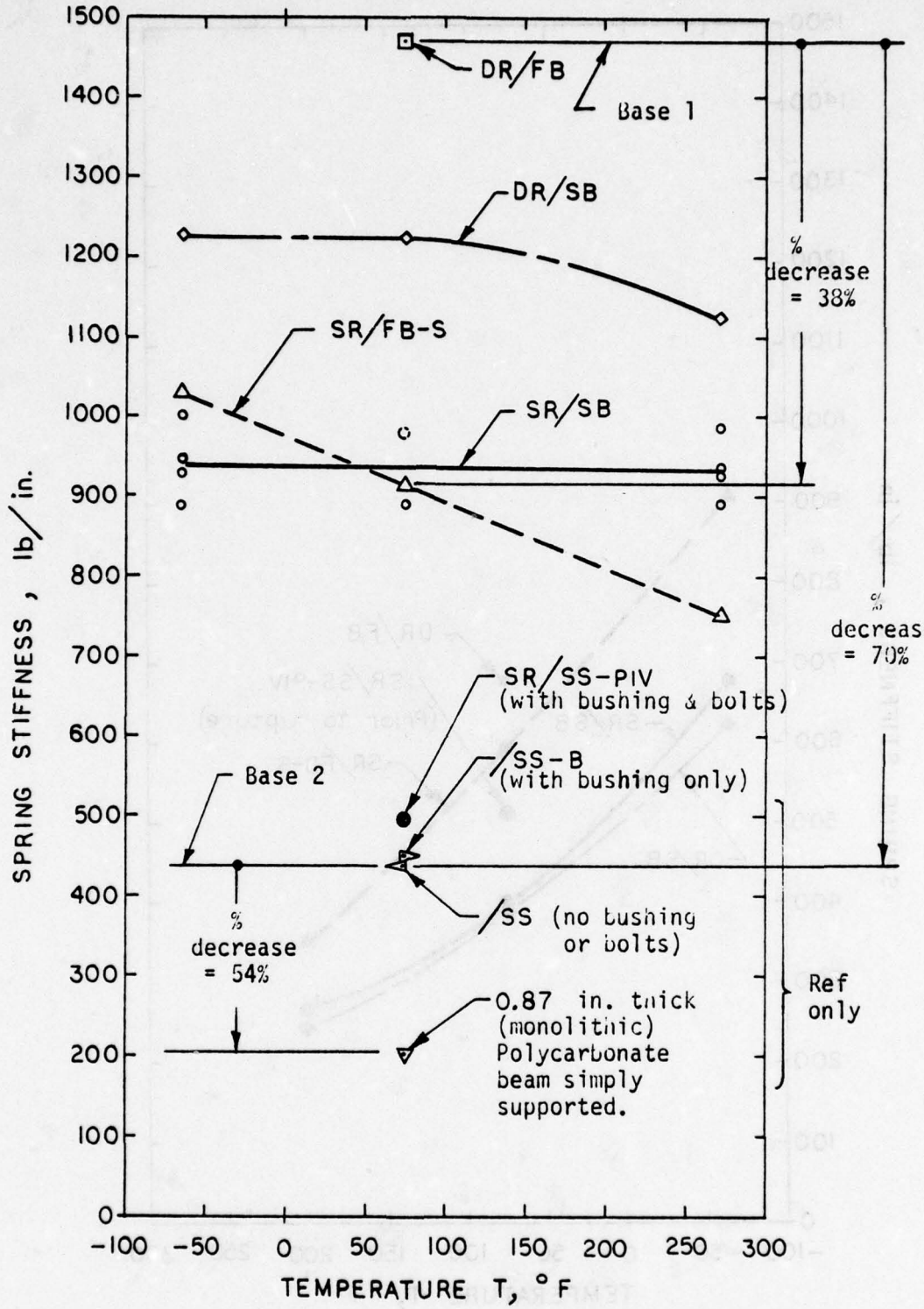

Figure 69. Spring stiffness versus Temperature change for thick core beam with different edge restraints.

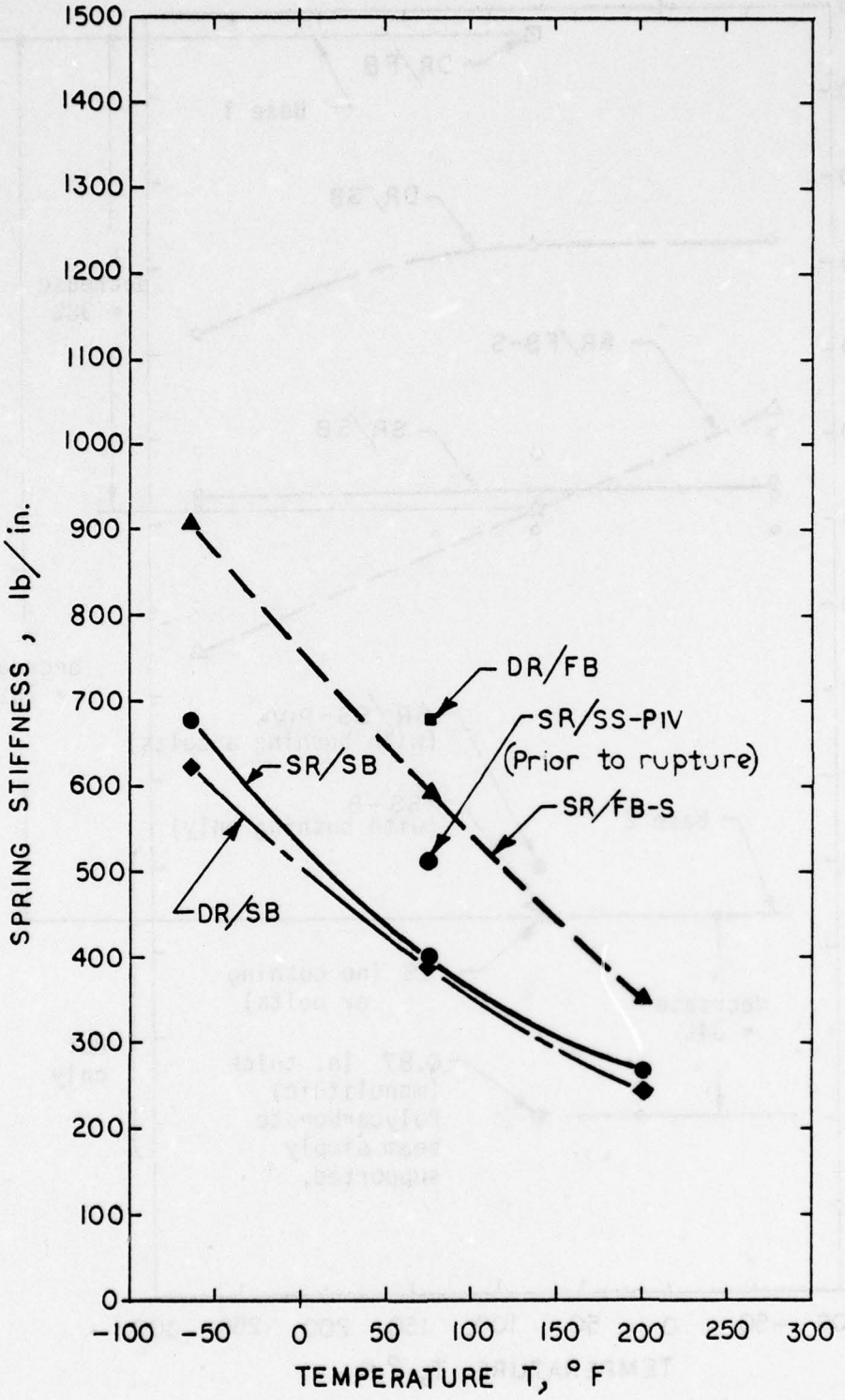

Figure 70. Spring stiffness versus Temperature change for Multi-Layered beam with different edge restraints.

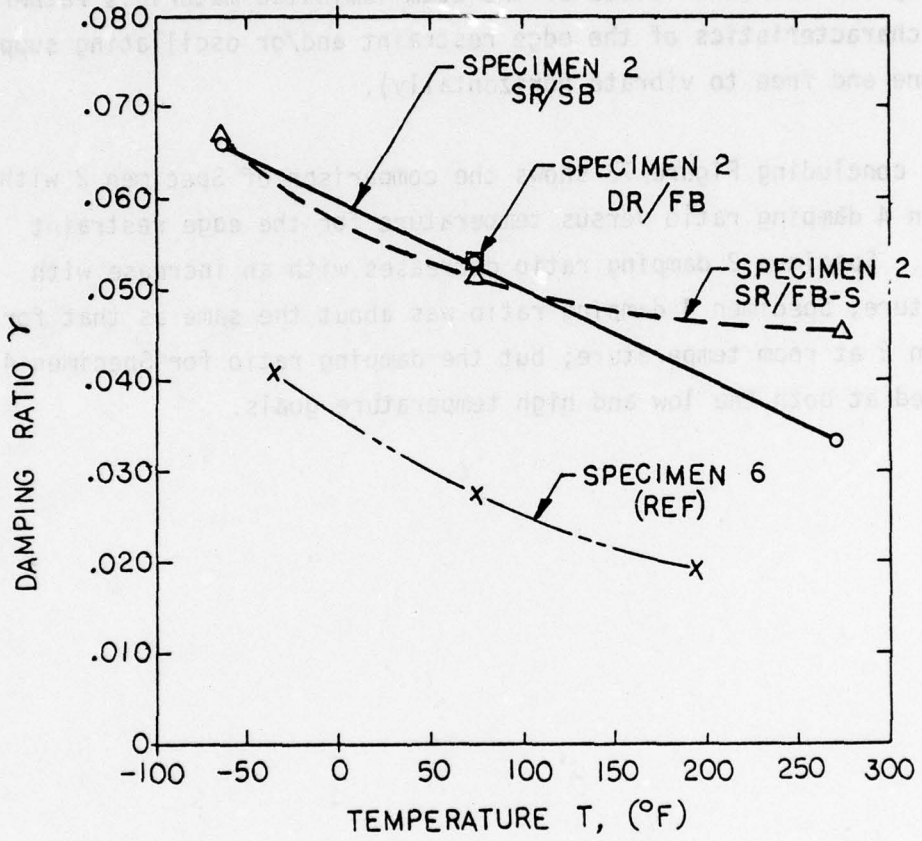

Figure 71. Damping ratio versus Temperature for the thick core beam specimen 2 with CIP interlayers.

Specimen 2 (with CIP interlayers), for edge restraint Conditions 19, 21 and 23 (SR/SB) and 63, 65 and 67 (SR/FB-S). A single point for Condition 29S (DR/FB) is also included. Also shown is the curve for the damping beam, Specimen 6, for reference purposes. Likewise, a set of curves are shown in Figure 72 for the multi-layered Specimen 4. Both sets of curves show similarity to their referenced damping beam specimen curves. It is assumed that the temperature effect as shown by these curves was mainly caused by the characteristics of the beam laminated materials rather than by the characteristics of the edge restraint and/or oscillating support base (one end free to vibrate horizontally).

The concluding Figure 73 shows the comparison of Specimen 2 with Specimen 4 damping ratio versus temperature for the edge restraint SR/FB-S. Specimen 2 damping ratio decreases with an increase with temperature, Specimen 4 damping ratio was about the same as that for Specimen 2 at room temperature; but the damping ratio for Specimen 4 decreased at both the low and high temperature goals.

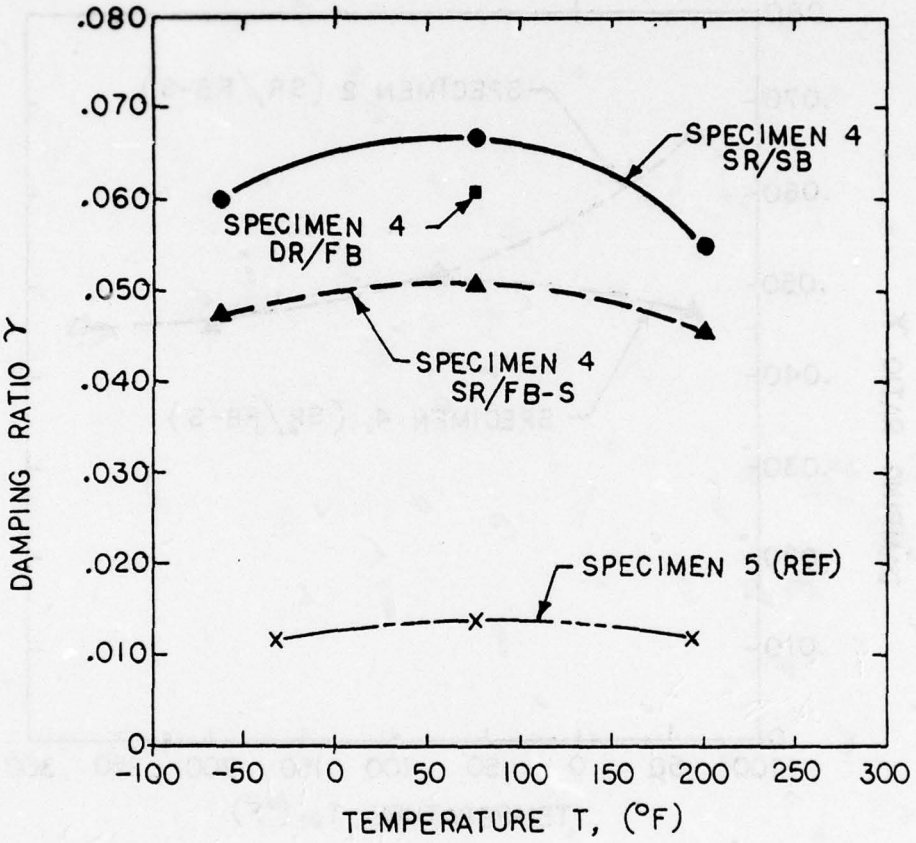

Figure 72. Damping ratio versus temperature for the multi-layered beam Specimen 4, with PPG-112 interlayers.

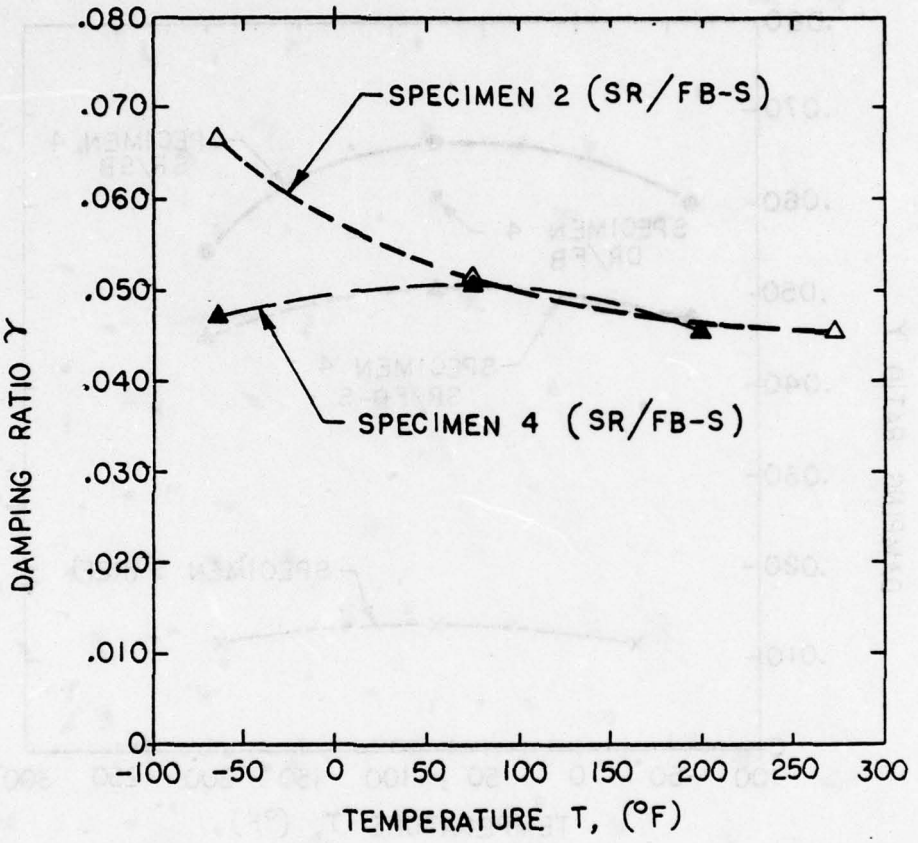

Figure 73. Comparison of Specimen 2 with Specimen 4 damping ratio versus temperature.

SUMMARY

The salient features derived from this study of the laminated beam strain distribution characteristics caused by various temperatures, loads, and edge restraints are summarized in subsequent paragraphs.

A comparison of the longitudinal strains in a thick core ply beam, simply supported versus fixed-end, was made. In theory, a simply supported beam would have zero end moments (or strain), and the strains at the beam ends were zero for test Condition 15 (SR/SS-PIV), even though the plies were interlocked with edge fasteners. Theoretically, the fixed-end beam end moments, with two-point equal loading conditions at one-third of the beam length locations should be 2 M/3 (negative) and M/3 (positive) in the constant bending section. Two fixed-end beam conditions and the simply supported beam longitudinal strain diagrams were superimposed in Figure 37. It should be noted that the strain diagram curves for the simply supported and fixed-end beams were not parallel. The most likely reason for this is that the simply supported beam interlayer experiences greater shear strains caused by the deflected geometry of the beam in respect to that of the fixed-end beam condition. Utilizing the one-third, two-thirds strain distribution theory, the percentage of end fixity was assessed to be 24 percent fixity for the single row attached beam and 94 percent fixity for the two row attached beam.

The longitudinal strains in the simply supported beam with and without attachments were compared. Condition 107A had bushings and bolts removed and Condition 107B had bushings only installed locking the plies together at the attach points. This test was conducted to study the interlayer shear load transfer characteristics (Figure 38). Figure 41 shows Condition 107A multi-strain distribution for each back-to-back strain gage set at each structural ply station. It was noted that the lower spall ply bending strain diagram component had been translated to the right, indicating potentially induced tensile strains caused by interlayer shear load transfer.

It was also noted that the upper glass ply indicated only a slight compressive strain component; this can most likely be attributed to the high modulus of elasticity of glass relative to polycarbonate (approximately 30 times greater). The percentage of axial strain increase caused by the addition of the tight fitting aluminum bushing does increase the tensile (25 percent in the lower spall ply) and the compression (10 percent in the core ply) strain components (see Figure 49). This upper glass ply did not seem to be affected by this condition because it is considered to be a floating ply.

The longitudinal strain distribution in beams with a single row of attachments (Condition 65) and sealant filled holes was compared to a beam with a double row of attachments (Condition 29S). Condition 65 displayed a 22 percent strain increase, in the attachment area, over the Condition 29S. The beam center displacement for Condition 65 was also 64 percent greater than for Condition 29S.

The longitudinal strain distribution characteristics for the multi-layered beams tested were similar to the thick core ply beam. The multi-layered beam, with PPG112 interlayer, strain acts more like a monolithic beam. The multi-strain diagrams display strain slopes that are almost in-line from the upper to the lower surface for each station location (Figure 58).

The thick core ply and multi-layered beams were compared for both spring stiffness and damping ratios. The spring stiffness (at room temperature) for the thick core ply beam was 1500 lb/in. for the double row attached condition with bases locked from sliding, and 910 lb/in. for the single row attached condition with sealant filled holes and locked bases. The multi-ply beam maximum spring stiffness was 680 lb/in. for the double row attached condition with the bases locked from sliding, 400 lb/in. for the single row attached condition, and 595 lb/in. for the single row attached condition with sealant filled holes (Reference Figures 69 and 70).

The damping ratio, with respect to temperature change, for each of the two beams is shown in Figure 73. Both curve patterns are similar to the corresponding damping beam specimen curves, and it is assumed that the temperature effect was due mainly to the characteristics of the beam materials.

SECTION VI
TEST RESULTS AND ANALYSES FOR IMPACT BEAM SPECIMENS

Section II of this report described the objectives, specimens, conditions, set-ups, and procedures for this series of impact tests.

The instrumentation developed for this series of specimen tests was described in Section III.

Within Section V the results and assessment of the strain distribution for the static/dynamic beam specimens were presented. Although both static and dynamic strain data were tabulated, only the static strain data was assessed. These strain distributions were assessed for various temperature and edge restraint conditions. The relevance of Section V to this section is that the impact specimens were previously tested as the static/dynamic beams.

This section presents the results and analysis of a series of three impact beam tests. The purpose of these impact tests were to evaluate the strain distribution, strain rate, strain gage failure point, and beam failure mode. To evaluate the stated impact effects, the beams were to be subjected to plastic deformation.

SPECIMEN DEFINITION AND TEST TEMPERATURES

The paragraphs that follow present the specimen definitions and testing temperatures.

Specimen Definition

The three specimens used in this test were the thick core ply beam specimens Numbers 1 and 2, and the multilayered beam specimen Number 4. Idealized specimen diagrams defining the installed beam edge restraints are shown in Figure 74. The referenced drop weight is also shown.

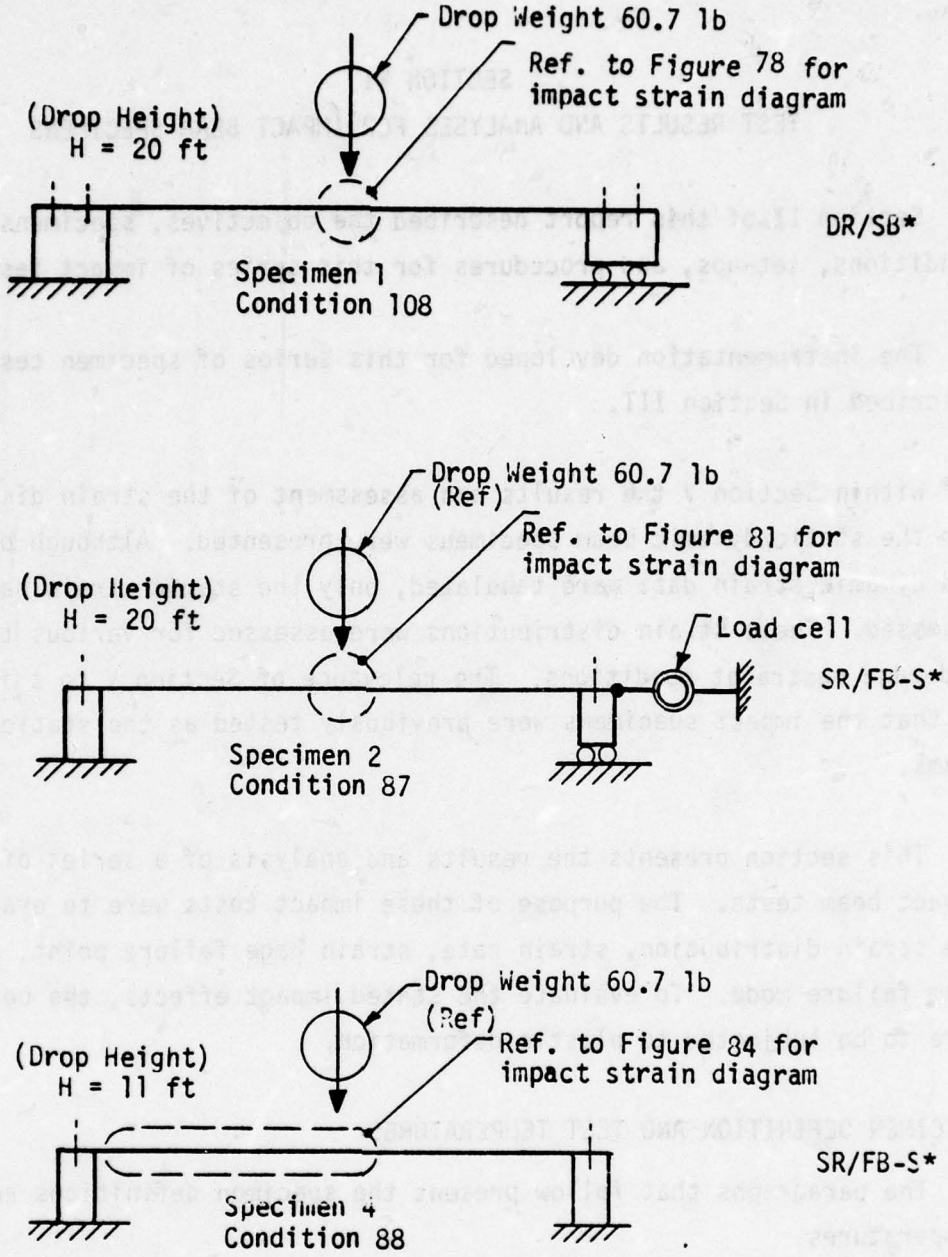

*Refer to Table 5 for Edge Restraint codings.

Figure 74. Idealized Specimen Diagrams, Impact Beam Test.

Test Temperature

The impact specimens were tested to destruction at room temperature.

DATA DOCUMENTATION PRESENTATION METHODS AND ASSESSMENT OF TESTING ERRORS

A method of reducing the numerical strain data from the impact beam responses into meaningful strain diagrams is presented, and a means of assessing testing errors is discussed in subsequent paragraphs.

Data Documentation Presentation Methods

The strain data is presented in the form of oscillograph recordings for the strain magnitudes in respect to time, and multi-strain diagrams within the structural plies. Only the beam center multi-strain diagrams for the thick core ply beam Specimens 1 and 2 were shown, since these were the highest recorded strains. For the multilayered beam Specimen 4, all multi-strain diagrams are shown.

Assessment of Testing Errors

In addition to the method used for the "assessment of testing errors" described in the preceding Section V, the oscillograph strain recordings were assessed for strain continuity. In the area where the maximum strains occurred (either rupture point of a structural ply and/or a strain gage failure), the multi-strain diagrams were constructed and are shown for assessment of possible strain error distribution.

RESULTS AND ASSESSMENT OF SPECIMEN STRAIN DISTRIBUTION, STRAIN RATE AND FAILURE

This subsection presents the results and the assessment of the strain distribution, strain rate and failure for each specimen. A comparison is made between the thick core and multilayered impact beams in tabular form.

Thick Core Beam Specimen 1 Impact Strain Distribution

Figure 75 shows the Specimen 1 strain gage arrangement for this test. The specimen instrumentation was limited to external strain gages. Test instrumentation was a horizontal (LVDT) device to measure the displacement of the support slide-plate.

A 60.7-pound weight was dropped from a 20-foot height onto the beam Specimen 1 as noted in Figure 76. The weight impacted a wooden load-distribution block. This block had a cylindrical radius that was representative of the main core-ply impacted beam curvature that may force the beam into plastic failure range.

By means of geometrical analysis the vertical deflection of the beam center was determined to be approximately 4 inches. The maximum horizontal displacement measured by the LVDT was approximately 1.00 inch.

Figure 77 shows the actual chart recording of the impact beam test results of strain versus time. The highest recorded strain was for strain gage Number 6 (ε_6 = 33,061 μ in./in. at time t = 22.5 milliseconds). It is believed that the highest reading should have occurred at strain gage Number 4 near the fixed-end, but this gage failed at t = 13 ms, as a result of the impact.

In Figure 78 the structural-ply strain diagrams shown represent only approximations, because no internal strain gages were present to verify the strain values within the structural plies.

Thick Core Beam Specimen 2 Impact Strain Distribution

This thick core beam Specimen 2 (laminated beam with one thick polycarbonate core-ply) had all three structural plies strain gaged as described in Section III. In addition to the impact strain data collected, deflection data was obtained with high-speed camera coverage of a grid board displayed behind the specimen, and with a vertical displacement potentiometer (LVDT).

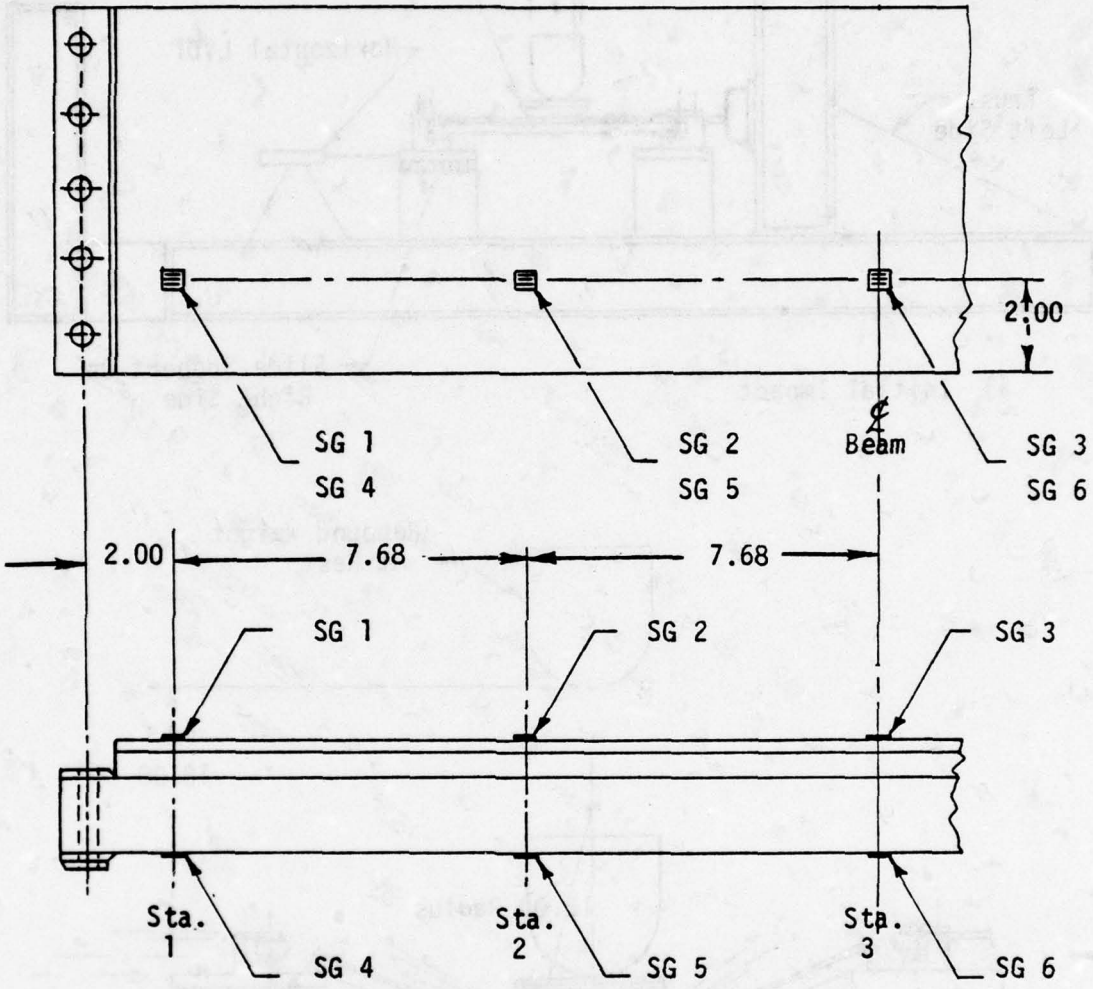

Figure 75. Specimen 1 strain gage arrangement for impact beam test of Specimen 1.

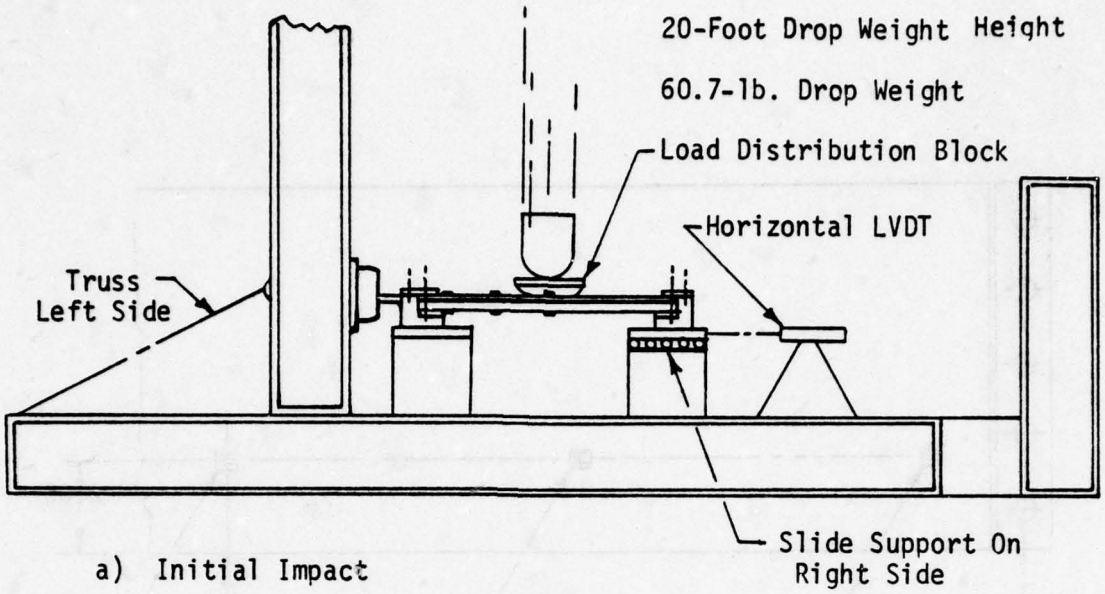

a) Initial Impact

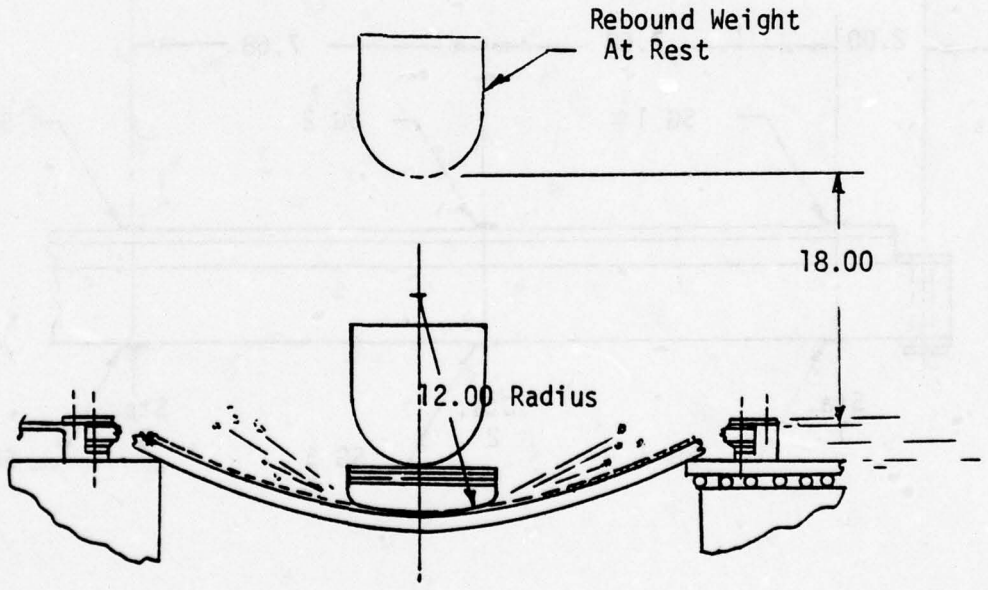

b) After Beam Rupturing

Figure 76. Test setup for impact beam test of Specimen 1, Condition 108 (DR/SB-S).

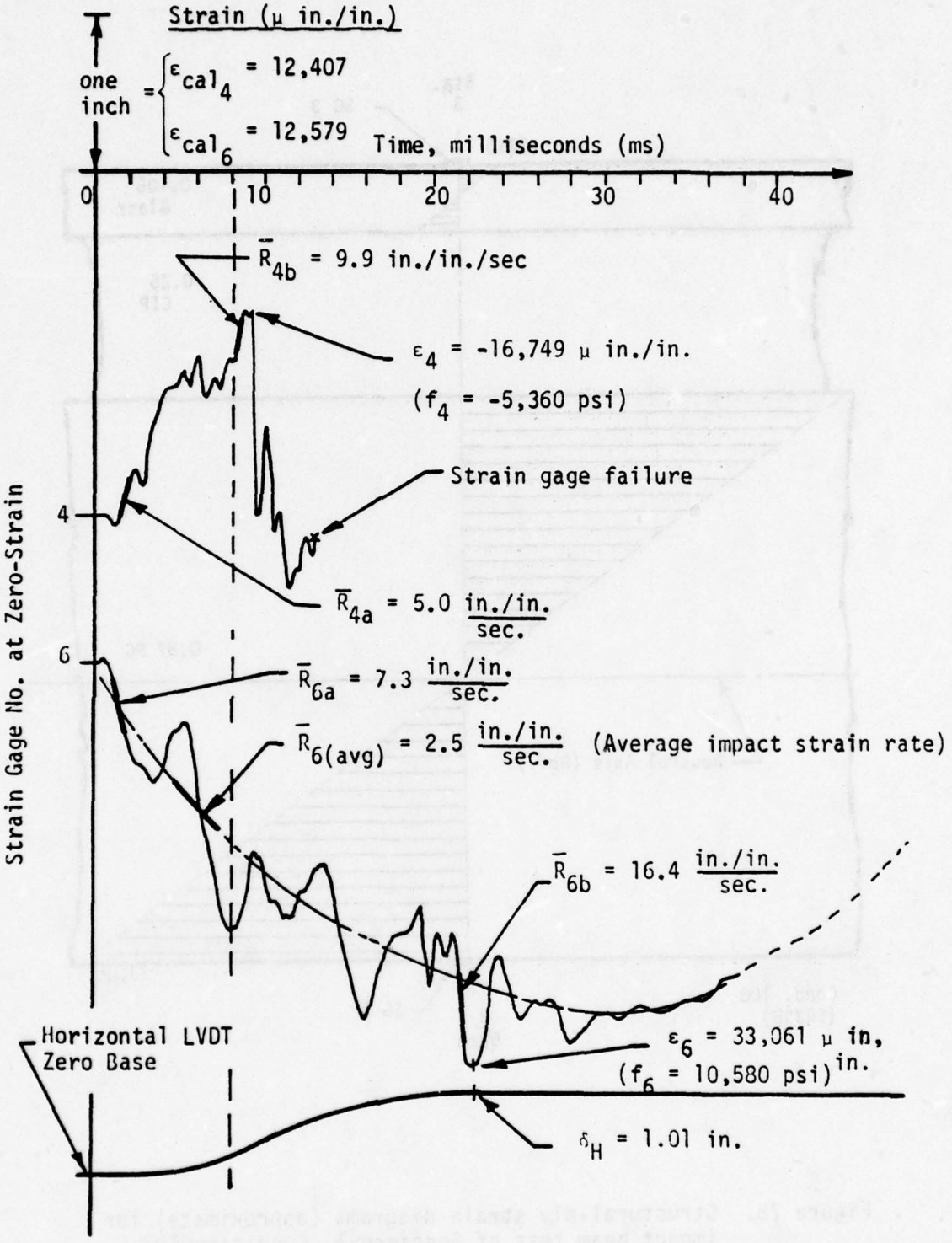

Figure 77. Oscillograph recording of strain gages 4 and 6 response versus time for impact beam test of Specimen 1.

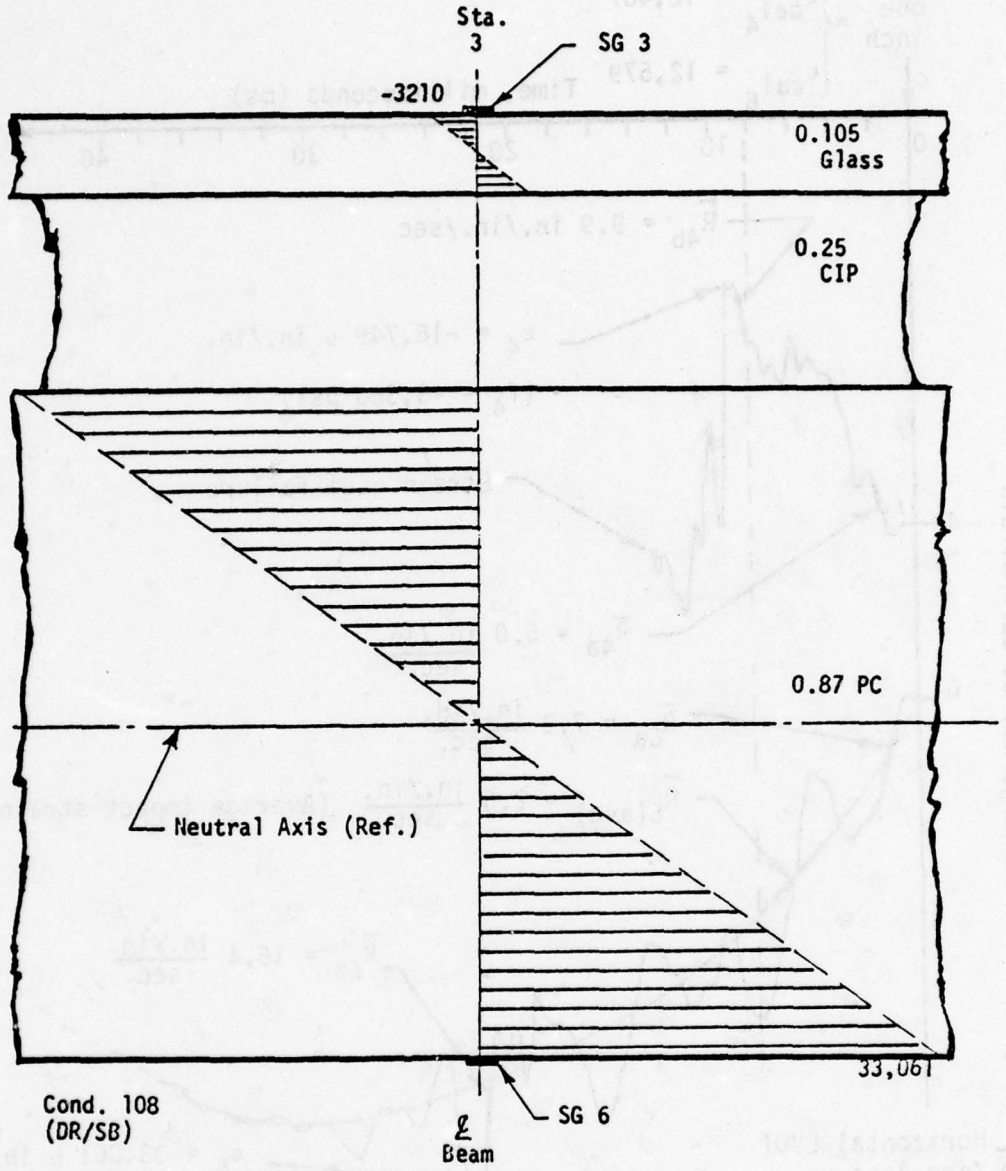

Figure 78. Structural-ply strain diagrams (approximate) for impact beam test of Specimen 1, Condition 108.

Figure 79 shows the test set-up for Condition 87. The test required a 20-foot drop of the 60.7-pound weight onto the approximate center of the beam. The horizontal reaction load was measured. The test data compiled indicated that the drop weight reached a velocity of 36 feet per second at impact and the beam center deflection was measured by the Linear Voltage Differential Transducer (LVDT) to be approximately 5.25 inches. Subsequently, the LVDT measurement was verified by high-speed camera coverage. The beam deflected mode shape is illustrated in the figure. To prevent direct contact with the strain gages the target impact location was directed to be one inch off the center line and misguided one inch to the rear, thus, causing transverse wave motion in both the longitudinal and lateral direction.

Recordings were made of the strain gage readings as a function of time and are shown in Figure 80. The strain rate was approximately 6 in./in./sec. and 7.6 in./in./sec respectively at Gages 15 and 18. The heavy lines represent the readings for strain gage Numbers 15 and 18, located on the main core ply which showed maximum strains at Gage Number 15, 17,616 μ in./in. (compression), and at gage Number 18, 20,078 μ in./in. (tension). It is believed that the maximum strains were the result of either the gages failing or caused by the rupturing of the core-ply. The dashed lines represent the readings for strain gage Numbers 6 and 12 located on the spall ply.

To illustrate the strain on the various plies of the laminate, Figure 81 was developed to show the relationships at selected times. The strains shown were determined at time (t) equal to 8.6 milliseconds. The strains on the spall ply at t = 14.3 milliseconds is shown as a dashed line.

Multilayered Beam Specimen 4 Impact Strain Distribution

This was the first impact test performed. Knowledge gained from this test was applied to the impact tests for Specimens 1 and 2.

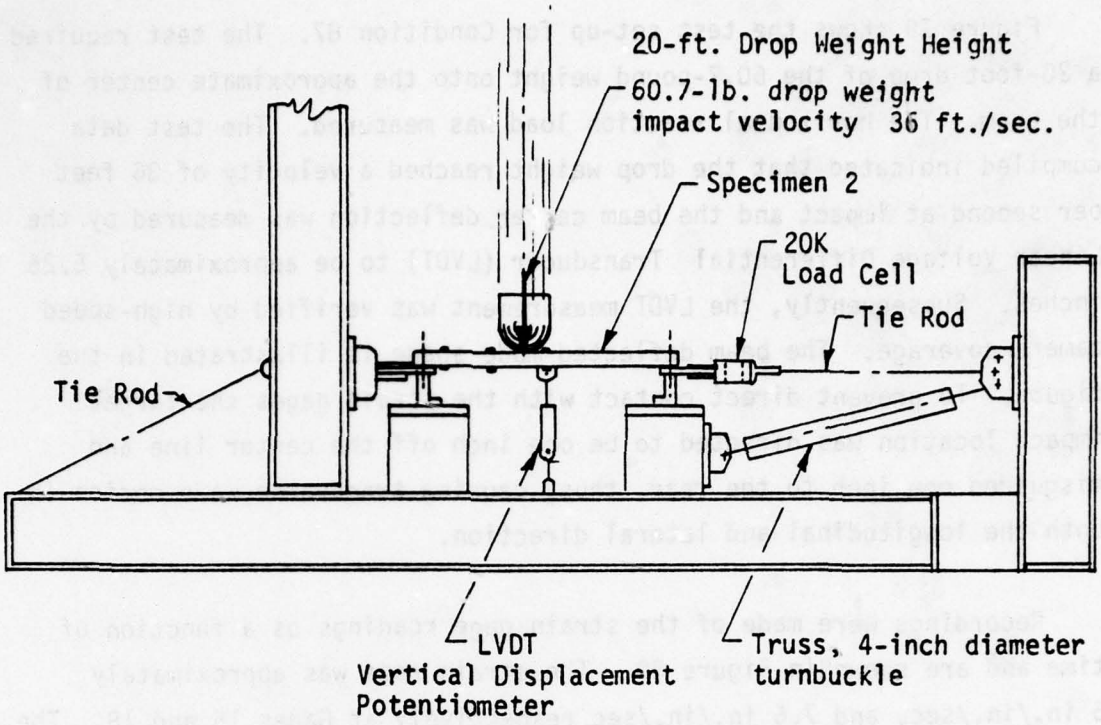

a) Initial Impact

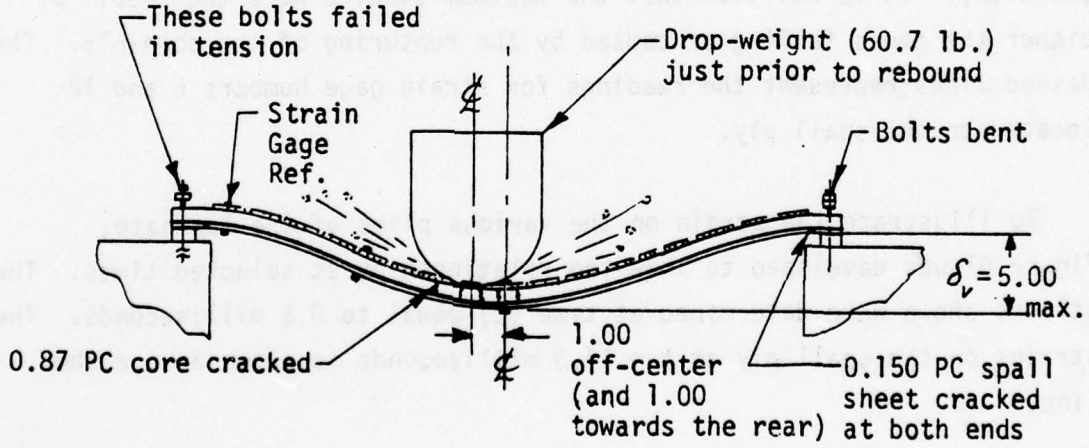

b) Beam Rupturing

Figure 79. Test set-up for impact test of Specimen 2, Condition U7 (SR/FB-S).

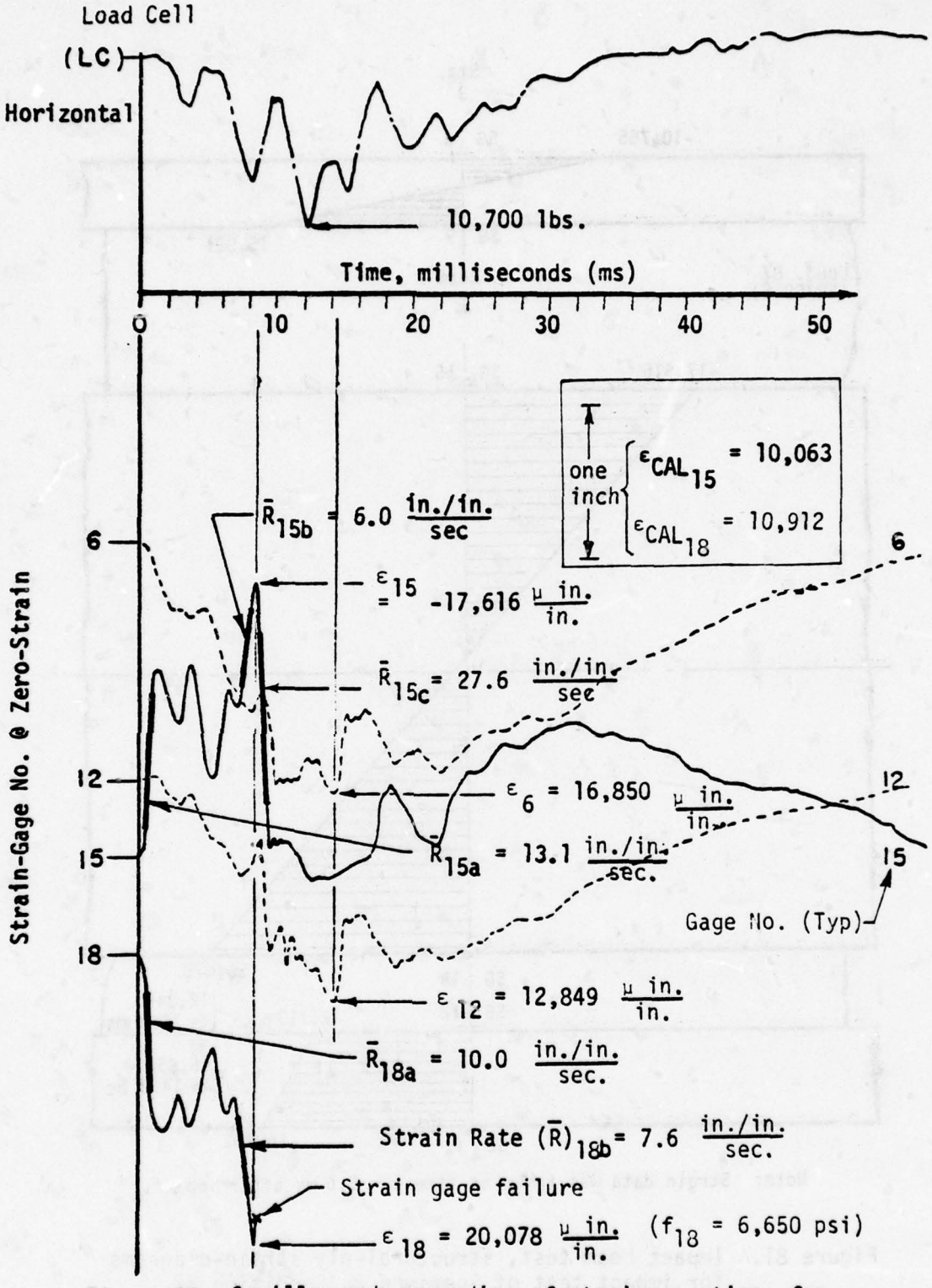

Figure 80. Oscillograph recording of strain vs. time, for impact beam test of Specimen 2, Condition 87.

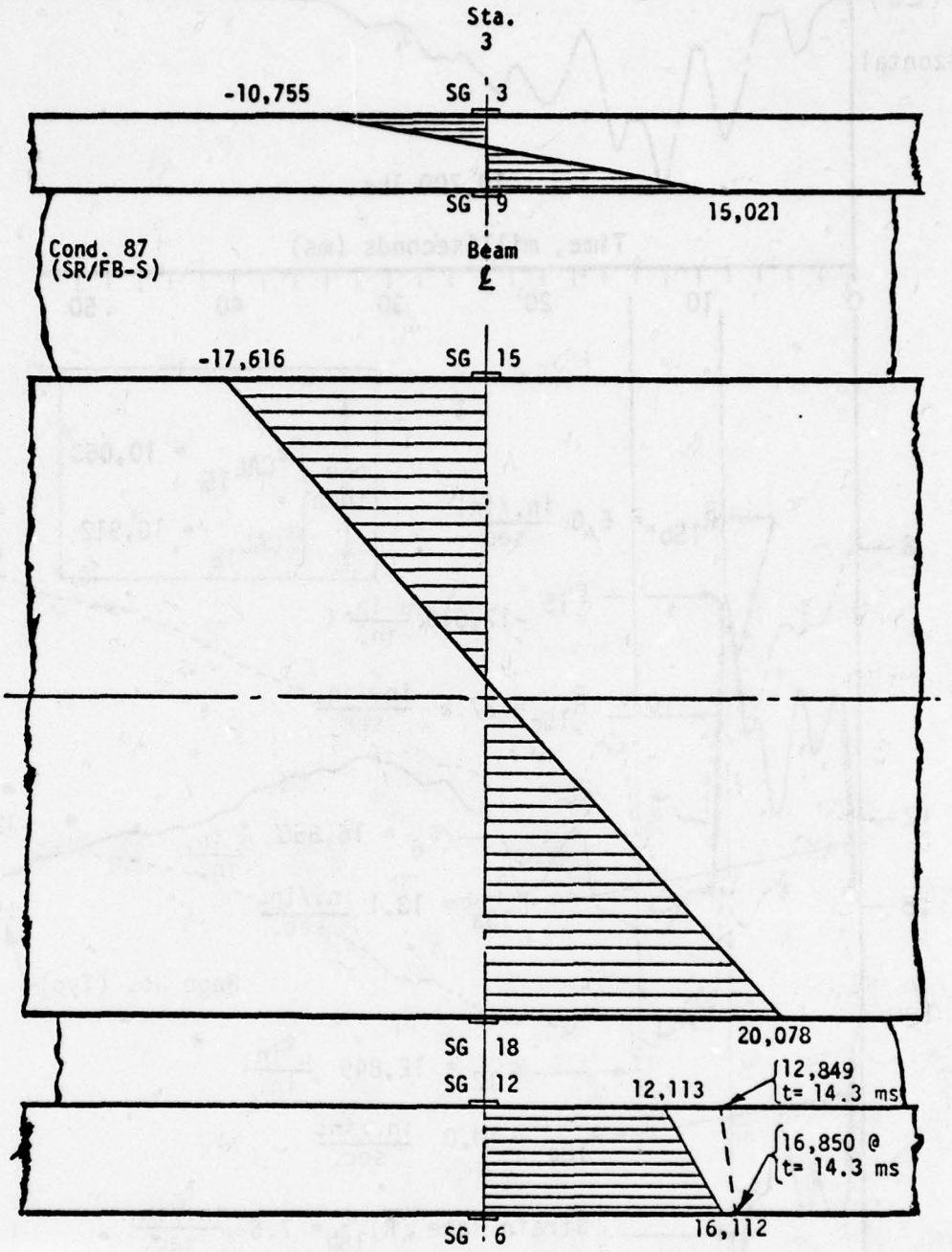

Note: Strain data was taken at time t = 8.6 ms after impact.

Figure 81. Impact beam test, structural-ply strain-diagrams for impact test of Specimen 2, Condition 87.

This beam specimen (two structural plies of 0.188-inch polycarbonate, with two outer floating plies of acrylic) had all four plies strain gaged as described in Section III. Strain data was recorded for all gages except for Gages 16, 18, and 24.

The test set-up for this test was similar to the set-up for Sierracin Specimen 2 (shown in Figure 79), specified as Condition 88; the drop height was 11 feet, and the impact velocity was 26.6 fps. The impact beam test is illustrated by Figure 82 showing the test configuration just prior to impact, just prior to rupture of the beam, and after the beam had ruptured.

Figure 83 shows a typical strain gage oscillograph recording, which shows the strain as a function of time for the various strain gages. The strain sequence from the initial impact through beam rupture is effectively shown in the figure.

Figure 84 graphically shows the peak strains achieved within each structural ply of Specimen 4. These are the strain readings at time t= 0.0094 second (9.4 milliseconds) after impact. Maximum strains occurred at this time. Subsequently, all strain gages failed at this location except strain Gage Number 3.

Strain Rate of Impact Beams

The strain rate ($\bar{R}$) (in./in./sec) is defined as the instantaneous slope of the strain per time curve. That is, $\bar{R}$ is equal to the change of strain divided by the change of time. The strain rates near the beginning of impact and near the maximum strain occurrence for Specimens 1, 2, and 4 are shown in Figures 77, 80, and 83, respectively. The strain rate near the beginning of impact is subscripted with its gage number and the letter "a"; the strain rate near the maximum strain occurrence is subscripted with its gage number and the letter "b". For gage location see Figure 78 (Specimen 1), Figure 81 (Specimen 2), and Figure 84 (Specimen 4).

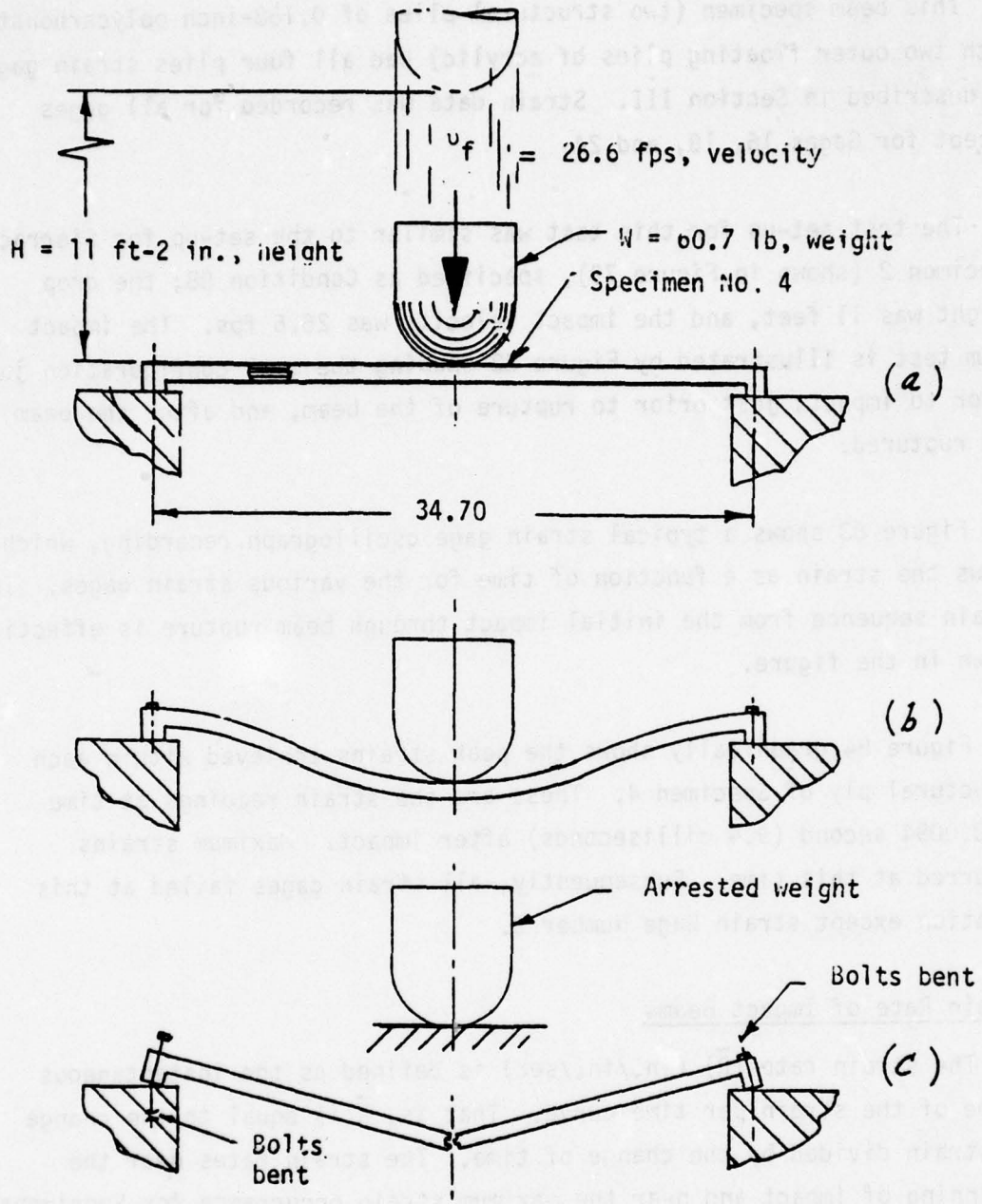

VIEW (a) JUST PRIOR TO IMPACT;
VIEW (b) JUST PRIOR TO BEAM RUPTURE;
VIEW (c) BEAM RUPTURED.

Figure 82. Impact sequence for Specimen 4, Condition 88 (SR/FB-S).

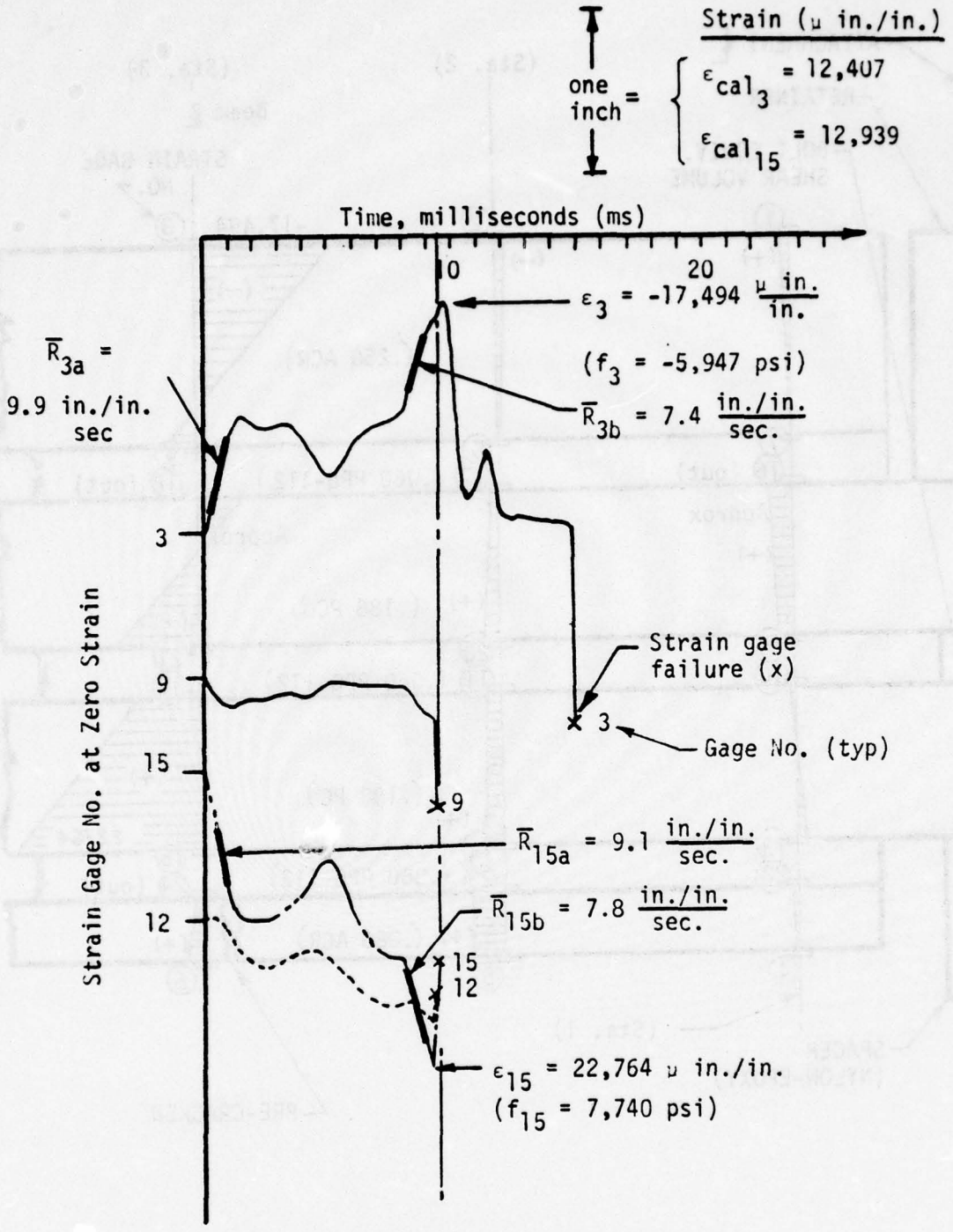

Figure 83. Oscillograph recording of strain versus time for impact beam test of Specimen 4, Condition 88.

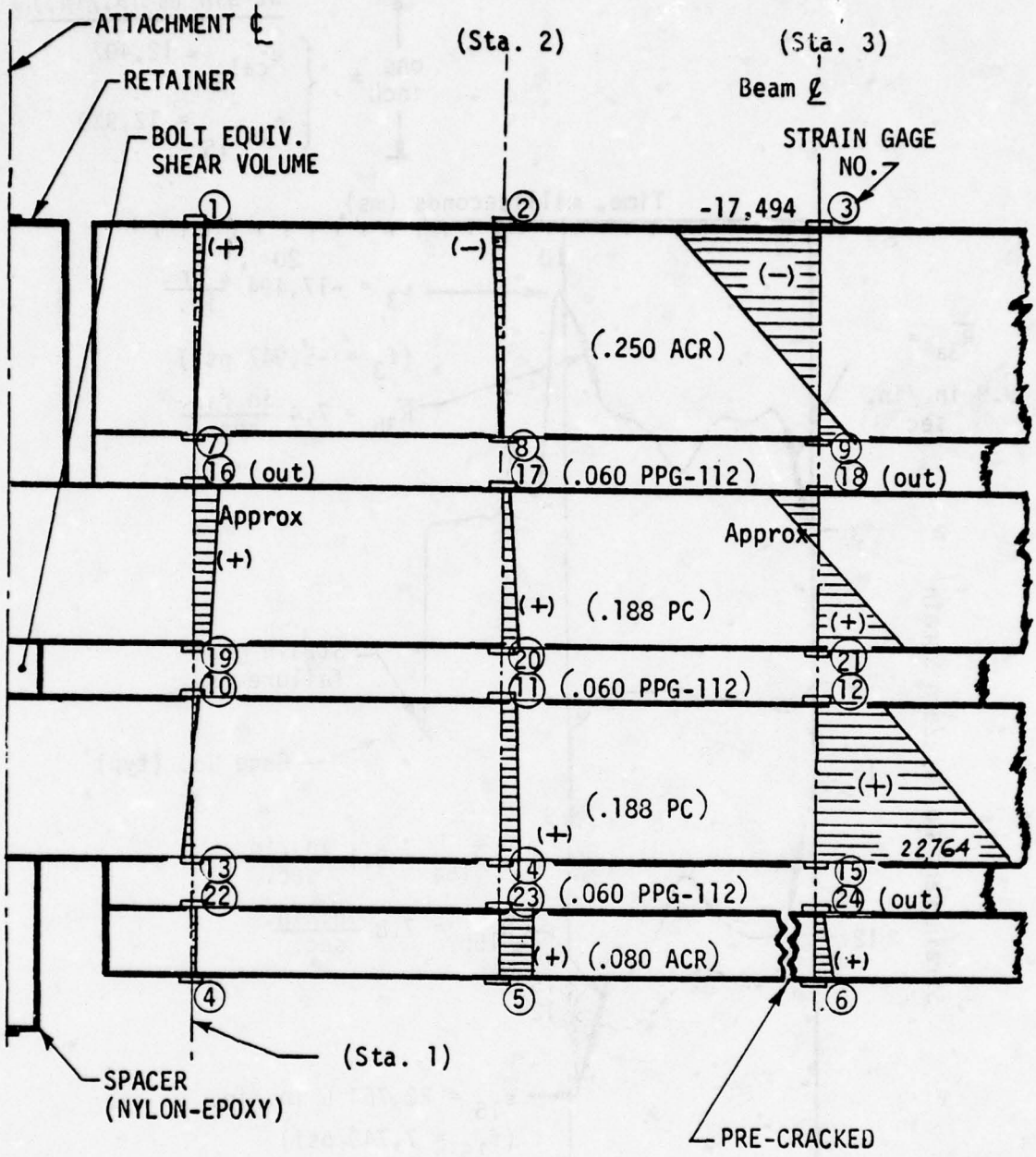

Figure 84. Structural-ply diagrams for impact beam test of Specimen 4, Condition 88 (SR/FB-S).

Shown in Figure 77 are the average impact strain curves (phantom curves) for Gages 5 and 6 of Specimen 1. The average impact strain rate ($\bar{R}_{6\ AVG}$) was 2.5 in./in./sec. Secondary wave motion caused higher recorded local strains, such as 16.4 in./in./sec. for $\bar{R}_{6b}$. This was a center bottom gage located on the main core ply. This was the highest recorded tensile strain rate for all three specimens. A higher strain rate for Specimen 2, where $\bar{R}_{15c}$ = 27.6 in./in./sec., was recorded; although, this was probably due to the cracking of the core ply or strain gage slippage.

Beam Failure Analyses and Edge Attachment Evaluation

Beam failure analyses and edge attachment evaluation for the three impact specimens follow.

The thick core beam, Specimen 1, had both ends fixed with two rows of attachments that prevented the ends from rotating, but one end was free to slide inward. Thus, the largest bending moments and strains should occur near the beam attachment areas. Although the beam did sever at its ends, as would be expected; the maximum recorded strain, ε_6 = 33,061 μ in./in., occurred at the beam center lower surface, as noted in Figure 77.

Figure 85 shows a sketch of the approximate ruptured condition of Specimen 1. In review of the beam ruptured areas, the failure mode appeared to be a brittle fracture of the polycarbonate material in both shear and tensile failure modes. An examination of the edge attachment area showed that no failure occurred in the polycarbonate material at the edges, and the bolt holes, bolts, and bushings were observed to be in good condition.

The thick core beam, Specimen 2, had both ends fixed with a single row of attachments that prevented the end from rotating, except through means of bolt bending.

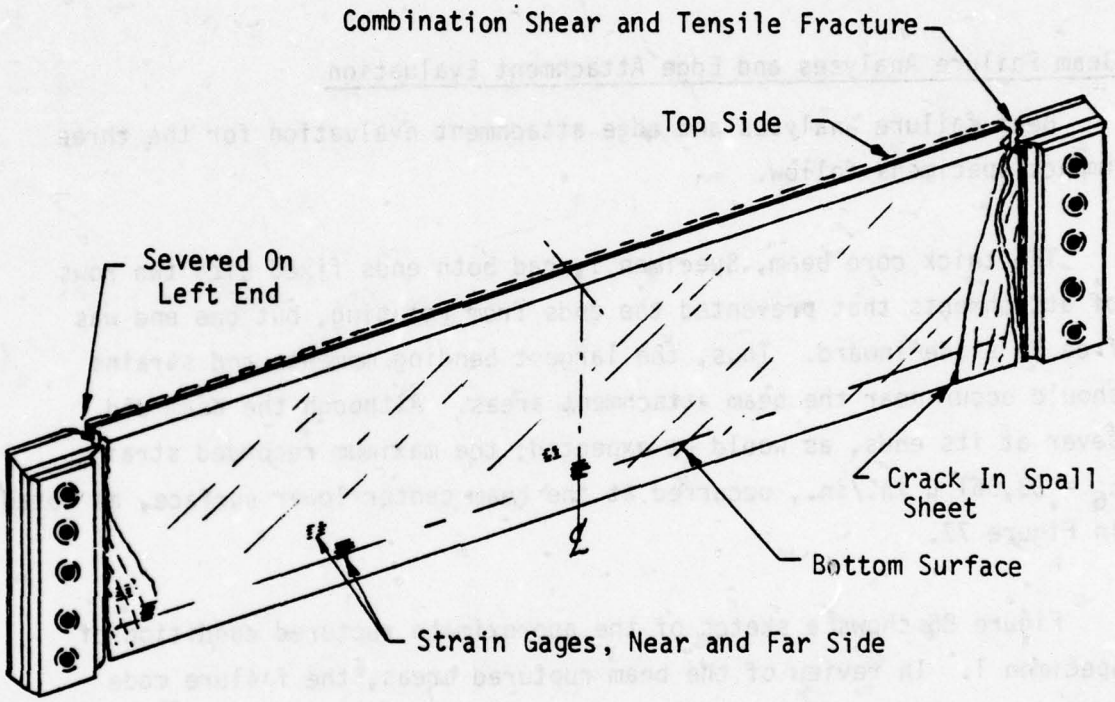

Figure 85. Sketch of approximate ruptured shape of impact beam test of Specimen 1, Condition 108.

Specimen 2 was examined after the impact test and it was determined that all of the structural plies had fractured, as shown in Figure 86. The outer glass ply, being chemically strengthened glass, was completely fractured as expected. The main core ply fractured under the point of impact and at one end; and the spall ply failed at each end adjacent to the attachment area. A phenomenon that was observed was a localized thinning or necking of the spall ply immediately below the point of impact. This thinning was 0.020-inch in depth by 0.20-inch in width by 1.00 inch in length.

A determination could not be made regarding the cause of failure of the main core ply at the one end. The horizontal load cell (LC) indicated that there was a maximum load of 10,700 pounds. Assuming that the main core ply would absorb the entire tensile load through the bolt attach area (5.05 square inches), the resulting stress would have been only 2120 psi. Yet, this tensile load would have been additive to the stresses resulting from the high bending moment which could not be assessed because the strain gages were inoperative. These important strain gages were Numbers 10 and 13. They were laminated in the initial beam specimen, but had failed previously, as noted in Section V.

The multilayered beam, Specimen 4, had an end-fixity that allowed only rotation through bolt bending by having only one row of attachments at each end. As noted previously this was the first impact test conducted. The beam was examined and it was found that the beam was severed at the middle with no apparent damage in the attachment areas and it was determined that the two halves of the beam remained straight indicating that there was no permanent deformation of the materials at impact. The fractured beam and bent attachments are illustrated in Figure 82. The maximum recorded strain was determined to be ε_{15} = 22,764 μ in./in., noted in Figure 83. This gage was located at the beam center bottom on the polycarbonate ply surface as shown in Figure 84.

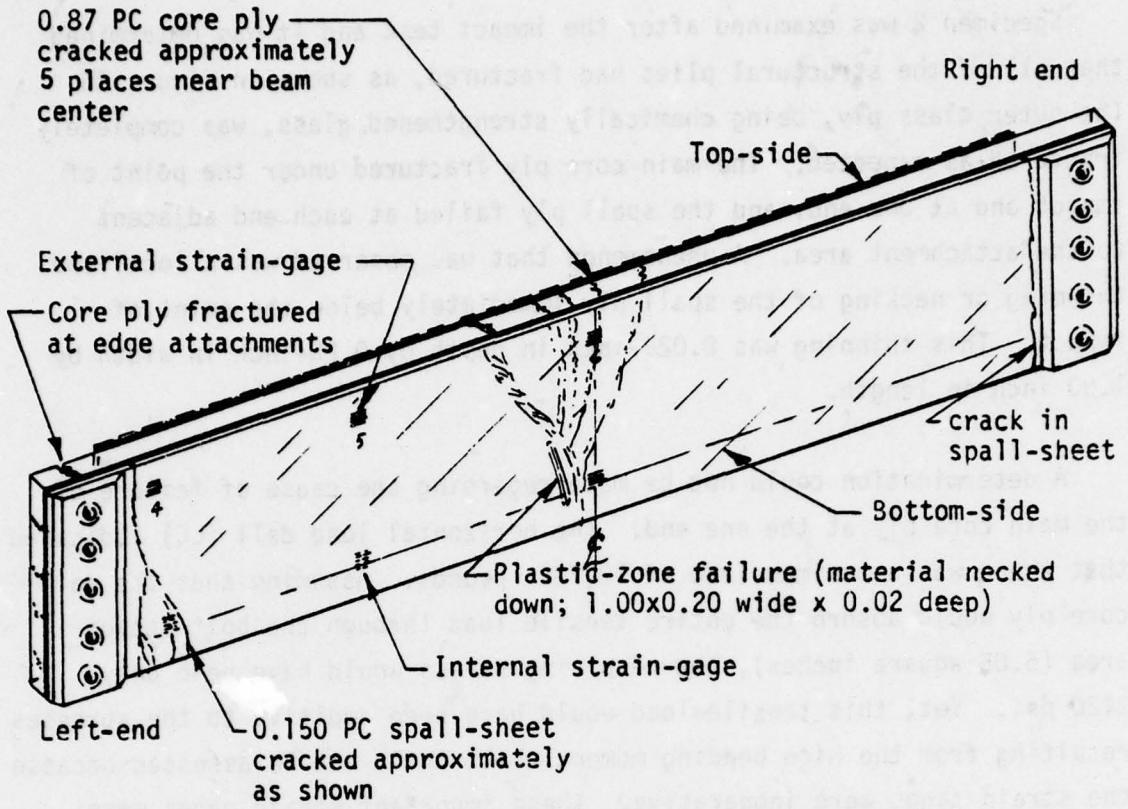

Notes:
1. Bolts were bent between the beam and support - surface.
2. Four bolts on the left end failed in tension through the cotter pin hole within nuts, and one failed between the beam and support surface.
3. The beam returned to a straight (flat) configuration after impact deflection.

Figure 86. Approximate location and mode of cracks in Specimen 2 (Part No. Z5942626-501).

Comparison of Thick Core Ply Beam Versus Multilyaered Ply Beam Impact Tests

An impact test summary, Table 37, is presented for a consise summary of the beam characteristics, and impact characteristics for comparison.

For each specimen number and condition, the edge restraint code, drop weight and height, are listed. The velocity shown is the instantaneous drop weight velocity at the time of impact. The maximum strain shown is for that strain that occurred at the beam center. The corresponding stress and strain rate is also listed. Also included is an index to the figures in this subsection.

TABLE 37. IMPACT BEAM TEST SUMMARY

Specimen No.		1	2	4
Condition No.		108	87	88
Edge Restraint[3]		DR/SB	SR/FB-S	SR/FB-S
Drop Weight (lb)		60.7	60.7	60.7
Drop Height[2] (ft)		20	20	11
Max. Velocity (fps)		36	36	26.6
Vertical Deflection Maximum (in)		4	5.25	4 to 5
Max. Strain, ε, at center (μin/in)		ε_6=33,061	ε_{18}=20,078	ε_{15}=22,764
Corresponding Stress,[1] f (psi)		11,241	6,827	7,740
Corresponding Strain Rate, (in/in/sec)		R_{6b}=16.4	R_{18b}=7.6	R_{15b}=7.8
TEST DATA INDEX	Set-up and Impact Figure No.	76	79	82
	Oscillation Record Figure No.	77	80	83
	Strain Map Figure No.	78	81	84
	Post Test Figure No.	85	86	

NOTES: 1) The corresponding stress was calculated from the basic stress equation, $f = \varepsilon E$, where the assumed Modulus of Elasticity, E, =340,000 psi.

2) Drop weight height calculated per method described in Section II, equation (3).

3) Refer to TABLE 5 for explanation of Edge Restraint coding.

SECTION VII
MATRIX ANALYSIS METHOD FOR THE DETERMINATION OF DAMPING FACTORS AND CORRELATION OF BEAM STRAIN RESPONSE WITH THEORETICAL ANALYSIS

This section presents the method of calculating structural ply, interlayer and air damping constants from data obtained by testing the damping specimens described in Section II. Results of test analysis correlation studies conducted on a damping beam, and a 36-inch specimen are described.

The analytical method of reducing the damping beam test data, and of calculating beam responses for test correlation purposes, is based upon the dynamic finite element analysis technique which is incorporated into the Bird Impact Math Model, Reference 1.

The present correlation studies apply to damping specimen Number 6, test Condition 5; and 36-inch specimen Number 2, test Condition 15. These studies include no case of dynamic impact, but the results of a correlation study of a 36- by 36-inch laminated transparency subjected to bird impact may be found in Reference 1.

MATRIX ANALYSIS METHOD AND PROCEDURE FOR THE DETERMINATION OF DAMPING FACTORS, AND RESULTS

This subsection presents the method of determining structural ply, interlayer, and air damping constants for laminated cantilevered beams. This includes a summary of the matrix analysis procedures for determining damping factors, a description of the finite element model required in this analysis, and a tabulation of the results. The damping/stiffness ratio h, as a function of temperature for various windshield materials, and a visual comparison of the calculated oscillatory response of damping specimen Number 6, with test data for Condition 5, are presented (Figures 89 and 90).

Matrix Analysis Method for Determining Damping Factors

A laminated cantilever beam was selected as the specimen for determining interlayer damping properties. The beam consisted of two structural plies separated by interlayer material, as shown in Figure 87. The rationale for this approach was that the specimen should represent the laminated transparency to be analyzed, as nearly as possible, in order to minimize errors involved in test-data reduction, and to aid in subsequent analysis of the transparency.

The laminated design of the specimens, however, precluded the use of the elementary beam methods often employed in determining damping constants. The figure shows the deformed shape of the vibrating beam as determined from a finite element analysis employing the Bird Impact Math Model. The figure shows the large shear strains present in the interlayer. In the Math Model, interlayer strains are represented by shearing strains in finite elements that represent the actual interlayer, as the figure indicates. Elementary beam methods do not account for these strains, consequently such methods are not applicable.

Two feasible approaches are: (1) the finite element method, and (2) a differential equation approach similar to the static analysis of Reference 11. The latter method can possibly be extended to dynamic cases, as mentioned in the section on "Recommendations". The development of the differential-equation method was not feasible within the time constraints of the present program; consequently, the Bird Impact Math Model was employed. The following paragraphs explain the applications of the Math Model for establishing the damping properties.

The differential equation for the response of a finite element model of the laminated beam to an initial tip displacement, assuming linear viscous damping is

$$M\ddot{\Delta} + C\dot{\Delta} + K\Delta = 0, \qquad (37)$$

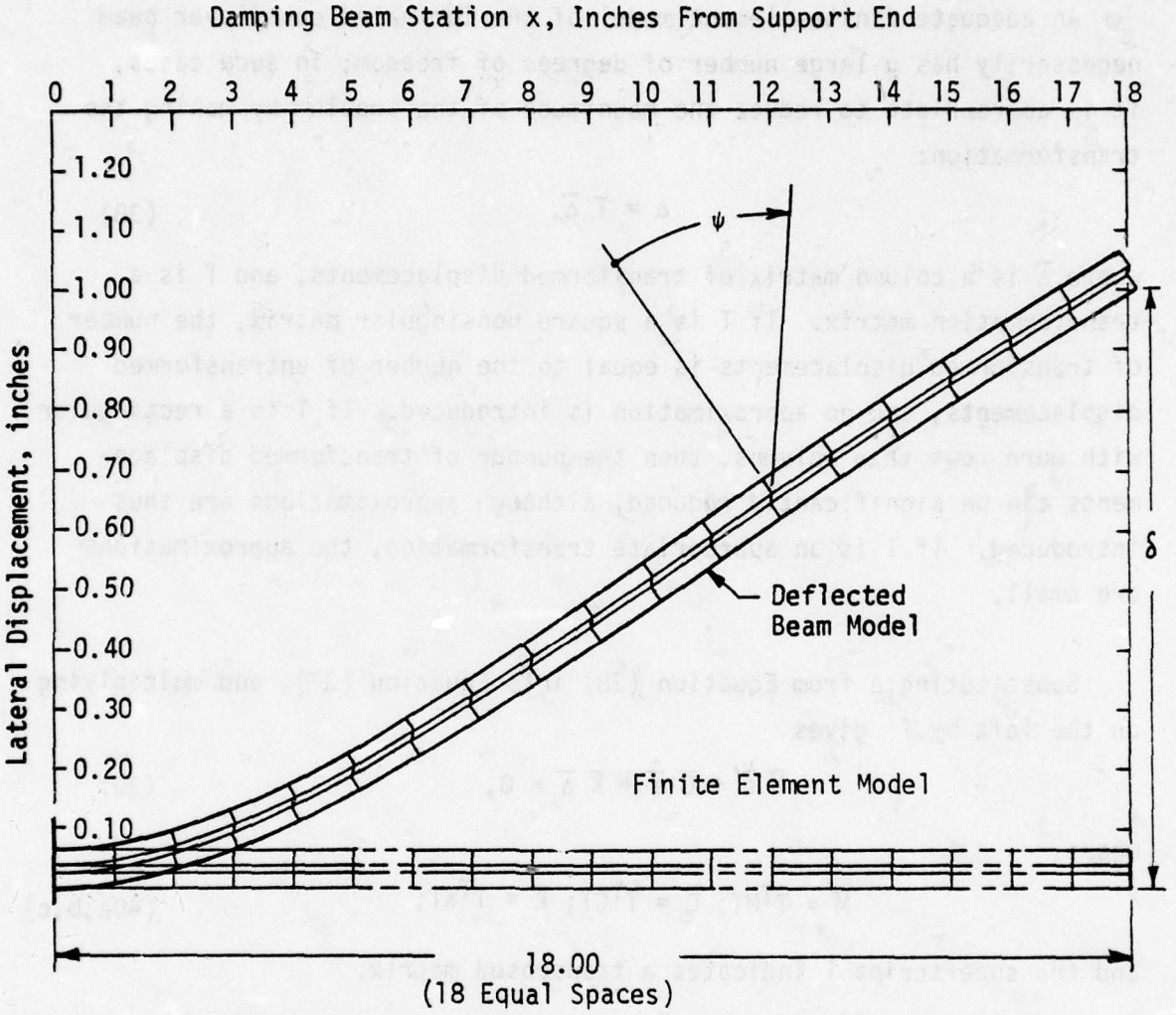

- Specimen 6, Condition 5
- Polycarbonate Structural Plies with CIP Silicone Interlayer
- 1st Natural Vibration Mode Shape
- ψ denotes interlayer distortion angle (shear strain).

Figure 87. Deflected beam model of finite elements.

where Δ = a column matrix of displacements, and M, C and K are square matrices consisting of mass, damping and stiffness coefficients.

An adequate finite-element model of the laminated cantilever beam necessarily has a large number of degrees of freedom; in such cases, it is appropriate to reduce the magnitude of the problem by making the transformation:

$$\Delta = T\,\bar{\Delta}, \tag{38}$$

where $\bar{\Delta}$ is a column matrix of transformed displacements, and T is a transformation matrix. If T is a square nonsingular matrix, the number of transformed displacements is equal to the number of untransformed displacements, and no approximation is introduced. If T is a rectangular with more rows than columns, then the number of transformed displacements can be significantly reduced, although approximations are thus introduced. If T is an appropriate transformation, the approximations are small.

Substituting Δ from Equation (38) into Equation (37), and multiplying on the left by T^T gives

$$\bar{M}\,\ddot{\bar{\Delta}} + \bar{C}\,\dot{\bar{\Delta}} + \bar{K}\,\bar{\Delta} = 0, \tag{39}$$

where:

$$\bar{M} = T^T M T;\ \bar{C} = T^T C T;\ \bar{K} = T^T K T; \tag{40a,b,c}$$

and the superscript T indicates a transposed matrix.

One way to establish a suitable transformation is to employ the natural modes of vibration for the beam. Setting C = 0 in Equation (37) gives the differential equation for free undamped vibrations:

$$M\,\ddot{\Delta} + K\,\Delta = 0. \tag{41}$$

In the free vibration, the motion is a simple harmonic; therefore;

$$\Delta = \Delta_m \sin \omega t. \tag{42}$$

Eliminating Δ from Equation (41) and (42), and combining the two equations gives

$$(K - \omega^2 M)\ \Delta_m = 0. \tag{43}$$

This characteristic equation can be solved for the eigenvalues, ω^2 (natural frequencies squared), and the eigenvectors, Δ_m (natural modes of vibration). The natural vibration modes can then be used as columns of the transformation matrix T. In this case, the matrix T is called a model transformation, and $\overline{\Delta}$ is called a matrix of "modal coordinates".

The justification for using undamped modes to analyze a damped mechanical system is that if all of the modes are used, no approximation is introduced, since the transformation T is square and nonsingular, and the number of modal coordinates is equal to the number of untransformed coordinates. If fewer modes are used, the analysis can still provide a satisfactory response for the damped system, even though the displacements of an equivalent undamped system will be different, because a linear combination of the undamped modes can be found, from the analysis, which will represent the damped response, provided that a sufficient number of suitable modes are employed. In the laminated beam, the damping introduced by the interlayer is rather small, so that the shape of the deflection curve is quite similar to the curve for an undamped beam. Also, the method of excitation, by initial tip displacement, produces a simple response which can be represented by a small number of undamped modes.

We now assume that the lowest natural mode of vibration is sufficient to represent the motion. Subsequent test-analysis correlations have shown that this assumption is satisfactory. Consequently, T becomes a column matrix and $\overline{\Delta}$ is a scalar. The transformation has the effect of reducing the vibrating beam to a single degree of freedom system. Consequently the following standard equation for damped single degree of freedom systems applies:

$$\bar{C} = 2\gamma\sqrt{\bar{M}\,\bar{K}}, \tag{44}$$

where $\bar{M}$, $\bar{C}$ and $\bar{K}$ are the transformed mass, damping, and stiffness constants for the beam, based on a single modal degree of freedom, and γ is the ratio of actual damping to critical damping.

The damping ratio, γ, is calculated from the logarithmic decrement of the motion subsequent to tip release, as determined from test data. The transformed mass $\bar{M}$ and the transformed stiffness $\bar{K}$ are determined from the untransformed mass and stiffness matrices, M and K, according to Equation (40). The matrices, M and K, can be determined from the finite-element model, since the mass and stiffness properties of the structural ply and interlayer materials are known. Consequently, $\bar{C}$ can be calculated from Equation (44). The damping constant, C_I, for the interlayer material can be derived from $\bar{C}$.

Assume that all of the damping in the laminated beam arises from three sources: interlayer damping, structural ply damping, and air damping; although we expect structural-ply and air damping to be small. Therefore, we can write,

$$C = C_S + C_I + C_A, \tag{45}$$

where:

C_S = damping matrix for structural plies,

C_I = damping matrix for interlayer, and

C_A = damping matrix for air.

Now assume that the structural-ply and interlayer damping matrices, C_S and C_I, are proportional to the corresponding stiffness matrices. Therefore,

$$C = h_S K_S + h_I K_I + c_A C_{A1}, \tag{46}$$

where,

h_S, h_I = material damping-to-stiffness ratios for structural plies and interlayer

K_S, K_I = stiffness matrices for structural plies and interlayer, and

c_A = an air damping constant

C_{A1} = C_A for a unit values of the air damping constant c_A.

The significance of c_A is now investigated.

The air damping matrix C_A has as many rows and columns as the structure has degrees of freedom. It can be seen, from Equation (45), that the element in the i^{th} and the j^{th} column of C_A is the air damping force in the i^{th} degree of freedom resulting from a unit value of the velocity component in the j^{th} degree of freedom. Consider only air damping forces normal to the surface, and, as a simplification, assume that C_A is diagonal, so that the air damping force in a given degree of freedom is dependent only on the velocity component in that degree of freedom. Each element on the diagonal of C_A therefore, represents the damping force on the portion of the beam surface adjacent to that degree of freedom resulting from a unit value of the velocity component in the degree of freedom. Now each element on the diagonal of C_{A1} is taken equal to the amount of surface area adjacent to the corresponding degree of freedom. Therefore, c_A represents the damping force on a unit area of surface resulting from a unit component of velocity normal to the surface. The units of c_A are lb-sec/in.^{3}.

The purpose of defining C_{A1} and c_A in this manner is to separate the geometry of the structure, represented by C_{A1}, from the damping property of the air, represented by c_A. The matrix C_{A1} is known, the scalar c_A remains to be determined. Because of the way in which c_A is defined, it is expected to be roughly independent of velocity, and of the surface to which it is applied. Therefore, the value of c_A determined from the beam can be applied to other windshield and/or canopy shapes.

The matrices K_S, K_I and C_{Al} are obtained from the finite element analysis. Therefore, since $\overline{C} = T^T C T$ (see Equation (40)),

$$\overline{C} = T^T (h_S k_S + h_I K_I + c_A C_{Al}) T, \tag{47}$$

or

$$\overline{C} = h_S \overline{K}_S + h_I \overline{K}_I + c_A \overline{C}_{Al}, \tag{48}$$

where

$$\overline{K}_S = T^T K_S T, \ \overline{K}_I = T^T K_I T, \text{ and } \overline{C}_{Al} = T^T C_{Al} T. \tag{49a,b,c}$$

This approach is now applied to specific cases to define the damping constants:

1. Monolithic Beam with Negligible Material Damping:

   Let $$h_S = h_I = 0. \tag{50}$$

   This equation applies to the aluminum beam. Therefore,

   $$\overline{C} = c_A \overline{C}_{Al}, \tag{51}$$

   or

   $$c_A = \frac{\overline{C}}{\overline{C}_{Al}}. \tag{52}$$

   This establishes the air-damping constant c_A.

2. Monolithic Beam with Significant Material Damping:

   Let $$h_I = 0. \tag{53}$$

   This equation is assumed to apply to the monolithic polycarbonate beams. Therefore,

   $$\overline{C} = h_S \overline{K}_S + c_A \overline{C}_{Al}, \tag{54}$$

   or

   $$h_S = \frac{1}{K_S} (\overline{C} - c_A \overline{C}_{Al}). \tag{55}$$

   This establishes the structural ply damping-to-stiffness ratio, h_S.

3. Laminated Beam with significant interlayer material damping and structural-ply damping: The damping constant equation is

$$\overline{C} = h_S\overline{K}_S + h_I\overline{K}_I + c_A\overline{C}_{A1}, \qquad (56)$$

or

$$h_I = \frac{1}{\overline{K}_I}\ (\overline{C} - h_S\overline{K}_S - c_A\overline{C}_{A1}). \qquad (57)$$

This establishes the interlayer damping-to-stiffness ratio, h_I.

This method of calculating damping constants is also applicable to beams composed of more than 3 layers, provided that the structural ply materials are all the same, and the interlayer materials' properties are also the same.

Matrix Analysis Procedure for Extracting Damping Factors

The procedure for reducing the data applicable to cantilever beams consists of the following steps:

1. Produce a finite element model of the test specimen and generate the stiffness, mass and unit damping matrices: K_S, K_I, K, M, and C_{A1} as explained in the preceding discussion.

2. Calculate the static strain in the finite element model at the strain-gage location, resulting from the same tip deflection as that imposed in the test.

3. Compare the calculated strain to the measured strain.

4. Calculate the first natural vibration mode based on K and M. The mode is a column matrix T.

5. Calculate the transformed stiffress, mass and unit damping matrices from Equations (40a,b,c) and (49a,b,c):

$$\overline{K}_S = T^T K_S T, \quad \overline{K}_I = T^T K_I T, \quad \overline{K} = T^T K T,$$
$$\overline{M} = T^T M T, \quad \overline{C}_{Al} = T^T C_{Al} T.$$

6. Record the average damping ratio for specimen(s) noted in Table 14 of Section IV; and also compare

$$\omega_d = \omega_n \sqrt{1-\gamma^2} \tag{58}$$

with the observed damped frequency where:

$$\omega_n = \sqrt{\overline{K}/\overline{M}} \tag{59}$$

7. Transformed damping matrix using Equation (44): (a scalar)

$$\overline{C} = 2\gamma \sqrt{\overline{M}\,\overline{K}},$$

where

$\overline{M}$, $\overline{K}$ = transformed mass and stiffness matrices.

8. Air-damping constant:

For a monolithic beam with negligible material damping (aluminum or perhaps glass) compute c_A using Equation (52):

$$c_A = \frac{\overline{C}}{\overline{C}_{Al}},$$

where

$\overline{C}_{Al}$ = transformed air-damping matrix (a scalar) computed on the basis of a unit air-damping constant, and

c_A = air-damping constant.

9. Structural-ply damping constant:

For a monolithic beam of the structural-ply material, compute h_S using Equation (55):

where:

$\bar{K}_S$ = transformed structural-stiffness matrix (a scalar), and

h_S = structural-ply damping-to-stiffness ratio.

10. Interlayer-damping constant:

For a laminated beam, compute h_I using Equation (57):

$$h_I = \frac{1}{\bar{K}_I} (\bar{C} - h_S \bar{K}_S - c_A \bar{C}_{A1}),$$

where:

$\bar{K}_I$ = transformed interlayer-stiffness matrix (a scalar), and

h_I = interlayer material damping-to-stiffness ratio.

Note that the matrices $\bar{C}_{A1}$, $\bar{K}_S$ and $\bar{K}_I$ are not necessarily the same for all of the specimens, since they are derived for each specimen from the appropriate finite element model. Also, all quantities in a given equation must correspond to the same temperature. In the preceding list, Steps 2, 3 and in Step 6, the calculation of ω_d, are not necessary steps in the procedures for finding the damping constants. They are included to provide checks on the calculations.

Finite-Element Model and Results

The finite-element model shown in Figure 88 was configured according to Specimen 6, and its strain response and amplitude envelope were computed at several time-points. Specimen 6 has outer polycarbonate layers 0.246 and 0.248-inch thick, laminated with a CIP interlayer 0.120-inch thick.

The finite-element model cell elements 1, 20 and 39 are rigid and represent the clamped support at the base of the cantilever test specimen. Spring $k_{\Delta 1}$ and $k_{\Delta 2}$ are provided for the purpose of introducing a partially

clamped condition, if this is needed to represent the test conditions. Cells 2 through 38 represent structural plies, and Cells 40 through 57 represent the interlayer. By giving appropriate material properties and thicknesses to these cells, the same model can be used to represent any of the several test specimens, whether laminated or monolithic. The model is a one-inch wide strip along the longitudinal centerline of the eight-inch wide specimen. Since such a segment is constrained against anticlastic bending because of the eight-inch width, the model was also constrained in the Y degree-of-freedom along both sides.

The data reduction procedure outlined in the preceding subsection resulted in the characterizing parameters, static strain comparisons, frequency comparisons, and damping ratios tabulated in Tables 38 to 49. The damping ratios were summarized in Table 14 of Section IV.

The air-damping constant and material-damping ratios found in the damping beam test/analysis procedure (Ref. Tables 42 and 43) were used to generate the structural damping matrix. A modal transformation based on the first natural vibration mode of the model was used to calculate the transformed stiffness, mass, and damping matrices.

Utilizing the appropriate data for the damping parameters with the Bird Impact Math Model program, the Damping-To-Stiffness Ratios, h_S and h_I, were extracted. A summary of these results is presented in Figure 89 for various structural plies and interlayer materials.

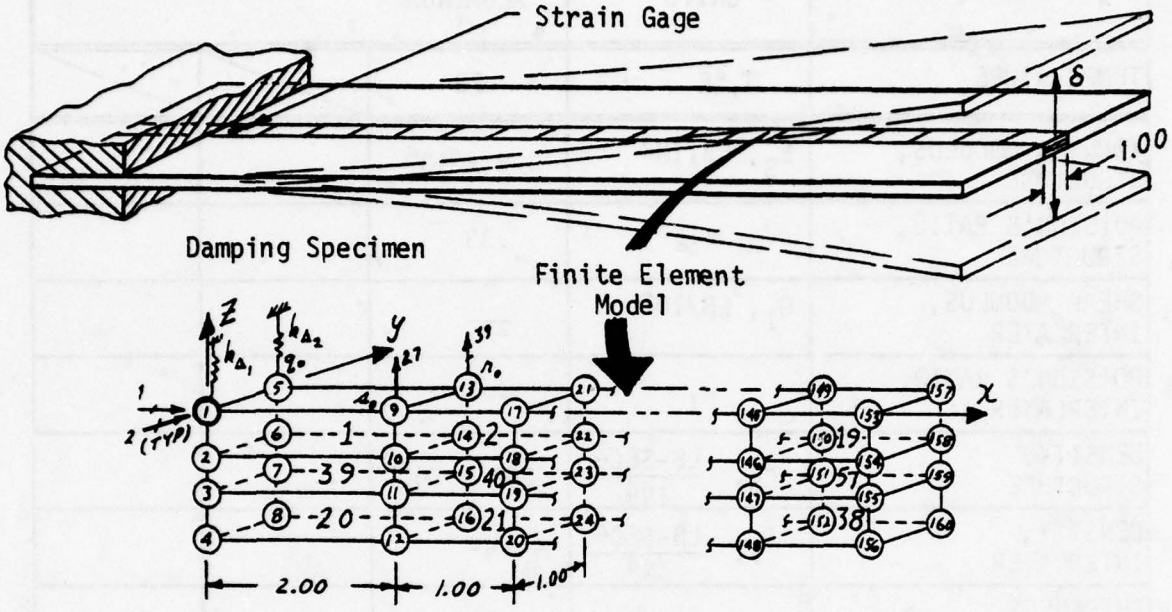

832 Degrees of Freedom, 2052 Element Forces

Figure 88. Finite element model for damping specimen analysis.

TABLE 38. SPECIMEN 8 (CONDITION 11.2) ANALYSIS PROPERTIES AND TEST/ANALYSIS CORRELATIONS

ITEM DESCRIPTION	SYMBOL, UNITS	SPECIMEN NO. 8 ALUMINUM		
TEMPERATURE	T, °F	75		
YOUNG'S MODULUS, STRUCTURE	E_S, LB/IN^2	10.3×10^6		
POISSON'S RATIO, STRUCTURE	ν_S	.33		
SHEAR MODULUS, INTERLAYER	G_I, LB/IN2	---		
POISSON'S RATIO, INTERLAYER	ν_I	---		
DENSITY, STRUCTURE	ρ_S, $\frac{\text{LB-SEC}^2}{\text{IN}^4}$	$.259 \times 10^{-3}$		
DENSITY, INTERLAYER	ρ_I, $\frac{\text{LB-SEC}^2}{\text{IN}^4}$	---		
THICKNESS, STRUCTURE	t_S, IN	.250		
THICKNESS, INTERLAYER	t_I, IN	---		
SPRING CONSTANT	k_Δ, LB/IN	2989.4		
FREQUENCY, COMPUTED	f_C, HZ	24.6		
FREQUENCY, TEST	f_T, HZ	23.2		
$(f_C - f_T)/f_T \times 100$	%	6.0		
DEFLECTION, IMPOSED	δ_I, IN	.998		
STRAIN, COMPUTED	ε_C	1070		
STRAIN, TEST	ε_T	1047		
$(\varepsilon_C - \varepsilon_T)/\varepsilon_T \times 100$	%	2.2		

TABLE 39. CALCULATION OF AIR DAMPING CONSTANT, c_A, FOR SPECIMEN 8.

ITEM DESCRIPTION	SYMBOL, UNITS	SPECIMEN NO. 8 ALUMINUM		
TEMPERATURE	T (°F)	75		
CRITICAL DAMPING RATIO FROM TEST (REF.)	γ_{TEST}	.00379		
TRANSFORMED MASS MATRIX	$\overline{M}$, $\frac{LB\text{-}SEC^2}{IN}$	$.301091 \times 10^{-3}$		
TRANSFORMED STIFFNESS MATRIX FOR STRUCT. LAYERS	$\overline{K}_S$, $\frac{LB}{IN}$	7.20569		
TRANSFORMED STIFFNESS MATRIX FOR INTERLAYER	$\overline{K}_I$, $\frac{LB}{IN}$	---		
TRANSFORMED STIFFNESS MATRIX $K = \overline{K}_S + \overline{K}_I$	$\overline{K}$, $\frac{LB}{IN}$	7.20569		
TRANSFORMED UNIT AIR DAMPING MATRIX	$\overline{C}_{A1}$, IN^2	9.32009		
TOTAL DAMPING $\overline{C} = 2\sqrt{\overline{M}\,\overline{K}}\,\gamma_{TEST}$	$\overline{C}$, $\frac{LB\text{-}SEC}{IN}$	$.353066 \times 10^{-3}$		
AIR DAMPING PER UNIT AREA	c_A, $\frac{LB\text{-}SEC}{IN^3}$	$.37882 \times 10^{-4}$		
DAMPING/STIFFNESS RATIO FOR STRUCTURAL LAYERS	h_S (SEC)	0 (Assumed)		
DAMPING/STIFFNESS RATIO FOR INTERLAYERS	h_I (SEC)	---		

TABLE 40. SPECIMEN 7B ANALYSIS PROPERTIES AND TEST/ANALYSIS CORRELATIONS.

ITEM DESCRIPTION	SYMBOL, UNITS	SPECIMEN NO. 7B POLYCARBONATE (Mfd. by Sierracin)		
TEMPERATURE	T, °F	-35	75	195
YOUNG'S MODULUS, STRUCTURE	E_S, LB/IN^2	3.66×10^5	3.41×10^5	3.25×10^5
POISSON'S RATIO, STRUCTURE	ν_S	.38	.38	.38
SHEAR MODULUS, INTERLAYER	G_I, LB/IN2	---	---	---
POISSON'S RATIO, INTERLAYER	ν_I	---	---	---
DENSITY, STRUCTURE	ρ_S, $\frac{\text{LB-SEC}^2}{\text{IN}^4}$	$.11138 \times 10^{-3}$	$.11138 \times 10^{-3}$	$.11138 \times 10^{-3}$
DENSITY, INTERLAYER	ρ_I, $\frac{\text{LB-SEC}^2}{\text{IN}^4}$	---	---	---
THICKNESS, STRUCTURE	t_S, IN	.636	.636	.636
THICKNESS, INTERLAYER	t_I, IN	---	---	---
SPRING CONSTANT	k_Δ, LB/IN	∞	∞	∞
FREQUENCY, COMPUTED	f_C, HZ	19.5	18.9	18.5
FREQUENCY, TEST	f_T, HZ	19.2	18.2	17.4
$(f_C - f_T)/f_T \times 100$	%	2.1	3.8	6.3
DEFLECTION, IMPOSED	δ_I, IN	.485	.521	.485
STRAIN, COMPUTED	ε_C	1440	1547	1438
STRAIN, TEST	ε_T	1525	1515	1365
$(\varepsilon_C - \varepsilon_T)/\varepsilon_T \times 100$	%	-5.6	2.1	5.3

TABLE 41. DAMPING RATIOS h_S FOR POLYCARBONATE, SPECIMEN 7B

ITEM DESCRIPTION	SYMBOL, UNITS	SPECIMEN NO. 7B POLYCARBONATE (Mfd. by Sierracin)		
TEMPERATURE	T, (°F)	-35	75	195
CRITICAL DAMPING RATIO FROM TEST (REF)	γ_{TEST}	.01264	.00667	.00740
TRANSFORMED MASS MATRIX	$\overline{M}$, $\frac{LB\text{-}SEC^2}{IN}$	.319758 x 10^{-3}	.319753 x 10^{-3}	.319750 x 10^{-3}
TRANSFORMED STIFFNESS MATRIX FOR STRUCT. LAYERS	$\overline{K}_S$, $\frac{LB}{IN}$	4.84457	4.51385	4.30218
TRANSFORMED STIFFNESS MATRIX FOR INTERLAYER	$\overline{K}_I$, $\frac{LB}{IN}$			
TRANSFORMED STIFFNESS MATRIX $K = \overline{K}_S + \overline{K}_I$	$\overline{K}$, $\frac{LB}{IN}$	4.84457	4.51385	4.30218
TRANSFORMED UNIT AIR DAMPING MATRIX	$\overline{C}_{Al}$, IN^2	9.045054	9.04491	9.04482
TOTAL DAMPING $\overline{C} = 2\sqrt{\overline{M}\,\overline{K}}\,\gamma_{TEST}$	$\overline{C}$, $\frac{LB\text{-}SEC}{IN}$	9.949824 x 10^{-4}	5.06800 x 10^{-4}	5.48922 x 10^{-4}
AIR DAMPING PER UNIT AREA (Ref. Table 11)	c_A, $\frac{LB\text{-}SEC}{IN^3}$	.37882 x 10^{-4}	.37882 x 10^{-4}	.37882 x 10^{-4}
DAMPING/STIFFNESS RATIO FOR STRUCTURAL LAYERS	h_S (SEC)	1.346534 x 10^{-4}	3.636823 x 10^{-5}	4.79492 x 10^{-5}
DAMPING/STIFFNESS RATIO FOR INTERLAYERS	h_I (SEC)	---	---	---

TABLE 42. SPECIMEN 6 ANALYSIS PROPERTIES AND TEST/ANALYSIS CORRELATIONS

ITEM DESCRIPTION	SYMBOL, UNITS	SPECIMEN NO. 6 LAMINATE: POLYCARBONATE AND CIP		
TEMPERATURE	T, °F	-35	75	195
YOUNG'S MODULUS, STRUCTURE	E_S, LB/IN^2	3.66×10^5	3.41×10^5	3.25×10^5
POISSON'S RATIO, STRUCTURE	ν_S	.38	.38	.38
SHEAR MODULUS, INTERLAYER	G_I, LB/IN2	60.0	50.0	45.0
POISSON'S RATIO, INTERLAYER	ν_I	.50	.50	.50
DENSITY, STRUCTURE	ρ_S, $\frac{LB\text{-}SEC^2}{IN^4}$	$.11138 \times 10^{-3}$	$.11138 \times 10^{-3}$	$.11138 \times 10^{-3}$
DENSITY, INTERLAYER	ρ_I, $\frac{LB\text{-}SEC^2}{IN^4}$	$.95855 \times 10^{-4}$	$.95855 \times 10^{-4}$	$.95855 \times 10^{-4}$
THICKNESS, STRUCTURE	t_S, IN	.246 .248	.246 .248	.246 .248
THICKNESS, INTERLAYER	t_I, IN	.120	.120	.120
SPRING CONSTANT	k_Δ, LB/IN	∞	∞	∞
FREQUENCY, COMPUTED	f_C, HZ	13.6	12.8	12.4
FREQUENCY, TEST	f_T, HZ	13.9	12.6	12.2
$(f_C - f_T)/f_T \times 100$	%	-2.1	1.6	1.6
DEFLECTION, IMPOSED	δ_I, IN	.495	.505	.560
STRAIN, COMPUTED	ε_C	1128	1125	1234
STRAIN, TEST	ε_T	1138	1130	1284
$(\varepsilon_C - \varepsilon_T)/\varepsilon_T \times 100$	%	-.9	-.4	-3.9

TABLE 43. DAMPING RATIOS h_I FOR CIP INTERLAYER, SPECIMEN 6

ITEM DESCRIPTION	SYMBOL, UNITS	SPECIMEN NO. 6 LAMINATE: POLYCARBONATE AND CIP		
TEMPERATURE	T, (°F)	-35	75	195
CRITICAL DAMPING RATIO FROM TEST (REF)	γ_{TEST}	.04095	.02752	.01895
TRANSFORMED MASS MATRIX	$\overline{M}$, $\frac{LB\text{-}SEC^2}{IN}$	.349100 $\times 10^{-3}$	.34872 $\times 10^{-3}$	.348408 $\times 10^{-3}$
TRANSFORMED STIFFNESS MATRIX FOR STRUCT. LAYERS	$\overline{K}_S$, $\frac{LB}{IN}$	1.59181	1.39875	1.29326
TRANSFORMED STIFFNESS MATRIX FOR INTERLAYER	$\overline{K}_I$, $\frac{LB}{IN}$	.942892	.863208	.813823
TRANSFORMED STIFFNESS MATRIX $K = \overline{K}_S + \overline{K}_I$	$\overline{K}$, $\frac{LB}{IN}$	2.53470	2.26196	2.10709
TRANSFORMED UNIT AIR DAMPING MATRIX	$\overline{C}_{AI}$, IN^2	10.5143	10.5029	10.4936
TOTAL DAMPING $\overline{C} = 2\sqrt{\overline{M}\,\overline{K}}\,\gamma_{TEST}$	$\overline{C}$, $\frac{LB\text{-}SEC}{IN}$	2.43625 $\times 10^{-3}$	1.54582 $\times 10^{-3}$	1.026889 $\times 10^{-3}$
AIR DAMPING PER UNIT AREA (Ref. Table 11)	c_A, $\frac{LB\text{-}SEC}{IN^3}$	.37882 $\times 10^{-4}$	.37882 $\times 10^{-4}$	.37882 $\times 10^{-4}$
DAMPING/STIFFNESS RATIO FOR STRUCTURAL LAYERS	(Ref. Table 4) h_S (SEC)	1.346534 $\times 10^{-4}$	3.636823 $\times 10^{-5}$	4.79492 $\times 10^{-5}$
DAMPING/STIFFNESS RATIO FOR INTERLAYERS	h_I (SEC)	1.93405 $\times 10^{-3}$	1.27093 $\times 10^{-3}$	6.97154 $\times 10^{-4}$

TABLE 44. SPECIMEN 7A ANALYSIS PROPERTIES AND TEST/ANALYSIS CORRELATIONS

ITEM DESCRIPTION	SYMBOL, UNITS	SPECIMEN NO. 7A POLYCARBONATE (Mfd. by PPG Ind.)		
TEMPERATURE	T, °F	-35	75	195
YOUNG'S MODULUS, STRUCTURE	E_S, LB/IN^2	3.66×10^5	3.41×10^5	3.25×10^5
POISSON'S RATIO, STRUCTURE	ν_S	.38	.38	.38
SHEAR MODULUS, INTERLAYER	G_I, LB/IN2	---	---	---
POISSON'S RATIO, INTERLAYER	ν_I	---	---	---
DENSITY, STRUCTURE	ρ_S, $\frac{LB\text{-}SEC^2}{IN^4}$	$.11138 \times 10^{-3}$	$.11138 \times 10^{-3}$	$.11138 \times 10^{-3}$
DENSITY, INTERLAYER	ρ_I, $\frac{LB\text{-}SEC^2}{IN^4}$	---	---	---
THICKNESS, STRUCTURE	t_S, IN	.621	.621	.621
THICKNESS, INTERLAYER	t_I, IN	---	---	---
SPRING CONSTANT	k_Δ, LB/IN	∞	∞	∞
FREQUENCY, COMPUTED	f_C, HZ	19.1	18.5	18.0
FREQUENCY, TEST	f_T, HZ	18.3	17.4	16.4
$(f_C - f_T)/f_T \times 100$	%	4.4	6.3	9.7
DEFLECTION, IMPOSED	δ_I, IN	.591	.576	.579
STRAIN, COMPUTED	ε_C, $\frac{\mu \text{ in.}}{\text{in.}}$	1713	1670	1678
STRAIN, TEST	ε_T, $\frac{\mu \text{ in.}}{\text{in.}}$	1608	1429	1407
$(\varepsilon_C - \varepsilon_T)/\varepsilon_T \times 100$	%	6.5	16.8	19.2

TABLE 45. DAMPING RATIOS h_S FOR POLYCARBONATE, SPECIMEN 7A

ITEM DESCRIPTION	SYMBOL, UNITS	SPECIMEN NO. 7A POLYCARBONATE (Mfd. by PPG Ind.)		
TEMPERATURE	T, °F	-35	75	195
CRITICAL DAMPING RATIO FROM TEST (REF)	γ_{TEST}	.01254	.00812	.00792
TRANSFORMED MASS MATRIX	$\overline{M}$, $\frac{LB\text{-}SEC^2}{IN}$	.312193 x 10^{-3}	.312189 x 10^{-3}	.312186 x 10^{-3}
TRANSFORMED STIFFNESS MATRIX FOR STRUCT. LAYERS	$\overline{K}_S$, $\frac{LB}{IN}$	4.51007	4.20219	4.00513
TRANSFORMED STIFFNESS MATRIX FOR INTERLAYER	$\overline{K}_I$, $\frac{LB}{IN}$			
TRANSFORMED STIFFNESS MATRIX $K = \overline{K}_S + \overline{K}_I$	$\overline{K}$, $\frac{LB}{IN}$	4.51007	4.20219	4.00513
TRANSFORMED UNIT AIR DAMPING MATRIX	$\overline{C}_{Al}$, IN^2	9.04459	9.0446	9.04437
TOTAL DAMPING $\overline{C} = 2\sqrt{\overline{M}\,\overline{K}}\,\gamma_{TEST}$	$\overline{C}$, $\frac{LB\text{-}SEC}{IN}$	9.41089 x 10^{-4}	5.88210 x 10^{-4}	5.60106 x 10^{-4}
AIR DAMPING PER UNIT AREA (Ref. Table 11)	c_A, $\frac{LB\text{-}SEC}{IN^3}$	.37882 x 10^{-4}	.37882 x 10^{-4}	.37882 x 10^{-4}
DAMPING/STIFFNESS RATIO FOR STRUCTURAL LAYERS	h_S (SEC)	1.326946 x 10^{-4}	5.84415 x 10^{-5}	5.430215 x 10^{-5}
DAMPING/STIFFNESS RATIO FOR INTERLAYERS	h_I (SEC)	---	---	---

TABLE 46. SPECIMEN 5 ANALYSIS PROPERTIES AND TEST/ANALYSIS CORRELATIONS

ITEM DESCRIPTION	SYMBOL, UNITS	SPECIMEN NO. 5 LAMINATE: POLYCARBONATE & PPG 112		
TEMPERATURE	T, °F	-35	75	195
YOUNG'S MODULUS, STRUCTURE	E_S, LB/IN^2	3.66×10^5	3.41×10^5	3.25×10^5
POISSON'S RATIO, STRUCTURE	ν_S	.38	.38	.38
SHEAR MODULUS, INTERLAYER	G_I, LB/IN2	670	500	100
POISSON'S RATIO, INTERLAYER	ν_I	.50	.50	.50
DENSITY, STRUCTURE	ρ_S, $\frac{LB\text{-}SEC^2}{IN^4}$	$.11138 \times 10^{-3}$	$.11138 \times 10^{-3}$	$.11138 \times 10^{-3}$
DENSITY, INTERLAYER	ρ_I, $\frac{LB\text{-}SEC^2}{IN^4}$	$.10363 \times 10^{-3}$	$.10363 \times 10^{-3}$	$.10363 \times 10^{-3}$
THICKNESS, STRUCTURE	t_S, IN	.250 .254	.250 .254	.250 .254
THICKNESS, INTERLAYER	t_I, IN	.121	.121	.121
SPRING CONSTANT	k_Δ, LB/IN	∞	∞	∞
FREQUENCY, COMPUTED	f_C, HZ	18.2	17.3	14.3
FREQUENCY, TEST	f_T, HZ	18.2	17.0	15.0
$(f_C - f_T)/f_T \times 100$	%	0	1.7	-4.7
DEFLECTION, IMPOSED	δ_I, IN	.510	.510	.515
STRAIN, COMPUTED	ε_C, $\frac{\mu IN.}{IN.}$	1501	1495	1335
STRAIN, TEST	ε_T, $\frac{\mu IN.}{IN.}$	1720	1607	1451
$(\varepsilon_C - \varepsilon_T)/\varepsilon_T \times 100$	%	-12.7	-7.0	-8.0

TABLE 47. DAMPING RATIOS h_I FOR PPG 112 INTERLAYER, SPECIMEN 5

ITEM DESCRIPTION	SYMBOL, UNITS	SPECIMEN NO. 5 LAMINATE: POLYCARBONATE AND PPG 112		
TEMPERATURE	T, (°F)	-35	75	195
CRITICAL DAMPING RATIO FROM TEST (REF)	γ_{TEST}	.01165	.01356	.01190
TRANSFORMED MASS MATRIX	$\overline{M}$, $\frac{LB\text{-}SEC^2}{IN}$	.326872 x 10^{-3}	.330066 x 10^{-3}	.356996 x 10^{-3}
TRANSFORMED STIFFNESS MATRIX FOR STRUCT. LAYERS	$\overline{K}_S$, $\frac{LB}{IN}$	3.81321	3.42027	2.00156
TRANSFORMED STIFFNESS MATRIX FOR INTERLAYER	$\overline{K}_I$, $\frac{LB}{IN}$	.453099	.491869	.889598
TRANSFORMED STIFFNESS MATRIX $K = \overline{K}_S + \overline{K}_I$	$\overline{K}$, $\frac{LB}{IN}$	4.26631	3.91213	2.89116
TRANSFORMED UNIT AIR DAMPING MATRIX	$\overline{C}_{AI}$, IN^2	9.53674	9.62978	10.4150
TOTAL DAMPING $\overline{C} = 2\sqrt{\overline{M}\,\overline{K}}\,\gamma_{TEST}$	$\overline{C}$, $\frac{LB\text{-}SEC}{IN}$	8.701036 x 10^{-4}	9.745334 x 10^{-4}	7.646183 x 10^{-4}
AIR DAMPING PER UNIT AREA (Reference Table 11)	c_A, $\frac{LB\text{-}SEC}{IN^3}$	.37882 x 10^{-4}	.37882 x 10^{-4}	.37882 x 10^{-4}
DAMPING/STIFFNESS RATIO FOR STRUCTURAL LAYERS	h_S (SEC) (7A)	1.326946 x 10^{-4}	5.84415 x 10^{-5}	5.430215 x 10^{-5}
DAMPING/STIFFNESS RATIO FOR INTERLAYERS	h_I (SEC)	6.27 x 10^{-6}	8.3326 x 10^{-4}	2.9383 x 10^{-4}

TABLE 48. SPECIMEN 10 ANALYSIS PROPERTIES AND TEST/ANALYSIS CORRELATIONS

ITEM DESCRIPTION	SYMBOL, UNITS	SPECIMEN NO. 10 ACRYLIC		
TEMPERATURE	T, °F	-35	75	200
YOUNG'S MODULUS, STRUCTURE	E_S, LB/IN^2	8.0×10^5	4.9×10^5	1.9×10^5
POISSON'S RATIO, STRUCTURE	ν_S	.35	.35	.35
SHEAR MODULUS, INTERLAYER	G_I, LB/IN^2	---	1.81×10^5	---
POISSON'S RATIO, INTERLAYER	ν_I	---	---	---
DENSITY, STRUCTURE	ρ_S, $\frac{\text{LB-SEC}^2}{\text{IN}^4}$	$.1114 \times 10^{-3}$	$.1114 \times 10^{-3}$	$.1114 \times 10^{-3}$
DENSITY, INTERLAYER	ρ_I, $\frac{\text{LB-SEC}^2}{\text{IN}^4}$	---	---	---
THICKNESS, STRUCTURE	t_S, IN	.679	.67	.679
THICKNESS, INTERLAYER	t_I, IN	---	---	---
SPRING CONSTANT	k_Δ, LB/IN	∞	∞	∞
FREQUENCY, COMPUTED	f_C, HZ	30.5	23.9	14.9
FREQUENCY, TEST	f_T, HZ	28.8	25.2	19.1
$(f_C - f_T)/f_T \times 100$	%	5.9	-5.1	-22
DEFLECTION, IMPOSED	δ_I, IN	.460	.507	.305
STRAIN, COMPUTED	ϵ_C, $\frac{\mu\text{IN.}}{\text{IN.}}$	1481	1633	983
STRAIN, TEST	ϵ_T, $\frac{\mu\text{IN.}}{\text{IN.}}$	1470	1470	845
$(\epsilon_C - \epsilon_T)/\epsilon_T \times 100$	%	.7	+11.0	+16.3

TABLE 49. DAMPING RATIOS h_S FOR ACRYLIC, SPECIMEN 10

ITEM DESCRIPTION	SYMBOL, UNITS	SPECIMEN NO. 10 ACRYLIC		
TEMPERATURE	T, (°F)	-35	75	200
CRITICAL DAMPING RATIO FROM TEST (REF)	γ_{TEST}	.01467	.03886	.04930
TRANSFORMED MASS MATRIX	$\overline{M}$, $\frac{LB\text{-}SEC^2}{IN}$	.341578 x 10^{-3}	.341516 x 10^{-3}	.341456 x 10^{-3}
TRANSFORMED STIFFNESS MATRIX FOR STRUCT. LAYERS	$\overline{K}_S$, $\frac{LB}{IN}$	12.5531	7.69297	2.98456
TRANSFORMED STIFFNESS MATRIX FOR INTERLAYER	$\overline{K}_I$, $\frac{LB}{IN}$			
TRANSFORMED STIFFNESS MATRIX $K = \overline{K}_S + \overline{K}_I$	$\overline{K}$, $\frac{LB}{IN}$	12.5531	7.69297	2.98456
TRANSFORMED UNIT AIR DAMPING MATRIX	$\overline{C}_{Al}$, IN^2	9.04814	9.04651	9.04494
TOTAL DAMPING $\overline{C} = 2\sqrt{\overline{M}\,\overline{K}}\,\gamma_{TEST}$	$\overline{C}$, $\frac{LB\text{-}SEC}{IN}$	1.921235 x 10^{-3}	3.983688 x 10^{-3}	3.147635 x 10^{-3}
AIR DAMPING PER UNIT AREA (Ref. Table 11)	c_A, $\frac{LB\text{-}SEC}{IN^3}$	.37882 x 10^{-4}	.37882 x 10^{-4}	.37882 x 10^{-4}
DAMPING/STIFFNESS RATIO FOR STRUCTURAL LAYERS	h_S (SEC)	1.25744 x 10^{-4}	4.73288 x 10^{-4}	9.398352 x 10^{-4}
DAMPING/STIFFNESS RATIO FOR INTERLAYERS	h_I (SEC)	---	---	---

Note:

(SK) denotes Sierracin product.

(PPG) denotes PPG Industries product.

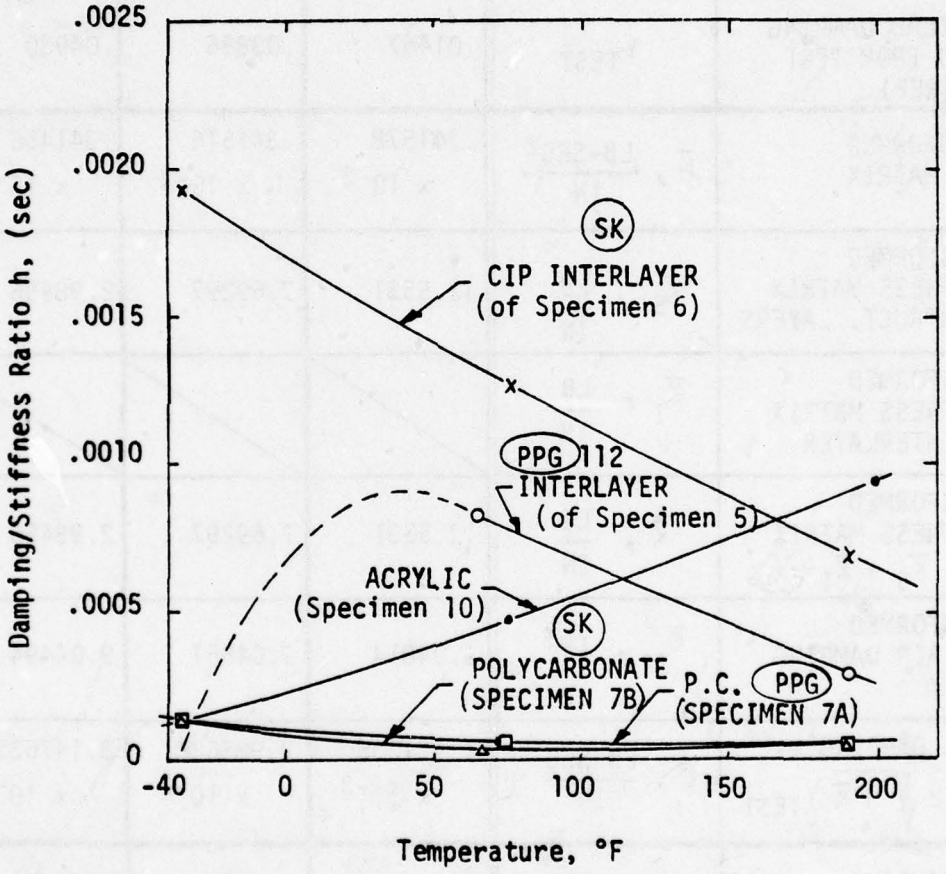

Figure 89. Damping to stiffness ratio (h) versus temperature for structural and interlayer components. (Specimens 5, 6, 7A, 7B, and 10)

CORRELATION OF TEST/ANALYSIS FOR DAMPING BEAM STRAIN RESPONSE

A primary reason for needing the parameters h_S and h_I, is to allow a realistic analytical calculation of the response of a laminated windshield to a dynamic impulse. Figure 90 shows a comparison of the response of Specimen 6 subjected to Test Condition 5, as measured and calculated by the Bird Impact Math Model computer program, employing the damping constants h_S and h_I.

A basic linear analysis capability was used in this analysis. Program modules developed for this level of capability includes a rectangular cell element generator, core resident complex eigenvalue/eigenvector solutions, complex exponentiation, and improved large-order matrix operators for multiplication, solution of linear simultaneous equations, and real eigenvalue/eigenvector solutions associated with the calculations of natural modes and frequencies (Reference 1).

CORRELATION OF TEST/ANALYSIS FOR STATIC/DYNAMIC BEAM STRAIN RESPONSE

This subsection presents the test/analysis correlation of the strain response from a 36-inch beam test (Specimen 2, Condition 15) at room temperature. The beam was pin-ended and simply supported. Aluminum bushing inserts and clamping edge attachments kept the inner plies from slipping. Figure 91 shows the test/analysis correlations of the beam static deflection and strains for the beam centerline.

The theoretical maximum strain equation shown in Figure 91 was derived from the simple beam theory. That is, from the beam centerline deflection Equation (9)

$$\delta_{\mathcal{L}} = \frac{23Pa^3}{24EI} . \tag{60}$$

Solving this equation in terms of moments gives

$$M = \frac{24}{23} \frac{EI}{a^2} \delta , \tag{61}$$

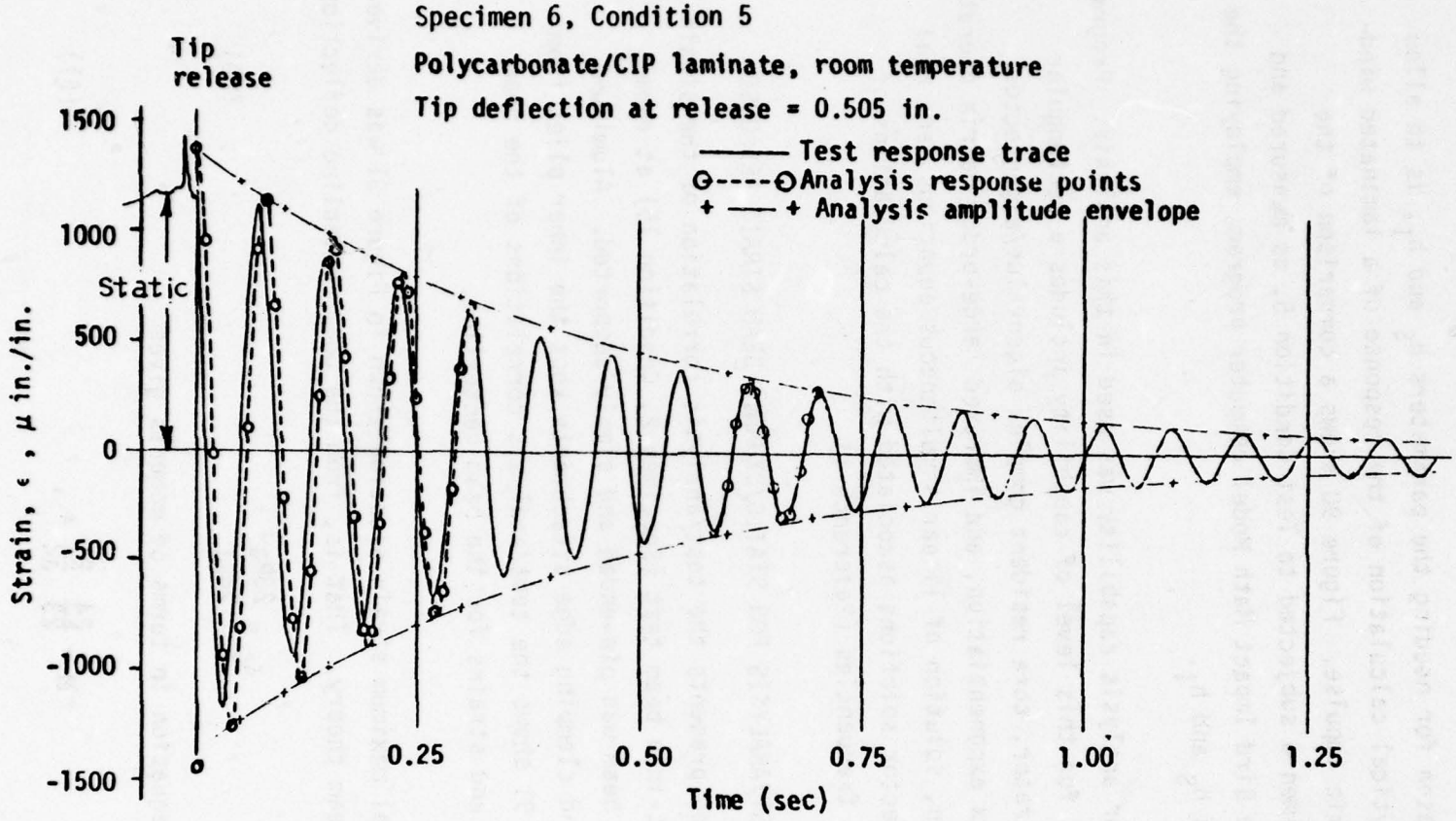

Figure 90. Damping beam response to an initial tip displacement.

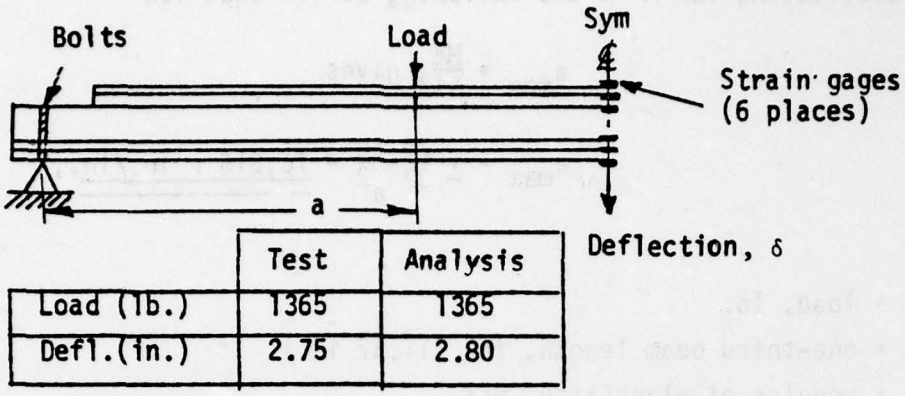

	Test	Analysis
Load (lb.)	1365	1365
Defl.(in.)	2.75	2.80

(a) Static deflection

SPECIMEN 2, COND. 15
SR/SS-PIV
@ ROOM TEMPERATURE

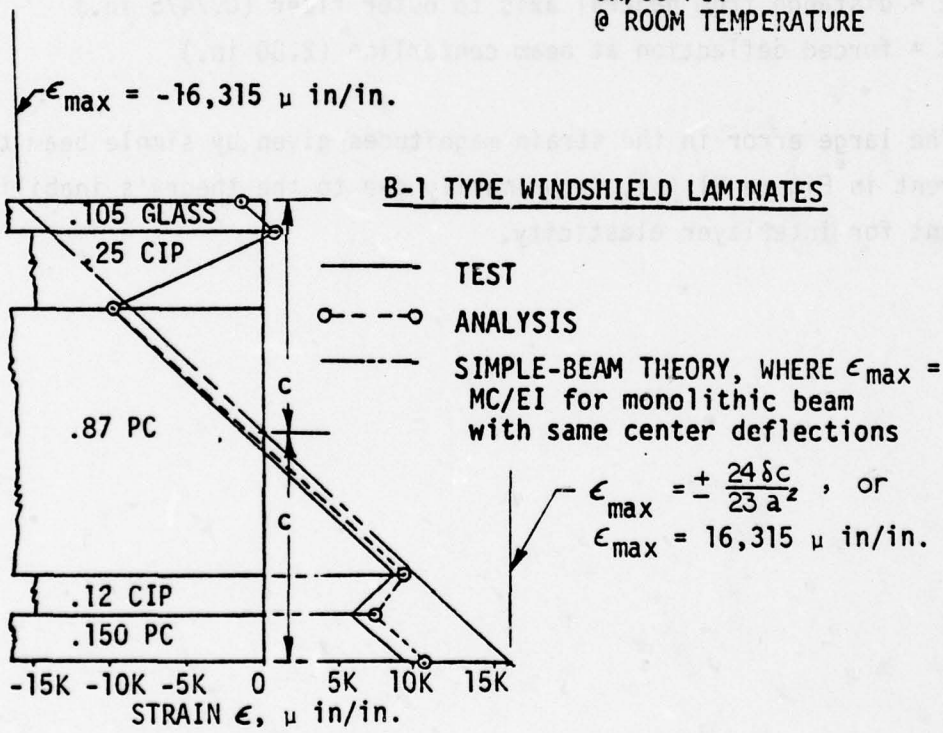

(b) Strain correlations

Figure 91. (a) Static deflection and (b) strain correlations for 36-inch beam model.

and substituting for M in the following strain equation

$$\varepsilon_{max} = \frac{Mc}{EI}, \text{ gives}$$

$$\varepsilon_{max} = \pm \frac{24\,\delta c}{32\,a^2} = \underline{16{,}315\ \mu\ \text{in./in.}}, \qquad (62)$$

where

P = load, lb.
a = one-third beam length, in. (11.57 in.)
E = modulus of elasticity, psi
I = moment of inertia, $in.^4$
M = moment, in.-lb.
c = distance from neutral axis to outer fiber (0.7475 in.)
δ = forced deflection at beam centerline (2.80 in.)

The large error in the strain magnitudes given by simple beam theory, apparent in Figure 91 (b), is primarily due to the theory's inability to account for interlayer elasticity.

SECTION VIII
CONCLUSIONS AND RECOMMENDATIONS

The conclusions derived from the three major types of testing are provided in the following subsections.

DAMPING BEAM TESTING

1. Cantilevered beam tests provided an effective means of obtaining damping parameters (Tables 11 and 14, and Figure 30). These tests also provided a data base for correlation with analytical results (Figure 90), for both static and dynamic conditions. It was observed during testing that the local stiffening effect of gages mounted on low-modulus polycarbonate material does not appear to be a problem.

2. The Damping-To-Stiffness Ratio, (h) provides an effective means for comparison of transparent windshield materials at various temperatures (Figure 89).

3. Damping ratios are dependent upon the relative magnitude of oscillatory displacements (Figures 28, 71 and 72). (Theoretically, like-material damping ratios are independent of material size or shape.)

4. Higher damping ratios, such as 0.039 for an acrylic beam, causes early decay of beam oscillatory motion, while lower damping ratios, such as 0.003 for an aluminum beam, allows a beam to vibrate relatively longer (Table 13 and Figure 29).

5. The percentage deviation of the recorded testing strains versus theoretical strains for the monolithic beam Specimen 7A, was 1341 versus 1429 μ in./in. respectively, which is a 6.16% deviation, that was considered to be reasonable.

STATIC/DYNAMIC BEAM TESTING

For detailed descriptions of end conditions and test condition details refer to Tables 4 and 5 as well as Figure 5.

1. The simply supported laminated beams represented by Figure 31a, with bolts and bushings, present higher beam stiffness than those with the fixed-end conditions represented by Figure 31c. This can be deduced by comparing the slopes of the strain diagrams of Figure 37. Attachments (bolts and/or bushings) prevent structural ply slippage at the ends of the simply supported beam, thus providing a type of inner fixity (Figures 38 and 43). This was observed as being pronounced on Specimen 2 to a greater degree than that for Specimen 4. The fixed end beam condition has negligible ply slippage occurring in the attachment areas.

2. The specimens tested all have an approximately linear relationship with respect to applied loads, structural-ply strains, and centerline deflections, as indicated in Figure 44. Specifically, after deformation of the beam occurs, plane sections of individual plies remain plane, as shown in Figures 46 and 58.

3. Beam Specimen 2, with the CIP silicone interlayers, allowed the structural plies to behave more independently than beam Specimen 4, with PPG-112 interlayers. Specimen 4 behaved relatively more like a monolithic beam (Figures 43 and 48); that is, the slopes of the multi-strain diagrams at a station location are approximately in line.

4. For the fixed-end beam configuration, the single-row attached beam had approximately 84 percent fixity and the double-row attached beam had approximately 96 percent fixity with respect to a theoretical fixed end beam (Figure 37).

5. The beam stiffness for single-row attachments installed in oversized bushings allowing loose holes that were sealant filled, (Specimen 2) Condition 65, was reduced by 38 percent in respect to the double-row attached beam, Condition 29S (Figures 51 and 69). This reduction in stiffness may be a desirable attribute in the area of the windshield attachments when bird impact shock waves travel from the windshield into the surrounding structure.

6. For Beam Specimen 2, with single-row attachments installed in oversized bushings allowing loose holes that were filled with sealant, the high temperature test at 272°F indicated a reduction of the beam spring stiffness by 18 percent with respect to the room temperature test condition (Figure 54). The majority of this beam stiffness reduction may be attributed to the softening of the sealant. A post inspection however, of the sealant formed bushings showed no apparent permanent set.

7. For single-row attached Beam Specimen 2, installed in tight fitting aluminum bushings, the high temperature condition had little effect on its spring stiffness (beam total load divided by the beam center deflection). Although, an increase of strain at the attachment area of 26 percent was observed. This was probably caused by the softening of the polycarbonate material (Figures 57 and 69).

8. Similar conclusions can be drawn from the multi-layer beam Specimen 4, with respect to those for Specimen 2, for similar test conditions. The beam stiffness for both a thick core ply beam, Specimen 2, and a multi-layered beam, Specimen 4, were approximately the same (500 pounds per inch). These beams and restraints had (SR/SS-PIV) single-row attachments installed in tight fitting aluminum bushings with both ends free to pivot in simple supports.

9. Using the stiffest thick core ply beam condition 29S (DR/FB) as the base (see Figure 69), comparatively, beam condition 107A (/SS) shows a 70% decrease in stiffness. Condition 107A for Specimen 2 was simply supported, with no bushings or bolts. Using Condition 107A as a new Base 2, comparatively, if the outer face plies and interlayers were removed, it appears that the beam stiffness would be decreased by approximately 54%.

10. Under the beam bending Condition 107A, the interlayer maximum shear strain occurs at the edge of the beam, decreasing approximately linearly to zero strain at the beam center (Figure 39).

11. These tests provided a data base for correlation with results through analysis. Figure 91 shows that the correlation was well within 10% of the accuracy requirement.

IMPACT BEAM TESTING

1. This type of test was effective in providing the highest practical strain rate in the beam specimens under laboratory test conditions. The strain rate achieved was approximately 10 in./in./sec in the area of failure (Figure 77). This value compares favorably with the maximum strain rate levels of 50 to 150 in./in./sec expected in transparencies subjected to high speed bird impact. The amount of variation in material properties caused by strain rate changes is reported in Reference 13.

2. The failures of the strain-gage system appeared to closely follow the structural ply failures. This was expected (Figures 77, 80 and 83) and preferred over early failure of strain gages.

3. The methods used for instrumenting the beams for this series of tests proved to be viable and not to appreciably effect the dynamic response of the beam.

4. The impact strain distribution through the structural plies, at a specific time, appeared to be uniform much like the static load test results (Figure 84). The maximum recorded strain for the three impact test beams occurred at the beam's center lower surface of Specimen 1.

5. Post-test observations showed the failures to be of a brittle-fractured type (Figures 85 and 86), similar to failures occurring in bird struck windshields.

6. The high stresses developed in the polycarbonate material near the attachment area of Specimen 2 could not be evaluated due to inoperative strain gages; although, fractures in this area did occur (Figure 86) in the left end of the thick core ply.

7. The post yield gages installed on Specimen 1 were 1/8-inch in length, which strain limits were rated at approximately 20 percent (200,000 μ in./in.); but, the maximum recorded strain was 33,061 μ in./in., which was well within the gage limitation. The larger internally mounted gages were 1/4-inch in length and also had the 200,000 μ in./in. strain limit capability. This indicated that reliable impact strain readings could be obtained through proper strain gage installations.

8. The edge restraint of a single row of attachments with oversize aluminum bushings and soft snug-fitting inner bushings appears to be an acceptable method of attaching aircraft windshields.

RECOMMENDATIONS

The recommendations derived from the three major types of testing are provided in the following subsections.

Damping Beam

Damping ratio statistical criteria for candidate transparent materials are required for the initial design stages of canopy or windshield designs.

These criteria are not included in MIL-HDBK-17. There is a need for an inexpensive and an accurate method for determining design damping ratios.

Other engineering test methods were investigated; and it was determined that the "free-free" vibration beam method, where the beam would be supported at its two vibratory node points by a simple string and rubber band suspension system, would meet these requirements. This method eliminates possible errors that may develop from the support base of the cantilevered vibrating beam method.

The "free-free" vibratory beam initial amplitude should be in the order one to two inches, to represent bird impacted transparency initial displacement. Damping ratio curves should then be developed and published for initial displacements of two inches, one inch, and "bop test" amplitudes. ("Bop test" is exciting the beam's vibratory mode by rapping the beam with a hammer or mallet.)

Most likely, a minimum of five specimens per test condition, in compliance with MIL-HDBK-5 statistical analysis methods for normal (or gaussian) distribution, would be required. However, if the distribution form is not normal, the number of test specimens required would be greatly increased.

In addition, it is recommended that an analytical differential-equation method for the determination of material damping ratios be pursued. This would encompass and extend the method used in Reference 11. This analytical differential-equation method should be less expensive to accomplish than a full scale math model computer program.

Static and Impact Beam

MIL-HANDBOOK-17 does not publish the modulus of rupture bending stress (F_b) for polycarbonate material. The present available polycarbonate material properties are based upon tensile and compression tests. These types of tests, result in uniform stressess across the specimen

test section. It is believed that the main failure mode in polycarbonate material occurs in high strain rate bending modes. It appears that polycarbonate in the bending mode is very sensitive to surface stress, and that these allowables are considerably reduced due to degradations caused by surface coatings, various surface defects, surface polishing, and/or thermal treatment.

Some Charpy and Izod impact test data are available but these data are used for energy comparison relationship between one specimen to another.

It is recommended that a series of beam bending tests be conducted in suffficient number, and variations in thickness (8 inches wide x 36 inches long) in order that statistical analyses can be performed. These should be conducted for both static and high strain rate (50 to 200 in./in./sec) conditions at various temperatures, and in the pure bending test condition (no axial loads).

The recommended data to be collected would be: A continuous record of the applied test load, the test temperature, and the resulting strain. Bending moments should be developed from the various applied loads. These data should be graphically presented with the ordinate axis as the bending stress (f_b) calculated from the "Mc/I" equation, and the abscissa axis as the resulting bending strain (ε_b). The modulus of bending rupture stress at failure should also be developed. It is also recommended that a continuous record of the beam's instantaneous bend radii be documented. The bend radii (R) would provide a means of counter-checking the strain gage readings, where $\varepsilon_b = c/R$, where c is the distance from the neutral axis to the upper or lower surface.

This data, in turn, would assist in determining when the windshield/canopy failure should occur as a result of normal structural loads or bird impact conditions.

REFERENCES

1. Denke, P. H., Eide, G. R., and Morris, R. C., "Aircraft Windshield Bird Impact Math Model"; Part I, Theory and Application, Part II, User's Manual, Part III, Programming Manual, (Douglas Aircraft Co.) Report No. AFFDL-TR-77-99, December 1977.

2. Singer, F. L., "Strength of Material", Harper and Row, Publishers, Inc., New York, New York, 1962, 2nd Edition.

3. Dove, R. C. and Adams, R. H., "Experimental Stress Analysis and Motion Measurements", (Theory, Instruments and Circuits, Techniques), C. E. Merrill Books, Inc., Columbus, Ohio, 1964, pp. 98-103.

4. Haberman, C. M., "Vibration Analysis", C. E. Merrill Publishing Co., Columbus, Ohio, 1968, pp. 22-33.

5. Scanlan and Rosebaum, "Introduction to the Study of Aircraft Vibration and Flutter", MacMillan Co., New York, 1962, pp.72.

6. Davis, H. E., Troxell, G. E., and Wiskocil, C. T., "The Testing and Inspection of Engineering Materials", McGraw-Hill Book Company, Inc., New York, 3rd Edition, 1965, pp. 150-183. (Static Shear and Bending Tests).

7. American Society for Testing and Materials, ASTM STP497; A conference sponsored by the ASTM, Anaheim, California, 20-22 April 1971, pp. 219-236. (Strain diagrams)

8. Seely, F. B. and Smith, J. O., "Advance Mechanics of Materials", John Wiley and Son, Inc., New York, 2nd Edition, 1967, pp. 64-75.

9. American Society for Testing and Materials. ASTM STP460; A symposium presented at a meeting of Committee D-30 on High Modulus Fibers and Their Composites, New Orleans, Louisiana, 11-13 February 1969, pp. 140-149. (Cylindrical testing of composites)

10. Perry, J. P., "Aircraft Structures", International Text Book Co., Inc., New York, 1950, pp. 113-125 & 317, 419-440. (Strain energy of beams)

11. Denke, P. H., and Hoffman, J. B., "The Determination of Deflection and Stress Distribution for a Laminated Transparent Beam". (Douglas Aircraft Company) Report No. AFFDL-TR-76-114, August 1976.

12. MIL-HDBK-17A, "Plastics for Aerospace Vehicles", Part II "Transparent Glasing Materials", July 1977.

13. Greene, F. E., Beck, R. I., Kozmata, J. W., and Magnusson, R. H., "Testing for Mechanical Properties of Monolithic and Laminated Polycarbonate Materials". (Douglas Aircraft Company) Report No. AFFDL-TR-77-96, October 1977.

BIBLIOGRAPHY

Hurty, W. C. and Rubinstein, M. F., "Dynamics of Structures", Prentice-Hall, Inc., Englewood Cliffs, New Jersey, 1964, pp. 173. (Free-free vibrating beam analysis.)

Johnson, Paul E., "Design and Testing of F-111 Bird Resistance Windshield/ Support Structure, Vol. II - Mechanical Properties Testing". University of Dayton Research Institute, Report No. UDRI-TR-76-44, University of Dayton, Dayton, Ohio; August 1976.

McCormac, J. C., "Structural Analysis", International Text Book Co., Pennsylvania, 2nd Edition, 1960, pp. 443-465. (Plastic analysis)

Pestel, E. C. and Leckie, F. A., "Matrix Methods in Elastomechanics", McGraw-Hill Book Co., Inc., New York, pp. 29-50, 95-124.

Sechler, E. C., and Dun, L. G., "Airplane Structural Analysis and Design", Dover Publishing, Inc., New York, 1963, pp. 124-153, (Strain energy methods for bending, shear, and torsion).

Sechler, E. E., PhD., "Elasticity in Engineering", John Wiley & Sons, Inc., New York, 1952, pp. 97-116, Equations 7.71 & 7.72. (Castigliano's strain energy equations)

Shigley, J. E., "Mechanical Engineering Design", McGraw-Hill Book Co., Inc., New York, 1963, pp. 66-76, (Strain energy in shear and bending).

Zienkiewiz, O. C., "The Finite Element Method in Engineering Science", McGraw-Hill Book Co., Inc., New York, 1971, pp. 124-153 (energy, $\frac{1}{R} = \frac{M}{EI}$, and Castigliano's Second Theorem).

APPENDIX A

LIST OF APPLICABLE DRAWINGS

APPENDIX A
LIST OF APPLICABLE DRAWINGS

Douglas Drawing Numbers	Title
Z7942620 (TAD)	Instrumented Transparency Beam Test
Z5942626	Transparent Beam - Instrumented
Z5942627	Support - Transparency Beam Test
Z5942628	Transparent Beam Assy - Instrumented
Z5942629	Transparent Beam - Damping Test
Z5942630	Instrumentation - Transparency Beam Test
Z5942631	Set Up - Transparency Beam Test

APPENDIX B

DATA COLLECTION FORMAT

DATA COLLECTION

Test form shall be simple and complete with a summary, witnessed and approved by the cognizant engineers. These data sheets shall be maintanined and may be supplied to the USAF (AFFDL/FEW).

Data Section shall be as follows:

A. Damping Test Data

B. Instrumented Beam Test Data

C. Drop-Weight Test Data

DATA COLLECTION FORM

Test No. _____ Date _____

Condition No._____ Drawing No._____

Specimen No. _____ Vendor _____

Temperature _____

Deflection @ Center_____ Drop Weight Distance_____

Dial Indicator @ Positions	Initial	Final
	_____	_____

Load Reading _____

Frequency _____HZ

Strain Gage Readings

(micro inch/inch)

Thermocouple Reading Gradient

(°F)

Test Remarks and Results:

Test Witnessed by: Test Conducted by:

_____ _____

Sheet _____ of ____

APPENDIX C

DAMPING RATIO BY ALTERNATE METHOD

DAMPING RATIO BY ALTERNATE METHOD

An alternate method for determining the approximate damping ratio, γ, of a single degree of freedom system with viscous damping, subjected to free vibration, is presented in Reference 4.

The logarithmic decrement (δ_L), Equation (1-46) of Reference 4, is

$$\delta_L = \frac{2\pi\gamma}{\sqrt{1 - \gamma^2}},$$

and $\delta_L = \frac{1}{n-1} \ln \frac{x_1}{x_n}$, from Equation (1-48) of Reference 4.

Solving for γ from Equation (1-46) of Reference 4 gives

$$\gamma = \frac{\delta_L}{\sqrt{(2\pi)^2 + \delta_L^2}} \approx \frac{\delta_L}{2\pi}, \text{ if } \delta_L << 1. \qquad (C.1)$$

Substituting for δ_L from Equation (1-48) of Reference 4 into Equation (C.1) gives

$$\gamma \approx \frac{1}{2\pi\ (n-1)} \ln \frac{x_1}{x_n} \qquad (C.2)$$

where
- n = the n^{th} cycle
- $(n-1)$ = total number of full cycles
- x_1 = first good peak amplitude value
- x_n = peak amplitude value at the n^{th} cycle
- ln = natural log
- γ = damping ratio

Using polycarbonate damping Specimen 12, Condition 97 (room temperature), as an example,

where

$(n-1)$ = 25 full cycles

x_1 = 1.26 divisions (strain amplitude)

x_n = 0.50 divisions (strain amplitude)

then from eq (C.2)

$$\gamma = \frac{1}{2\pi(25)} \ln \frac{1.26}{0.50}$$

or

$$\gamma = \underline{\underline{0.005884}}$$

which is the average damping ratio for this specimen condition.

Table C.1 and Table C.2 allow comparison between data and results for the two methods indicated.

TABLE C.1. DATA USED IN EQUATION (C.2) FOR THE DETERMINATION OF THE DAMPING RATIO FOR SPECIMEN 12, CONDITION 97.

Temperature	35°F	RT	135°F
Initial Deflection (inch)	1	1	1
$(n-1)$	22	25	14
x_1	1.20	1.26	1.01
x_n	0.26	0.50	0.43
γ	.011064	.005884	.009708

TABLE C.2. DATA USED IN EQUATION 26 (of Section IV) FOR THE DETERMINATION OF THE DAMPING RATIO FOR SPECIMEN 12, CONDITION 97

Temperature	-35°	RT	135°F
Initial Deflection (inch)	1	1	1
(q-p)	(45-1)	(51-1)	(29-1)
x_p	1.20	1.26	1.01
x_q	0.26	0.50	0.43
γ	.011063	.005884	.009707

*U.S.Government Printing Office: 1978 — 757-080/493